THE
PHYSICAL REVIEW

A journal of experimental and theoretical physics established by E. L. Nichols in 1893

SECOND SERIES, VOL. 79, NO. 3 AUGUST 1, 1950

Transition Curves of 330-Mev Bremsstrahlung*

WADE BLOCKER, ROBERT W. KENNEY AND WOLFGANG K. H. PANOFSKY
Radiation Laboratory, Department of Physics, University of California, Berkeley, California
(Received April 17, 1950)

Transition curves produced by 330-Mev bremsstrahlung from the Berkeley synchrotron have been measured in carbon, aluminum, copper and lead. The measurements have been made with a thin ionization chamber "immersed" in the materials under study. The results are in agreement with expected shower behavior. An important part of this investigation is to provide a suitable means for standardizing the synchrotron beam. This is accomplished in two ways. (1) The area of the shower curves gives a good measure of the beam energy. (2) Analysis of transition curves with thin converters permits separation of Compton and pair electron ionization. The pair ionization can be compared with theory and the primary energy deduced. Agreement between these methods is very good. As a result of these measurements absolute cross section measurements in the synchrotron beam become possible.

I. INTRODUCTION

SINCE the discovery of electron-gamma-ray cascade showers in the cosmic radiation by Blackett and Occhialini[1] numerous investigations on the properties of these showers have been carried out. All such experiments fall essentially into three classes. (1) Experiments in which the progress of a shower is traced visually by counting the numbers of particles at a given depth between converters.[2] (2) Experiments in which the ionization is measured as a function of depth.[3] (3) Experiments studying the radial extent of the cascade radiation.

Cascade theory in its present form[4] gives expressions for the functions $P(E, t)$ and $\gamma(E, t)$ which give the probabilities of finding an electron or a gamma-ray, respectively, of energy E at a depth t. Evaluation of these functions depends on initial "boundary conditions," i.e., on the primary energy spectrum of the initiating particles or particle. Experiments of type (1) as enumerated above give a direct count of the numbers of particles; however, the primary energy can only be inferred from the track count and the "critical energy"[4a] of the electrons in the material studied.

Ionization experiments on the other hand constitute a more direct measurement of shower energy but their interpretation in terms of number of particles at a given depth is more tenuous. This is particularly true in the case of heavy elements for which the large scattering angles[5] of the low energy electrons make the ionization corresponding to a given particle uncertain. When such an experiment is carried out in the cosmic radiation the primary event cannot be identified. A more definite initial condition for a shower can be established by studying the transition from the equilibrium distribution in a light material to a heavy material, as has been done by Vernov and Vavilov[6] and others.

In this experiment the method of ionization measurement in an effectively infinite medium has been used to study the longitudinal, and also to some extent the transverse, behavior of a shower. A definite initial condition is established by using as the initial radiation the bremsstrahlung of the Berkeley synchrotron with 330-Mev quantum limit. Transition curves in matter, initiated by accelerator produced radiation, have been studied previously only at energies where cascade effects are essentially negligible.[7] Showers initiated by syn-

* This work was performed under the auspices of the AEC.

[1] P. M. S. Blackett and G. P. S. Occhialini, Proc. Roy. Soc. A139, 699 (1933).

[2] E. Hayward, Phys. Rev. 72, 937 (1947). G. Pfotzer, Zeits. f. Physik 102, 41 (1936). S. Nassar and W. E. Hazen, Phys. Rev. 69, 298 (1946). W. E. Hazen, Phys. Rev. 66, 254 (1944).

[3] Bowen, Millikan, and Neher, Phys. Rev. 52, 80 (1937). J. C. Street and R. T. Young, Phys. Rev. 46, 823 (1934); Phys. Rev. 47, 572 (1935).

[4] H. Snyder, Phys. Rev. 76, 1563 (1949).

[4a] The critical energy is the energy loss by ionization per radiation unit traversed.

[5] B. Rossi and K. Greisen, Rev. Mod. Phys. 13, 240 (1941).

[6] S. N. Vernov and O. N. Vavilov, Phys. Rev. 70, 769 (1946).

[7] Koch, Kerst, and Morrison, Radiology 40, 120 (1943).

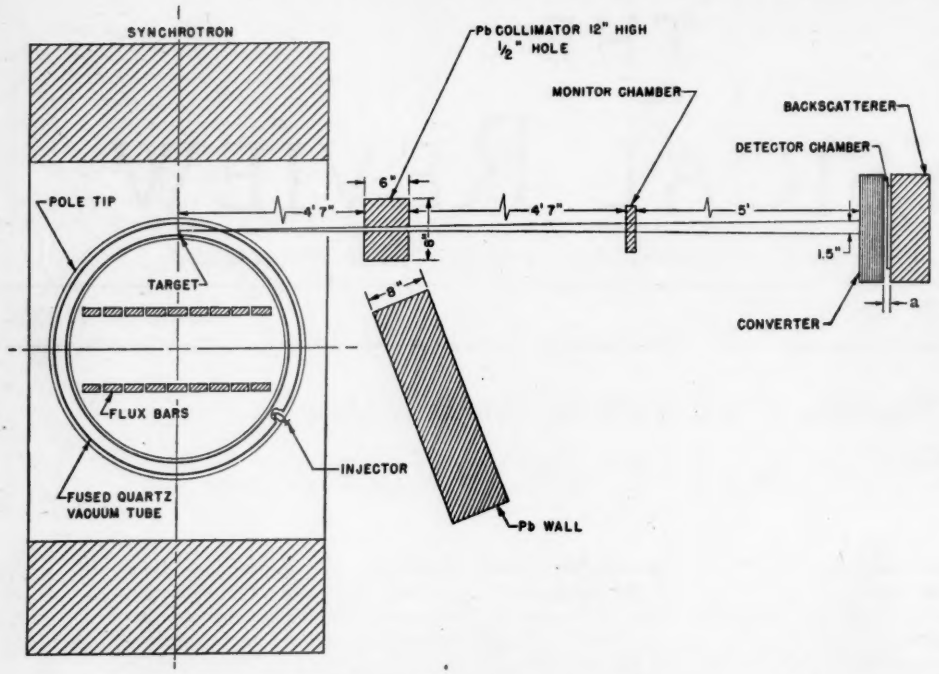

FIG. 1. Schematic arrangement of the apparatus with respect to the synchrotron. The collimator absorbers and ionization chambers are coaxial with the beam. The lead wall shields the apparatus from x-rays originating at the injector. The slot width, a, is variable.

chrotron bremsstrahlung are not exactly equivalent to showers initiated by a single electron owing to the fact that (a) only 15 percent of the incident electron energy is lost by radiation in the synchrotron target, and (b) the target material, platinum, is not the same as the converter in which the shower propagation was studied (Pb, Cu, Al, and C). The synchrotron bremsstrahlung spectrum is, on the other hand, not the ideal thin target spectrum because of finite target thickness. This modifies somewhat the primary gamma-ray energy distribution by lessening the steepness of the spectrum near the quantum limit.

In addition to serving as a contribution to the experimental material bearing on cascade theory this work serves the practical purpose of providing a primary standard of beam energy of the synchrotron radiation. The magnitude of the ionization during the first part of the gamma-ray initiated shower can be interpreted simply in terms of the cross sections for pair production and Compton electrons. Let the cross section for pair production and production of Compton electrons be $\phi_{\text{pair}}(k)$ and $\phi_C(k)$ respectively and let the energy contained in the primary x-ray beam be given by

$$U=\int N_k k dk, \tag{1}$$

where N_k is the number of primary quanta in the energy interval between k and $k+dk$. The cross sections per atom will have the form

$$\phi_{\text{pair}}=(Z^2+Z)\phi_{\text{pair}}{}^0 \quad \text{and} \quad \phi_C=Z\phi_C{}^0, \tag{2}$$

where the ϕ^0 are functions essentially independent[7a] of the atomic number Z. If N_e is the number of electrons per unit area in a converter, then the ionization $I(N_e)$ produced in an ionization chamber of thickness g by secondaries from the converter of a primary beam of energy U is given by

$$I(N_e)=N_e g I_0\left\{\int (kN_k)\phi_C{}^0(k)\frac{dk}{k} +2(Z+1)\int (kN_k)\phi_{\text{pair}}{}^0(k)\frac{dk}{k}\right\}, \tag{3}$$

where I_0 is the ionization per unit length in air of an electron near minimum ionization. The Z-dependence of the beginning of the shower curve, where cascade processes are as yet negligible, in combination with (1) and (3) gives, therefore, a measurement of U. Such an evaluation will depend on the theoretical expressions for $N_k\phi_{\text{pair}}{}^0$, and therefore for large values of Z will show up deviations from the (Born approximation) theory previously found by Lawson[8] and others.[9] This deviation has in fact been observed.

The Compton integral in Eq. (3) as it stands is divergent. Actually it has a definite finite value due to the self-absorption of the Compton electrons in the converter. In addition to this, the Compton integral would be modified by the fact that the low energy spectrum N_k is affected by the quartz vacuum chamber walls. Theoretical evaluation of the first term is therefore not very fruitful.

An independent way of arriving at the energy of the primary beam is from the area of the shower curve. Let $I(t)$ be the observed ionization at a depth t of

[7a] The variation of ionization with energy, the small variation of ϕ^0 with atomic number, and the variation of pair production in the field of an electron, will be considered later in the more detailed calculations.

[8] J. L. Lawson, Phys. Rev. 75, 433 (1949).
[9] R. L. Walker, Phys. Rev. 76, 1440 (1949).

converter. If $(-dE/dt)$ is the stopping power for electrons near minimum ionization in the material under study, then the total beam energy is closely given by

$$U=\int_0^\infty (-dE/dt)[I(t)/I_0 g]dt, \qquad (4)$$

since all energy is lost eventually by ionization. It is of course assumed here that the converters and ion chamber used contain the total radial extent of the shower. This method is not very accurate since it is difficult to take account of the small variation of dE/dt with electron energy.

The degree of agreement of the energy values calculated from Eqs. (3) and (4) for various values of Z furnishes a valuable check on the internal consistency of the data as well as on the behavior of the pair cross section as a function of Z.

These two methods serve to determine the total energy in a 330-Mev x-ray beam or an effective number of quanta defined by

$$Q=U/k_{\max}, \qquad (5)$$

where $k_{\max}$ is the energy of the quantum limit. This analysis of the shower curves thus provides a basis for the determination of absolute photo cross sections in the synchrotron beam. This method is considerably simpler and more reliable than the use of a graphite lined chamber as carried out by Lax;[10] as proposed in his work both the Compton and pair effects must be calculated in detail, and also specific calculations of the behavior of the electrons as to scattering, etc., are necessary. Studying the Z-dependence of the ionization for converters of a small fraction of a radiation length thickness eliminates either complication.

FIG. 2. Cross section (side view) of the monitor ionization chamber.

[10] M. Lax, Phys. Rev. 72, 61 (1947).

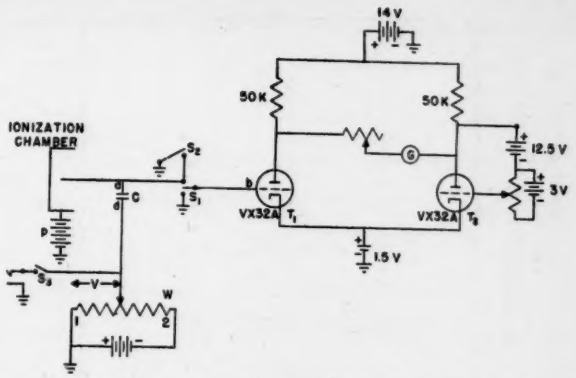

FIG. 3. Schematic diagram of the ionization chamber and associated circuits. The voltage, V, is measured with a potentiometer and decade voltage divider.

A remark might be made here concerning the usual manner in which the intensity of the x-ray beam from a high energy electron accelerator is specified. It is customary to give a value of a certain number of roentgens per hour at a definite distance from the target. This quantity is measured usually with a small cylindrical ionization chamber of wall material of given composition. As has been pointed out by Lax[10] such a method gives easily interpretable results if the electron range is small compared with the wall thickness, which in turn is small compared to a radiation length. This condition can be met at small electron energies (up to 1 to 2 Mev), but is not applicable at higher energies.

II. APPARATUS

The progress of the shower produced by the synchrotron x-ray beam was observed by inserting a thin integrating ion chamber in plane parallel geometry into an effectively infinite slab of the converter under study at a distance, t, from the front face of the converter. The material both from the front and rear of the chamber contributes greatly to the observed ionization, as was pointed out recently by Vernov and Vavilov.[6] A back scatterer is therefore necessary to account for the total energy in the shower.

In principle the slit into which the ion chamber is inserted would need to be infinitely thin in order that the chamber measure a quantity corresponding to the ionization at a given depth in the converter, and also that no energy be lost by side leakage across the edges of the chamber. The latter point is particularly important for heavy materials, since a shower initiated in a heavy element will contain a large number of electrons traveling at large angles to the initial beam direction. It was therefore found necessary to extrapolate the data to effectively zero chamber thickness.

The location of the apparatus with respect to the synchrotron is shown in Fig. 1. The beam of x-rays originated in the synchrotron target, which was a strip of platinum 0.020 inch thick located within the vacuum chamber. For external experimental use, the beam

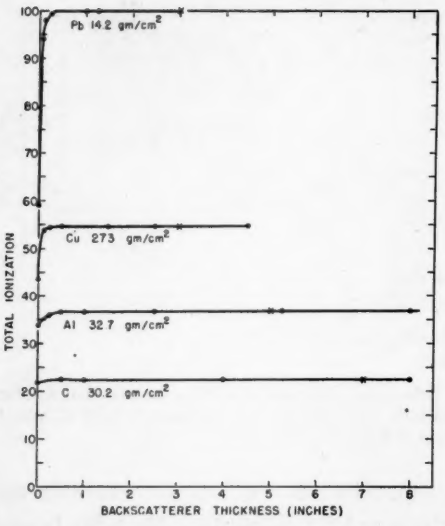

FIG. 4. The observed total ionization, in arbitrary units, plotted against the thickness of the backscatterer. The thickness of the converter corresponds approximately to the maximum of the shower curve for that element (see Figs. 7 and 8). The cross on each curve indicates, for that element, the thickness of backscatterer used to obtain the data for the corresponding shower curve in Fig. 7 or 8. Converter thickness ahead of the chamber is indicated on each curve.

passes through the wall of the vacuum chamber made of fused quartz approximately $\frac{3}{8}$ inch thick. At the position of the collimator, the beam has a diameter of $\frac{7}{8}$ inch, measured at the half-intensity circle. The intensity at 2 inches from the beam axis is 2 percent of the intensity at the beam axis. The lead collimator block is 6 inches thick, 8 inches wide, 12 inches high, and has approximately a $\frac{1}{2}$-inch diameter tapered collimating hole through its center which is coaxial with the beam.

The shower intensity in the converter is measured by comparing the integrated ionization current of the ion chamber inserted into the thin slot in the converter with the reading of a monitor chamber located beyond the collimator (see Fig. 1).

At the position occupied by the monitor ionization chamber, the x-ray beam diameter is approximately 1 inch; the sensitive volume of the monitor chamber is 6 inches in diameter. Adequate beam monitoring intensity was obtained from a sensitive volume of 1-inch depth. Both the monitor and detector ionization chambers contain air and are vented to the atmosphere. Details of the monitor chamber are shown in Fig. 2. The cylindrical walls are constructed of Lucite. All foils are of 0.00035-inch aluminum. The active volume of the chamber is bounded by foils, in the planes *bb'* and *dd'*, which were applied to the Lucite with polystyrene dope and stretched slightly. The collecting foil is in the plane *cc'* and is completely surrounded by the active volume. A grounded electrostatic shield surrounds the entire chamber and serves incidentally as a dust shield. It was also applied in the above manner to the surfaces *aa'* and *ee'* of the outer rings which serve as high voltage insulation from the foils *bb'* and *dd'*, but over surfaces *ae* and *a'e'* this shield was not allowed to touch the Lucite, thus minimizing leakage to ground. The diameter of the monitor chamber is small enough so that the foils remain tight when supported only by the Lucite. In passing through the monitor, the beam traverses 0.00175 inch of aluminum.

The soft x-ray background in the vicinity of the synchrotron is appreciable, with a harder component apparently originating at the injector. A wall of lead bricks shields both the ionization chambers from direct

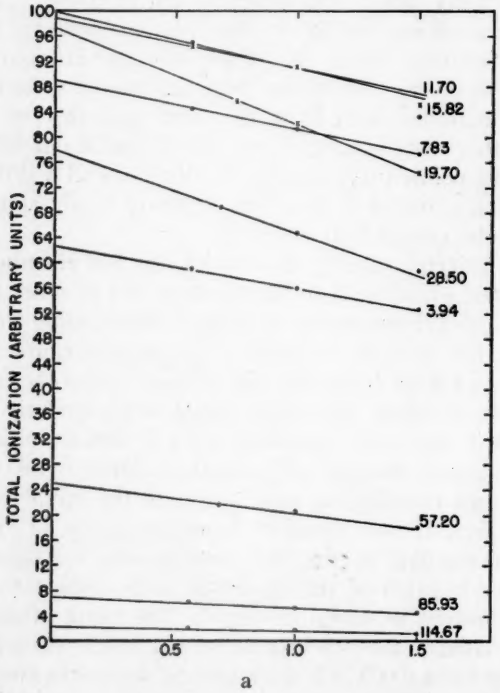

FIG. 5. Extrapolation curves for lead.

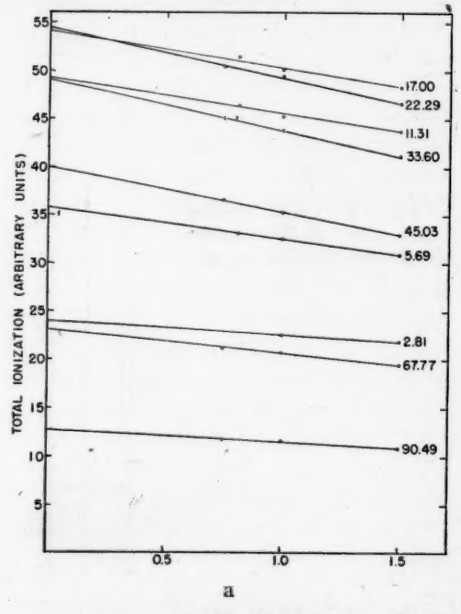

FIG. 6. Extrapolation curves for copper.

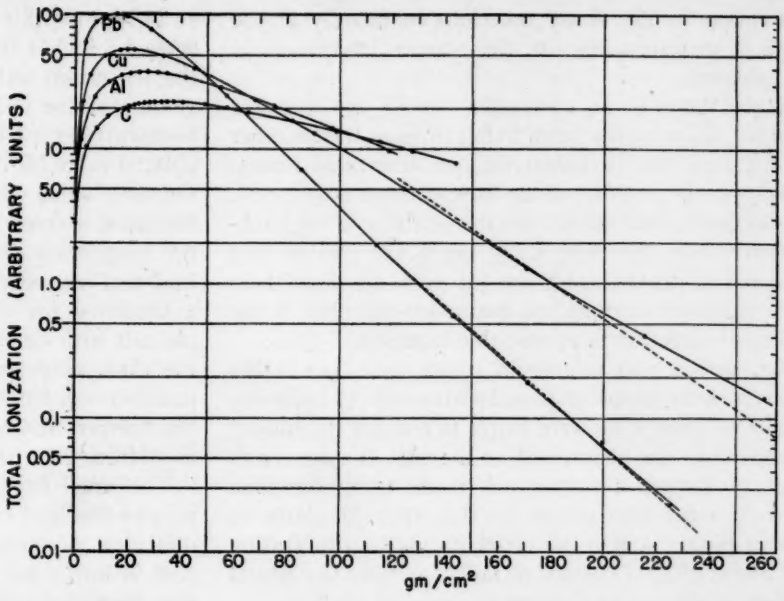

FIG. 7. The total ionization, in arbitrary units, in an effectively infinite block of converter, plotted against the depth (g/cm²) in the converter. The dashed lines have slopes calculated from the minimum absorption coefficients given by Heitler (reference 12), and are plotted for comparison with the data. The discrepancies in the slopes are considered to be within the experimental errors

radiation coming from the region of the injector, while a $\frac{1}{8}$-inch thick lead hood placed over the monitor, extending 30 inches from the monitor in both directions along the beam, shields it from the general soft x-ray background.

The construction of the detector chamber is basically the same as that of the monitor (see Fig. 2); however, no outer rings *aa'b'b* and *dd'e'e* are used. The converter plates (see Fig. 1) serve in lieu of electrostatic shield foils. The sensitive volume, 11 inches in diameter and $\frac{1}{2}$ inch deep, is bounded by 0.00035-inch aluminum foils which were applied to the surfaces *bb'* and *dd'* with polystyrene dope and stretched slightly. The diameter of the chamber is large enough so that a mesh of 0.003-inch stainless steel wire, spaced two inches apart, is required to support the outer foils *bb'* and *dd'*.

The centers of the ionization chambers were positioned to within $\frac{1}{8}$ inch of the beam axis by means of a transit located coaxially with the beam. The line of sight of the transit was adjusted and checked photographically so that it was within $\frac{1}{16}$ inch of the beam axis at all points where the apparatus was placed.

The collimator was provided with a peepsight insert which allowed it to be checked photographically for coaxial alignment with the beam.

The ionization current of each chamber was collected on a low leakage, polystyrene insulated capacitor, *C* (see Fig. 3). The voltage on the condenser was measured by a null method. The principle of the method is to maintain the condenser terminal connected to the ion collecting electrode at ground potential by sliding back the other terminal by a voltage exactly measurable by a potentiometer. This system also makes any correction for lead capacities, etc., unnecessary. The zero voltage condition of the collector can be checked by an electronic voltmeter which serves only as a null indicator.

The complete circuit is shown in Fig. 3. The electronic voltmeter is disconnected from the collector electrode during the run (in order to avoid possible grid rectification of high transient pulses, such as might be produced by voltages induced by microphonic pulses of the ion chamber in the noise field of the synchrotron). After the run the collector is slid back to zero and the slide-back voltage is measured. The grid current of the voltmeter is 10^{-15} amp. so that the charge loss during measurement is negligible. Leakage resistance between the high voltage foil and the collecting foil of the chamber was held above 10^{15} ohms without benefit of guard rings. Less than $\frac{1}{2}$ percent of the minimum voltage utilized for an ionization measurement was attributable to leakage. The condenser used was a 0.01 μf condenser and the voltage collected of the order of 1 volt.

The collecting voltage *P* applied to the detector chamber was varied, and it was found that with fields between 800 and 1500 volts per inch the ionization readings for a given set of conditions remained a constant within the experimental error. 1200 volts per inch collecting field was used in both monitor and detector chambers.

III. EXPERIMENTAL PROCEDURE

The block of converter was formed of closely stacked plates of the element under study, located both ahead and behind the ion chamber. The x-ray beam, after passing through the monitor, fell normally on the stack and the shower electrons were observed by the detector ionization chamber situated in a slot of width *a* and depth *t* in the stack. In all cases, as shown in Fig. 4, only a few inches of backscattering converter were required behind the chamber to serve in place of the remainder of the ideal infinite block. The ionization due to the backscatterer, essentially at shower maximum, is expressed as a fraction of the total ionization by the following: Pb, 0.41; Cu, 0.20; Al, 0.09; C, 0.04.

The curves in Fig. 4 are taken approximately at the depth t corresponding to the shower maximum in each element.

When there is no converter before the detector chamber, allowing the beam to fall through the chamber directly onto the backscatterer, no detectable ionization due to the presence of the backscatterer is observed. This indicates that shower electrons arising in the backscatterer from the pure x-ray beam are created and scattered at depths which are too great to allow them to be scattered through the ionization chamber in the backward direction in appreciable numbers.

The carbon and aluminum plates were ten inches square and the copper and lead plates were 12 inches by 14 inches. These sizes were ample to contain the shower diameter[11] in the absence of an air gap. A very rough check of shower diameter was made using Eastman Type K x-ray film placed in the stack of plates at various points, and in all elements used no indication was found of the presence of radiation near the lateral borders of the stack of plates.

The elements studied were obtained from stock. The carbon was graphite, type C-18, of nominal density 1.58. The 2S aluminum used was found to contain less than 0.5 percent impurities. The copper and lead used were of commercial graed.

It was found to be unfeasible to construct a detector chamber of large enough diameter to intercept all the ionization from shower electrons in the slot, even though the showers were initiated by an x-ray beam less than 2 inches in diameter. Appreciable fractions of the electrons were backscattered into the slot at angles approaching 90 degrees with respect to the shower axis, especially in the case of a lead converter. It was thus necessary to observe the total ionization, at a given depth t, corresponding to several slot widths from 1.5 inches to 0.75 inch, and then to extrapolate the ionization values to zero slot width. The active volume of the chamber was kept in contact with the backscatterer plates at all slot widths. This extrapolated value for the total ionization was assumed to be the same value which one would find in the ideal case discussed above. The curves in Figs. 5* and 6* show the magnitude of the necessary extrapolation for the lead and copper converters. In the case of aluminum, a tendency for the ionization values to approach a plateau with decreasing slot width was observed, and the extrapolations were made accordingly. No extrapolation was found to be necessary in the case of a carbon converter. Complete shower curves and results derived from them are based upon these extrapolated data.

The small energy discrepancies associated with the area of the lead curve (Section V) may be due to the difficulty of extrapolating in the correct manner. Also in lead some of the electrons have such low energies that the range in the chamber itself cannot be considered entirely negligible, nor is it necessarily true that all electrons are at minimum ionization. Small discrepancies in the energy balance of the heavy elements are thus expected. The construction of a chamber thinner than $\frac{1}{2}$ inch was not considered compatible with reasonable accuracy, since flexibility of the window foils would result in untenable variations in the sensitive volume.

The x-ray beam was contaminated by electrons arising from the wall of the fused quartz vacuum chamber and from the air through which the beam passed before striking the apparatus. This background contamination was of small intensity, compared with the maximum shower intensity observed, principally due to the fact

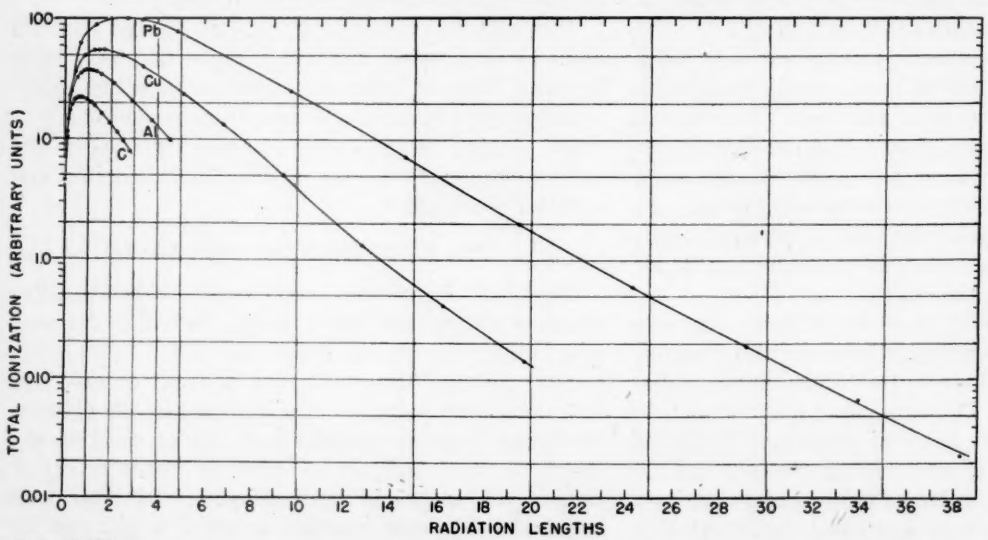

FIG. 8. The total ionization, in arbitrary units, in an effectively infinite block of converter, plotted against the depth (radiation lengths) in the converter.

[11] J. M. Blatt, Phys. Rev. 75, 1584 (1949). B. Rossi and K. Greisen, Rev. Mod. Phys. 13, 306 (1941).

* The total ionization, in arbitrary units, measured by the detector chamber is plotted against the distance, a, in inches, between the converter and the backscatterer, for the converter thicknesses (g/cm^2) noted at the right of the curves. The curve for each converter thickness is extrapolated to $a=0$, and these limiting values are assumed to give the total ionization within an infinitesimally thin slot in an infinite block of converter.

that the quartz vacuum chamber walls are at a point where the synchrotron magnetic field has a value of approximately one-half of the value at the orbit. The fraction of a radiation length of air traversed by the beam is very small. The detector chamber is largely shielded against this background by the converter plates, except at very small values of t, at which the contamination was adequately treated as a background. The intensity of this contamination background was proportional to the beam intensity so that the monitor chamber, which keeps only a proportional check on the beam intensity, was not affected.

An ionization value observed under any conditions was taken to be the ratio of the detector condenser voltage to the corresponding monitor condenser voltage, both voltages resulting from charge collection during a single run of approximately 1 minute duration. This ratio was extrapolated in the manner discussed in the preceeding section to arrive at the value for total ionization (Figs. 7† and 8†). Two successive runs were made for every slot width a at each depth t in the converter. The internal consistency is about 1.5 percent for points within a factor of 50 in intensity of the shower peak; for points farther down the curve the consistency drops to 10 percent. Long time changes in background were checked and found to be negligible.

IV. RESULTS ON SHOWER CURVES

The data for the normalized shower curves in Figs. 7 and 8 were obtained for the elements lead, copper, aluminum, and carbon. On repeating a run it was found that while the shape of the curve was unaltered, the values of the ordinates may have changed slightly. It is believed that these changes were due in part to differences in the electron contamination of the x-ray beam at the times of the experimental runs, since the geometry was not precisely reproduced for all runs.

The ordinates are proportional to the ratios of the voltages measured on the integrating condenser of the detector to the corresponding voltages measured for the monitor. The changes in absolute value discussed above required that the ordinates be normalized to some standard in order that the curves for the different elements might be compared. This was done by obtaining the ratio of the ordinate for the experimental point nearest the peak of a shower curve to that of the peak point for the copper curve for each of the elements. Each ratio was obtained once with the exception of the C/Cu ratio which was later checked, the two values agreeing to within 0.3 percent. This agreement is fortuitous since for successive runs for the same point the mean ordinate was reproducible to only about 1.5 percent on the average. In reducing the data, all points

† The ionization was observed by a thin ionization chamber in a slot of width, a, and depth, t, in the converter. Data were obtained at various slot widths and then extrapolated to $a=0$ in Figs. 5 and 6. The extrapolated values thus obtained are the ordinates of Figs. 7 and 8.

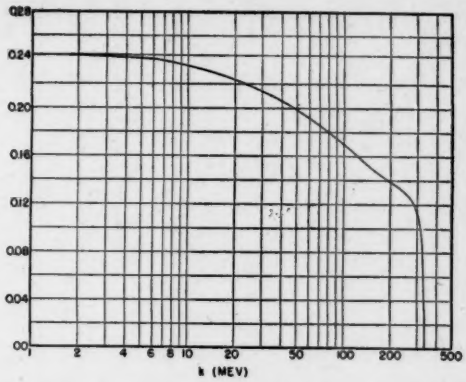

FIG. 9. The theoretical bremsstrahlung energy distribution kN_k for the Berkeley synchrotron, calculated for a single electron of energy 330 Mev incident normally upon a platinum target 0.020 inch in thickness. The area under this curve divided by k_{max} is the target x-ray efficiency.

were normalized to correspond to the value 100 for the peak of the lead curve.

It is seen that the zero points for all the curves do not coincide. This is probably due to differences in electron contamination of the beam incident upon the converter. This means that the initial portions of the curves are slightly in error. This is not significant however, since the slopes are so great at this point that the maximum difference would correspond to a converter thickness of only about 0.1 g/cm².

After the synchrotron beam has passed through a sufficiently great thickness of converter, it should be attenuated along the remainder of its path in such a manner that the absorption coefficient has a constant and minimum value. The curves of Figs. 7 and 8 show that the required thicknesses have been approached for lead and copper. The converter thickness of aluminum or carbon is not great enough to give this condition, but it is large enough so that absorption coefficients determined from the curves can be used without serious error in the integration of the area of the shower curves as described below.

The dashed lines in Figs. 7 and 8 are lines having slopes which correspond to the minimum absorption coefficient for gamma-rays given by Heitler.[12] The pair contribution to the lead absorption coefficient has been decreased by 10 percent to take account of Lawson's[8] values for the lead pair production cross section. These lines are plotted for comparison with the experimental data.

V. SEPARATION OF PAIR AND COMPTON CONTRIBUTIONS IN THE IONIZATION

As has been shown in Section I, the Z-dependence of the ionization for small values of N_e can be used to separate the Compton and pair contributions to the total ionization. Let us rewrite Eq. (3), adding some detail as to the behavior of ϕ_{pair}^0. In the notation of

[12] W. Heitler, *The Quantum Theory of Radiation* (Oxford University Press, London, 1944), p. 215 ff.

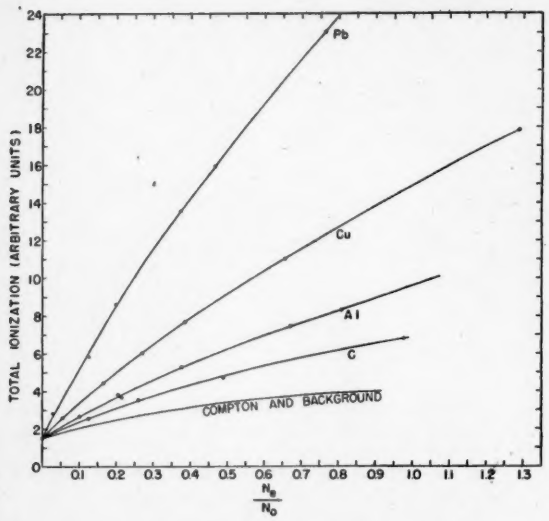

FIG. 10. The total ionization, in arbitrary units, observed by a thin ionization chamber plotted against an abscissa proportional to the number of electrons per square centimeter of the converter. No backscatterer was present and no extrapolation to zero ionization chamber thickness was found necessary. Contributions to the total ionization due to Compton recoils and background are given by the lowest curve, which is independent of Z.

Section I

$$I(N_e)=N_e Ig\left\{\int (kN_k)\phi_C{}^0\frac{dk}{k}+2(Z+1)\int_{-\infty}^{0}\left[\left(\frac{\phi_{\text{pair}}}{Z^2}\right)\left(\frac{Z+\alpha}{Z+1}\right)\cdot\left(\frac{I(\frac{1}{2}k)}{I_0}\right)(kN_k)\right]d\left(\ln\frac{k}{k_{\max}}\right)\right\}. \quad (6)$$

The individual terms in the pair integral have been written to be slowly varying functions of Z and k respectively. Here ϕ_{pair} is the cross section for pair production in the field of the nucleus, α is the fractional contribution to the total pair cross section due to "triplet" production in the field of an electron. According to the calculations of K. M. Watson[13] and of A. Borsellino,[14] α has a value from 0 to 0.9 in the range of interest, but the effective average value is 0.49, and hence the factor $(Z+\alpha)/(Z+1)$ is only a small correction. It has been assumed that only two of the three triplet members are observed. Similarly the term ϕ_{pair}/Z^2 has only a small Z-dependence, arising from the variation of the screening correction[15] as a function Z. $I(\frac{1}{2}k)$ represents the ionization per unit length in air of a pair electron of energy $(\frac{1}{2}k)$, it being assumed that each pair electron receives half of the quantum energy in all cases. Since $I(\frac{1}{2}k)/I_0$ is a correction factor close to unity, it is not necessary to consider the detailed division of energy among the pair members.

The bremsstrahlung spectrum kN_k corrected for the finite target thickness has been kindly calculated for us by W. Aron; the spectrum is shown in Fig. 9. The integral in the second term of Eq. (6) can thus be evaluated numerically as a ratio to the total beam energy $U=\int kN_k dk$. Let us designate this ratio by $R(Z)$, i.e., let

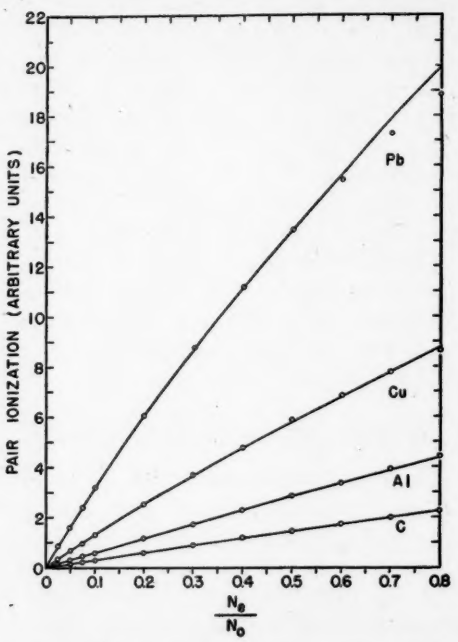

FIG. 11. The pair ionization, in arbitrary units, plotted against an abscissa proportional to the number of electrons per square centimeter of the converter. These curves are obtained from the curves of Fig. 10 by subtracting the Compton plus background curve from the total ionization curves.

$$R(Z)=\frac{\int_{-\infty}^{0}\left\{\left(\frac{\phi_{\text{pair}}}{Z^2}\right)\left(\frac{Z+\alpha}{Z+1}\right)\frac{I(\frac{1}{2}k)}{I_0}(kN_k)\right\}d\left(\ln\frac{k}{k_{\max}}\right)}{\int_0^1 (kN_k)d(k/k_{\max})}. \quad (7)$$

This quantity represents the cross section for pair production (normalized to $Z=1$) averaged over the primary bremsstrahlung spectrum. $R(Z)$ is tabulated in Table I. The quantity ϕ_{pair}/Z^2 in the integrand contains both the screening correction and also, in the case of lead, the 10 percent correction as obtained by

[13] K. M. Watson, Phys. Rev. 72, 1060 (1947), and private communications concerning corrections to this paper.

[14] A. Borsellino, Nuovo Cimento 4, No. 3–4, (June 1, 1947).

[15] H. Bethe and W. Heitler, Proc. Roy. Soc. A146, 83 (1934).

TABLE I. The cross section for pair production, $R(Z)$.

Z	6	13	29	82
$R(Z)$ in cm²	2.54×10^{-26}	2.55×10^{-26}	2.50×10^{-26}	2.20×10^{-26}

Lawson.[8] $I(\frac{1}{2}k)/I_0$ is obtained from the curve of Rossi and Greisen.[5]

Figure 10 shows the initial parts of the shower curves (taken without backscatterer) plotted as a function of the number of electrons per unit area of converter. In addition to the experimental curves a curve is plotted labeled "Compton and Background." This curve is obtained by subtracting the proper fraction, computed from Eq. (6), of the difference between the aluminum and the carbon curve from the carbon curve; this fraction is nearly unity if α in Eq. (6) is unity and if ϕ_{pair}/Z^2 is constant. It is not feasible here to compare the Compton curve with theory, since it is difficult to separate from the background, and also since the Compton contribution cannot be evaluated without consideration of the converter self-absorption. After subtraction of the "Compton and Background" curve, the curves presumably representing the pair ionization are obtained (Fig. 11).

If cascade effects were negligible, the curves of Fig. 11 should be straight lines. This is not the case and the observed curvature is a measure of the loss of the pair electrons by radiation and of primary absorption. For thicknesses of converter which are a small fraction of a radiation length, the slope will decay with distance essentially exponential with a characteristic decay distance of the order of a radiation length. The slopes of the curves of Fig. 11 conform to this interpretation; points computed under the assumption that the slope falls exponentially from its observed initial value are plotted on the curves on Fig. 11. The initial slopes thus represent the pair contribution to the total ionization, and according to Eq. (6) should be a linear function of $Z+1$, after correction for the variation of $R(Z)$ with Z has been made. This correction has been applied and the resultant slopes are plotted against $Z+1$ in Fig. 12; it is seen that the agreement is good. As has been mentioned above, in agreement with the deviations observed by Lawson[8] for the pair cross sections in heavy elements for 88-Mev radiation, and by Walker[9] at 17.5 Mev, a 10 percent correction has been applied to $R(Z)$ in the case of lead. The point is also plotted without the correction, with significantly poorer agreement.

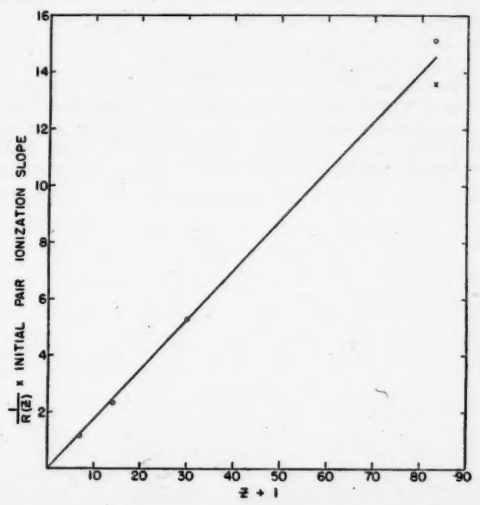

FIG. 12. The initial slopes of the curves in Fig. 11, divided by the function R (Z) (as tabulated in Table I), plotted against $Z+1$. A point (x) is also shown indicating the deviation if the Lawson correction (reference 8) is *not* used in computing $R(Z)$. The units are arbitrary.

TABLE II. Normalized values of the energy flux in the collimated beam measured by the "two-element" method, in units of 10^8 Mev/sec.[a]

Converter pair / N_e/N_0	Pb−Cu	Pb−Al	Pb−C	Cu−Al	Cu−C	Al−C
0.0	102.3	102.2	101.0	102.0	98.5	90.7
0.025	101.0	101.0	99.9	101.1	97.8	90.5
0.05	99.7	99.8	98.8	100.1	97.0	90.2
0.075	98.5	98.6	97.7	99.1	96.3	90.0
0.1	97.2	97.5	96.6	98.2	95.5	89.6
0.2	92.3	92.9	92.4	94.4	92.6	88.6
0.3	87.7	88.5	88.4	90.8	89.8	87.6
0.4	83.2	84.3	84.5	87.2	87.0	86.5
0.5	79.0	80.3	80.8	83.8	84.3	85.5

[a] Various pairs of converters are used. The energy flow is tabulated against the thickness of the converter measured in terms of electrons/cm.² N_0 = Avogadro's number. The variability of the entries indicates the effect of primary absorption and of radiation. This table serves as a guide to select proper converter thicknesses and also as a means to convert to zero converter thickness. This table is normalized to a reference intensity on the beam axis of about 1400 R/hr behind ½ inch of lead 1 meter from the target. This intensity was estimated from the reading of a large Zeus meter using the effective Zeus meter area and the measured value of 1.6 for the ratio of central intensity to average intensity in the beam emerging from a 1-inch collimator. This reference performance corresponds to about one-fourth of the usual operating intensity.

VI. STANDARDIZATION OF THE SYNCHROTRON BEAM

The separation of the pair and Compton contributions described above makes it possible to obtain a direct measurement of the total beam energy, using the theoretically calculated values $R(Z)$ given in Table II. It will be recalled that $(Z^2+Z)R(Z)$ is the cross section for the production of pair and "triplet" electrons when averaged over the primary bremsstrahlung spectrum.

Analysis of the initial part of the shower curve, by the subtraction method outlined above, measures directly the number of pairs produced and thus the data of Table II immediately yield the primary energy for a given ion current due to pairs. In case it is not intended to obtain complete transition curves, then the beam can also be standardized by a "two element" method. Consider the measurement of the ionization I_1 and I_2 behind two converters of atomic numbers Z_1 and Z_2 of equal numbers (N_e) of electrons per square centimeter. N_e must not be great enough to allow cascade effects to enter appreciably. It follows from Eq. (7) that the

TABLE III. Beam energy flow through a one inch collimator distant 55 inches from the synchrotron target in units of 10^8 Mev/sec., or 10^8/330 quanta/sec., as computed by the various methods outlined. This tabulation is normalized to an axial beam intensity of 1400 R/hr at 1 meter from the synchrotron target, which is the same reference intensity used in Table II.

Method / Material	I	II	III
	Pair production using Fig. 11	Pair production using two converters of equal electron surface density in the limit of zero converter thickness (see Table II)	Shower curve area
C	90.8		100.4
Al	90.7		103.0
Cu	96.7		94.6
Pb	100.0		84.6
Pb−Cu		102.3	
Pb−Al		102.2	
Pb−C		101.0	
Pb−C		101.0	
Cu−Al		102.0	
Cu−C		98.5	
Al−C		90.7	

primary energy and the number of quanta (see Eq. (5)) is given by

$$Q=\frac{U}{k_{\max}}=\frac{1}{2N_e g I_0}\,\frac{I_2(N_e)-I_1(N_e)}{(Z_2+1)R(Z_2)-(Z_1+1)R(Z_1)}. \quad (8)$$

This equation assumes that the converter thickness (N_e) has been chosen to be small enough that no correction is necessary for the radiation effect noticeable in Fig. 11. Table III gives a typical tabulation of the calculated energy as a function of converter thickness, which indicates the effect of losses by radiation and primary absorption. Table III was computed directly from the experimental results plotted in Fig. 11. The data are smoothed, however, by assuming an exponential decay of the slope. This table can be used for a decision on the maximum converter thickness, permissible and for a derivation of the corrections necessary for extrapolation to zero thickness.

As a further alternate means of beam standardization the beam energy has been evaluated using the areas of the shower curves (Fig. 8) and Eq. (4). The areas were evaluated numerically except for the exponential tail of the curves; the tail area was evaluated analytically using the asymptotic absorption coefficients. This latter method is considered to be less accurate, for reasons discussed above. In particular, for heavy elements appreciable deviations are expected.

Table III shows the beam energy evaluated for typical operation of the Berkeley synchrotron. The value I_0 used is 62.5 ion pairs/cm.[16]

The values of beam energy as entered in Table III are not of equal reliability. In the measurement by shower curve area (column III) the values observed in the heavy elements are of lesser reliability owing to the large extrapolation to zero chamber thickness and the low energy and range of the ionizing electrons. The two element method (column II) will lead to the best results for pairs of most dissimilar Z, since errors in the background and Compton subtraction are then less significant. It is gratifying to note that the low Z shower data and large differential Z "converter pair" data are in good agreement.

The method of standardization based on the pair cross section (using Eq. (8)) can be executed quite rapidly and is being used for the calibration of chambers serving as secondary standards.

This work, including the method used, was proposed to us by Professor E. M. McMillan. He has guided the work throughout its progress and in particular is responsible for the method of separating pair and Compton effects. We are also indebted to the crew of the Berkeley synchrotron for their efficient operation of the machine during the bombardments. The calculation of the primary spectrum, pair cross sections, and the stopping powers used in these calculations was made by W. Aron.

[16] This value corresponds to the theoretical energy loss for fast electrons divided by 32 volts. It is thus not equal to the number of ions/cm as observed by a droplet count in cloud-chamber work. The latter number does not include secondary ionization. The effect of electrons of insufficient range to cross the ionization chamber has been evaluated also and found to be negligible.

The Disintegration of Ruthenium 103 and Palladium 103*

J. Y. Mei, C. M. Huddleston, and Allan C. G. Mitchell
Indiana University, Bloomington, Indiana

(Received April 26, 1950)

The beta- and gamma-ray spectra of Ru^{103} (43 days), Pd^{103} (17 days), and Rh^{103m} (56 min.) have been investigated in a magnetic lens spectrograph. Ru^{103} disintegrates with the emission of two beta-ray groups of end-point energies 0.684 Mev (six percent) and 0.204 Mev (94 percent) together with a gamma-ray of 0.494 Mev and an internally converted gamma-ray of 40.4-kev energy. Pd^{103} disintegrates by orbital electron capture. The spectrum consists of an electron line at 36.9 kev, shown to be due to L electrons from a highly converted gamma-ray of 40.4-kev energy, together with Auger electrons. The spectrum of the metastable Rh^{103m}, whose half-life has been determined as 56 min., consists of an L conversion line for a gamma-ray of 40.4 kev, with some indication of the presence of the K-line. Ru^{97} (2.8 days) was also measured and found to emit a gamma-ray of 0.217 Mev.

I. INTRODUCTION

THE two elements Ru^{103} and Pd^{103} both disintegrate to form Rh^{103}, the first by the emission of beta-rays, accompanied by gamma-rays and internal conversion electrons, and the second by K-electron capture. In both cases there is evidence that the metastable state of Rh^{103}, approximately 50-min. half-life, is formed. As will be shown below, Pd^{103} gives no radiation except that associated with the metastable state of Rh^{103}, together with x-rays and Auger electrons. Since the half-life of Pd^{103} is 17 days and since it can be produced with high specific activity, this element provides an excellent means of studying the radiations from Rh^{103m}.

Sullivan, Sleight, and Gladrow[1] have investigated two ruthenium activities produced by neutron and deuteron bombardment. Activities of half-life 42 days,[2] ascribed to Ru^{103}, and 2.8 days ascribed to Ru^{97}, were reported. The absorption experiments of Sullivan, Sleight, and Gladrow suggest that the 42-day Ru^{103} emits a gamma-ray of approximately 0.56 Mev energy and two beta-ray groups of approximately 0.3 (95 percent) and 0.8 (five percent) Mev. They report that Ru^{97} decays by orbital electron capture followed by a gamma-ray of approximately 0.23 Mev energy.

Hole[3] has measured the beta-ray spectrum of Ru^{103} in a spectrometer. The results of his investigation show that the spectrum is complex and that the energy of the highest energy component has an end point of 0.665 Mev. In addition, he finds three internal conversion lines of energies 34 kev, ascribed to Rh^{103m}, 217 kev and 290 kev. Mandeville and Shapiro[4] have made coincidence studies of the disintegration of Ru^{103} and find results essentially similar to those of Sullivan, Sleight, and Gladrow.

The radiations from Pd^{103} have been investigated by Matthews and Pool[5] and Brosi[6] who have shown that this element decays by K-electron capture with a half-life of 17 days. The former authors state that the decay takes place entirely through x-ray emission. They also observed the radiations from Rh^{103m} associated with the decay.

The metastable state Rh^{103m}, half-life 45 to 57 min., has been studied by various authors. Glendenin and Steinberg,[7] Flammersfeld and Bruna,[8] Wiedenbeck,[9]

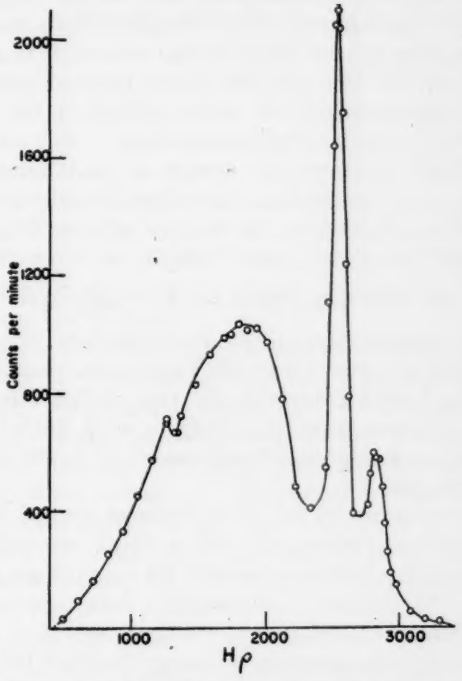

FIG. 1. Distribution of photo-electrons produced by gamma-rays of ruthenium.

* This research was assisted by the joint program of the ONR and AEC.

[1] Sullivan, Sleight, and Gladrow, Phys. Rev. **70**, 778 (1946); Plutinium Project Reports CCl493 (March, 1944).

[2] For other measurements of the half-life see E. Bohr and N. Hole, Arkiv. f. Mat. Astr. o. Fys. **32A**, No. 15 (1948); Nishkima, Kimura, Yasaki, and Ikawa, Zeits. f. Physik **119**, 195 (1942); W. E. Grummitt and G. Wilkinson, Nature **158**, 163 (1946).

[3] N. Hole, Arkiv. f. Mat. Astr. o. Fys. **36A**, No. 2 (1948).

[4] C. E. Mandeville and E. Shapiro, Phys. Rev. **77**, 439 (1950).

[5] D. E. Matthews and M. L. Pool, Phys. Rev. **72**, 163(A) (1947).

[6] A. R. Brosi, Plutonium Project Reports—Mon-N150 (July, 1946), as reported by Seaborg and Perlman.

[7] L. E. Glendenin and E. P. Steinberg, Plutonium Project Reports CC579 and CC680 (1943).

[8] A. Flammersfeld and O. Bruna, Zeits. f. Naturforschung **2a**, 241 (1947).

[9] M. L. Wiedenbeck, Phys. Rev. **67**, 267 (1945); **68**, 237 (1945).

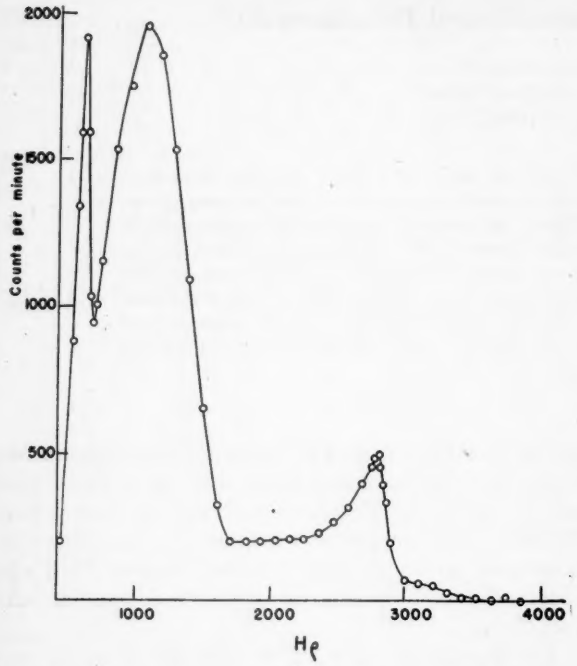

FIG. 2. Beta-rays and internal conversion electrons from Ru^{103}.

Hole,[10] and Gunlock and Pool[11] have all made observations on this element. The metastable state has been formed from normal Rh^{103} by fast neutrons[8] (n,n), by deuterons[8,10,11] (d,d^1) and by x-rays.[9] Gunlock and Pool found that x-rays of Rh were emitted in the disintegration and also found electron lines at 39.9 and 42.7 kev. Hole[10] measured the energy of the internal conversion lines in a magnetic spectrograph and found one line of energy 34 kev. He was not able to determine whether the electrons come from the K or L shell.

II. THE SPECTRUM OF Ru^{103} AND Ru^{97}

The present experiments on ruthenium were performed with a source of normal ruthenium prepared by neutron bombardment in the Oak Ridge Pile. The ruthenium was purified by distilling it as RuO_4 from a strongly acid solution, and was converted to the metallic state for use.

The spectrum of the photoelectrons ejected from a lead radiator of 16 mg/cm² surface density was measured in a magnetic lens spectrometer. The results are shown in Fig. 1. The K- and L-photoelectric lines corresponding to a gamma-ray of energy 0.494 ± 0.002 Mev and a K-line for a gamma-ray of energy 0.217 ± 0.002 Mev are to be seen. The line at 0.494 Mev decays with a period of 42 days and is to be ascribed to Ru^{103}. The line at 0.217 Mev decays with a period of 2.8 days and belongs to Ru^{97}.

The particle spectrum was next investigated. In the source which was used for this purpose the 2.8-day Ru^{97} had been allowed to die out. The first observations were made with a thin source, the activity of which was quite low. The measurements showed that there is a main group of beta-particles with a maximum energy of 0.204 Mev and a much weaker group of considerably higher energy. In addition, an internal conversion line corresponding to the gamma-ray at 0.494 Mev was found and also an internal conversion line of energy approximately 0.035 Mev, presumably emitted from the daughter substance Rh^{103m}.

In order to determine the end point of the higher energy group, and to get some information on the relative intensities of the two groups, a thicker source was measured. The results of the measurement are shown in Fig. 2. The internal conversion lines corresponding to the 0.494 Mev gamma-ray and the low energy line from Rh^{103m} are clearly seen. A Fermi plot of the beta-ray data was made and two beta-ray groups were found; one with an end point at 0.204 ± 0.010 Mev (94 percent) and the other at 0.684 ± 0.010 Mev (six percent). The ft-values for the two groups are $ft_{0.204}=3.9\times10^5$ and $ft_{0.684}=1.8\times10^8$. The lines at 0.217 and 0.290 Mev, mentioned by Hole, were not observed. It is believed that the lines which he reported were probably due to impurities.

Owing to the low specific activity of the source and the presence of the strong group of beta-rays of low energy, it is not possible to tell whether the line at 35 kev occurs as a result of electrons being ejected from the K or L shell. It was therefore decided to attempt to produce this line under circumstances in which there would be no beta-rays and under which the source would be as free as possible of inert material. This can be done best through an investigation of Pd^{103}.

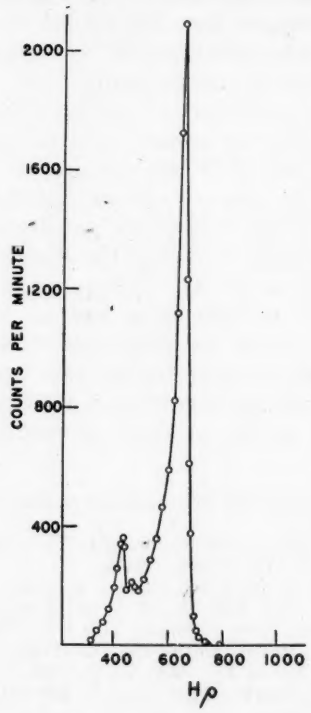

FIG. 3. Internal conversion electrons and Auger electrons from Pd^{103}.

[10] N. Hole, Arkiv. f. Mat. Astr. o. Fys. **34B**, No. 5 (1947).
[11] H. F. Gunlock and M. L. Pool, Phys. Rev. **74**, 1264(A) (1948).

III. THE SPECTRUM OF Pd^{103}

Pd^{103} was made by bombarding rhodium metal with 23-Mev alpha-particles in the cyclotron. The rhodium was hard-soldered to a probe and given a bombardment of several hundred microampere-hours of alpha-particles. The rhodium was put into solution by fusing. A few milligrams of palladium carrier were added and the palladium was precipitated as palladium-dimethylglyoxime. The material was then converted to the oxide for use as a gamma-ray source. The oxide was dissolved in *aqua regia* and a drop of this solution was evaporated and used as a beta-ray source.

The gamma-ray source, using a lead radiator, was measured in the spectrometer. No photo-electrons at all were seen. The line of energy 0.494 Mev was entirely absent. In an attempt to find the gamma-ray which gives rise to the internally converted line at 35 kev, a thin copper radiator, instead of the lead radiator was used, and a search was made for photo-electrons. If the line at 35 kev results from conversion in the K shell the gamma-ray energy should be 59 kev, and if it results from conversion in the L shell the gamma-ray energy should be 40 kev. No photo-electrons were found corresponding to a gamma-ray of either energy. This suggests that the gamma-ray giving rise to the line is very highly internally converted.

The beta-ray spectrum of Pd^{103} was investigated using a counter fitted with a thin zapon window. The result of the investigation is shown in Fig. 3. It will be noted that only three low energy lines appear in the spectrum. There are no positrons.

The most intense line of the spectrum corresponds to that observed in Ru^{103}. The energy of the line is 36.9 $\pm$0.5 kev. If it be assumed that this line can be attributed to the ejection of electrons from the K shell by a gamma-ray of energy 60 kev, the L-line should easily be seen. Since no line is seen corresponding to the ejection of electrons from the L shell by a gamma-ray of 60 kev it must be assumed that the line in question is either an L-line or that the K/L ratio is at least 100:1. In order to explain the half-life of the Rh^{103m} state, it is necessary to assume a spin change of approximately 4 units. This would entail, at these energies, a $K/L<1$. This suggests that the line in question arises from the conversion in the L shell of a 40.4 kev gamma-ray.

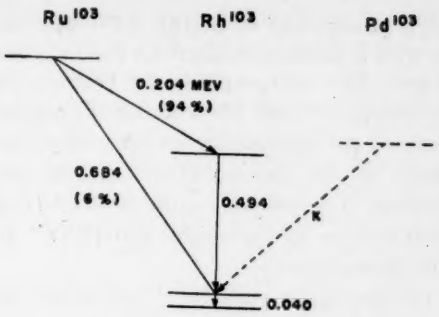

FIG. 5. Energy levels of Rh^{103}.

It will be noted also that there are two lower energy lines in the spectrum. These come at a setting of 0.22 and 0.2025 amp. for the current in the field coils. If the 40.4 kev gamma-ray is internally converted in the K shell, the electrons should have an energy of 16.89 kev and should be focused at 0.2041 amp. On the other hand, the Auger electrons ($K-2L_I$), arising from orbital electron capture will have a energy of 16.40 kev and will be focused at 0.2075 amp. It is impossible to tell what fraction of the line at 0.2025 amp. is due to Auger electrons and to electrons internally converted in the K shell. The line at 0.22 amp. is clearly an Auger line corresponding to $K-L_I-M$, which should be focused at 0.2185 amp.

Finally, a source of Rh^{103m} was prepared by adding a small amount of rhodium to the Pd^{103} parent and precipitating the palladium away from the rhodium. The period of the rhodium was measured and found to be 56 min. A beta-ray source was prepared and measured using the same counter and window as that used for the investigation of Pd^{103}. The results are shown in Fig. 4. In order to get sufficient intensity the spectrometer had to be used at lower resolution than in the experiments on Pd^{103}. The results show the line at 36.9 kev together with a small line at the correct position to be a K-line. This line, at 0.205 amp., is not as intense, relative to the main group as is the similar line in Pd^{103}. It would appear, therefore, that the low energy line seen in Pd^{103} owes most of its intensity to Auger electrons and only slightly to electrons converted in the K shell.

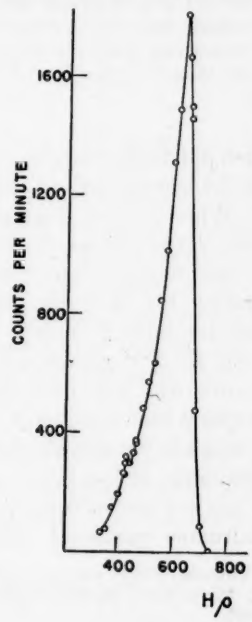

FIG. 4. Internal conversion electrons from Rh^{103m}.

IV. CONCLUSION

The present experiments on Ru^{103} show that this element disintegrates with the emission of two beta-ray groups of end-point energies 0.684 and 0.204 Mev. In

addition, a gamma-ray of energy 0.494 Mev is found together with L conversion electrons from a gamma-ray of 40.4 kev. The energy difference between the two beta-ray groups is 0.480 Mev, somewhat smaller than the energy of the gamma-ray as determined from the distribution of the photo-electrons. While not absolutely certain, it seems reasonably probable that both transitions lead to the metastable state Rh^{103m} 40.4 kev above the ground state.

That the metastable state Rh^{103m}, of 56-min. half-life, decays by the emission of an internally converted gamma-ray of energy 40.4 kev is shown by the work on Pd^{103} and Rh^{103m}. As has been pointed out above, the absence of any L-line attributable to a gamma-ray of 60 kev, definitely shows that the line at 36.9 kev must be an L-conversion line of a 40.4 kev gamma-ray. One can account for the mean life of Rh^{103m} by assuming a spin change $l=4$ and a value of $N_e/N_\gamma \sim 10^3$. In addition the ratio N_K/N_L would be extremely small, in agreement with experiment. From the results of the above experiments a tentative energy level scheme for Rh^{103} is given in Fig. 5.

The authors wish to express their thanks to Dr. Milo B. Sampson and the cyclotron crew for making the bombardments. They are also indebted to Miss Elma Lanterman for preparing the chemical separations.

Note Added in Proof: Since this paper was sent to press, a fission product source of Ru^{103}, also containing Ru^{106} and its daughter Rh^{106}, has been measured. Using a source and counter window 3 mm in diameter, the conversion line at 0.494 Mev has been examined. Under these conditions the breadth of the K-line at half-maximum is 1.3 percent and the K and L lines have been resolved. The ratio $N_K/N_L=6.5$. In addition the low energy beta-ray group has been re-examined. The end point is somewhat higher, 0.222 Mev. The internal conversion coefficient, $(N_e)_K/N_\gamma$, for the line at 0.494 Mev is $5.5\pm0.5\times10^3$. The line is either electric quadrupole or magnetic dipole since the conversion coefficient values calculated by Rose *et al.* give $\alpha_2=5.37\times10^{-3}$ and $\beta_1=5.10\times10^{-3}$.

PHYSICAL REVIEW VOLUME 79, NUMBER 3 AUGUST 1, 1950

Nuclear Energy Level Argument for a Spheroidal Nuclear Model*

JAMES RAINWATER
Columbia University, New York, New York
(Received April 17, 1950)

Recently there has been notable success, particularly by Maria Mayer, in explaining many nuclear phenomena including spins, magnetic moments, isomeric states, etc. on the basis of a single particle model for the separate nucleons in a spherical nucleus. The spherical model, however, seems incapable of explaining the observed large quadrupole moments of nuclei. In this paper it is shown that an extension of the logic of this model leads to the prediction that greater stability is obtained for a spheroidal than for a spherical nucleus of the same volume, when reasonable assumptions are made concerning the variation of the energy terms on distortion. The predicted quadrupole moment variation with odd A is in general agreement with the experimental values as concerns variation with A, but are even larger than the experimental values. Since the true situation probably involves considerable "dilution" of the extreme single particle model, it is encouraging that the present predictions are larger rather than smaller than the experimental results. A solution is given for the energy levels of a particle in a spheroidal box.

I. INTRODUCTION

RECENTLY considerable evidence has been pointed out for the existence of nuclear shell structure on such basis as nuclear spins, magnetic moments, and on the degree of forbiddenness of various β-ray spectra.[1] Probably the most successful scheme is that of Maria Mayer who treats the nuclear energy levels as due to a filling-up of individual particle levels for nucleons in a spherical box. It is assumed that the strong interaction of each nucleon with all other nucleons in the nucleus can be approximated as a (roughly constant) interaction potential extending over the nuclear volume such that the assemblage of nucleons forms a "self consistent" box. When an even number of neutrons or protons are present, it is well known that they pair off to give zero spin and moment, and great success is obtained by attributing the spin and moments to the odd nucleon alone for odd A nuclei. Maria Mayer assumes that strong $L-S$ coupling splits the levels for a given L, but otherwise maintains the normal order nearly intact to explain the closed shell values Z_c or $N_c=2$, 8, 20, 50, 82, and 126 "magic numbers."

Similarly, it has been emphasized[2] that evidence for the nuclear shell structure is also shown by the nuclear quadrupole moments. The material of the following

* Supported by the AEC.

[1] Maria Mayer, Phys. Rev. **75**, 1969 (1949). E. Feenberg and K. C. Hammack, Phys. Rev. **75**, 1877 (1949). L. W. Nordheim, Phys. Rev. **75**, 1894 (1949). Also Symposium X at the 1950 New York Physical Society Meeting. Maria Mayer, Phys. Rev. **78**, 16, 22 (1950).

[2] Townes, Foley, and Low, Phys. Rev. **76**, 1415 (1949). R. D. Hill, Phys. Rev. **76**, 998 (1949). W. Gordy, Phys. Rev. **76**, 139 (1949).

discussion is mainly contained in the paper by Townes, Foley, and Low, with particular reference to their plot of Q/R^2 *vs.* Z_{odd} (R=nuclear radius). The following features of the evidence are mainly emphasized.

(1) The plot of Q/R^2 *vs.* Z_{odd} shows a regular shape related to the filling of individual particle levels. The curve passes through zero at the closed shell values, Z_c, and is negative for Z_c+1 and positive for Z_c-1 as expected for the odd particle since $m=l$.

(2) Q/R^2 has a peak of ~ 9 at $Z_{\text{odd}}=71$, 73 and decreases to zero near $Z=55$ and 82. This is the region where the $5g_{7/2}$, $4d$, $3s$, and $6h_{11/2}$ subshells are being filled,[1] on the Mayer scheme. The position of the broad peak in this region agrees with the shell picture but the magnitudes are much too large to assign to the wave function of the odd proton alone. For $_{71}\text{Lu}^{176}$ Townes, Foley, and Low estimate that Q/R^2 is 35 times larger than the value expected for a single odd proton. Also the large values for some odd neutron nuclei are not explained.

II. GENERAL ARGUMENT FOR A SPHEROIDAL NUCLEAR MODEL

The above evidence strongly indicates that the basic nuclear shape in this case is *not* spherical, but corresponds to a considerable distortion of the whole nucleus into a spheroidal shape. It is the purpose of this paper to point out that this is exactly the shape to be expected for minimum energy on the basis of the model discussed above. One notes that a distortion of the nucleus into a spheroidal shape means that the "self-consistent" box in which each nucleon moves also assumes the same spheroidal shape. One must then solve the eigenvalue problem for a particle in a spheroidal box. This has been done for the case of small distortions and is described in the last section. In this case solutions are obtained which are similar to those for the spherical case and become identical for zero distortion. Note that the distortion applies to filled shells as well as unfilled ones and *it is this distortion of the core that gives the main contribution to* Q.

We shall assume, in agreement with the method used to investigote nuclear fission[3] that, for closed shell nuclei, the nucleus is treated as an incompressible drop and only the surface and Coulomb energy terms are considered. These partly cancel and give an increased energy proportional to e^2 on distortion, where $e=(b-a)/R$ (a and b are the semiaxes) is proportional to the distortion. Using Feenberg's expression for E_s and E_c and selecting E_c^0 and E_s^0 from the semi-empirical binding energy formula gives

$$\Delta E_s+\Delta E_c=e^2[2.74A^{\frac{1}{3}}-0.054Z^2A^{-\frac{1}{3}}]\ \text{Mev}.$$

It is to be emphasized that the coefficient of e^2 is relatively small and permits large distortions for relatively small energies.

[3] N. Bohr and J. A. Wheeler, Phys. Rev. **56**, 426 (1939). E. Feenberg, Phys. Rev. **55**, 504 (1939).

The quantum numbers n, l, m for r, θ, φ still apply for a spheroidal box but l is no longer a strict angular momentum quantum number. The levels can be specified by the same notation as for the spherical box and we still speak of filling a subshell with a given l. In the spherical problem the eigenvalues are degenerate with respect to m for a given l, but in the spheroidal case this degeneracy is removed and there is a splitting which is linear in e and depends on l and m^2. In particular, distortion to oblate (disk) shape lowers the (kinetic) energy for $|m|\approx l$ and increases it for $m^2\ll l^2$.

The expected effect of these considerations on the nuclear shape is: (a) for closed shells $\Delta E\approx$ const. e^2, so $e=0$ is most stable; (b) for $Z=Z_c+1$, $\Delta E\approx c_1e^2-c_2e$ if e is chosen positive for the oblate case. Then $e=c_2/2c_1$ gives the stable shape for minimum energy.

The basis for the linear term is easily seen by noting that the kinetic energy $T=(E-V)$ is proportional to $\hbar^2/mR^2$ and, for a Bohr orbit with $m=l$, the particle goes around the equator. Thus $R\to b>R$ and

$$\Delta T=-\tfrac{2}{3}eT_0 \quad \text{for} \quad m=l\gg 0.$$

This result applies asymptotically for large l, but should be only a little too large for $l=4$. Using $l=4$ for a single odd proton with $m=l$ (near Lu^{175}) gives $T_0=33.5\hbar^2/mR^2$, $e=1/5.2$, and $Q/R^2=-11$ which is of the order of magnitude of the largest observed Q/R^2 values. (This uses the relation $Q=2Z(a^2-b^2)/5$ or $Q^2/R^2=-4Ze/5$.) So far only $Z=Z_c\pm 1$ has been considered. For a nearly half-filled shell of high l we might assign $m=l$ for the odd proton (to defined the axis and I) and put the rest in low m^2 levels. *The linear coefficients should add for all nucleons in unfilled shells* so the low m^2 terms will predominate to give Q/R^2 large and positive as for Lu^{175}. Also, following this plan, it is easy to see that Q increases as the shell is filled until the levels with oppostite slope are reached, after which Q steadily decreases until a closed shell is reached. The presence of both neutron and proton unfilled shells complicates matters since both should be effective.

Clearly the above discussion merely gives a bare outline rather than the finished theory required for exact predictions and comparison with theory.

III. THE INDIVIDUAL PARTICLE LEVELS IN A SPHEROIDAL BOX

In the previous section it was pointed out that a "self-consistent" spheroidal nuclear shape is expected for a model where the nucleons are considered as filling individual particle levels in the nuclear "box." It is assumed that the nuclear volume remains constant during the distortion and that only surface and coulomb energy terms apply for the core of closed shells. We consider the solution of the problem of a particle in such a spheroidal box in the region of small distortions, assuming infinite walls.

If ρ, φ, Z are cylindrical coordinates, and $b>a$, then

$$Z^2/(a^2-\lambda)+\rho^2/(b^2-\lambda)=1$$

defines two families of orthogonal surfaces in oblate spheroidal coordinates[4] as λ is varied. We choose $ab^2=1$=spherical nuclear radius (to define the unit length) and let $c^2=b^2-a^2=2e$. For $0\leqslant\lambda\leqslant a^2$ let $a^2r^2=(a^2-\lambda)$ so $0\leqslant r\leqslant 1$ corresponds to the radius in spherical coordinates. For $b^2\geqslant\lambda\geqslant a^2$ let $c^2w^2=\lambda-a^2$ where $-1\leqslant w\leqslant 1$ corresponds to $\cos\theta$, and φ is the third coordinate. Then

$$(\nabla^2+k^2)\psi=\frac{\partial}{\partial r}\left[(c^2/a^2+r^2)\frac{\partial\psi}{\partial r}\right]+\frac{\partial}{\partial w}\left[(1-w^2)\frac{\partial\psi}{\partial w}\right]$$
$$+\frac{(r^2+c^2w^2/a^2)}{(c^2/a^2+r^2)(1-w^2)}\frac{\partial^2\psi}{\partial\varphi^2}+k^2(a^2r^2+c^2w^2)\psi=0.$$

This may be factored into $\psi=R(r)\Theta(w)\Phi(\varphi)$ where $\Phi=e^{im\varphi}$ as in the spherical case. Then we obtain

$$\frac{1}{R}\left\{\frac{d}{dr}\left[(r^2+c^2/a^2)\frac{dR}{dr}\right]+\left[k^2a^2r^2+\frac{c^2m^2}{a^2r^2+c^2}\right]R\right\}$$
$$=-\frac{1}{\Theta}\left\{\frac{d}{dw}\left[(1-w^2)\frac{d\Theta}{dw}\right]+\left[c^2k^2w^2-\frac{m^2}{(1-w^2)}\right]\Theta\right\}=l(l+1)-s.$$

The spherical case is obtained by setting $c=s=0$ and $a=1$ to give functions R_0 and Θ_0. Here s is a small correction on $l(l+1)$ which is easily evaluated. Multiply the differential equation for Θ by Θ_0 and vice versa. Subtract and integrate between $w=0$ and 1. Note that Θ corresponds to Θ_0 and both are either even or odd functions of w. This gives

$$s=c^2k^2\left(\int_0^1 w^2\Theta_0\Theta dw\right)\Big/\left(\int_0^1\Theta_0\Theta dw\right).$$

To obtain an expansion as $e\to 0$ set $\Theta=\Theta_0$ in these expressions to give

$$s=c^2k^2\langle w^2\rangle_{Av}=c^2k^2\left[\frac{2l(l+1)-2m^2-1}{(2l+3)(2l-1)}\right].$$

We now examine the equation for R, simplifying it to include only first order correction terms in e (or c^2). We are principally interested in evaluating $k^2=k_0^2+\Delta k^2$ which gives the change in the (kinetic) energy on distortion. Multiply the differential equation for R by R_0 and vice versa. Subtract and integrate from $r=0$ to 1, noting the boundary condition $R=R_0=0$ at $r=1$ and also at $r=0$, for the case of interest $l>0$. This gives

$$\frac{\Delta k^2}{k_0^2}=2e\left\{\frac{2}{3}-\frac{\left[m^2\int_0^1(R_0^2dr/r^2)+k_0^2\langle w^2\rangle_{Av}\int_0^1 R_0^2dr+\int_0^1 R_0R_0''dr\right]}{k_0^2\int_0^1 r^2R_0^2dr}\right\},$$

where $R_0''=d^2R_0/dr^2$ and $\langle w^2\rangle_{Av}$ is given above and depends on l and m^2. It is not clear that an average of the above expression over all values of m gives zero, but it is easy to show that it is true asymptotically for large l and the first radial solution, since R_0 then has a value only near $r=1$ and $R_0''\approx[-k_0^2+l(l+1)]R_0$ near $r=1$. (Note that $k_0\approx l$ in these units.)

If we *assume* that this will average to zero over all m values, then

$$\frac{\Delta k^2}{k_0^2}=2e[l(l+1)/3-m^2]\frac{\left[\int_0^1\frac{R_0^2dr}{r^2}-\frac{2k_0^2\int_0^1 R_0^2dr}{(2l+3)(2l-1)}\right]}{k_0^2\int_0^1 r^2R_0^2dr}.$$

(For $l\to\infty$ and $m=l$, this gives the value for $\Delta T/T_0$ expected from the orbit argument in the preceding section.) For $l\to\infty$ this becomes

$$\Delta T/T_0=\Delta k^2/k_0^2=e[\tfrac{1}{3}l(l+1)-m^2]/k_0^2.$$

We note that l is no longer an exact angular momentum quantum number. For the nucleus as a whole, the distortion of the core probably requires that angular momentum be associated with the core part of the time. This might help in explaining the deviation of the magnetic moments from the "Schmidt lines," for example.

It should be pointed out that this model seems capable of giving even larger Q values than are experimentally observed. In this connection Aage Bohr has pointed out that if the nucleus is a spheroid with a component of angular momentum $m=l$ along its axis, it will precess about the total **I** vector to reduce the "experimental" Q-value to an "intrinsic" Q-value ratio by a factor $I(2I-1)/(I+1)(2I+3)$ which is equal to 1/10, 2/7, 5/12, and 28/55 for $I=1, 2, 3, 4$.

I wish to thank Aage Bohr for many helpful discussions of this problem and the AEC for their support of this research.

[4] Smythe, *Static and Dynamic Electricity* (McGraw-Hill, Book Company, Inc., New York, 1939), Chapter 5.

The 4n+1 Radioactive Series: The Decay Products of U^{233}*

FRENCH HAGEMANN, L. I. KATZIN, M. H. STUDIER, G. T. SEABORG,† AND A. GHIORSO†
Argonne National Laboratory, Chicago, Illinois

(Received March 13, 1950)

The path of the artificially produced $4n+1$ radioactive decay series between U^{233} and Bi^{209} and the properties of the individual members of the chain are developed.

I. INTRODUCTION

THE three families of radioactive heavy isotopes found in nature are differentiated by their mass characteristics. Thus, the family represented by thorium (Th^{232}) and its decay products has masses corresponding to the formula $4n+0$; the family represented by U^{238} and its decay products corresponds to $4n+2$; and the family represented by U^{235} and its decay products corresponds to $4n+3$, where n in all cases represents an integral multiplier. The family corresponding to the formula $4n+1$ has not been found in nature, except for the stable end-member of the chain, bismuth (Bi^{209}).

Previous experiments[1–7] in artificial production of nuclei have resulted in the formation of the isotopes Pb^{209}, Th^{233}, Pa^{233}, U^{233}, and Np^{237}, whose masses correspond to the $4n+1$ formula. From the isotope Np^{237}, which decays by emission of an alpha-particle, beta-active Pa^{233}, and from it alpha-active U^{233}, are formed by successive decays. We may therefore consider Np^{237} to represent the long-lived parent of a $4n+1$ radioactive decay family, and in analogy with natural series this may be called the neptunium series.[8]

The purpose of this paper is to trace the path of the decay chain between the isotopes U^{233} and Bi^{209}, and to give the properties which have been found for the isotopes which are members of the chain. The findings may be summarized as in Fig. 1 and Table I. Work in another laboratory, where parallel studies have been made of the U^{233} decay chain,[9] has resulted in essentially similar findings.

Various predictions have been made in the literature with regard to the properties of the $4n+1$ series. Russell[10] suggested the following decay scheme:

$$U^{237} \xrightarrow{\alpha} Th^{233} \xrightarrow{\beta^-} Pa^{233} \xrightarrow{\alpha} Ac^{229} \xrightarrow{\beta^-} Th^{229} \xrightarrow{\alpha} Ra^{225} \xrightarrow{\alpha}$$

$$Em^{221} \xrightarrow{\alpha} Po^{217} \xrightarrow{\alpha} Bi^{213} \begin{cases} \xrightarrow{\beta^-} Po^{213} \xrightarrow{\alpha} \\ \xrightarrow{\alpha} Tl^{209} \xrightarrow{\beta^-} \end{cases} Pb^{209} \xrightarrow{\beta^-} Bi^{209}.$$

On the basis of analogy with the three known series Ra^{225} was predicted to be alpha-active, decaying to alpha-active Em^{221}. Later Widdowson and Russell[11] revised this prediction to suggest branching decay of Ra^{225} and beta-decay of the emanation isotope. The chain would thus proceed through isotopes of elements 87 and 85 to predominantly beta-active Bi^{213} as shown below, rather than through the even-numbered elements as in the natural series.

$$\begin{matrix} & & Em^{221} & & \\ & \overset{\alpha}{\nearrow} & & \overset{\beta^-}{\searrow} & \\ Ra^{225} & & & & 87^{221} \xrightarrow{\alpha} 85^{217} \xrightarrow{\alpha} Bi^{213} \xrightarrow{\beta^-} \text{etc.} \\ & \underset{\beta^-}{\searrow} & & \underset{\alpha}{\nearrow} & \\ & & Ac^{225} & & \end{matrix}$$

Sometime later Turner[12] predicted that U^{237} would be a beta- rather than an alpha-emitter and supported Meitner, Strassman, and Hahn's[3] assignment of a 25-day Pa activity to Pa^{233}. The decay scheme proposed by Turner was:

$$U^{237} \xrightarrow{\beta^-} Np^{237} \xrightarrow{\alpha} Pa^{233} \xrightarrow{\beta^-} U^{233} \xrightarrow{\alpha} Th^{229} \xrightarrow{\alpha} Ra^{225} \xrightarrow{\beta^-}$$

$$Ac^{225} \xrightarrow{\alpha} 87^{221} \xrightarrow{\alpha} 85^{217} \xrightarrow{\alpha} Bi^{213} \begin{cases} \xrightarrow{\beta^-} Po^{213} \xrightarrow{\alpha} \\ \xrightarrow{\alpha} Tl^{209} \xrightarrow{\beta^-} \end{cases} Pb^{209} \xrightarrow{\beta^-} Bi^{209}.$$

Turner's scheme leads through elements 85 and 87, as did the prediction of Widdowson and Russell, but an emanation would not be formed in the main line.

---

* Preliminary report, Phys. Rev. **72**, 252 (1947). Except where otherwise indicated, these studies were made during 1944–46, at the Metallurgical Laboratory, University of Chicago (now the Argonne National Laboratory), under the auspices of the Manhattan Engineer District.

† Present address: Radiation Laboratory and Department of Chemistry, University of California, Berkeley, California.

[1] R. L. Thornton and J. M. Cork, Phys. Rev. **51**, 383 (1937); R. S. Krishnan and E. H. Nahum, Proc. Camb. Phil. Soc. **36**, 490 (1940); K. Fajans and A. F. Voight, Phys. Rev. **60**, 619 (1941); W. Maurer and W. R. Ramm, Zeits. f. Physik, **119**, 602 (1942).

[2] Fermi, Amaldi, D'Agostino, Rasetti, and Segrè, Proc. Roy. Soc. **A146**, 483 (1934).

[3] Meitner, Strassmann, and Hahn, Zeits. f. Physik **109**, 538 (1938).

[4] Grosse, Booth, and Dunning, Phys. Rev. **59**, 321 (1941).

[5] Seaborg, Gofman, and Kennedy, Phys. Rev. **59**, 321 (1941).

[6] Seaborg, Gofman, and Stoughton, Phys. Rev. **71**, 378 (1947).

[7] A. C. Wahl and G. T. Seaborg, Phys. Rev. **73**, 940–941 (1948).

[8] G. T. Seaborg, *The Transuranium Elements: Research Papers* (McGraw-Hill Book Company, Inc., New York, 1949), Paper No. 22.3, National Nuclear Energy Series, Plutonium Project Record, Vol. 14B.

[9] English, Cranshaw, Demers, Harvey, Hincks, Jelley, and May, Phys. Rev. **72**, 253 (1947).

[10] A. S. Russell, Phil. Mag. **46**, 642–656 (1923).

[11] W. P. Widdowson and A. S. Russell, Phil. Mag. **48**, 293–306 (1924).

[12] L. A. Turner, Phys. Rev. **57**, 950 (1940).

TABLE I. The $4n+1$ radioactive series.

Isotope	Type of radiation	Half-life[a]	Energy of radiation (Mev)
Np^{237}	α	2.20×10^{6} yr.[b]	4.77
Pa^{233}	β^-	27.4 days[c]	0.23[f]
U^{233}	α	$1.62(\pm0.01)\times10^{5}$ yr.[d]	4.80[g]
Th^{229}	α	$(7.34\pm0.16)\times10^{3}$ yr.	4.85; (~70%) 4.94; (~20%) 5.02; (~10%)
Ra^{225}	β^-	14.8 ± 0.2 days	*ca.* 0.2
Ac^{225}	α	10.0 ± 0.1 days	5.80
Fr^{221}	α	4.8 ± 0.1 min.	6.30
At^{217}	α	0.018 ± 0.002 sec.	7.00
Bi^{213}	β^-(98%), α(2.0%)	47 ± 1 min.	*ca.* 1.2(β^-); 6.0(α)
Po^{213}	α	Very short	8.34
Tl^{209}	β^-	2.20 ± 0.07 min.	1.8
Pb^{209}	β^-	3.3 hr.[e]	0.7[e]
Bi^{209}	Stable		

[a] Limits of error for Ra^{225}, Ac^{225}, Fr^{221}, and At^{217} are estimates rather than true probable errors.
[b] L. B. Magnusson and T. LaChapelle, J. Am. Chem. Soc. **70**, 3534–8 (1948).
[c] See reference 4.
[d] E. K. Hyde, Paper No. 19.15, National Nuclear Energy Series, Plutonium Project Record, Vol. 14B; AECD Doc. No. 2457.
[e] See reference 1.
[f] E. Haggstrom, Phys. Rev. **62**, 144–150 (1942).
[g] A. H. Jaffey (private communication).

Feather[13] believed Turner's predictions should be correct, and in actual fact the only deviation from our experimental findings is his prediction that the major decay of Bi^{213} would be by alpha-emission, whereas this mode accounts for only two percent of the disintegrations.

Ponisovsky,[14] from independent studies of the regularities in the stable isotopes, predicted essentially the same series, with the difference that the Th^{229} was predicted to be beta-active, leading to an alpha-active Pa^{229} which would give the Ac^{225} without the appearance of a radium isotope in the chain.

With respect to possible alpha-branching of the Ra^{225}, our experiments on separating this isotope from its daughter Ac^{225} have enabled us to set 0.5 percent as an upper limit on the amount of such branching. No emanation has been detected. No evidence for beta-decay of the Th^{229} has been found. The properties of the theoretical product, Pa^{229}, are known from material produced by cyclotron bombardment.[15]

II. EXPERIMENTAL

U^{233}

The U^{233} used in these experiments was prepared by neutron irradiation of thorium in the uranium-graphite pile. Following decay of most of the intermediate Pa^{233} and Th^{233}, the uranium was separated by extraction with ether.[16] A series of extractions and precipitations of sodium uranyl acetate, ammonium diuranate, and uranyl peroxide served to give complete chemical and radiochemical purification of the uranium. The nuclear properties of this isotope are described elsewhere.[17]

The U^{233} prepared in this way contained four to five percent of U^{238} since the thorium compounds irradiated normally contained a part or so per million of natural uranium impurity. Account was taken of the UX activity introduced from this isotopic impurity in experiments involving thorium isotopes. Lower members of the uranium decay chain were present in amounts which were insignificant because of the long half-life of U^{234} and its low concentration.

An important impurity was found to be U^{232},[18] which decays to radiothorium of 1.9-yr. half-life, followed by ThX(Ra^{224}) and its short-lived daughters. The RdTh half-life is so short relative to that of the Th^{229} that even with only one disintegration of U^{232} in 5700 disintegrations of U^{233} (the concentration actually found in one sample of the material by a mica absorption method), a significant fraction of the daughter radioactivities extracted after a decay period of a few weeks or months is due to this impurity. The ratio of Th^{229} activity to RdTh activity was found to vary from about 2 to 3.5 for different samples of U^{233}. The origin of the U^{232} is probably a small Pa^{231} impurity in the thorium irradiated, since Pa^{231} has a high neutron capture cross section.[19] The capture product, Pa^{232}, decays to U^{232} by

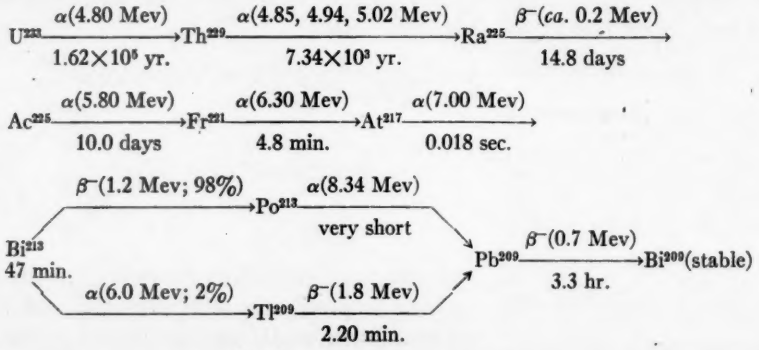

FIG. 1. Decay scheme of the neptunium series.

[13] N. Feather, British Atomic Energy Projects, Report Br-339 (1943).
[14] L. Ponisovsky, Nature **152**, 187–8 (1943).
[15] Hyde, Studier, Hopkins, and Ghiorso, Paper No. 19.17, National Nuclear Energy Series, Plutonium Project Record, Vol. 14B.
[16] Hagemann, Katzin and Studier, Paper No. 3.15, National Nuclear Energy Series, Plutonium Project Record, Vol. 17B.
[17] M. H. Studier, Paper No. 1.3, National Nuclear Energy Series, Plutonium Project Record, Vol. 17B; AECD Doc. No. 2444.
[18] J. W. Gofman and G. T. Seaborg, Paper No. 19.14, National Nuclear Energy Series, Plutonium Project Record, Vol. 14B.
[19] A. H. Jaffey and Q. Van Winkle, Paper No. 9.16, National Nuclear Energy Series, Plutonium Project Record, Vol. 17B.

beta-emission with a half-life of 1.4 days.[18] An alternative possibility is that there is a sufficient flux of fast neutrons to give a sufficient $(n, 2n)$ reaction with the thorium to yield the Pa^{231}. A second-order absorption would then give rise to the U^{232}.

III. ISOTOPIC ASSIGNMENTS

Assignments of the periods and radiations to definite isotopes were made on the basis of radiochemical separations together with range analyses of the alpha-particles by means of a pulse analyzer.[20]

The isolated thorium activity showed the anticipated alpha-activity. After RdTh daughters had grown to equilibrium, alpha-activity continued to grow over a period of time at a rate corresponding to a half-life of the order of three weeks. The number of alpha-activities growing from the Th^{229} was shown to be four, both from range analysis by the pulse analyzer, and from the increase in alpha-activity. Radiochemical isolation of a combined radium-actinium fraction (e.g., on barium sulfate) gives an alpha-active preparation into which two alpha-activities grow with a 5-min. half-life, followed by growth with a $\frac{3}{4}$-hr. half-life. Separation into radium and actinium fractions shows the radium isotope to possess a soft beta-particle of about 0.2-Mev energy, while the actinium fraction repeats the alpha-activity growth pattern noted above. Four alpha-activities (the actinium isotope and its daughters) grow into the radium fraction on a time relation dependent on the 14.8-day radium period and the 10.0-day actinium period. The fact that two alpha-activities (and no beta-) grow in with a 5-min. period indicates that the half-life of At^{217} is considerably shorter than the 5-min. period of Fr^{221}. This is borne out by the period determined from coincidence measurements (0.018 sec.). A bismuth fraction free of lead isotopes shows an alpha-activity and a beta-activity decaying with the same half-life, leaving a beta-activity ascribable to daughter Pb^{209}. The short half-life of the alpha-emitter and the long range of its particle indicate it to be due to Po^{213}, produced by beta-decay of Bi^{213}. Evidence from range analysis of the Bi^{213} activity indicates some branching by alpha-decay.

Th^{229}

This isotope, together with the radiothorium impurity mentioned above, was isolated from the purified U^{233} solution after a suitable period of time by co-precipitation with zirconium iodate.

One- to two-tenths of a milligram of zirconium nitrate and sufficient iodic acid solution to give a final iodate concentration of $0.05M$ were added per milliliter of solution of U^{233} in $0.1N$ nitric acid. The precipitated zirconium iodate was washed by centrifugation, dissolved in sulfur dioxide-water, heated to remove liberated iodine, diluted, and the zirconium reprecipitated with iodic acid. Four to five of these cycles served to decontaminate completely from uranium, radium, and most of the actinium. Bismuth and lead activities were removed by one or two lead sulfide by-product precipitates.

In order to prepare samples sufficiently free from carrier for alpha-particle range measurements in the pulse analyzer, and to remove any traces of actinium activity, the following procedure was used. The thorium isotopes were co-precipitated from the final zirconium iodate solution with lanthanum fluoride carrier (0.1–0.2 mg/ml), the fluoride precipitate was

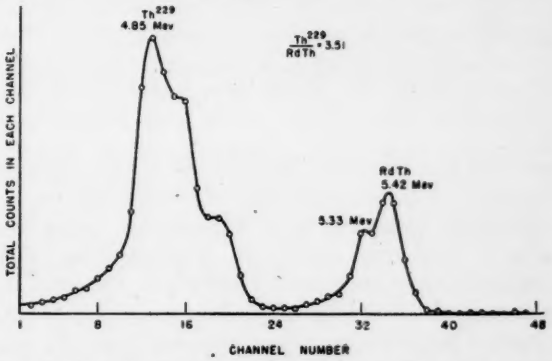

FIG. 2. Pulse analyzer curve of thorium alpha-activity showing the three alpha-peaks of Th^{229} together with the peaks due to RdTh impurity.

metathesized to hydroxide with concentrated potassium hydroxide and the hydroxide dissolved in $0.05M$ nitric acid. Separation of the thorium activity from the lanthanum carrier was accomplished by extraction with a solution[21] of $0.15M$ thenoyl trifluoracetone (TTA) in benzene. The change from zirconium to lanthanum carrier was necessary since the former extracts into TTA solution under the conditions used, whereas the latter does not. In some cases, TTA extraction of the thorium isotopes was made directly from the uranium solution. The TTA benzene solution was in either case evaporated directly on the counting plate or re-extracted with $8N$ nitric acid and the latter solution evaporated. Ignition of the resulting plates left an essentially weightless film of the thorium activity.

Since the Th^{229} half-life is several thousand years, indirect methods of determining this property were necessary. A known amount of freshly purified U^{233} was allowed to decay for a measured time. UX_1 tracer was then added and the thorium activity isolated as above. The UX_1 tracer provided a means of determining the yield of thorium through the separation procedure without introducing any foreign alpha-activity. The ratio of Th^{229} to radiothorium was determined by alpha-pulse analysis. Applying corrections for yield and for radiothorium impurity the amount of Th^{229} activity which had grown into the U^{233} could be calculated, and

[20] Ghiorso, Jaffey, Robinson, and Weissbourd, Paper No. 16.8, National Nuclear Energy Series, Plutonium Project Record, Vol. 14B.

[21] J. C. Reid and M. Calvin, AECD Doc. No. 1405.

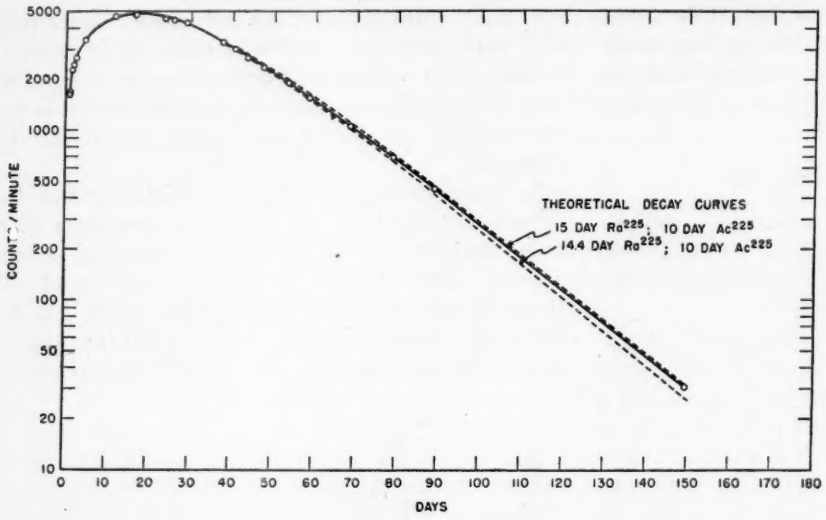

FIG. 3. Growth and decay of alpha-activity from Ra^{225} preparation. Theoretical decay curves calculated on the basis of 10-day Ac^{225} and 15-day and 14.8-day Ra^{225} are shown by the broken lines.

from this the Th^{229} half-life. The mean value obtained from eight such determinations was 7340±160 yr.

The alpha-radiations of Th^{229} have been found to be complex. The main group of alpha-particles, which constitutes approximately 10 percent of the total, has an energy of 4.85±0.01 Mev. Two small longer-range groups of particles have been resolved from the main group, differing from it by 90 and 170 kev, respectively. The less energetic of these two small groups contains roughly about twice the number of alpha-particles in the other. Figure 2 is a typical curve obtained with the pulse analyzer of the thorium activity which shows the two longer-range groups of the Th^{229} alpha-particles together with the RdTh impurity mentioned above. The energy of the Th^{229} particles was determined by placing a standard containing some Po^{210} (5.30 Mev) and ionium (4.66 Mev)[22] in the chamber together with the sample. The Th^{229} energy was found by interpolation from the resulting calibration curve using the Po^{210}, Io, and RdTh peaks[23] as reference points of known energy.

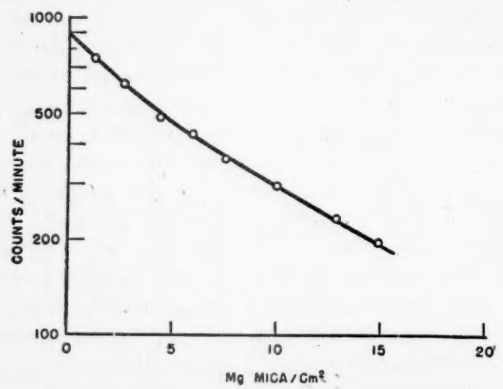

FIG. 4. Absorption of Ra^{225} beta-particles in mica.

[22] Clark, Spencer-Palmer, and Woodward, British Atomic Energy Projects, Report Br-522.
[23] Clark, Spencer-Palmer, and Woodward, British Atomic Energy Projects, Report Br-584.

Ra^{225}

The Ra^{225} (and ThX from the U^{232} impurity) was isolated from the U^{233} solution from which the thorium activity had been separated. Both barium sulfate and barium chloride were used as carriers for the radium activity; the latter was found to be preferable with regard to decontamination from actinium. With barium chloride the procedure was to add 1 mg of barium as nitrate to the U^{233} solution, reduce the volume to a few tenths of a milliliter and add seven times the volume of hydrochloric acid-ether solution (six parts conc. HCl to one part ethyl ether). After cooling with ice the precipitated barium chloride was centrifuged and reprecipitated in the same manner. Two or three precipitations were sufficient to remove the U^{233}; however, appreciable actinium activity still remained at this point. This was removed either by precipitating lanthanum fluoride from the solution or by adding lanthanum nitrate, evaporating to dryness and extracting the lanthanum and actinium nitrates with absolute ethyl alcohol. Lead sulfide was precipitated from the solution to remove bismuth and lead activity and the barium finally precipitated and mounted for counting as the sulfate.

Because of the low energy of its beta-particles, the half-life of the Ra^{225} was determined indirectly by following the growth and decay of the alpha-activity in the fraction isolated as above. Figure 3 shows an experimental curve and theoretical curves calculated on the basis of a 10.0-day Ac^{225} daughter (see below) assuming different values for the Ra^{225} half-life and using the observed maximum count. The growth of the alpha-activity does not follow precisely the theoretical values due to the presence of the ThX impurity. However, by the time the maximum value has been passed the short-lived ThX has largely decayed away. The experimental points best fit a theoretical curve for a 14.8-day radium half-life. Since the Ra^{225} and Ac^{225} half-lives are similar,

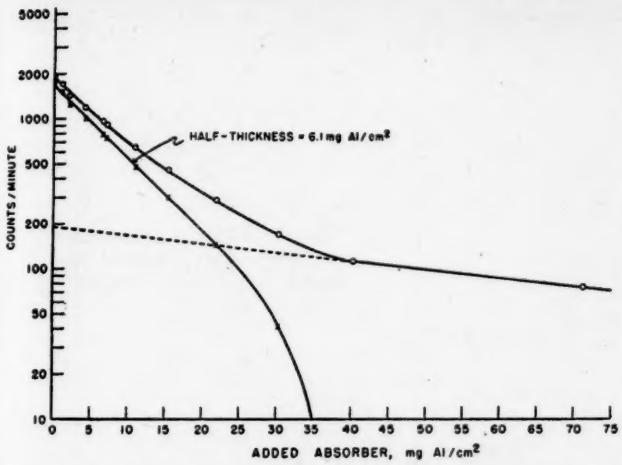

FIG. 5. Absorption of Ra^{225} beta-particles in aluminum measured with a mica-window Geiger tube (3 mg mica/cm²).

transient equilibrium is approached very slowly and direct determination of the Ra^{225} half-life from the decay curve with reasonable accuracy would be possible only after some hundreds of days of decay.

Beta-ray absorption curves were taken on samples of Ra^{225} repurified after having been allowed to stand for some weeks in order to eliminate the effects of the ThX daughters. The original Ra fraction was isolated from the U^{233} solution upon barium chloride carrier and reprecipitated to remove uranium and thorium activities. After about 30 days the Ra^{225} was purified from daughter activities by the above procedure, mounted on platinum, and absorption curves taken. Figure 4 is the curve of the absorption in mica obtained in a windowless G-M counter 5 hr. after separation. One-half hour after separation this sample showed 30 alpha-counts/min. Other curves taken with a low absorption counter using a thin (*ca.* 0.1 mg) zapon window and aluminum absorbers were similar. The amount of Ra^{225} activity which should have been present initially was calculated from the growth of alpha-activity in the sample to be about 650 counts/min., making approximate corrections for counting geometry. This agrees well with the value for zero absorber extrapolated from the curve after correcting for backscattering and self-absorption. Figure 5 shows the curve taken on another sample, 8 hr. after separation, with an ordinary thin window (3.3 mg/cm² of mica) Geiger counter using Al absorbers. The absorption half-thickness of the Ra^{225} beta-particle from these curves is about 6 mg/cm² and the range about 35 mg Al/cm², corresponding to an energy of *ca.* 0.2 Mev. No reliable information is available about gamma-rays.

Ac^{225}

Ac^{225} was separated by means of lanthanum fluoride carrier from the U^{233} solution from which Th^{229} had been removed. The fluoride precipitate was metathesized by means of potassium hydroxide and then dissolved in nitric acid. After two or three such cycles barium nitrate was added to "holdback" radium, the solution was evaporated to dryness and the lanthanum and actinium extracted from the residue with absolute ethyl alcohol.[24] The alcohol was evaporated, more barium nitrate added, and the extraction repeated. After precipitating lead sulfide to remove any bismuth or lead activity remaining, the lanthanum and actinium were precipitated as fluoride and mounted. A typical growth and decay curve for the Ac^{225} fraction is shown in Fig. 6 from which the half-life of 10.0 days was obtained by least-squares analysis.

Fr^{221}

Analysis of the growth curves of the alpha-activity in the Ac^{225} sample showed that three alpha-activities grew in, two with a half-life of about 5 min. followed by a third with a half-life of about 45 min. The 5-min. growth appeared to start with the flaming of the plate containing the activity, and after equilibrium had been reached, the 5-min. growth reappeared if the sample

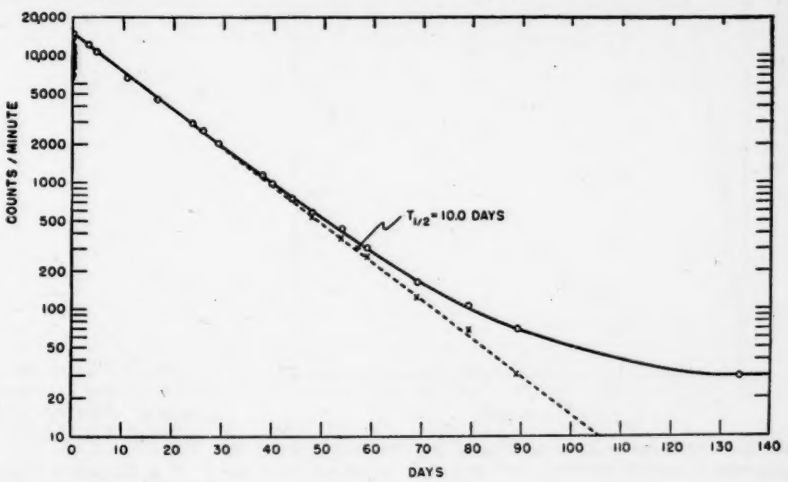

FIG. 6. Growth and decay of alpha-activity from Ac^{225}.

[24] M. Haissinsky, Comptes Rendus **196**, 1778–9 (1933).

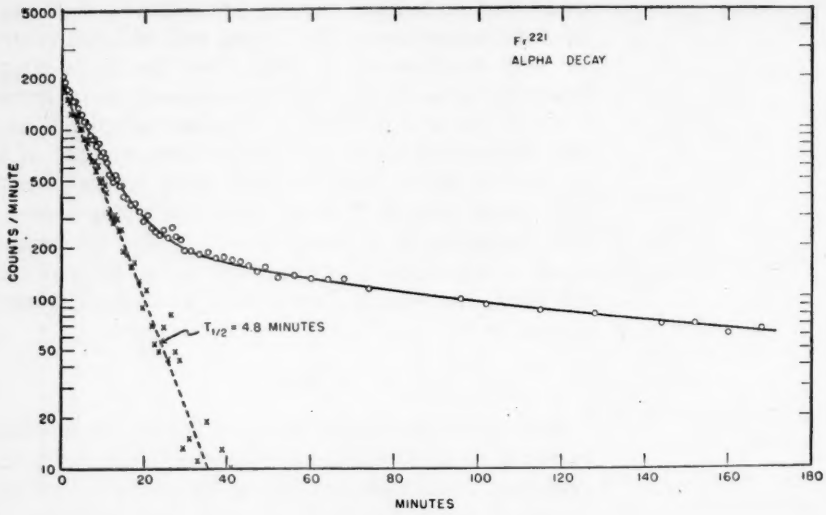

FIG. 7. Decay of alpha-activity from Fr^{221}. The long-lived background is probably unseparated Ac^{225}.

was reflamed. Experiments with Cs^{134} tracer indicated that this activity could be volatilized by flaming under similar conditions. These facts indicated that the daughter of Ac^{225}, Fr^{221}, was an alpha-emitter of about 5-min. half-life and its daughter was also an alpha-emitter of much shorter life.

The half-life of the Fr^{221} was determined more accurately by precipitating lanthanum hydroxide from a small volume of a solution of Ac^{225} and its daughters with ammonia, mounting the supernatant solution and following the decay of the alpha-activity obtained. Figure 7 shows the observed decay curve together with the curve resulting from subtraction of the non-decaying background (probably Ac^{225}). The half-life obtained from the latter curve gave a value of 4.8 min.

At^{217}

The half-life of At^{217} was determined by measuring the time interval between successive alpha-particle emissions by Fr^{221} and At^{217}. A sample of Ac^{225} was mounted upon a very thin zapon film supported on a 2-mil wire ring of about 1-cm diameter. The ring was placed in a vertical position on the bottom electrode of the chamber of a standard alpha-counter.[25] A resistor and condenser in series were connected between the

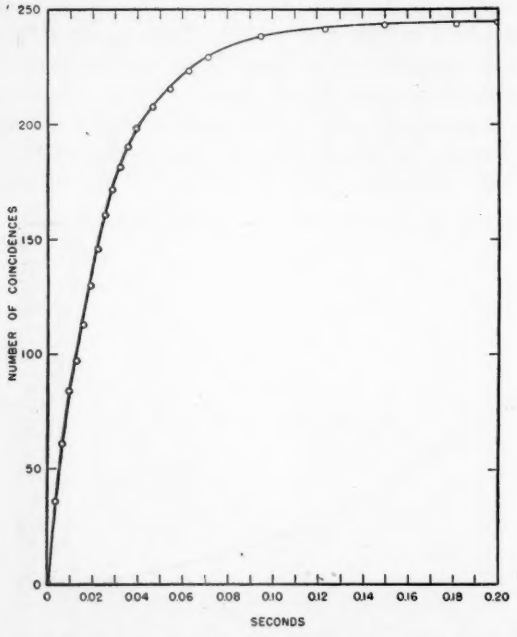

FIG. 8. Integral curve obtained by plotting the total number of coincidences observed between Fr^{221} and At^{217} alpha-particles in fixed time intervals against the time intervals. Corrections for chance coincidences have been applied.

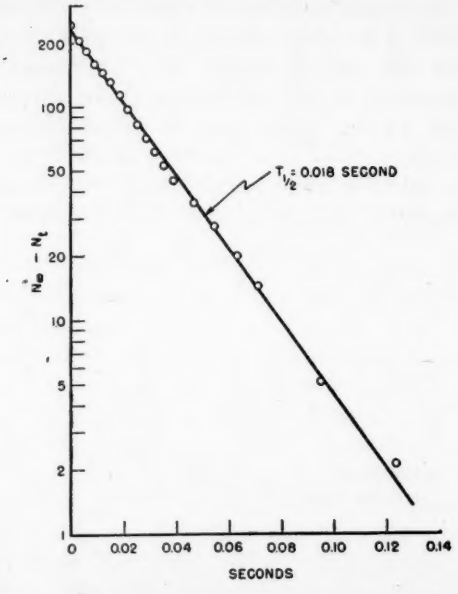

FIG. 9. Plot of the difference between asymptotic value of the total number of observed coincidences, N_∞ (from Fig. 8), and the number observed within a fixed interval, N_t, against the time interval. The slope of the line gives directly the half-life of At^{217}.

[25] A. H. Jaffey, Chapter 16, "Radiochemical assay by alpha and fission measurements," National Nuclear Energy Series, Plutonium Project Record, Vol. 14A.

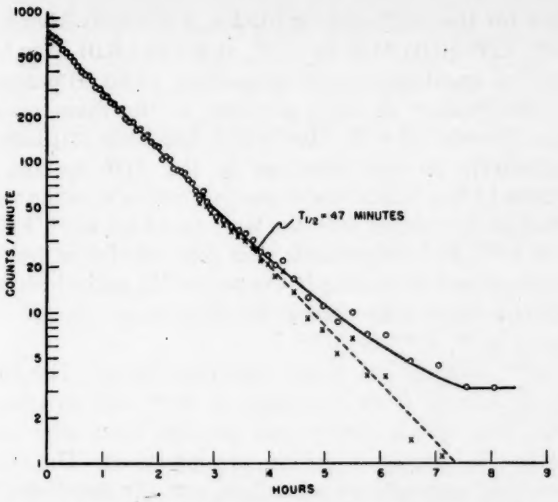

FIG. 10. Decay of alpha-activity from Bi^{213} and daughters.

plate and cathode of one of the tubes of the first Eccles-Jordan trigger pair[26] in the scaling circuit of the counter. The voltage changes across the condenser were followed by an oscilloscope, the plates of which were connected directly across the condenser. Thus a single alpha-particle would cause the electron beam of the oscilloscope to sweep across the screen at a rate dependent upon the time constant of the circuit. If two successive alpha-particles were emitted within this time interval the beam would be returned to its original position and the distance through which it swept would be a measure of the interval between the pulses. The time constant of the circuit was such that 0.2 sec. was required for the beam to sweep across the screen. The distances swept for successive emissions were observed visually. A detailed description of the circuit and method may be found in another paper from this laboratory.[27]

The purpose of the special mounting of the sample was to increase the geometry factor to approximately 100 percent in order to obtain as high a ratio of coincident to single pulses as possible. A low counting rate (9 counts/min.) was used in order to reduce corrections for coincidences due to random emission of single particles. This correction varied linearly in the range of interest, from nil at zero time to about three percent at 0.2 sec.

Figure 8 shows the integral curve obtained by plotting the total number of coincidences within a given time interval against the time interval. The mean interval was 0.026 sec. from which was obtained the value 0.018 sec. for the half-life of At^{217}. The same half-life was obtained by graphical analysis (Fig. 9). Essentially all the coincidences were observed within the maximum time interval. By plotting the difference between the total number of coincidences and the number within a given time interval against the interval on semi-logarithmic paper a straight line was obtained the slope of which determined the half-life of At^{217}.

Bi^{213}

The Bi^{213} was isolated from a solution of Ac^{225} by precipitation with bismuth sulfide carrier. Four or five cycles consisting of solution of the sulfide in hot concentrated hydrochloric acid, dilution with water and reprecipitation of bismuth with hydrogen sulfide served to remove all except lead activity, which was separated upon lead sulfate precipitates.

The Bi^{213} half-life was determined by following the

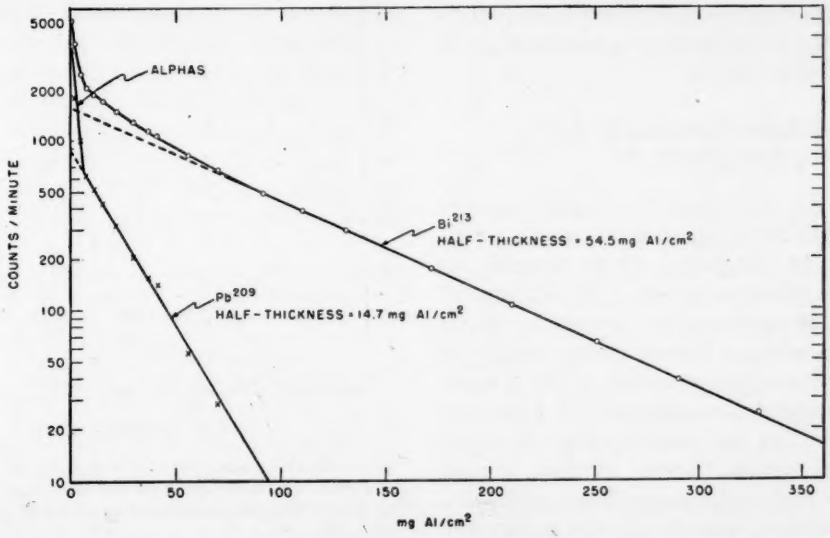

FIG. 11. Absorption curve in aluminum of beta-particles from Ac^{225} and daughters showing the two components due to Pb^{209} and Bi^{213}.

[26] W. H. Eccles and F. W. Jordan, Radio Rev. 1, 143 (1919).
[27] M. H. Studier and E. K. Hyde, Phys. Rev. 74, 591–600 (1948).

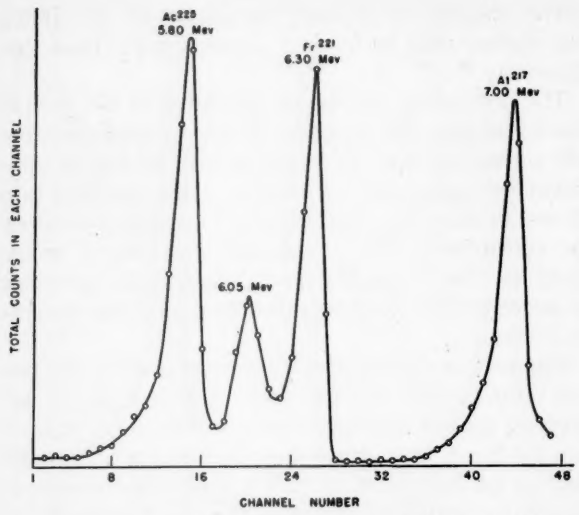

FIG. 12. Typical pulse analyzer curve of the alpha-particles from Ac^{225} and daughters.

very short-lived alpha-emitting daughter Po^{213} rather than the beta-particles of Bi^{213} itself since the growth of beta-particles of 3.3 hr. Pb^{209} is a complicating factor in the latter case. Figure 10 shows a sample decay curve of the Bi^{213} fraction which, after subtracting the non-decaying counter background, gives a value of 47 min. for the Bi^{213} half-life. This same isotope has been identified as a decay product of Pa^{229} by other workers in this laboratory.[15]

Absorption curves in aluminum of the beta-particles from Bi^{213} and Pb^{209} were taken with samples of Ac^{225} in equilibrium with its daughters. Figure 11 shows an experimental curve which has been resolved into the two components; the beta-particles of Bi^{213} have a half-thickness of 54.7 mg Al corresponding very roughly to an energy of 1.2 Mev and those of Pb^{209} have a half-thickness of 14.7 mg corresponding approximately to the reported value[1] of 0.7 Mev.

Energies of Alpha-Particles of Ac^{225}, Fr^{221}, At^{217}, and Po^{213}

The energies of the alpha-particles of these isotopes were determined with the pulse analyzer using a standard of RdTh and its daughters, whose energies are known, to establish reference points. The instrument[20] which was used has 48 electronic channels which register all the alpha-pulses within a narrow energy band; the 48 channels cover 48 contiguous energy bands of equal width increasing in energy from channel No. 1 to channel No. 48. By plotting the total number of alpha-counts per channel against channel number, a peak will be observed for each alpha-group. The position and size of the peak measure, respectively, the energy and abundance of the alpha-group.[28]

The values obtained for the energies were 5.80±0.05 Mev for the Ac^{225} alpha-particles, 6.30±0.05 Mev for Fr^{221}, 7.00±0.05 Mev for At^{217}, and 8.34±0.01 Mev for Po^{213}. A small peak containing about 25 to 30 percent of the number of alpha-particles in the main peaks was observed at 6.05 Mev which has been attributed tentatively to fine structure in the Fr^{221} spectrum. Figure 12 is a typical pulse analyzer curve showing this small peak together with the large peaks for Ac^{225}, Fr^{221}, and At^{217}. It is improbable that this activity is due to unrecognized branching in the series. No radiochemical evidence has been found for branching decay[29] of Th^{229}, Ac^{225}, Fr^{221}, or At^{217}.

Bi^{213} does exhibit some branching decay. The bismuth activity from a solution of Ac^{225} was separated with lead sulfide carrier and purified from other activities by repeated sulfide precipitations. The lead was then precipitated as sulfate and the supernatant containing the carrier-free bismuth activity was mounted and examined in the pulse analyzer. In some cases plates were prepared by direct electrodeposition of the bismuth from 1*N* HCl solution of the actinium. In addition to the normal peak of Po^{213} at 8.34 Mev a small peak at about 6.0 Mev was observed. The sample was followed for a period of several half-lives and both peaks decayed with the Bi^{213} half-life of 47 min. The number of alpha-particles in the shorter range peak was 2.0±0.2 percent of the total in both, based on 15 determinations. An experimental curve is shown in Fig. 13. Although the energy of this small peak is close to that mentioned above attributed to Fr^{221}, the number of alpha-particles from the Bi^{213} is insufficient to account for more than a fraction of the total in that peak.

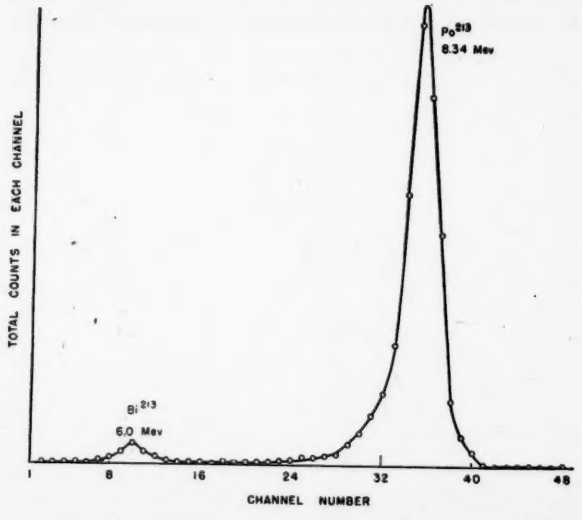

FIG. 13. Pulse analyzer curve of alpha-particles from Bi^{213} and daughters. The small peak at 6.0 Mev containing two percent of the total alpha-particles is due to alpha-branching of Bi^{213}.

[28] We are indebted to B. Weissbourd and J. Mech for assistance with the pulse analyses of our numerous samples.

[29] Systematics of decay of the heavy elements [Perlman, Ghiorso, and Seaborg, Phys. Rev. 77, 26 (1950)] suggest that At^{217} and Fr^{221} may not be beta-stable. There is also the suggestion that At^{217} may have an as yet unobserved alpha-group of higher energy.

With the quantities of material available at the time of these experiments, attempts to isolate the Tl^{209} activity were unsuccessful. Since then one of us[30] has been able to characterize the isotope as decaying with a 2.2-min. half-life by emission of a 1.8-Mev beta-particle. Gamma-rays if present constitute a maximum of one percent of the Geiger activity.

[30] French Hagemann, Phys. Rev. **79**, 534 (1950).

PHYSICAL REVIEW VOLUME 79, NUMBER 3 AUGUST 1, 1950

Interaction of 12- to 13-Mev Neutrons with Deuterons*†

G. L. GRIFFITH,** M. E. REMLEY, AND P. G. KRUGER
University of Illinois, Urbana, Illinois

(Received March 22, 1950)

By use of a CD_4-filled high pressure cloud chamber, the angular distribution of recoils from 12- to 13-Mev neutrons has been studied. The angular range 0° to 140° in the center-of-mass system was covered by these measurements. The distribution indicates a rather large asymmetry in the forward and backward directions with a minimum at about 60° in the center-of-mass system. The existence of a $D(n, 2n)p$ reaction was evident by the presence of tracks between 60° and 90° in the laboratory system which were too long to be accounted for by either deuteron or proton elastic recoils.

I. INTRODUCTION

THEORETICAL predictions which have been developed up to the present time concerning the angular distribution of neutrons elastically scattered by deuterons show a marked dependence on the type of nuclear forces assumed. Massey and Buckingham[1] have made extensive calculations concerning this problem below 11.5 Mev, and Verde[2] has recently published calculations concerning this problem for neutron energies up to 20 Mev. Since 1937 there have been several experimental determinations made of the angular distribution of $n-d$ elastic scattering.[3] Unfortunately, the discrepancies existing among these various experimental determinations of the angular distribution and the theoretical predictions are such that no definite conclusions can be drawn concerning the nature of the nuclear forces involved in $n-d$ elastic scattering. Rosenfeld[4] has presented an excellent summary of the experimental and theoretical work done on this problem up to 1948. The importance which this problem may have in the eventual understanding of the nature of nuclear forces makes it reasonable to accumulate more experimental evidence concerning $n-d$ elastic scattering.

II. APPARATUS

The high pressure cloud chamber used by Laughlin and Kruger[5] to measure $n-p$ scattering has been used to investigate $n-d$ scattering. A thin deuterium gas target bombarded by 10-Mev deuterons from the University of Illinois cyclotron served as a source of 12- to 13-Mev neutrons. The cloud chamber was filled with CD_4 and used D_2O and isopropyl alcohol as the vapor mixture. This served as a source of deuteron scattering centers as well as a detector of the deuteron recoils. Details of the cloud chamber, neutron source and collimator, and the resultant neutron spectrum may be found in reference 5.

The cloud chamber was surrounded by a temperature-controlled water-cooling system which was maintained at 21°C.

An Illex No. 3 Universal shutter was mounted directly in front of the camera lens to determine the exposure time. In case of shutter failure, caused by the excessive strains of solenoid operation, the shutter could be replaced without disturbing the camera lens position. The use of two General Electric A-H6 mercury arc lamps for chamber illumination, a coated $f/2.0$ Ektar 45 mm lens, and Linagraph Ortho 35 mm film gave satisfactory exposures at $f/3.5$ and 1/20 of a sec.

Neutrons were introduced into the cloud chamber only during expansion by placing a deuteron beam shutter made of sheet tungsten ahead of the thin deuterium gas target. At each expansion this beam

* This report is part of a thesis submitted in partial fulfillment of the requirements for the degree of Doctor of Philosophy at the University of Illinois, 1950. A preliminary report of these data was given in Phys. Rev. **77**, 748 (1950).

† Assisted by a joint program of the ONR and the AEC.

** Now at the Westinghouse Research Laboratories, East Pittsburgh, Pennsylvania.

[1] H. S. W. Massey and R. A. Buckingham, Phys. Rev. **71**, 558 (1947). R. A. Buckingham and H. S. W. Massey, Proc. Roy. Soc. **A179**, 123 (1941).

[2] Mario Verde, Helv. Phys. Acta. **22**, 339 (1949).

[3] Kruger, Shoupp, Watson, and Stallman, Phys. Rev. **52**, 678 (1937). H. Barschall and M. Kanner, Phys. Rev. **58**, 590 (1940). Coon, Davis, and Barschall, Phys. Rev. **70**, 104 (1946). J. Coon and H. Barschall, Phys. Rev. **70**, 592 (1946). J. Darby and J. Swan, Nature **161**, 22 (1948). J. Coon and R. Taschek, Phys. Rev. **76**, 710 (1949).

[4] L. Rosenfeld, *Nuclear Forces* (Interscience Publishers, Inc., New York, 1948), Chapter XIV.

[5] J. Laughlin and P. G. Kruger, Phys. Rev. **73**, 197 (1948). J. Laughlin, Ph.D. thesis, University of Illinois, 1947.

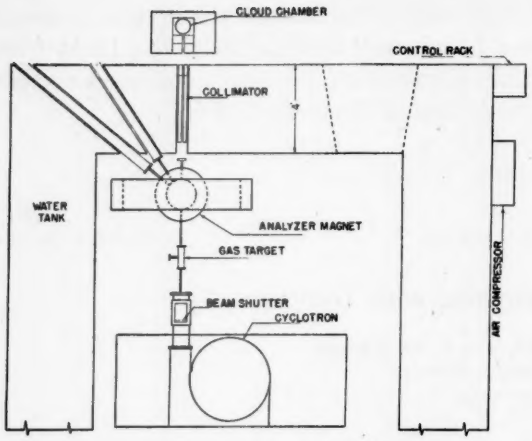

FIG. 1. Arrangement of experimental apparatus.

shutter was lowered out of the deuteron beam by means of an air-ram controlled from the cloud chamber cam system. Tungsten was used as a beam shutter since it has a low yield of gamma-rays and neutrons when bombarded by deuterons. The arrangement of the experimental apparatus is shown in Fig. 1.

The exposed film, after being processed, was projected through the same camera and mirror system as was used to photograph the interior of the cloud chamber. The stereoscopic projections were viewed on the screen of the measuring engine which is shown in Fig. 2. Tests were made on this projection and measuring system to study the effects of film shrinkage and the failure of the camera gate mechanism to relocate the film exactly. These tests showed that the reproducibility in a measurement of the recoil angle was $\pm 1°$ for the recoil range 0° to 70°, and the azimuthal angle measurements were reproducible to $\pm 2°$ for the azimuthal range of 0° to 360°.

The heavy methane gas used in the cloud chamber was synthesized by Tracerlab, Inc., Boston, Massachusetts. A sample of this gas was analyzed in a mass spectrograph by Dr. N. D. Coggeshall of the Gulf Research and Development Company. The following analysis was obtained:

CD_4	85.4 percent	N_2	4.6 percent
CD_3H	9.2 percent	O_2	0.8 percent.

III. EXPERIMENTAL PROCEDURE

These data were taken in two separate runs. During the high pressure run the cloud chamber was operated at a compressed pressure of 15.84 atmos., an expanded pressure of 13.84 atmos., and a 162 sec. cycle time. A compressed pressure of 6.33 atmos., an expanded pressure of 5.60 atmos., and a cycle time of 90 sec. were used during the low pressure run. The laboratory recoil angular range investigated was 0° to 60° in the high pressure run and 31° to 70° in the low pressure run. The chamber pressures used were such that the entire range of a deuteron recoiling from a 12- to 13-Mev neutron was contained within the chamber. This was necessary since the neutron spectrum[5] incident on the chamber showed a d, d peak of neutrons at 12- to 13-Mev superimposed on a continuous background. For this reason it was necessary to use a track length selection criterion in order to choose only those tracks which could have been deuterons elastically recoiling from 12- to 13-Mev neutrons.

Since the cycle time of the chamber was long, it was desirable to make the yield of recoils as large as possible by allowing neutrons to enter the chamber slightly before and throughout the expansion process. Thus the pressure differential in the chamber and the one Mev energy spread of the incident d, d neutrons made it necessary to accept a spread of recoil track lengths for each recoil angle. The maximum and minimum acceptable recoil ranges as a function of recoil angle are plotted for the two runs in Fig. 3. These were calculated from the usual range-energy curves and the energy-momentum considerations for the $n-d$ elastic scattering process. The stopping power of the chamber gas as a function of recoil range in air was used to convert the recoil range in air to range in the chamber.

The range limits shown in Fig. 3 assured that all recoils from 12- to 13-Mev neutrons would be accepted. However, recoils from 13- to 14-Mev neutrons formed while the chamber was compressed as well as any recoils from 11- to 12-Mev neutrons formed while the chamber was expanded also would have ranges falling within these limits. From the known time, relative to expansion, that neutrons were allowed to enter the chamber

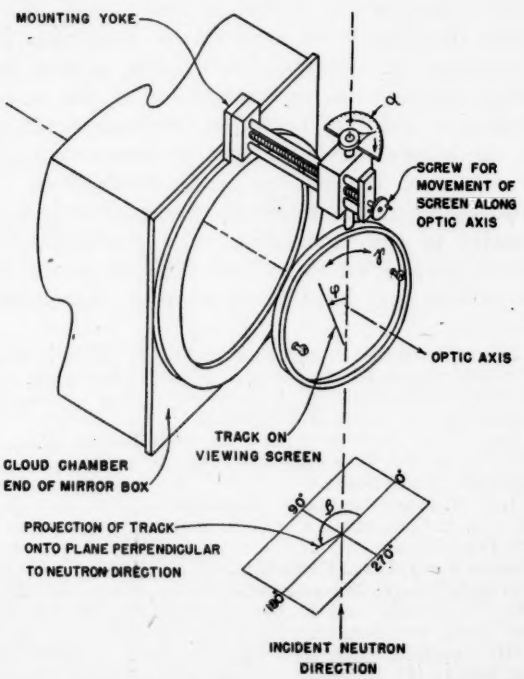
MOUNTING YOKE
SCREW FOR MOVEMENT OF SCREEN ALONG OPTIC AXIS
OPTIC AXIS
TRACK ON VIEWING SCREEN
CLOUD CHAMBER END OF MIRROR BOX
PROJECTION OF TRACK ONTO PLANE PERPENDICULAR TO NEUTRON DIRECTION
INCIDENT NEUTRON DIRECTION

FIG. 2. Schematic diagram of the measuring engine. The angles φ and β are the laboratory recoil angle and the azimuthal angle, respectively.

and from the shape of the neutron spectrum it was calculated that 88 percent of the recoils were due to 12- to 13-Mev neutrons while the remaining 12 percent were due to 11- to 12-Mev and 13- to 14-Mev neutrons.

A total of 4009 photographs was taken during the high pressure run, and 3042 photographs were taken during the low pressure run. All of the photographs from the low pressure run and half of the photographs from the high pressure run were examined twice, and independent measurements on acceptable tracks made. Satisfactory agreement was obtained in the two independent measurements. For this reason the remaining photographs were examined only once. 3271 tracks from the high pressure run and 958 tracks from the low pressure runs were found to have acceptable range-angle correlation as defined by the curves in Fig. 3. These acceptable tracks were grouped into 10° recoil angular intervals.

The use of two correction factors was necessary in conversion of the observed tracks to an angular distribution. A length correction factor was necessary because: (1) the portion of the cloud chamber in which a recoil could originate and not strike the opposite chamber wall is a function of the recoil range, recoil angle, and the azimuthal angle; (2) it was difficult to detect a short range recoil near the beam entrance side of the chamber because of the presence of electron tracks produced by gamma-rays from the collimator. An azimuthal correction was necessary since a different fraction of the azimuthal interval was used in the observation of recoils in each 10° recoil interval. The fraction of the azimuthal interval used was determined by the following factors: (1) the light beam illuminating the chamber was 1½ inches high, thus placing a geometrical limit on the azimuthal interval in which all recoils of a given recoil angle were fully illuminated; (2) it was determined experimentally that the observer failed to detect some of the very short range recoils if the azimuthal angle was near 90° or 270°.

These two corrections were determined experimentally. For each 10° recoil interval a track origin distribution was plotted showing the experimentally observed number of tracks originating per centimeter across the chamber along the path of the neutron flux. The usable length of the chamber for each 10° recoil interval was taken as that portion of the chamber in which the number of recoils originating per centimeter was constant within statistical limits. The experimental length correction factor was the reciprocal of the usable length of the chamber and for convenience was normalized so that the smallest value was unity.

The azimuthal correction factor was determined by making azimuthal distribution plots for each 10° recoil interval. Since the four azimuthal quadrants were symmetrical with respect to the light beam and to the point of observation, all of the tracks were folded into the first azimuthal quadrant. From these plots the fraction of the quadrant in which all tracks were fully illuminated and detected by the observer was determined, and the experimental azimuthal correction factor was the reciprocal of this fraction. In plotting the azimuthal distributions only those tracks originating in the usable length of the chamber for each 10° recoil interval were used.

These two correction factors allowed these data to be converted to an angular distribution. The corrected number of tracks per unit solid angle for each 10° recoil interval was determined by the product of the observed number of tracks in the azimuthal interval where all tracks were observed, the azimuthal correction factor, the length correction factor, and the reciprocal of the solid angle included in each recoil interval.

IV. EXPERIMENTAL RESULTS

Figure 4 shows some examples of the tracks photographed in the chamber. The length correction factors and the azimuthal correction factors were experimentally determined as outlined above and are given in Tables I and II.

It was determined experimentally that 93 percent of all recoils with tracks longer than 4 mm originated in the collimated region of the chamber. Presumably the remaining 7 percent of the tracks were due to uncollimated neutrons which were scattered into the chamber and produced recoils. It was observed that 7.2 percent of those recoils originating outside of the collimated region had a length such as to be an acceptable track

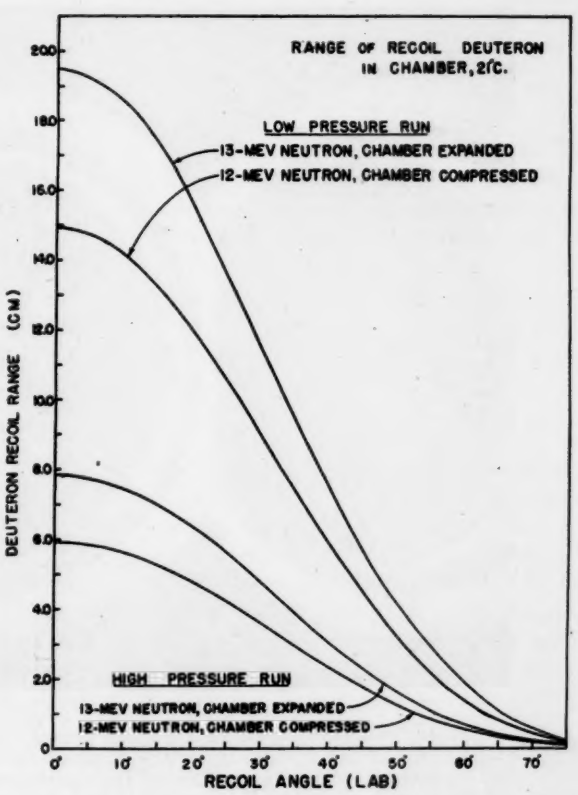

FIG. 3. Range of deuteron recoils in the chamber.

if the neutron direction was assumed parallel to the collimator axis. Assuming a uniform distribution of these uncollimated neutrons throughout the entire chamber, it was calculated that 0.5 percent of the acceptable tracks originating in the collimated region could have been due to random, uncollimated neutrons.

The experimental results are summarized in Tables I and II. The results of the low pressure run were fitted to the high pressure run in the three overlapping recoil intervals by the method of least squares. The errors assigned to the relative numbers of tracks per unit solid angle in each recoil interval are the probable errors. The calculation of these errors is considered in the following section. It is to be noted that only those usable tracks which fell in the azimuthal intervals where all tracks were detected were used in the final analysis of these data. Thus while a total of 4229 tracks were measured as having an acceptable range-angle relation, only 1534 of these were used.

Figure 5 shows the angular distribution of the observed tracks. A comparison also is made with some experimental results of Coon and Taschek,[3] the two curves being normalized at the 60° center-of-mass recoil angle. It is to be noted that these data have not been corrected for the presence of confusable recoil or disintegration protons. The recoil protons could arise from the presence of ordinary hydrogen in the scattering material, and a $D(n, 2n)p$ reaction would give rise to reaction protons. This background of confusable protons will be discussed further in a following section.

The data of Coon and Taschek shown in Fig. 5 also include a background of protons of the same order of magnitude, so that a direct comparison of data seems reasonable. Considering the difference in incident neutron energies the two curves are in fair agreement in the 0° to 140° center-of-mass recoil interval. A comparison of these data to the theoretical predictions[1,2] shows agreement only in the sense of a pronounced asymmetry with a minimum near the 60° center-of-mass recoil angle. No good fit of these experimental data with any of the theoretical curves could be made.

V. EXPERIMENTAL ERRORS

The errors assigned to the experimental points in Fig. 5 are probable errors based on the probable errors in the following factors:

(1) Probable error in the number of usable tracks in each recoil interval which were in that fraction of the azimuthal quadrant where all tracks were detected.
(2) Probable error in the length correction factor.
(3) Probable error introduced by confusable recoils from uncollimated neutrons.

The azimuthal correction factor is a pure numerical ratio and the solid angle included is a trigonometric calculation. Hence these factors introduce no errors.

Other sources of error such as small temperature and

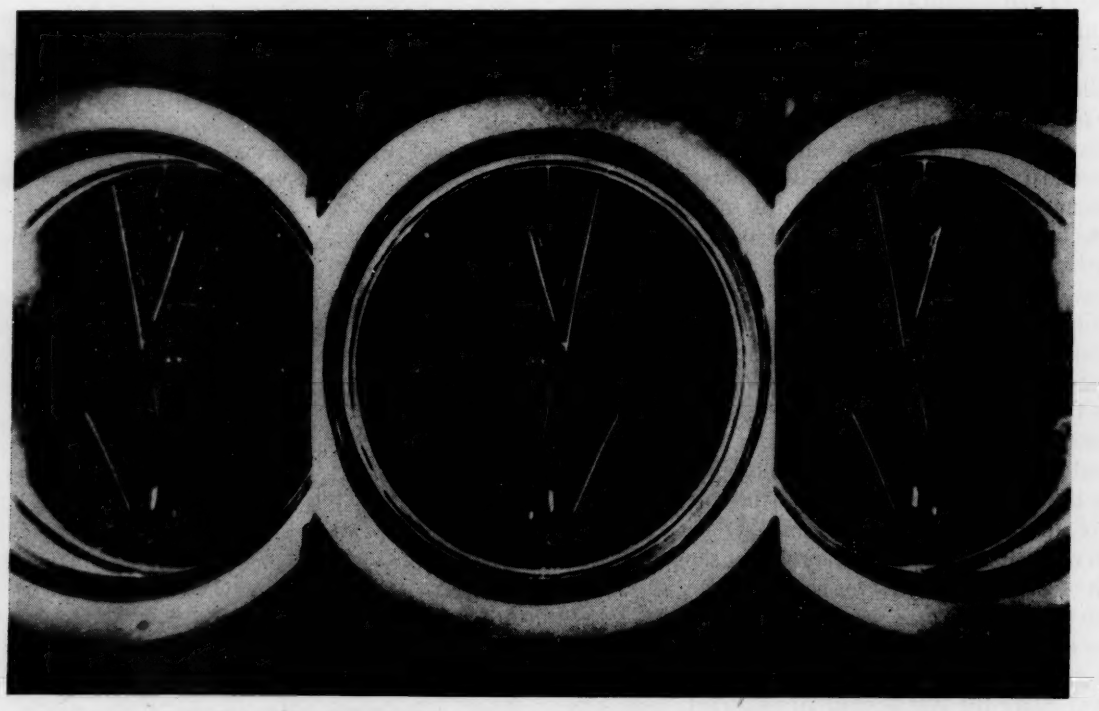

FIG. 4. Photograph taken during the high pressure run with cloud chamber filled to 15.84 atmos. with CD_4. The tracks due to recoils are easily discernible, accompanied by some electron tracks produced by the gamma-rays incident on the chamber wall from the collimator. The neutron collimation is evident by the restricted region across the chamber in which recoils originated. The direction of the incident neutrons is from the bottom to the top of the picture along the diameter of the chamber.

TABLE I. Results of high pressure run.

Lab recoil angle CM recoil angle CM scattering angle	0°–10° 0°–20° 180°–160°	11°–20° 20°–40° 160°–140°	21°–30° 40°–60° 140°–120°	31°–40° 60°–80° 120°–100°	41°–50° 80°–100° 100°–80°	51°–60° 100°–120° 80°–60°
No. of acceptable tracks	399	499	260	382	779	952
No. of acceptable tracks in usable part of chamber	297	405	206	314	596	704
Usable length of chamber	6.0 cm	7.0 cm	8.0 cm	9.0 cm	9.0 cm	9.0 cm
Length correction factor	1.50	1.29	1.12	1.00	1.00	1.00
No. of usable tracks in azimuthal interval where all tracks are detected	209	170	96	145	281	441
Azimuthal correction factor	1.50	3.00	3.00	3.00	3.00	3.00
CM solid angle	0.379	1.09	1.67	2.05	2.18	2.05
Corrected no. of tracks per unit CM solid angle	1240	604	190	213	387	645
Relative no. of tracks per unit CM solid angle	6.53±0.32	3.18±0.17	1.00±0.07	1.12±0.06	2.03±0.08	3.39±0.11

pressure variations in the chamber and small uncertainties in the accepted values of the atomic stopping power of the elements in the chamber gas all lead to small uncertainties in the incident neutron energy. These uncertainties are negligible compared to the spread of one Mev in the accepted neutron energies. The calculated probable errors are set forth in Table I and II.

VI. PROTON BACKGROUND

There were three possible sources of protons in this experiment which could have produced protons having track lengths confusable with those of acceptable deuteron recoils. These processes were $n-p$ elastic scattering, (n, p) reactions, and the $D(n, 2n)p$ reaction.

Because of the presence of the elements N, O, and C in the chamber gas, it was necessary to investigate the possibilities of an (n, p) reaction on these elements. The $C(n, p)B$ reaction has a Q-value of -11.2 Mev and hence protons from this reaction are of too low an energy to be confusable. The atomic ratio of O and N atoms to D atoms in the chamber gas was 0.42 and 2.5 percent, respectively. These small atomic ratios combined with the relatively small cross sections[6] for (n, p) reactions on N and O leads to a negligible number of confusable protons from this process.

The presence of CD_3H and isopropyl alcohol in the chamber made possible confusable protons from $n-p$ elastic scattering. The atomic H/D ratio was determined to be 3 percent from the chamber gas analysis. Energy considerations showed that 8.0 to 8.6 Mev neutrons would produce confusable proton recoils. If it is assumed that the experimental angular distribution is approximately that for $n-d$ elastic scattering, a rough calculation of the number of confusable protons can be made relative to $n-d$ scattering. The relation

[6] *The Science and Engineering of Nuclear Power* (Addison-Wesley Press, Inc., Cambridge, Massachusetts, 1947), Appendix C.

TABLE II. Results of low pressure run.

Lab. recoil angle CM recoil angle CM scattering angle	31°–40° 60°–80° 120°–100°	41°–50° 80°–100° 100°–80°	51°–60° 100°–120° 80°–60°	61°–70° 120°–140° 60°–40°
No. of acceptable tracks	33	150	436	339
No. of acceptable tracks in usable part of chamber	17	92	360	264
Usable length of chamber	3.0 cm	6.0 cm	10.0 cm	10.0 cm
Length correction factor	3.33	1.67	1.00	1.00
No. of usable tracks in azimuthal interval where all tracks are detected	7	26	77	82
Azimuthal correction factor	6.00	6.00	6.00	6.00
CM solid angle	2.05	2.18	2.05	1.67
Corrected no. of tracks per unit CM solid angle	68	120	226	295
Relative no. of tracks per unit CM solid angle fitted to high pressure run	1.06±0.27	1.88±0.25	3.54±0.27	4.62±0.35

used is

$$\frac{Y_{n-p}}{Y_{n-d}} = KN \frac{\int_{\varphi_1}^{\varphi_2} 2\pi d\sigma_{n-p}(\varphi) \sin\varphi d\varphi}{\int_{\varphi_1}^{\varphi_2} 2\pi d\sigma_{n-d}(\varphi) \sin\varphi d\varphi},$$

where K is the ratio of numbers of 8.0- to 8.6-Mev neutrons to the numbers of 12- to 13-Mev neutrons, N is the H/D atomic ratio, the Y's are the relative yields, and where the $n-p$ scattering is assumed to be isotropic in the center of mass system. K was determined from the observed spectrum[5] of neutrons. The above integrals were evaluated numerically after the total area under the integrand curves had been normalized to the following total cross sections,[4]

$$\sigma_{n-p} = 0.85 \text{ barn at } 8.3 \text{ Mev},$$
$$\sigma_{n-d} = 0.78 \text{ barn at } 12.5 \text{ Mev}.$$

The $n-d$ angular distribution was extended by the

extrapolation of Coon and Taschek[3] in the 140°–180° center-of-mass recoil interval. The results of these calculations are given in Table III.

An inelastic $n-d$ scattering process is energetically possible for incident neutron energies above 3.3 Mev. This $D(n, 2n)p$ process presumably will have a continuous spectrum of proton energies and thus represents a possible source of confusable protons in any $n-d$ elastic scattering experiment. If monoenergetic neutrons were used one probably could isolate the peak of $n-d$ recoils from the continuous proton spectrum by a suitable recoil length or energy analysis. No such discrimination was possible in this experiment because of the continuous background spectrum of incident neutron energies.

However in the 60°–90° laboratory recoil interval, the track lengths of the elastic recoils were very short, with an upper limit in length being imposed by $n-p$ scattering. In this angular interval, 44 tracks were observed in the low pressure run which were too long to be attributed to $n-p$ scattering. If it is assumed that $n-d$ elastic scattering accounts for most of the acceptable recoils observed in the low pressure run in the 31°–70° lab recoil interval, a rough value of the upper limit of the $(n, 2n)$ cross section can be calculated. The relation used for this calculation is

$$\frac{Y_{n,2n}}{Y_{n-d}} = \frac{2\pi \int_{\varphi 1}^{\varphi 2} d\sigma_{n,2n}(\varphi) \sin\varphi d\varphi}{2\pi \int_{31°}^{70°} d\sigma_{n-d}(\varphi) \sin\varphi d\varphi}$$

where the Y's are the observed yields corrected for azimuth and usable length of the chamber, and where

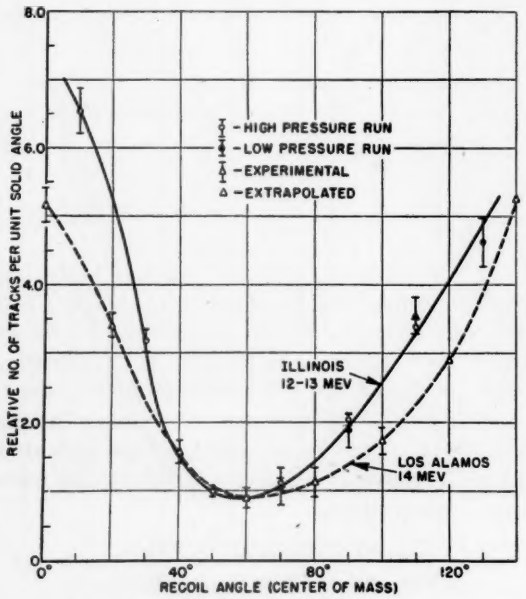

FIG. 5. Experimental angular distribution.

the integrated $n-d$ cross section was taken as 0.37 barn. Thus it was calculated that the integrated cross section for the disintegration process over the lab range 75° to 90° and yielding protons of energies between 1.0 and 3.4 Mev is about 0.014 barn. Similarly, the calculated value of the integrated cross section for the $(n, 2n)$ process over the laboratory range 60° to 90° and yielding protons of energies between 3.0 and 4.8 Mev is about 0.008 barn. These values represent upper limits on the integrated cross sections since, undoubtedly, a larger neutron energy interval, and hence a greater number of neutrons, was responsible for the production of disintegration protons than for the production of acceptable deuteron recoils. It is to be noted that the statistical errors to be attached to these values are of the order of 25 percent. It is impossible to make any calculation of the total cross section for the $D(n, 2n)p$ process from these data.

Chew[7] recently has made some theoretical calculations concerning the $D(n, 2n)p$ process. His ideas were developed for neutron energies above 90 Mev and are likely to be very inaccurate when applied to this experiment. These calculations are based primarily on phase space considerations, with the order of magnitude of the intensity derived from the known $p-p$ and $n-p$ cross sections in the 12.5-Mev range. Chew's calculations, when applied for 12.5-Mev neutrons, predict a total cross section for the $D(n, 2n)p$ reaction of about 0.24 barn with roughly 50 percent of the protons having energies between 0 and 2.0 Mev and 50 percent having energies between 2.0 and 10 Mev, with the high energy protons occurring in the forward directions. His calculations also predict cross sections of 0.013 barn and 0.007 barn corresponding to the experimental cross sections of 0.014 barn and 0.008 barn, respectively, which were mentioned above. It is felt that the agreement between these theoretical and experimental results is fortuitous in view of the very limited experimental data and the questionable application of Chew's calculations to 12.5-Mev neutrons.

A calculation of the ratio of confusable disintegration protons to acceptable deuteron recoils was made for each 10° recoil interval. For this calculation the $D(n, 2n)p$ cross section at 12.5 Mev was determined from Chew's predictions, and the experimental angular distribution curve, normalized to a total cross section of 0.78 barn, was used to determine the $n-d$ cross section for each 10° recoil interval. This method neglects the possibility that a larger number of neutrons may be responsible for disintegration protons than for elastic $n-d$ scattering. The results of these calculations are given in Table IV.

It is not believed by the authors that the results shown in Tables III and IV can be used to make a correction on the observed angular distribution in order

[7] G. F. Chew, University of California (private communications).

TABLE III. Confusable elastically scattered protons.

Lab recoil interval	Ratio of confusable proton recoils to acceptable deuteron recoils	
	High pressure run (percent)	Low pressure run (percent)
0°–10°	1.0	
11°–20°	1.8	
21°–30°	3.8	
31°–40°	4.5	5.2
41°–50°	2.9	3.4
51°–60°	1.9	2.2
61°–70°		1.3

TABLE IV. Confusable protons from the D(n, $2n$)p reaction.

Lab recoil interval	Ratio of confusable reaction protons to acceptable deuteron recoils (percent)
0°–10°	1.7
11°–20°	4.2
21°–30°	11
31°–40°	15
41°–50°	9.5
51°–60°	7.5
61°–70°	5.0

to obtain the true $n-d$ elastic scattering angular distribution. This is because of the unreliability of the estimated corrections for the $n-p$ and D(n, $2n$)p processes. The main errors in these are due to the questionable method of calculating the D(n, $2n$)p cross section and the fact that the corrections were derived on the assumption that the observed angular distribution was essentially that of $n-d$ elastic scattering. The purpose of including in this report the results shown in Tables III and IV is that they may indicate, approximately, the extent to which confusable protons are present in this experiment.

The angular distribution shown in Fig. 5 cannot be interpreted as the angular distribution for $n-d$ elastic scattering since as much as 20 percent of the tracks observed in some recoil intervals may have been confusable protons. It does seem reasonable to draw the conclusion that the general features of the distribution shown in Fig. 5 are those of $n-d$ elastic scattering. It is highly desirable to have more and better information concerning the D(n, $2n$)p reaction.

The authors are grateful to Dr. N. D. Coggeshall for his analysis of the CD_4 gas. They also wish to express their thanks to the members of the cyclotron staff for their help in carrying out this experiment.

A Redetermination of the Relative Abundances of the Isotopes of Neon, Krypton, Rubidium, Xenon, and Mercury*

ALFRED O. NIER
Department of Physics, University of Minnesota, Minneapolis, Minnesota
(Received April 19, 1950)

A careful redetermination of isotopic abundance ratios in neon, krypton, rubidium, xenon, and mercury has been made. The mass spectrometer employed was calibrated for mass discriminative effects with a synthetic argon isotope mixture made from essentially pure samples of A^{36} and A^{40}. The present results together with those obtained from an earlier study on carbon, nitrogen, oxygen, argon, and potassium enable one to use the several elements investigated as sub-standards for calibrating mass spectrometers for mass discriminative effects in other instances.

I. INTRODUCTION

IN a previous publication[1] the author reported on a redetermination of isotopic abundance ratios in carbon, nitrogen, oxygen, argon, and potassium. It is believed that this work is more accurate than earlier determinations because the mass spectrometers employed in the study were calibrated for mass discriminative effects with carefully made synthetic isotope mixtures of A^{36} and A^{40}. The investigation has now been extended to include the elements neon, krypton, rubidium, xenon, and mercury. For details on the preparation of the standards and the general procedure the reader is referred to the earlier publication. The instrument used in the present work is that previously designated as MSl. The rare gases used in the present study were all obtained from the Air Reduction Sales Corporation.

II. RESULTS

Neon

Table I gives the results obtained. In making analyses the procedure was to admit the standard and unknown alternately to the instrument. This procedure was repeated three times with an extra run of the standard at the end. Each number given is the average of 10 determinations, scanning of the spectrum being first in one direction and then in the other in order to eliminate the effect of any drift. This general procedure was also followed for the other elements studied. All errors given here and elsewhere in this paper are *probable errors* computed in the usual manner.

TABLE I. Comparison of mass spectrometer readings for neon and argon standard A V.

$(A^{36}/A^{40})^{2+}\times10^5$	$Ne^{21}/Ne^{20}\times10^5$	$Ne^{22}/Ne^{20}\times10^5$
1067[a]	286.9	9931
1080	286.1	9944
1067	286.1	9933
1052		
av. 1067±4	286.4±0.18	9936±3.7
corr. 1096±1.5	282.7±0.6	9703±40
Diebeler *et al.*[b]	309 ±20[c]	10180±200[c]
Vaughan *et al.*[d]	300	10810
Bleakney[e]	280[f]	8200[f]
	300[g]	9200[g]
Hibbs[h]	330±10	10800±10

[a] All members in this column corrected for H_2O^+ contribution to the mass 18 peak.
[b] See reference 11.
[c] Maximum deviation.
[d] Vaughan, Williams, and Tate, Phys. Rev. 46, 327 (1934).
[e] W. Bleakney, Phys. Rev. 43, 1056 (1933).
[f] For singly charged ions.
[g] For doubly charged ions.
[h] See reference 12.

The abundance ratios found for neon correspond to percentage abundances of 90.92±0.04, 0.257±0.001, and 8.82±0.04 for Ne^{20}, Ne^{21}, and Ne^{22} respectively. With a conversion factor[1] of 1.000278 from the physical to the chemical scale and the assumption that the isotopic weights[2,3] of Ne^{20} and Ne^{22} are 19.9987 and 21.9986 respectively, one computes the atomic weight of neon to be 20.172. This value is to be compared with the International value of 20.183. For convenience of reference the isotopic abundance ratios determined by other recent investigators are given at the bottom of Table I.

In making the present determination the problem was complicated by the fact that sensitive mass spectrometers always have a residual mass 18 peak caused by water vapor. Thus in determining the $(A^{36}/A^{40})^{2+}$ abundance ratio, the 18 peak, and hence the measured ratio, was too high. This effect was eliminated by the following procedure: (a) determination of the 17 as well as of the 18 and 20 peaks while the standard argon mixture was in the mass spectrometer; (b) determination of the ratio of the 18 and 17 peaks while pure A^{40} was admitted to the instrument at the same rate as the argon in (a); (c) from the measurements in (a) and (b) determining the correction to be made for H_2O^+ in the measured 18/20 abundance ratio. Step (b) was taken as an added precaution on the remote chance that the 18/17 abundance ratio for residual water vapor in the machine might depend on the presence of argon in the instrument.

* Research supported by joint program of ONR and AEC.
[1] A. O. Nier, Phys. Rev. 77, 789 (1950).
[2] K. T. Bainbridge, National Research Council, Preliminary Report No. 1, Nuclear Science Series, 1948.
[3] F. W. Aston, *Mass Spectra and Isotopes* (Longmans, Green and Company, New York, 1942).

Krypton

The procedure in this case was, first of all, to determine the Kr^{82}/Kr^{86} abundance ratio by taking readings alternately on $(Kr^{82}/Kr^{86})^{2+}$ and $(A^{36}/A^{40})^{+}$. The ions in the two cases had so nearly the same m/e value that it was felt that a linear mass discrimination correction factor could be applied safely. The result, $(6654\pm11)\times10^{-4}$ for Kr^{82}/Kr^{86}, was then used for making mass discrimination corrections for the remaining krypton isotopes in the spectrum of the singly charged krypton ions. Table II gives the ratios found. The results of earlier investigators are also tabulated for comparison. From the present work the percentage abundances are 0.354 ± 0.002, 2.27 ± 0.01, 11.56 ± 0.02, 11.55 ± 0.02, 56.90 ± 0.1, and 17.37 ± 0.02 for Kr^{78}, Kr^{80}, Kr^{82}, Kr^{83}, Kr^{84}, and Kr^{86} respectively. With a packing fraction[3] of -7.2 and a conversion factor of 1.000278 from the physical to the chemical scale, an atomic weight of 83.805 is computed from these results. The International value is given as 83.7.

Rubidium

Rubidium vapor was distilled into the electron beam from a small furnace mounted in the ion source. Since evaporation took place at a very slow rate from a liquid surface, it was assumed that the vapor leaving the liquid was enriched in light atoms. However, as the light atoms also travel faster to a cold region where they condense, it is assumed that the vapor composition in the electron beam is normal. The rubidium employed was of unknown origin and was the same material used in the author's earlier work.[4]

Two comparisons for rubidium were made. The first was between the previously determined krypton abundance ratio Kr^{86}/Kr^{84} and singly charged rubidium ions. The second comparison was made between doubly charged rubidium ions and argon standard[1] A V. The results are shown in Table III. The weighted average for the Rb^{85}/Rb^{87} abundance ratio from the two determinations is 2.591 ± 3. The error takes account of the fact that the Kr^{86}/Kr^{84} ratio also is based on A V. The new value is to be compared with the following most recent values: Nier,[4] 2.68 ± 0.02; Brewer,[5] 2.59–2.61; Paul,[6] 2.64 ± 0.03. The disagreement between the author's new and old values is perhaps not surprising. A recent determination of zinc and cadmium[7] has shown a similar discrepancy.

Xenon

A preliminary comparison was first made between the standard argon mixture and $(Xe^{128}/Xe^{136})^{3+}$. The value obtained for the latter abundance ratio was then employed for correcting the other isotope abundance radios when the singly charged xenon isotopes were examined. The results found are shown in Table IV. Again, for purposes of comparison the earlier work of Nier[8] and Lounsbury *et al.*[9] are included. The present ratios correspond to percentage abundances of 0.096 ±0.001, 0.090 ± 0.001, 1.919 ± 0.004, 26.44 ± 0.08, 4.08

TABLE II. Comparison of mass spectrometer readings for krypton and argon standard A V.

	$(A^{36}/A^{40})^{+}\times10^{5}$	$(Kr^{82}/Kr^{86})^{2+}\times10^{4}$
	1042	6516
	1043	6490
	1034	
	1040	6470
	1035	
Av.	1039±1.2	6492±8.5
Corr.	1096±1.5	6654±11

	$(Kr^{78}/Kr^{86})\times10^{5}$	$(Kr^{80}/Kr^{86})\times10^{4}$	$(Kr^{82}/Kr^{86})\times10^{4}$	$(Kr^{83}/Kr^{86})\times10^{4}$	$(Kr^{84}/Kr^{86})\times10^{3}$
	2115	1341	6741	6736	3314
	2103	1332	6726	6731	3297
	2086	1326	6795	6716	3288
Av.	2101±5.7	1333±2.9	6754±14	6728±4	3300±5
Corr.	2039±12	1308±6	6654±11	6653±13	3276±6
Dibeler *et al.*[a]	2088	1305	6710	6636	3314
Lounsbury *et al.*[b]	1962	1278	6598	6586	3271
Nier[c]	1985	1297	6597	6597	3268
Nier (recalculated)[d]	2060	1353	6759	6716	3307

[a] See reference 11.
[b] See reference 9.
[c] See reference 8.
[d] See discussion at end of present paper.

[4] A. O. Nier, Phys. Rev. **50**, 1041 (1936).
[5] A. K. Brewer, J. Am. Chem. Soc. **60**, 691 (1938).
[6] W. Paul, Zeits. f. Physik **124**, 244 (1947).
[7] W. T. Leland and A. O. Nier, Phys. Rev. **73**, 1206 (1948).
[8] A. O. Nier, Phys. Rev. **52**, 933 (1937).
[9] Lounsbury, Epstein, and Thode, Phys. Rev. **72**, 517 (1947).

TABLE III. Comparison of mass spectrometer readings for doubly charged rubidium and argon standard A V, rubidium and krypton.

	$(A^{36}/A^{40})^{+}$ $\times 10^5$	$(Rb^{85}/Rb^{87})^{2+}$ $\times 10^3$	$(Kr^{86}/Kr^{84})^{+}$ $\times 10^4$	$(Rb^{85}/Rb^{87})^{+}$ $\times 10^3$
	1070	2582	3075	2568
	1076	2580	3071	2588
	1068	2567	3072	2583
	1071			2576
Av.	1071±1.2	2576±3.2	3072±0.9	2579±3
Corr.	1096±1.5	2589±4	3053±6.5	2595±6

±0.01, 21.18±0.05, 26.89±0.07, 10.44±0.02, and 8.87±0.01 for Xe^{124}, Xe^{126}, Xe^{127}, Xe^{128}, Xe^{129}, Xe^{130}, Xe^{131}, Xe^{132}, Xe^{134}, and Xe^{136}, respectively. The mean mass number is 131.390 which when combined with a packing fraction[3] of −4.1 and a conversion factor of 1.000278 from the physical to the chemical scale yield an atomic weight of 131.300. The present International value is given as 131.3.

Mercury

In this case a sample of laboratory mercury was employed. Since this Laboratory has its own mercury purifying apparatus the sample chosen could be considered as a kind of average of the various samples of mercury employed in the laboratory in recent years. Approximately one cc of mercury was placed in a glass appendage attached to the main vacuum system of the mass spectrometer. The temperature of the appendage was adjusted to give the size peak desired and was in the neighborhood of −15°C. Table V gives the results obtained. The instrument was calibrated for mass discrimination by employing both the Kr^{80}/Kr^{86} and Xe^{128}/Xe^{136} abundance ratios previously determined. Since the doubly charged ions of mercury were employed, their m/e values were greater than those of the calibrating gas in the one case and less in the other. No significant differences in the two sets of results were observed. Because of the small size of the Hg^{196} peak no attempt was made to establish a new value for the relative abundance of the Hg^{196} isotope and the author's earlier Hg^{196}/Hg^{198} ratio, 0.0146, should be assumed to determine the Hg^{196} relative abundance.

The new values for the relative abundances lead to a mean mass number of 200.627 which when combined with a packing fraction[3] of 1.7 and the conversion factor 1.000278 from the physical to the chemical scale yield an atomic weight 200.605. The International value is 200.61.

III. DISCUSSION

The errors given in the present study are all probable errors based on the assumption that systematic errors have been reduced to negligible proportions. Thus one might expect that there would be a very good chance that the quantities measured here should agree with the true values within, let us say, three times the probable errors given. Thus it is hard to reconcile the present results on neon with any of the other determinations given in Table I. In all cases the neon was obtained from commercial sources. It is possible that the air reduction processes used in isolating the neon could have resulted in fractionation of the isotopes and that the fractionation effect was different in the various samples investigated. If this were true, one might expect a better correlation between the Ne^{21}/Ne^{20} and Ne^{22}/Ne^{20} ratios from sample to sample. It appears more likely that experimental errors of one kind or another were present in much of the work. The fact that the mass span of the neon isotopes is nearly ten percent of the mass means that systematic errors leading to mass discriminative effects could assume serious proportions. Also, the very low abundance of Ne^{21} makes it difficult to measure this isotope accurately.

As can be seen from Tables II and IV, the earlier work of the author on krypton and xenon[8] is in good agreement with the more recent work of Lounsbury and his co-workers.[9] However, the present determinations do not agree with either of these older measurements. In view of the care taken in all three researches it appears to be worth looking for sources of systematic error unknown to the investigators. It is seen from the

TABLE IV. Comparison of mass spectrometer readings for xenon and argon standard A V.

	$A^{36}/A^{40}\times 10^5$	$(Xe^{128}/Xe^{136})^{2+}\times 10^4$		
	1081	2149		
	1080	2137		
	1075	2145		
	1079			
	1079±0.9	2144±3		
	1096±1.5	2164±4		
	Xe^{124}/Xe^{136} $\times 10^5$	Xe^{126}/Xe^{136} $\times 10^5$	Xe^{128}/Xe^{136} $\times 10^4$	Xe^{129}/Xe^{136} $\times 10^3$
	1084	1006	2172	2983
	1078	1004	2158	2960
	1084	1017	2155	2985
Av.	1082±1.3	1009±2.7	2162±3.6	2979±5.6
Corr.	1084±4	1010±4	2164±4	2981±8
Dibeler *et al.*[a]	1136	1091	2149	2952
Lounsbury *et al.*[b]	1064	985	2147	2938
Nier[c]	1049	982	2121	2927
Nier (recalculated)[d]	1098	1020	2186	3004
	Xe^{130}/Xe^{136} $\times 10^4$	Xe^{131}/Xe^{136} $\times 10^3$	Xe^{132}/Xe^{136} $\times 10^3$	Xe^{134}/Xe^{136} $\times 10^3$
	4596	2389	3035	1179
	4566	2376	3010	1173
	4607	2396	3043	1178
Av.	4590±8.3	2387±4	3030±6.7	1177±1.3
Corr.	4594±11	2388±5	3032±7	1177±2
Dibeler *et al.*[a]	4100	2343	3020	1174
Lounsbury *et al.*[b]	4540	2378	3016	1178
Nier[c]	4540	2363	3009	1176
Nier (recalculated)[d]	4644	2406	3054	1184

[a] See reference 11.
[b] See reference 9.
[c] See reference 8.
[d] See discussion at end of present paper.

TABLE V. Comparison of mass spectrometer readings for mercury and krypton, mercury and xenon.

	Kr^{80}/Kr^{86} $\times 10^4$	$(Hg^{198}/Hg^{202})^{2+}$ $\times 10^4$	$(Hg^{199}/Hg^{202})^{2+}$ $\times 10^4$	$(Hg^{200}/Hg^{202})^{2+}$ $\times 10^4$	$(Hg^{201}/Hg^{202})^{2+}$ $\times 10^4$	$(Hg^{204}/Hg^{202})^{2+}$ $\times 10^4$
	1299	3370	5640	7756	4448	2305
	1297	3357	5637	7748	4429	2300
	1299					
Av.	1298±0.5	3363±5.2	5639±1.1	7752±2.7	4439±6.4	2302±1.7
Corr.	1308±6	3370±7	5648±6	7761±5	4441±7	2299±2.4
	Xe^{128}/Xe^{136} $\times 10^4$					
	2128	3348	5622	7701	4389	2300
	2136	3347	5657	7782	4440	2308
	2145					
Av.	2136±3.3	3347±0.5	5639±12	7743±27	4415±14	2304±2.7
Corr.	2164±4	3361±3	5657±12	7759±27	4420±14	2299±3
Average[a]		3362±3	5650±5	7761±5	4437±6	2299±2
Hibbs[b]		3371	5693	7773	4448	2301
Nier[c]		3420	5761	7869	4459	2270
Nier (recalculated)[d]		3386	5718	7753	4448	2281

[a] Two sets of data assumed independent except for dependence upon A^{36}/A^{40} ratio in original standard.
[b] Ratios given here computed from Hibbs' percentage abundances. Hg^{196} percentage abundance (not included in above table) was given as 0.16±0.03. See also reference 12.
[c] See reference 8.
[d] See discussion at end of present paper.

data in Tables II and IV that the older determinations differ from the present in that, in general, the relative abundances of the light isotopes are lower. This suggests a mass discriminative effect. In all but the most recent work on isotope abundances no effort was made to correct for possible mass discriminative effects produced by the "leak" used to introduce gaseous samples to the mass spectrometer. The assumption usually made was that the mass spectrometer diffusion pumps pumped off molecules at a rate inversely proportional to the square root of their masses and that somehow or other the inlet leak admitted gases in the same manner and hence no correction had to be made. It is now clearly recognized that the leak may have either molecular or viscous flow, or for that matter, anything between these two extremes.[10] Leaks used in earlier work usually consisted of a length of fine bore glass capillary drawn from glass tubing of larger diameter. The nature of the flow through a capillary depends upon the pressure, length, diameter, and upon whether or not the bore is uniform. In the author's earlier work on krypton and xenon the leak flow was assumed to be molecular. If the flow were actually viscous, the heavier isotopes would have too high an abundance relative to the lighter ones in the spectrometer. In the last rows of Table II and IV the author's earlier data have been "corrected" on the assumption that the leak flow may have been viscous. It is seen that the author's new results for both krypton and xenon lie between his "original" and "corrected" values. Thus it appears to be attractive to assume that the leak used in the earlier work came closer to being a viscous than a molecular leak. The close agreement between the author's earlier work and that of Lounsbury and his co-workers suggests that a similar situation may have existed also in the latter investigation. These speculations are, of course, based on the assumption that the rare gases employed were identical in composition.

The mass spectrometer used by Dibeler[11] and his coworkers employs a carefully designed molecular leak. Hence the gas composition in the mass spectrometer is accurately known. However, the apparatus was not designed specifically for making isotope analyses, and the precision, especially for rare isotopes, does not appear to be as good as the other work cited. Nevertheless, the results seem to agree reasonably well with the author's new work.

In the case of mercury the present results agree very well with both the author's earlier[8] values as well as Hibbs'[12] recent determinations. If a correction factor depending upon the square root of the mass ratio is applied to the author's earlier values the agreement between the new and old data is even better. A correction factor of this sort is possibly justified for the following reason: The author's earlier apparatus was evacuated by two mercury pumps each having it own trap. Ordinarily both traps were immersed in liquid air or dry ice. However, when the mercury determinations were made one of the traps was warmed to around 0°C in order to give a sufficiently high vapor pressure

[10] A manuscript based on a study of leaks in this laboratory is now in preparation. Published references include: R. E. Honig, J. App. Phys. 16, 646 (1945); A. O. Nier, Rev. Sci. Inst. 18, 398 (1947); A. O. Nier *et al.*, Anal. Chem. 20, 188 (1948). M. G. Inghram, *Advances in Electronics*, Vol. I (Academic Press, New York, 1948).

[11] Dibeler, Mohler, and Reese, J. Research Nat. Bur. Stand. 38, 617 (1947).

[12] R. F. Hibbs, "Mass Spectrometric Measurements of Natural Isotopic Spectra." Report No. AECU-556, August 1949, U. S. Atomic Energy Commission.

for making an analysis. Since the mercury in the trap was that which previously had been distilled over from the nearby pump (the amount distilled being small compared with the total amount of mercury in the pump) one might expect the distillate to be rich in the lighter isotopes. The author was aware of the possibility at the time but hesitated to make the correction since it was by no means clear that the conditions were proper for ideal distillation. The new results would seem to indicate that a correction should have been made. Of course, if the isotopic composition of the mercury used in the several investigations was different the apparent good agreement could be fortuitous. Until such time as the mercury from various sources is shown to have different isotopic compositions it seems best to accept the close agreement as real.

The writer wishes to express his appreciation to Mrs. R. C. Boe for the assistance given in making the many careful measurements and computations required in this work. The construction of the apparatus was aided materially by grants from the Graduate School and the Minnesota Technical research fund subscribed to by General Mills, Inc., Minneapolis *Star-Journal and Tribune*, Minnesota Mining and Manufacturing Company, Northern States Power Company, and Minneapolis Honeywell Regulator Company.

PHYSICAL REVIEW VOLUME 79, NUMBER 3 AUGUST 1, 1950

Study of Electron-Electron Scattering*

GERHART GROETZINGER, LEWIS B. LEDER, FRED L. RIBE, AND MARTIN J. BERGER
Institute for Nuclear Studies, University of Chicago, Chicago, Illinois

(Received March 13, 1950)

In the course of various cloud-chamber investigations pictures of 98 electron-electron collisions were obtained, in which the primary electrons ranged in energy approximately from 0.05 to 1.7 Mev and the deflections (in the center-of-mass system) exceeded 32°. By means of a statistical test suitable for the systematic evaluation of heterogenous data, a comparison was made of our results with the theory of Møller, relativistic versions of the theories of Mott and Rutherford, and the classical non-relativistic Rutherford theory. Our data discriminate definitely only against the latter theory. When combined with 122 electron-electron collisions observed by Champion, they are consistent only with the first two theories, but are insufficient to discriminate decisively between them.

I. INTRODUCTION

As a by-product of several cloud-chamber investigations carried out in this laboratory, a considerable number of photographs of fast electron-electron scattering events have been obtained. Since the amount of experimental evidence concerning this phenomenon is not very extensive, it was felt worth while to present our findings.

The first studies of this type of collision were made by Bothe[1] and by Wilson[2] using cloud chambers without a magnetic field. The observed cross sections agreed in order of magnitude with the results of a theory by Thomson.[3] Henderson[4] studied the scattering of electrons from RaE in several gases with a scattering chamber (filled with the gas to be investigated) and an ionization-chamber to record the scattered electrons. From the dependence of the scattering on the atomic number, he estimated the contribution made to it by electron-electron scattering.

All subsequent investigations were performed with cloud chambers using a magnetic field. As a source of electrons beta-ray emitters and gamma-ray sources were used. In all cases the energy of the electron before scattering was determined from the curvature of its path in the magnetic field. Some investigators determined the energy of the scattered electron of lower energy while others measured the angles between the directions of the tracks at the point of the collision. Furthermore, the investigations differed in the method used to compare the experimental results of various theories. Williams and Terroux[5] determined the energies of the scattered electrons of lower energy from their ranges. They divided the observed 72 events into four groups depending upon the magnitude of this energy. For electrons with energies between 0.13 and 1.6 Mev before the collision they compared the number of cases in these groups with the number resulting from the theory of Thomson[3] for an average energy of 0.46 Mev. The difference between the experimental and theoretical results is, according to Williams and Terroux, much greater than the experimental and statistical error. According to Hornbeck and Howell,[6] the above results also lead to cross sections which are more than twice

* This research was assisted in part by the joint program of the ONR and AEC.

[1] W. Bothe, Zeits. f. Physik **12**, 117 (1922).
[2] C. T. R. Wilson, Proc. Roy. Soc. **104**, 192 (1923).
[3] J. J. Thomson, Phil. Mag. **23**, 449 (1912). N. Bohr, Phil. Mag. **25**, 10 (1913).
[4] M. C. Henderson, Phil. Mag. **8**, 847 (1929).
[5] E. J. Williams and F. R. Terroux, Proc. Roy. Soc. **A126**, 289 (1929/30).
[6] G. Hornbeck and I. Howell, Proc. Am. Phil. Soc. **84**, 33 (1941).

those resulting from the theory of Møller.[7,7a] Williams,[8] using 20-kev electrons, finds agreement with the non-relativistic classical theory, corrected for quantum-mechanical exchange. Champion[9] divided the 250 events which occurred with electrons in an energy range from 0.38 to 1.1 Mev (before scattering) into three groups, depending upon whether the scattered electron of higher energy is deflected between 10 and 20, 20 and 30, or more than 30 degrees from the direction of the incident electron in the laboratory system. In order to make a comparison with the various theories, he integrated the theoretical angular distributions in the laboratory system over the three angular ranges and over the range of energies occurring in his experiments. The energy spectrum of the electron tracks was obtained by Champion in a separate investigation with the same experimental arrangement. He finds good agreement with Møller's theory, but not with the classical theory of Rutherford or that of Mott, even when these theories are amended to make them approximately relativistic. Hornbeck and Howell[6] measured the average cross section for electron-electron scattering for primary energies in six intervals from 0.67 to 2.64 Mev, selecting events in which both scattered electrons had energies in excess of 12 kev (116 cases) and, in the entire energy range, those events in which the secondaries had energies greater than 20, 30, and 40 kev, respectively (205 cases). They determined the energy of the scattered electron of lower energy from its range and concluded that their results, when averaged over the energy and angular distribution, were in "essential agreement" with Møller's theory. The work of Hornbeck and Howell was extended by Shearin and Pardue,[10] who divided their 180 cases in a similar way into three groups depending on the minimum energy of the scattered electron of lower energy (restricting the initial energies to a range between 1.3 and 2.6 Mev). Their results are in better agreement with Møller's theory.

The theory of electron-electron scattering now generally accepted is that of Møller,[8] according to which the angular scattering distribution, for collisions between free electrons, can be written in a form which contains separate terms for the exchange effects and for the retardation:

$$df_\gamma(\theta)=\frac{(\gamma+1)\pi e^4\sin\theta d\theta}{m^2\gamma^2v^4}\{\csc^4(\tfrac{1}{2}\theta)+\sec^4(\tfrac{1}{2}\theta)$$

$$-\csc^2(\tfrac{1}{2}\theta)\cdot\sec^2(\tfrac{1}{2}\theta)+[(\gamma-1)/\gamma]^2[1+4\csc^2\theta]\}, \quad (1)$$

where θ is the angle of scattering in a relativistic center-of-mass system,[10a] γ is the ratio of the total to the rest energy, v is the velocity of the incident electron in the laboratory system, m is the rest mass, and e is the charge of the electron. In the non-relativistic limit ($\gamma\approx1$) Møller's formula reduces to that of Mott.[11]

Dropping the fourth term in the bracket, which accounts for retardation, we are left with a formula which we shall refer to as the relativistic Mott formula, since, like the non-relativistic formula of Mott[11] it takes account of exchange. Similarly, if we drop the third (exchange) term also, we refer to the remaining expression as the relativistic Rutherford formula, since, in the limit it reduces to the classical Rutherford expression (with recoils taken into account).[12]

II. EXPERIMENTAL PROCEDURE

The cloud chamber used had a diameter of 22 cm and an illuminated depth of 2½ cm. The strength of the magnetic field was about 350 gauss. Photographs were taken using a camera in connection with a mirror arrangement to obtain stereoscopic pictures with a 26° difference in orientation, the direct view being inclined 3° with respect to the magnetic field. Owing to the different purposes for which the cloud chamber was operated, other experimental conditions varied somewhat. At different times the chamber was filled with the following gases, always at a pressure of one atmosphere: argon, a mixture of 40 percent argon and 60 percent helium, and a mixture of 40 percent nitrogen

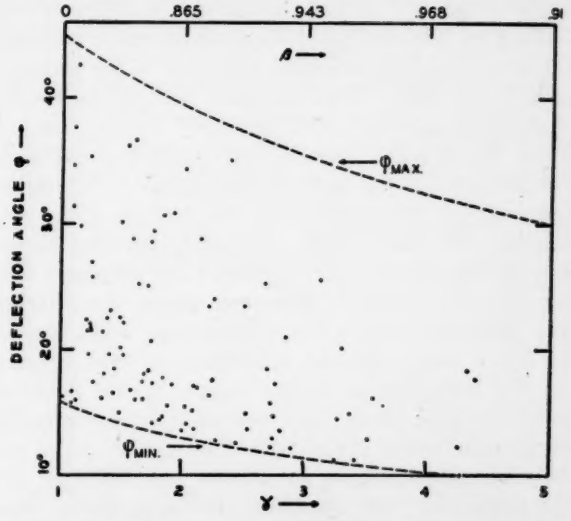

FIG. 1. Distribution of the angles between the direction of the electron before collision and the direction of the scattered electron of higher energy as a function of β and $\gamma[\beta=v/c$, and $\gamma=m/m_0=1/(1-\beta^2)^{\frac{1}{2}}]$ for 98 electron-electron scattering events larger than the arbitrary minimum angle $\varphi_{\min}$.

[7] C. Møller, Zeits. f. Physik **70**, 786 (1931). C. Møller, Ann. d. Physik **14**, 531 (1932). K. C. Kar and C. Basu, Ind. J. Phys. **18**, 223 (1944).

[7a] According to a private communication quoted in the paper of Hornbeck and Howell (reference 6), Williams and Cameron found in 1933 somewhat better agreement with Møller's theory.

[8] E. J. Williams, Proc. Roy. Soc. **A128**, 459 (1930).

[9] F. C. Champion, Proc. Roy. Soc. **A137**, 688 (1932).

[10] P. E. Shearin and T. E. Pardue, Proc. Am. Phil. Soc. **85**, 243 (1942).

[10a] That is, that Lorentz frame of reference in which the two electrons have equal and opposite momenta.

[11] N. F. Mott, Proc. Roy. Soc. **A126**, 259 (1930).

[12] It should be noted that the above expressions are not the same as the expressions used in columns 6, 7, 8 of Table I in Champion's paper (reference 9).

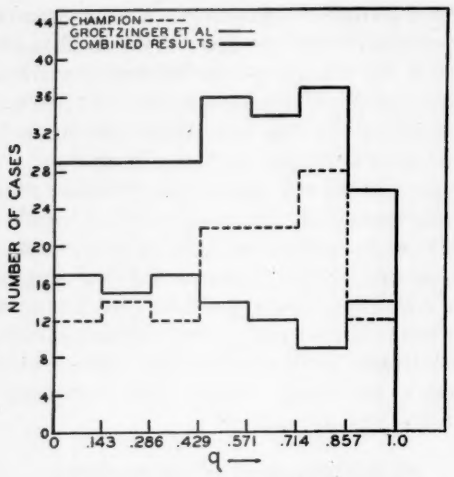

FIG. 2. Distribution of the q's calculated with the Møller formula.

and 60 percent helium. A P^{32} source[13] mounted at various positions in the center of the illuminated section of the chamber was used as a source of electrons ranging in energy up to approximately 1.7 Mev.

Approximately 7500 pictures were scanned for the purpose of finding the electron-electron scattering events. Since it is very important not to discriminate against certain angles of deflection, a strong effort was made to record all cases occurring in these pictures. For this reason two different observers investigated each picture at different times. The pictures containing the events were projected to their original size on a sheet of paper and both the direct and the mirror views were traced. The energy of the electron before collision was obtained in the following ways: (a) If the incident track, in the direct view, exceeded four cm in length, its average curvature was measured using a set of circles. (b) In some cases, where the track of the incident electron was too short, it was possible to determine its energy by measurements of the energies of the secondaries. In the energy determination the angle between the plane of the track and the magnetic field was taken into account. The space angles of scattering were determined from their projections appearing in the direct view, and the orientation of the primary and the secondary of higher energy at the point of collision in both views. This method of determining the space angle breaks down if the direction of one of the above-mentioned tracks approaches the direction of a line connecting corresponding points in both views (reference direction). For purposes of accuracy in the angle determination, we therefore excluded cases in which the direction of one of the tracks at the point of collision approached within ten degrees of the reference direction. There is no reason to assume that this exclusion of events, which is purely on the basis of orientation, will discriminate against any particular scattering events. As a check, many of these space angles were also measured by two observers using a stereoscopic projection method involving an adjustable ground-glass viewer, and in these cases good agreement between these two methods was found.

The space angles φ thus found were then converted to angles θ in the center-of-mass system by the relation

$$\cos\theta=[2-(\gamma+3)\sin^2\varphi]/[2+(\gamma-1)\sin^2\varphi]. \quad (2)$$

Only events resulting in angles θ larger than 32° were selected for consideration, which assured that even for the highest energies encountered the laboratory angles φ did not fall below 10°. This left us with 98 electron-electron collisions to be analyzed.

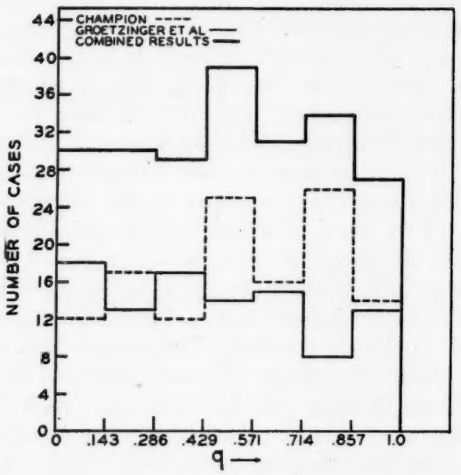

FIG. 3. Distribution of the q's calculated with the "relativistic Mott" formula.

The theories of electron-electron scattering considered here assume that both particles are free. This condition is not strictly fulfilled for scattering by atomic electrons; this does not matter, however, so long as the binding energy of the atomic electrons is small compared to the energy of the incident electron. For scattering in argon it would appear safe to neglect the binding energy of the K-shell electrons (3.5 kev) for incident energies greater than 100 kev, particularly in view of the fact that our measurements were made on the track of the more energetic secondary. Less than 10 percent of the events observed by us can be expected to involve collisions with K-shell electrons of argon. Moreover, none of these events involve incident energies below 50 kev, and only 10 percent involve incident energies between 50 kev and 100 kev. Thus in 99 percent of the recorded cases the binding energy can be expected to be less than 3.5 percent of the incident energy. In collisions involving K-shell electrons in argon there may also be appreciable deflections of the electrons by the coulomb field of the nucleus, especially at low energies of the incident electron (below about 200 kev). An estimate similar to the one above leads to the result that not more than

[13] The radioactive P^{32} was obtained from the Isotope Branch of the AEC, Oak Ridge, Tennessee.

two to three percent of all cases will be influenced by either effect.

III. METHOD OF ANALYSIS

In view of the diverse conditions under which our data were obtained, we have analyzed them on the basis of a comparison of relative rather than absolute angular differential cross sections of scattering which makes it unnecessary to know the "effective track length" per energy interval. We have applied a method originated by Pearson[14] which is suitable for the systematic evaluation of heterogenous data. Pearson's test, as originally proposed, had the purpose of testing whether a sample from a population of known composition had been drawn at random; we have here reversed the question: assuming the sample (in our case a set of scattering events) to have been selected at random, we test a hypothesis concerning the population (namely the scattering law).

Let $f_\gamma(\theta)$ be the angular scattering law, normalized to unity in the range $(\theta_{\min}, \theta_{\max})$. In the center-of-mass system, as explained above, $\theta_{\max}=\pi/2$ and $\theta_{\min}$ was chosen to be 32°. The lower cut-off is necessary, not only to avoid unduly large experimental errors for

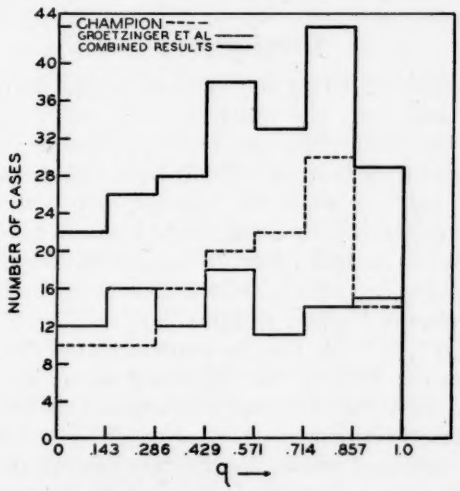

FIG. 4. Distribution of the q's calculated with the "relativistic Rutherford" formula.

small angles, but also because the scattering laws, in the formulations used by us, diverge at $\theta=0$. We define

$$q(\theta)=\int_\theta^{\pi/2} f_\gamma(\theta)d\theta; \tag{3}$$

so that $0\leq q\leq 1$. It follows that

$$f_\gamma(\theta)d\theta=-dq; \tag{4}$$

in other words, q is distributed rectangularly. It should be noted that while q is a function of the energy (γ), the distribution function of q is not. Thus one can lump together, for the purpose of statistical comparison, scattering events occurring at different energies without having to consider the energy distribution.

The statistical significance of a set of q's $(q_1, q_2\cdots q_N)$ can be summarized, following Pearson, by the statistic

$$z=-\ln\prod_{i=1}^{i=N} q_i=-\sum_{i=1}^{i=N}\ln q_i \tag{5}$$

which is thus a function of the observed scattering angles $\varphi_1, \varphi_2\cdots\varphi_N$ as well as of the assumed scattering law $f_\gamma(\theta)$. It can readily be shown that the distribution of z is:

$$dF(z)=[(N-1)!]^{-1}z^{N-1}e^{-z}dz, \tag{6}$$

which, for large N, approaches a Gaussian distribution with mean $\mu=N$ and standard deviation $\sigma=N^{\frac{1}{2}}$. The value of z obtained with a given number of observations will thus indicate the likelihood of the assumed scattering law.

In an investigation of the sensitivity of this method we have calculated the probabilities that the relativistic Mott theory, or the non-relativistic Rutherford theory, may be consistent with a set of (hypothetical) data in perfect accord with Møller's theory. It turns out that at an energy $\gamma=2$ the number of observed scattering events must exceed 1500 for the former and 350 for the latter theory in order to make these probabilities smaller than 5 percent. The number of cases necessary to get an equally low probability (5 percent) on the basis of a comparison of absolute cross sections for various angular ranges (method of Champion) was also estimated for the case of the relativistic Mott theory. At the same energy $(\gamma=2)$, subdividing the angular range in the laboratory system into five intervals (13°–20°, 20°–25°, 25°–30°, 30°–35°, 35°–$\varphi_{\max}$, where 13° corresponds to our minimum cut-off of 32° in the center-of-mass system) it was estimated, using the χ^2-test, that at least 1000 events are needed. It appears

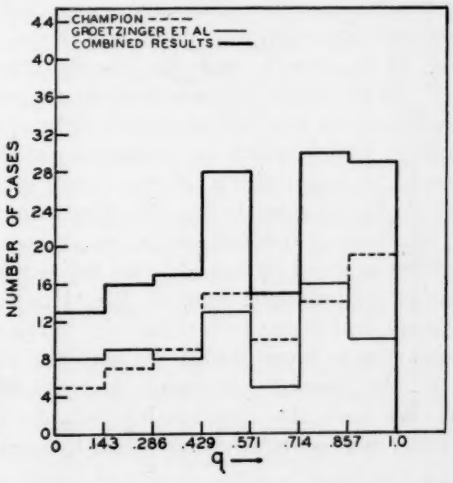

FIG. 5. Distribution of the q's calculated with the Rutherford formula with the angles transformed non-relativistically into the center-of-mass system.

[14] K. Pearson, Biom. **25**, 397 (1938).

TABLE I. Statistical analysis of electron-electron collisions.

Theory	z (exp.)	μ (statist. mean)	$\delta=0.6745\mu^{\frac{1}{2}}$ (probable error)	$(\mu-z)/\mu$	δ/μ
A: Groetzinger *et al.*					
Møller	105.57	98	±6.68	−0.075	±0.07
Mott	109.31	98	±6.68	−0.115	±0.07
Rutherford	90.53	98	±6.68	0.075	±0.07
Rutherford (non-rel.)	57.76	69	±5.60	0.165	±0.08
B: Champion					
Møller	103.63	122	±7.45	0.15	±0.06
Mott	107.65	122	±7.45	0.12	±0.06
Rutherford	92.30	122	±7.45	0.245	±0.06
Rutherford (non-rel.)	51.80	79	±5.99	0.345	±0.075
C: Combined data					
Møller	208.83	220	±9.98	0.05	±0.045
Mott	216.33	220	±9.98	0.015	±0.045
Rutherford	182.83	220	±9.98	0.17	±0.045
Rutherford (non-rel.)	109.56	148	±8.21	0.26	±0.055

that fewer cases are needed in the absolute cross section method than in our approach to be able to discriminate equally well between various theories. However, the measurement of absolute cross sections using beta- or gamma-ray sources and a cloud chamber involves the determination of an "effective track length" in which the scattering events occur, as a function of the energy. This quantity is difficult to determine because it depends in a complicated manner on the geometry of the chamber, and on the number of events which must be excluded, owing to the impossibility of their evaluation (tracks not long enough to allow an estimate of the energy, etc.).

IV. RESULTS

Figure 1 shows the scattering angles φ_i (in the laboratory system) plotted as functions of $\beta(=v/c)$ and of γ for the incident particle. The curves $\varphi_{\max}$ and $\varphi_{\min}$ represent the maximum and minimum angles, corresponding to $\theta_{\max}=\pi/2$, and the chosen cut-off of $\theta_{\min}=32°$, in the center-of-mass system, respectively. The relation of our data to the various theories can be seen in Figs. 2 to 5, which are histograms of the distribution of the quantities q. Figure 2 corresponds to Møller's theory as given in Eq. (1), Fig. 3 to Mott's theory transformed (relativistically) to the center-of-mass system as given by Eq. (1) with the last term in the bracket (retardation) omitted, Fig. 4 to Rutherford's theory, transformed relativistically to the center-of-mass system as given by Eq. (1) with the two last terms in the bracket (exchange and retardation) omitted. We have also included Rutherford's theory, transformed in a non-relativistic manner to a center-of-mass system by simply taking $\theta=2\varphi$ and using a cut-off angle of 32° in this system, which in this case simply corresponds to a cut-off of 16° in the laboratory system. The distribution of the q's based on this theory, whose number is reduced from 98 to 69 due to the different cut-off, is shown in Fig. 5.

We also applied our method to Champion's data, as given in Fig. 1 of his paper.[15] Use of the same minimum cut-off angles as applied to our data reduced his 250 cases to 122 and 79 cases respectively. Figures 2 to 5 contain, in addition to our distributions, those of Champion, and the combined distributions obtained by considering all data together. A comparison of the histograms shows that the proportion of small scattering angles is larger in Champion's data than in ours.

The histograms show deviations from rectangularity. To determine whether these deviations may be considered due to statistical fluctuations alone, we computed the statistic z (Eq. (5)) from our data, from Champion's data, and from the combined data for each of the theories. Table I gives the experimental values of z, as well as the statistical mean, μ, and the probable error, $\delta=0.6745\sigma$, all of which are functions of the number of cases. The last two columns give $(\mu-z)/\mu$ and δ/μ.

V. DISCUSSION

The results in part A of Table I show that deviations of our data from the relativistic theories of Møller, Mott, and Rutherford are within statistical fluctuations, indicating that our data fit these theories almost equally well. As might be expected, our results discriminate against the non-relativistic Rutherford theory. The data of Champion (part *B*) show deviations outside of statistical fluctuations, with a definite preference for the theories of Møller and Mott.

In part *C* of Table I we have combined our data with Champion's. Besides the improvement in statistics, this may have the advantage of decreasing the influence of systematic errors.

The combined results discriminate against the relativistic and non-relativistic Rutherford theories and indicate agreement to within statistical error with the theories of Møller and Mott. To discriminate between these two theories, that is, to test the effect of retardation, the data now available are not adequate, but there is the possibility that in the course of various cloud-chamber investigations enough electron-electron scattering data will accumulate which, when combined by using Pearson's test, will make such a discrimination possible.

[15] Champion's paper (reference 9) is the only one of those quoted which gives complete information about the observed events.

Magnetic Cloud-Chamber Analysis of Cosmic Rays at 3.4 Kilometers*

CHARLES E. MILLER, JOSEPH E. HENDERSON, DAVID S. POTTER, JAY TODD, JR., AND A. WILLIAM WOTRING†
*Applied Physics Laboratory,** University of Washington, Seattle, Washington*
(Received February 6, 1950)

About 18,000 magnetic cloud-chamber photographs (magnetic field of 8000 Gauss) have been taken at an altitude of 3.4 kilometers at Climax, Colorado. These were counter-controlled with single counters above and below the chamber forming a twofold telescope. The photographs were taken under three conditions: with no absorber over the chamber, and with 5 and 20 cm of lead above the chamber. The momenta of singly occurring particles have been measured and plotted to give momentum distributions. With sufficient absorber over the chamber, selection of exposures showing a single track has the effect of eliminating electrons. The momentum spectrum of the residual particles (mesons and some protons) shows a distribution closely similar to that found for mesons at sea level. Contrary to previously published reports, no appreciable increase in the relative number of low energy mesons is found. Particles selected in this way show a positive to negative ratio of 1.5 ± 0.05 as compared to reported values of about 1.3 at sea level. This confirms previous reports of an increase in this ratio with altitude. However, it is shown that the increase in positive excess is due in part to a greater number of protons at higher altitudes, and it is suggested that the entire increase may be thus accounted for, the positive excess of mesons remaining constant with altitude. Some estimate has been made of the abundance of protons at 3.4 kilometers.

I. INTRODUCTION

FEW studies in which a cloud chamber has been operated in a magnetic field sufficiently strong to give good momentum measurements have been made at higher altitudes. The observations of Adams, Anderson, *et al.*[1] in which a magnetic cloud chamber was operated from a B-29 airplane at altitudes between 30,000 and 40,000 feet, in particular their detection of large numbers of protons at this altitude, made a detailed study at an intermediate altitude seem worth while.

With this in mind, some 18,000 counter-controlled magnetic cloud-chamber photographs have been taken at an altitude of 3.4 kilometers at Climax, Colorado. Of these, 3000 are for a field strength of 10,000 Gauss while the remainder were taken with a field of 8000 gauss. To get additional information, and in order to remove effectively the electron component, exposures were made in which 5 and 20 cm of lead absorber were placed above the chamber, in addition to those exposures made with no absorber above the chamber.

The momenta of all singly occurring particles have been measured. Exposures showing a single and apparently counter-controlled track constitute about 60 percent of all photographs taken. Selection of single tracks for those exposures in which lead absorber was placed above the chamber effectively removes the electron component. The distribution in momenta for all singly occurring tracks and for the subgroup of heavily ionizing single tracks (protons) have been obtained.

II. THE APPARATUS

Figure 1 shows schematically the arrangement of magnet, cloud chamber, Geiger counters and absorbers used. The diaphragm type cloud chamber is 17 cm in diameter with a usable and illuminated depth of one inch. It differs from the conventional chamber of this type in being expanded through a $2\frac{1}{4}$ in. diameter hole through one of the pole pieces of the magnet with the pneumatic diaphragm outside the magnet structure. It is filled with argon gas and the saturated vapor of a 60–40 *n*-propyl alcohol-water mixture to a total pressure of 1.8 atmos. A very great improvement in its operating characteristics was achieved by loosely packing the tube connecting the chamber proper and the expansion compartment with a coarse form of copper wool. With this addition the tracks as photographed show an almost complete absence of background fog droplets, and the stability of operation is such that the expansion ratio need not be adjusted more often than once a day.

The camera photographs the chamber face through one of the magnet poles as shown in Fig. 1. Illumination is provided by the flash of four Sylvania Type R-4340 photo-flash lamps each operated from the discharge of a 32-μf condenser charged to 2600 volts. Each lamp is backed by a reflector and has its light partially collimated by a cylindrical lens between it and the chamber. The time interval between the occurrence of a coincidence count and the flash of the lamps can be set at any desired value. In this investigation delays of 0.04 to 0.06 sec. were used. The exact time for completion of expansion of the chamber is not known; however, the fact that tracks can be faintly photographed at 0.02 sec. following a coincidence count and the track width (0.5 to 0.7 mm) indicates an expansion time of less than 0.01 sec.

The magnet used was originally constructed for use aboard an aircraft and so was designed for minimum weight rather than most economical power consumption. The completed magnet weighs one ton, with the weight about equally distributed between copper and iron. The magnet coils are wound from 0.25×0.80 in. solid copper strip and are contained in a housing which

* This work supported by the Bureau of Ordnance, Navy Department, under Contract NOrd-7818, and by the joint program of ONR and AEC.
† Now with the Brookhaven National Laboratory.
** A division of the Department of Physics.
[1] R. V. Adams, C. D. Anderson, *et al.*, Rev. Mod. Phys. **20**, 334 (1948).

TABLE I. Coincidence counting rate in counts/second.

	No absorber	5 cm lead	20 cm lead
Field off	0.045	0.030	0.023
Field on	0.034	0.028	0.023

also forms the external portion of the magnetic circuit and through which transformer oil is circulated to provide cooling. The windings are similar to those used in most cyclotron magnets but with more efficient cooling and more rapid oil circulation. The oil is circulated through the magnet and a suitable water cooled heat-exchanger at a rate of 100 gallons per minute. With this circulation continuous current densities as high as 7000 amp. per square inch of copper can be used. The temperature of the oil as it enters the magnets is maintained constant to 0.01°C by use of a resistance thermometer which actuates a bypass on the heat-exchanger. The temperature rise in the oil in passing through the magnet structure (for 8000 gauss and 25 kw power consumption as used in most of the present work) is about 3.0°C. The magnet arrangement is such that the cloud chamber temperature is determined entirely by the temperature of the magnet structure which completely isolates the chamber from external influences. The magnet current was continuously recorded during the course of a run and occasional adjustments made.

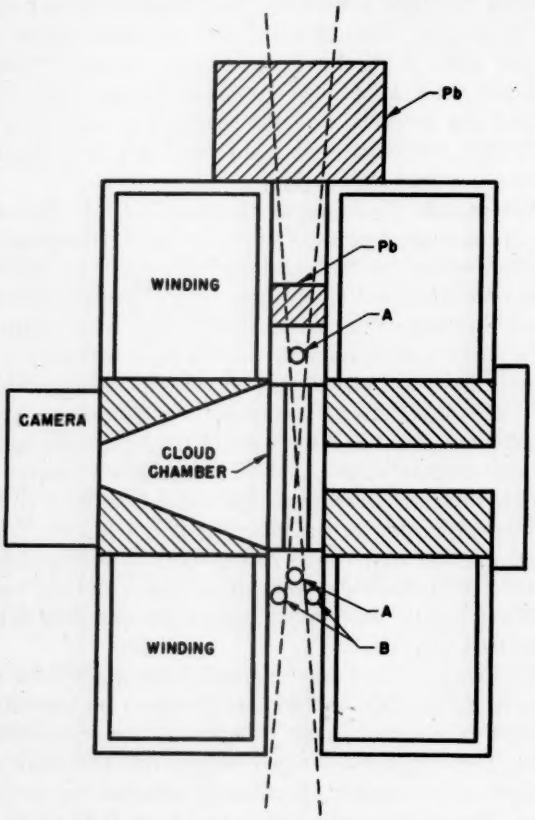

FIG. 1. Schematic diagram of the magnet, cloud chamber, counters and absorbers.

Only short period fluctuations as large as 1 percent occurred.

III. THE EXPERIMENT

The apparatus was installed on a surplus radar truck with power supplied to the magnets from a motor-generator set on a second truck. Exposures were made almost continuously for a period of six weeks at Climax, Colorado (elevation 3.4 kilometers). As is shown in Fig. 1, the chamber was triggered following a coincidence count from the A counters. These counters were $\frac{3}{4}$ in.$\times$6 in. and were placed directly above and below the chamber. They define a cone which does not include any of the magnet structure. Exposures were divided between those taken with no absorber above the chamber (except for the light weight sheet steel truck roof), with 5 cm of lead above the counter telescope and with 20 cm of lead placed above the magnet structure. Two counters, located as shown at B in Fig. 1, were used in anticoincidence with the A counters. These were included to reduce the number of shower photographs which were not of particular interest in the investigation. Exposures were taken both with and without the B counters in use. The counting rates of the A telescope showing the effect of the field and absorbers are shown in Table I. The rates do not include the 90 sec. chamber recovery time used.

The ratio of 2:1 of the no-absorber rate to the 20 cm lead rate (with field off) is just the ratio of the total to hard component at this altitude, as given by Rossi.[2] The agreement must be in part fortuitous since the two-counter telescope used was hardly adequate for a reliable rate determination. With no absorber above the telescope the field shows a strong effect in reducing the rate from 0.045 to 0.034 count/second. This reduction corresponds to the presence of large numbers of low energy electrons whose momenta lie below the magnetic cut-off of the equipment used. This cut-off comes at about 50 Mev/c as will be explained later. As shown by the rates in Table I, the field does not reduce the counting rate for the radiation that has been hardened by passage through 20 cm of lead.

IV. SELECTION OF TRACKS FOR CURVATURE MEASUREMENT

As explained previously, in obtaining momenta distributions only singly occurring tracks have been measured for curvature. However, tracks accompanied by others which from their appearance are obviously post or pre-expansion tracks have been included. Also, those single tracks whose angle in the chamber indicates that they could not have been counter-controlled have been excluded. These latter constitute only a few percent of all single tracks, which is a good indication that in the case of most single tracks the particle photographed was actually the counter-controlling particle

[2] B. Rossi, Rev. Mod. Phys. 20, 537 (1948).

and so could not have originated in any part of the surrounding absorber (with the exception of the lead absorbers deliberately placed above the chamber to modify the radiation). If this were not the case there is no obvious reason why large numbers of single tracks should not occur with angles in the chamber indicating that they could not have passed through both coincidence counters. As mentioned earlier, some 60 percent of all exposures showed single tracks. Because of the large number of tracks available only the longest (15 cm long or longer out of a chamber diameter of 17 cm) have been used. In this way only tracks long enough for good curvature measurements were used and those passing close to the chamber wall and so subjected to larger turbulence distortion were avoided. These selection criteria should be in no way selective. However, the selection of single tracks does discriminate strongly against electrons, except for those exposures taken under no absorber. In the case of most air showers, not more than one electron would be expected to be incident on the small cross-sectional area (about 30 cm²) represented by the equipment used. With no absorber above the chamber this electron usually would not form secondaries as the chamber wall and upper coincidence counter represent only a fraction of a radiation length. Other shower electrons intercepting the magnet structure are unlikely to produce secondaries which will reach the chamber because of the large amount of interposed absorber. For these reasons those single tracks photographed with no absorber above the chamber are expected to include large numbers of electrons. This is clearly shown by the large number of low momentum particles included in the momentum distribution for this case (Fig. 2). On the other hand, single tracks photographed under 5 or 20 cm of lead should include almost no electrons.

TABLE II. Momentum distribution for single tracks (of both signs) with no absorber over chamber.

Momentum in Bev/c	Number of particles in interval
0.00–0.08	25
0.08–0.13	64
0.13–0.21	99
0.17–0.27	100
0.21–0.31	67
0.27–0.39	87
0.35–0.49	104
0.41–0.57	131
0.49–0.68	144
0.57–0.88	176
0.68–0.88	160
0.88–1.20	115
1.03–1.46	154
1.20–1.85	167
1.46–2.50	204
1.85–2.50	130

V. MEASUREMENT OF TRACK CURVATURES

Curvatures were measured by direct comparison with standard curves. The standards were scribed full scale on Aquadag-coated plate glass by means of an Evans type mechanical linkage. In this way a graded set of

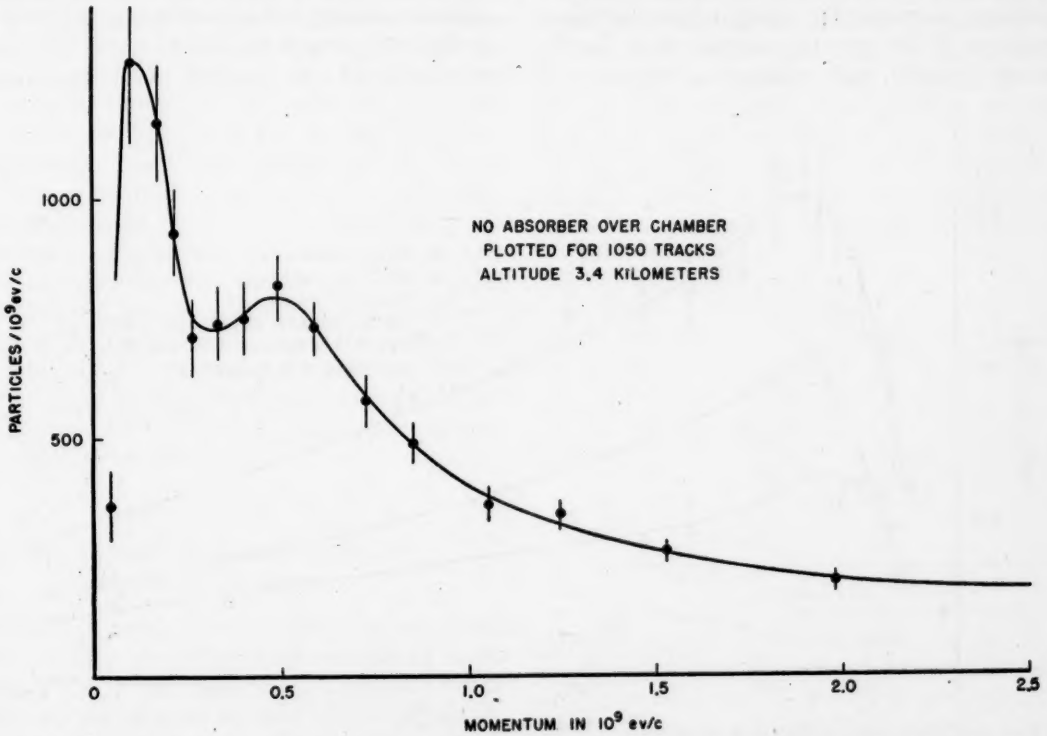

FIG. 2. Momentum spectrum of single tracks (positive and negative) with no absorber over chamber other than that represented by the glass chamber wall and upper coincidence counter. Includes mesons, electrons and protons.

TABLE III. Momentum distribution for single tracks with 5 cm of lead absorber over chamber.

Momentum in Bev/c	Number of particles in interval Positive	Negative
0.00–0.08	4	2
0.08–0.17	12	9
0.13–0.21	16	11
0.17–0.27	25	21
0.21–0.31	24	23
0.27–0.39	40	20
0.35–0.49	60	32
0.41–0.57	61	38
0.49–0.68	63	40
0.57–0.88	96	56
0.68–1.03	108	59
0.88–1.20	96	57
1.03–1.46	107	76
1.20–1.85	135	90
1.46–2.50	164	105
1.85–2.50	89	59

arcs increasing smoothly but in ever longer steps from a radius of 0.3 to 10.0 meters was prepared. The standards prepared in this way were photographed under identical conditions as in the photographing of actual cloud tracks. The photographs were then projected onto the screen of a comparator and the screen replaced by a photographic plate on which the image was recorded. The plates obtained in this way formed the standards which for comparison purposes were placed in contact with cloud track photographs projected on the same screen. Care was taken to show that no distortions resulted from different positioning in the field of the standard arc and cloud track during the photographic and projection processes. The comparator used gave an enlargement of 1.5 over the original track size in the chamber. Actually, each standard arc consisted of two arcs of the same radius and separated along the radius by 0.7 mm. In comparison the projected image of the cloud track was observed between these two arcs. The curvature range from 0.3 to 10.0 meters was divided into 48 segments and each track recorded as lying in one of these segments. The segments increased in length from about 0.1 meter at 0.3 meter radius to 1.5 meters at 10 meters radius. To obtain an idea of the consistency of measurement, a group of several hundred tracks were measured by different observers and their individual results plotted against each other as abscissa and ordinate. For perfect consistency this would give points all lying on the line $y=x$. The result gave a symmetrical distribution of points about this line showing agreement to 10 percent or better up to 3.5 meters and becoming rapidly worse at larger radii; at 10 meters the accuracy of measurement is not considered to be better than ± 3 meters. No attempt was made to estimate curvatures greater than 10 meters. No error resulted from non-uniformity of the magnetic field as this was found by measurement to be uniform to ± 1.0 percent over the usable volume of the chamber. The magnetic field for most of the exposures was 8200 Gauss. A radius of one meter is taken to correspond to a momentum of 250 Mev/c.

As stereoscopic pictures were not taken, lack of knowledge of the exact position and angle of the tracks in the chamber is a source of error in curvature measurements. Considering the limited depth of the illuminated region and the fact that the tracks used lie entirely in this region and extend almost a chamber diameter, the maximum possible error from this source is 4 percent and the average error less than 2 percent. For counter-controlled tracks the possible track displacement and

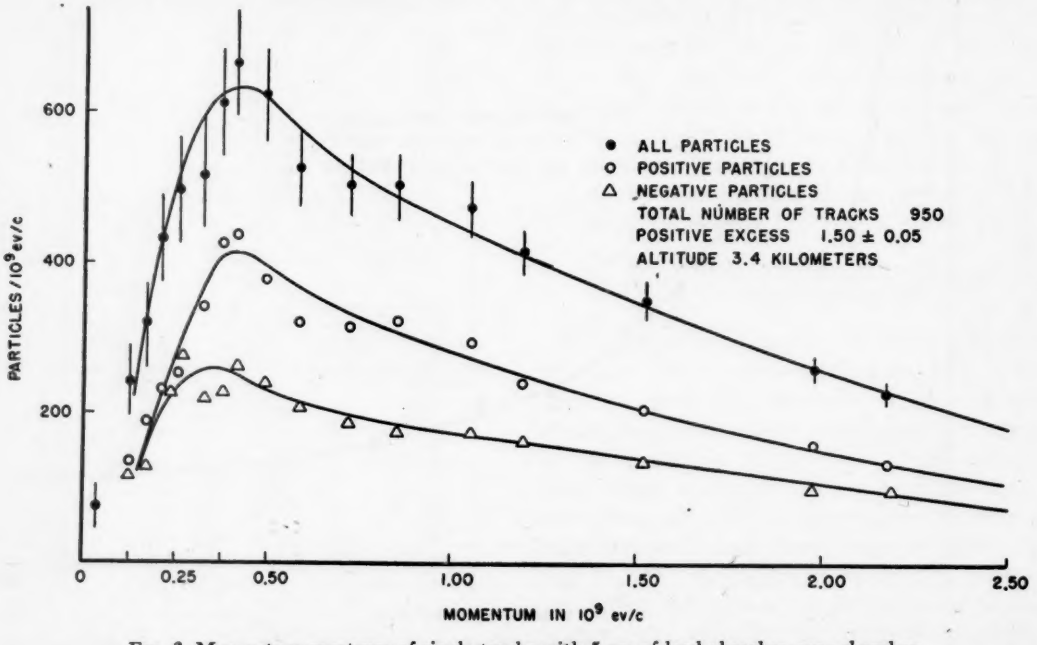

FIG. 3. Momentum spectrum of single tracks with 5 cm of lead absorber over chamber. Spectrum includes mesons and protons.

TABLE IV. Momentum distribution of heavily ionizing particles —including those found under no absorber and under 5 cm lead.

Momentum range Bev/c	Number of particles
0.00–0.25	0
0.25–0.30	7
0.30–0.35	12
0.35–0.50	49
0.43–0.58	44
0.50–0.65	39
0.58–0.75	31
0.65–0.88	27
0.75–1.00	16
>1.00	5

corresponding error in curvature measurement is about half this large (average error=1.0 percent).

VI. MAGNETIC CUT-OFF

The twofold coincidence triggering arrangement, used with counters above and below the chamber, has the effect of discriminating against particles of low momentum because of deflection by the magnetic field. This effect has been computed by use of a graphical construction and integration. Actually, the effect has been somewhat overestimated. For ease of computation the field was considered to extend in full strength to the position of the counters. Actually, it decreases very rapidly just beyond the chamber walls. For the computation, a knowledge of the intensity variation with zenith angle is necessary and the usual cosine-squared law was assumed. A less rapid decrease with zenith angle would give less cut-off while a much more rapid decrease seems unlikely for the low momentum range of interest here. The result shows complete cut-off for particles of momentum below about 50 Mev/c, 10 percent cut-off at 100 Mev/c and negligible cut-off for momenta above 150 Mev/c. As the intensity found for the non-electronic component is small at 100 Mev/c the effect of cut-off here is unimportant as compared with statistical uncertainties. It is assumed then that the momentum distribution found for protons and mesons is not seriously affected by magnetic cut-off above 100 Mev/c; the plots have not been continued below this value. On the other hand, the sudden decrease in intensity of low momentum particles shown in Fig. 2 is due to magnetic cut-off and occurs at the expected value. As will be shown later, the particles extending to cut-off here are electrons.

VII. RESULTS

A. Momentum Distribution with No Absorber over Chamber

The method of track selection has been explained. In addition, it may be well to point out that no single track meeting the specified length requirement (15 cm long) was omitted because of track quality or other considerations, except that several complete rolls of film were not used, being of rather poor quality. This left a residue of 1050 tracks of momentum less than 2.5 Bev/c for the no-absorber case, with a momentum distribution as given in Fig. 2. An additional 479 tracks were recorded as having momenta greater than 2.5 Bev/c. Figure 2 is plotted for overlapping intervals, the data being given in Table II. Each interval in Table II includes at least 3 of the 48 intervals into which the range from 0 to 2.5 Bev/c was divided in originally recording the curvatures. The deviations plotted in Fig. 2 are for statistics only.

B. Momentum Distribution under 5 Cm of Lead Absorber

The data for this case are given in Table III and plotted in Fig. 3. In addition to the 950 particles included in the plot, 535 were recorded as having momenta >2.5 Bev/c.

C. Particles under 20 Cm of Lead

Here only one-third as much data was taken as for the no absorber and 5 cm of lead cases, so the statistics are not adequate for a meaningful plot. In addition, exposures were made on Eastman Linograph Pan film, instead of the Linograph Ortho used in the other cases. This film proved too grainy for good momentum measurement. So far as can be told, the distribution does not differ appreciably from that of Fig. 3.

D. Heavily Ionizing Particles

The data of Figs. 2 and 3 include all single tracks regardless of their densities. Some show a density clearly indicating an ionization well above minimum. Of 5040 single tracks examined for the no absorber case, 99 (or 2.0 percent) clearly correspond in density to a particle of above minimum ionization. These figures are for *all* single tracks; not merely those of length 15 cm as plotted in Figs. 2 and 3. Similarly, of 2940 single tracks under 5 cm of lead, 50 (or 1.7 percent) are

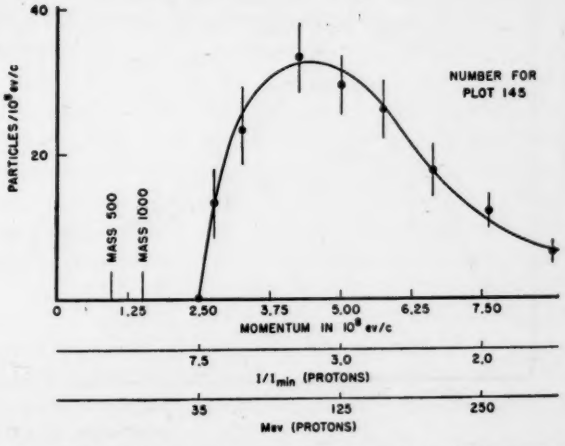

FIG. 4. Momentum spectrum of single heavily ionizing particles (protons), including those found under no absorber and those under 5 cm of lead.

heavily ionizing, while under 20 cm of lead the corresponding figures are 1560 and 12 (or 0.8 percent). Of the total of 161 heavily ionizing single tracks for the three cases, all but three show a direction of curvature corresponding to a positive particle moving downward.

The momentum distribution of the single heavily ionizing particles is given in Fig. 4 and the data of Table IV. Particles found under no absorber as well as under 5 cm of lead are included. Tracks 12 cm long and longer have been used. The distribution has been drawn to zero for the lowest momentum found for any single heavily ionizing track of length 12 cm. Within statistics the momentum distributions for heavily ionizing particles under no absorber and those under 5 cm of lead as plotted separately do not differ from the combined distribution of Fig. 4. The combined distribution is given to improve statistics and to show the low momentum cut-off which, as will be explained, does not depend on the nature of the absorber above the chamber.

VIII. DISCUSSION

A. Momentum Distribution

Momentum distributions from magnetic cloud-chamber measurements at sea level and at 30,000 feet have been given by Wilson[3] and by Adams, Anderson, *et al.*[1] In the case of Wilson's sea level measurements, sufficient absorber was used to insure cascade multiplication of electrons which were eliminated in this way. The distribution is then that of the non-shower-producing particles at sea level and as such is assumed to represent the meson distribution. This sea level result is quite similar to that found in the present investigation as given in Fig. 3. The 3.4 kilometer data of Fig. 3, as will be discussed later, contains significant numbers of protons. The distribution of experimental points as plotted in Fig. 3 seems to show a small secondary maximum at about 0.8 Bev/c; this is particularly true of the distribution of the positive particles only and does not show in the distribution of the negative particles. However, within the statistical uncertainty of the data no significance can be attached to this small maximum, and it is not included in the continuous curve sketched in. Figure 3 does not show the presence of large numbers of low energy mesons at higher altitudes (as compared to the number at sea-level) as found by Moore and Brode,[4] by Hall,[5] and others. Hall,[5] working at 14,000 feet, has obtained an integral range spectrum (in lead) from which a momentum spectrum has been derived through use of the meson range-momentum relationship. In this way he finds a sharp (meson) maximum at between 100 and 200 Mev/c and a rapid decrease in intensity at higher momenta. Hall's work is at an altitude 3000 feet higher than the present investigation. As he has pointed out, this large low momentum maximum would be unstable with increasing depth because of meson decay and in fact could reasonably exist at 14,000 feet only in the case of strong local production of low momenta mesons. Even allowing for decay (and no production) between 14,000 and 11,000 feet, the two results would not agree exactly, besides which it would be strange to find strong production of low momenta mesons at 14,000 feet, but not at 11,000 feet. In the present investigation momenta are measured directly without the assumption of any particular range-momentum relationship. The transformation from range

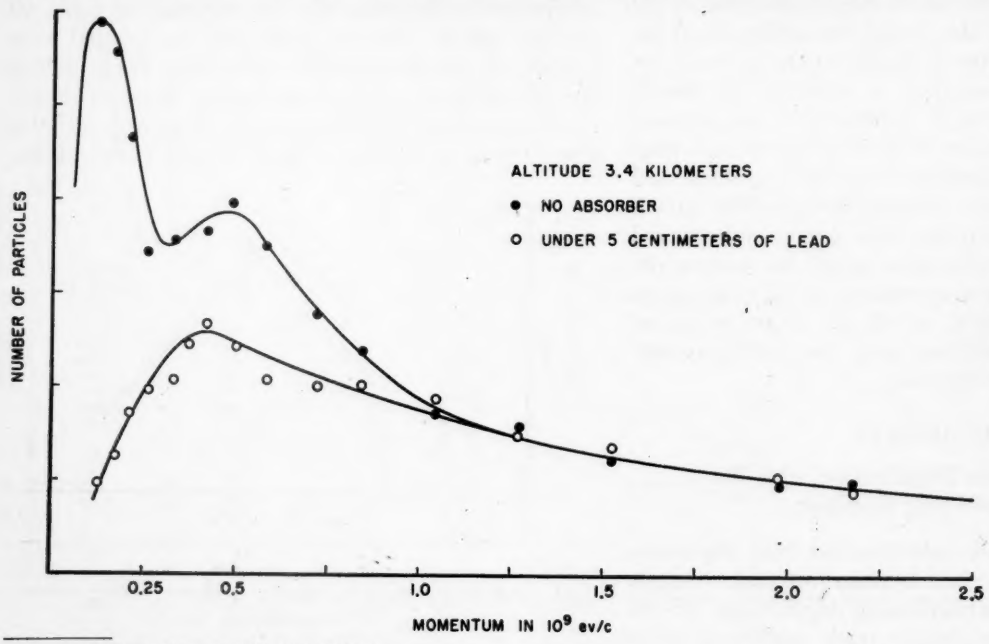

FIG. 5. Comparison of the momentum spectra under no absorber (electrons, mesons and protons) and under 5 cm lead (mesons and protons).

[3] J. G. Wilson, Nature 158, 414 (1946).
[4] D. C. Moore and R. B. Brode, Phys. Rev. 73, 532 (1948).
[5] D. B. Hall, Phys. Rev. 66, 321 (1944).

to momenta, as made in Hall's work, would, if there were an appreciable number of protons in the range 0 to 1.0 Bev/c, have just the effect of giving incorrectly too many particles below 200 Mev/c. In the present work there is a strong magnetic cut-off for momenta below 100 Mev/c, but this is negligible at 200 Mev/c. At this latter momentum there is no obvious reason why large numbers of mesons, if present, should not be detected. Possibly Hall's experimental arrangement fails to eliminate electrons completely, and certainly scattering in the lead absorbers has been inadequately considered. The strong maximum he has found at 100 to 200 Mev/c depends critically on the initial slope of the integral range curve where discrimination against electrons is difficult. From cloud-chamber observations made at 30,000 feet, Adams, Anderson, and Cowan[6] also point out that they fail to find large numbers of low energy mesons.

In the case of the momentum distribution obtained at 30,000 feet by Adams, Anderson, *et al.*,[1] no appreciable amount of absorber was present over the chamber so that the data includes electrons in addition to protons and mesons. The rapid rise that they find in the distribution at very low momentum is almost certainly due to electrons. The maximum occurring between a magnetic rigidity of 1 and 2 ($H\rho$ in 10^6 gauss-centimeter) is interpreted as due to protons, since when the distributions for positive and negative particles are plotted separately the maximum is present only for the positive particles. Protons could not be recognized (as they could in the present investigation) by their ionization density, as a bronze casting present between the cloud chamber and lower coincidence counter gave a proton cut-off at a momentum above that at which the increased density is easily recognized. Their result is to be compared to the distribution (Fig. 2) found in the present investigation and giving a similar plot obtained with almost identical experimental conditions but at a lower altitude. Figure 2 shows a small maximum at about the same momentum as the much more pronounced maximum found by Adams, Anderson, *et al.*[1] However, the maximum at about 0.5 Bev/c in Fig. 2 is so small as to be just resolved within the statistics, and it is doubtful that it is due entirely to protons, since the meson distribution (Fig. 3) also shows a maximum at about this momentum. In the present investigation the amount of absorbing material between the sensitive volume of the chamber and that of the coincidence counter below it was such as to give a proton cut-off at 250 Mev/c and so allowed identification of protons through their increased ionization density as will be discussed later.

In Fig. 5 we give a comparison of the momentum distribution of single tracks under no absorber to the distribution found for single tracks under 5 cm of lead. The distributions have been normalized to a common basis from a knowledge of the relative counting rates. The difference between the two distributions below a momentum of 1 Bev/c is considered to be due to electrons. As previously explained, for the no-absorber case there is not sufficient material above the chamber to insure cascade multiplication of single electrons incident on the equipment.

B. Positive Excess

Measurements of the ratio of the number of positive to negative mesons at sea-level have given values near 1.3. Thus, Jones[7] and Hughes[8] from magnetic cloud-chamber observations have given values for the positive excess of 1.22 ± 0.07 and 1.29 ± 0.05, respectively. The measurements in both cases extend to 10 Bev/c and do not in either case indicate a variation in positive excess with momentum; however, the statistics are not adequate to make this certain. More recently Brode[9] has measured the ratio at sea-level by a method depending on the deflection of charged particles in magnetized iron plates with Geiger counter detection, and has obtained a positive excess of 1.32 ± 0.24. The experimental work of Brode includes mesons between 1 and 2.5 Bev. Adams, Anderson, *et al.*,[1] have reported a very large positive excess at higher altitudes. However, the number of tracks on which this observation was based was inadequate to give much statistical weight to the observation. The present work confirms an increase in positive excess with increasing altitude. Figure 3 shows the momentum spectrum found for both positive and negative particles at 3.4 km as observed under 5 cm of lead. The method of track selection to eliminate electrons has been explained previously. The result gives a positive excess of 1.5 ± 0.05. This result is for mesons of momentum between the magnetic cut-off at 50 Mev/c and the maximum momentum measured of 2.5 Bev/c. Within statistical error no trend in the positive excess with momentum is indicated. It is difficult to understand why the ratio of positive to negative mesons should vary with altitude, and it is certain that the increase above the sea-level value is due in part, and perhaps entirely, to the greater number of protons (which are not distinguished from mesons in determinations of positive excess previously reported) at higher altitudes. As has been indicated, in the present investigation heavily ionizing protons alone were found to constitute 2 percent of all non-electronic charged particles under 5 cm of lead. Including only those particles below 2.5 Bev/c for which the positive excess of 1.5 was found, heavily ionizing protons constitute about 3 percent of all such non-electronic charged particles found. As only heavily ionizing protons (momenta below 500 Mev/c) could be recognized in this investigation, *all* protons at 3.4 km may well constitute

[6] Adams, Anderson, and Cowan, Rev. Mod. Phys. **21**, 73 (1949).

[7] H. Jones, Rev. Mod. Phys. **11**, 235 (1939).
[8] D. J. Hughes, Phys. Rev. **57**, 592 (1940).
[9] R. B. Brode, Phys. Rev. **76**, 468 (1949).

the 8 percent required to give the increase in positive excess from about 1.3 at sea-level to 1.5 at 3.4 km. Statistical uncertainties in both the sea-level and 3.4 km values are such that an even smaller percentage of protons may be adequate to account for the observed difference.

C. Protons

Figure 4 gives the distribution in momentum of heavily ionizing particles, combining those observed under no absorber and under 5 cm of lead. Only those tracks clearly more dense than the general run of tracks were included in the group selected. While this method of selection involves somewhat arbitrary judgment, it was found that different observers agreed almost absolutely on those tracks to be included. In any case, for protons of momenta below 500 Mev/c a mistake can hardly be made. At higher momenta it is probable that all protons have not been included. While the group of heavily ionizing tracks were selected on the basis of density alone, it was later found that all but three corresponded in direction of curvature to a positive particle moving downward; a good indication of the adequacy of the method of selection. The rapid decrease in numbers of protons at lower momenta, as shown in Fig. 4, results from the nature of the apparatus. The cut-off found at about 250 Mev/c represents the minimum momentum necessary for a proton to get from the sensitive volume of the chamber to the sensitive volume of the lower coincidence counter through the intervening absorbing material. Within experimental error the cut-off at 250 Mev/c checks the value to be expected for a proton and the amount of absorbing material present. Among all tracks examined, not a single heavily ionizing particle with a momentum less than 250 Mev/c was found. With increasing momentum the decreasing density of ionization for protons is such that the decrease in numbers above 500 Mev/c, as shown by Fig. 4, is almost certainly due in part to failure to distinguish their tracks from those of mesons. Thus, the form of the distribution (Fig. 4) is strongly influenced at low momenta by absorption cut-off (this occurs above the magnetic cut-off which thus has no effect) and at high momenta by failure to recognize the tracks of protons. Neither of these distortions is important for a momentum band from about 350 to 500 Mev/c between which values it is possible to use this information in estimating proton rates as measured by our apparatus. For protons in this momentum interval it is found that the rate does not change appreciably in passing from the no absorber case to the measurements made under 5 cm of lead. The agreement between the proton rates for the two cases may be in part fortuitous, as under 5 cm of lead there has been both proton absorption and production as compared to the original radiation. On the other hand, the meson intensity in this momentum interval should not be appreciably affected in passage through 5 cm of lead. In this way, by comparing the hourly proton rate as measured under no absorber with the hourly rate for all particles under 5 cm of lead, one finds that for this altitude the number of protons with momenta between 350 and 500 Mev/c is approximately 10 percent of the number of mesons lying in the same momentum interval. From the results obtained under 5 cm of lead and the assumption of no proton production in the lead, computation involving the range momentum relationship shows some 20 percent of the ionizing non-electronic component in the momentum band near 600 Mev/c to be protons. The assumption of no production of protons in the lead is very uncertain and further experimental work is being undertaken in an attempt to determine the proton intensity for this and higher momenta.

The authors wish to express their appreciation to the Climax Molybdenum Company and especially to its general manager, Mr. C. J. Abrams, without whose generous cooperation this investigation could not have been completed. The important contributions of Mr. Don Eng, electronics technician, and Mr. Elmer Wright, instrument maker, of our own staff, are particularly recognized.

Evidence for the Formation of Ce^{139} by an n-γ Reaction*,†

ALFRED J. MOSES AND DON S. MARTIN, JR.
Institute for Atomic Research and the Department of Chemistry, Iowa State College, Ames, Iowa
(Received March 23, 1950)

A radioactivity, found in old samples of pile-irradiated cerium, can be attributed to Ce^{139} (140d) formed by an n-γ process. This activity had a half-life of more than 120 days, and absorption curves indicated it possessed a larger component of x-rays than the more abundant Ce^{141} (28d). The activity followed Ce in chemical separations from La, Ca, Ba, Pb, Fe, and Zn. The ratio of cross sections, $\sigma_{138}/\sigma_{140}$, was estimated to be 1.4.

I. INTRODUCTION

Ce^{139}, which decays by K-capture, has been prepared by deuteron bombardment[1,2] of La, alpha-bombardment[1] of Ba and fission[3] of Bi. Besides the La x-rays the radiation contains a 0.18 Mev gamma, partly converted, and possibly harder radiations of low intensity.[1,2] Although it would be formed by the $n-\gamma$ reaction from Ce^{138} (abundance 0.25 percent), this process has not been previously observed because of the high intensity of radiation from Ce^{141} formed during the neutron irradiation of this element.[4] Ce^{141} has been reported to decay with a 28-day half-life by β-emission with a maximum energy of 0.53 Mev and with a partially converted 0.146 Mev γ-ray accompanying 70 percent of the disintegrations.[5–7]

II. EXPERIMENTAL

It was desired to use for tracer experiments some old samples of cerium activity which had been prepared by neutron irradiation in the Oak Ridge pile for 30 days. As a routine procedure two portions of the activity were mounted for observance of their decay by means of a thin-wall, hydrogen-filled G-M counter tube. One sample was arranged with little absorber so that the major contribution came from beta-particles; the other stronger sample was separated from the counter tube by 270 mg/cm² of Al, sufficient to stop all the betas. Individual counting rates were always compared with that of a U_3O_8 standard sample. A difference in the disintegration periods of the two samples was soon noted and the decay curves followed from 240 to 530 days after irradiation. The results, shown in Fig. 1, indicated that although the β-component decayed exponentially with about a 26-day half-life, the gamma-component contained in addition a long-lived fraction with a half-life greater than 120 days. Consequently the radiation was studied by absorption methods and a number of chemical separations performed in order to establish its identity. The first sample (A) had been formed by a one-month irradiation in the Oak Ridge pile of about one gram of carefully purified Ce metal which had been originally prepared by Dr. F. H. Spedding and co-workers. A similar long-lived activity was also found in a second sample of metal (B) which was irradiated for three months in the Oak Ridge pile. Both samples were employed in the various chemical tests.

Absorption curves for the radiation in Ta, appearing in Fig. 2, offered some information concerning the nature of the gamma-components. The upper curve shows the absorption of a sample of freshly irradiated ceric oxide. There was sufficient aluminum directly in front of the counter tube (225 mg/cm²) to stop completely all Ce^{141} betas. This curve was identical within experimental error to one obtained with sample (A) 203 days after irradiation. The half-thickness of the hard component (410 mg Ta/cm²) was consistent with either the 0.146 and 0.18 Mev gamma-rays of Ce^{141} and Ce^{139}. The original sample however contained a soft component

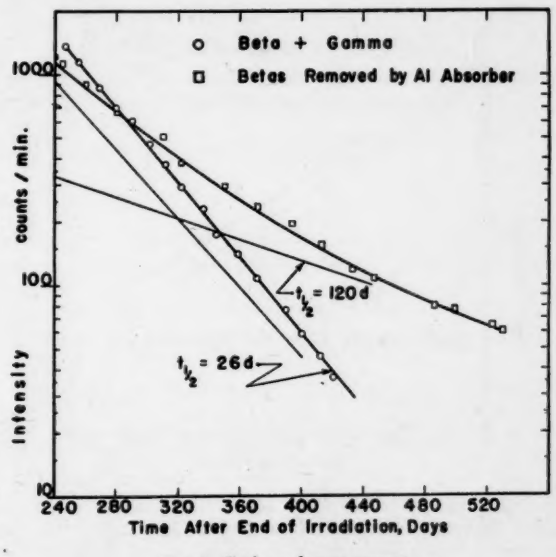

FIG 1. Cerium decay curves.

* This work was performed in the Ames Laboratory of the AEC.

† Contribution No. 93 from the Institute for Atomic Research and the Department of Chemistry, Iowa State College, Ames, Iowa.

[1] M. L. Pool and N. L. Krisberg, Phys. Rev. **73**, 1035 (1948).
[2] J. B. Chubuck and I. Perlman, Phys. Rev. **74**, 982 (1948).
[3] R. H. Soekerman and I. Perlman, Phys. Rev. **73**, 1127 (1948).
[4] G. T. Seaborg and I. Perlman, Rev. Mod. Phys. **20**, 585 (1948).
[5] W. H. Burgus reported in "Plutonium Project Report," CC-680, p. 13 (May, 1943).
[6] L. R. Shepard, Research **1**, 671 (1948).
[7] Ter-Pogossion, Cook, Goddard and Robinson, Phys. Rev. **76**, 909 (1949).

TABLE I. Results of chemical separations.

Series	Sample	Days after irradiation	Element	Percent of activity carried (beta and gamma)
1	*A*	460	La	1.2
			Ce	99.
2	*B*	230	Pb	0.3
			Ca—Ba	0.2
			Ce	99.
3	*B*	290	Fe	5.
			Zn	1.4
			Ce	94.

with half-thickness of 39 mg Ta/cm² which might correspond to a photon of about 34 kev and in agreement with a light rare earth K x-ray. Such an x-ray would not appear in the spectrometer determination of photo-electrons from a uranium foil reported in reference 7. They might arise as a result of internal conversion of the gamma-rays following the Ce^{141} disintegration. The ratio of intensities for the hard to soft component was 1.6. In a similar absorption curve on the same material 363 days after irradiation the ratio of the hard to soft components had decreased to 1.0. Because of the low activity in the sample the line for the hard component was fitted to the data by the least squares method. These results would be consistent with the presence of Ce^{139} which, decaying by electron capture, would emit the lanthanum K x-rays with high intensity.

There remained the necessity of associating the long-lived activity with Ce. A consideration of possible impurities in the metal indicated that the most probable chemical impurities would be other rare earths, alkaline earths from refractory liners, lead, iron, and zinc. A series of chemical separations were performed in which carriers from these groups of elements were added and then separated from the radioactive cerium.[7a] The results of these separations have been tabulated in Table I. In each case the major fraction of the activity followed the cerium. However, all of the separated elements, especially Fe, carried measurable activity. In each case the absorption curves of these activities appeared to be identical with the original Ce activity insofar as could be determined with the intensities at hand. In addition the decay rate of the photon component of radiation from cerium, which had undergone the chemical separations, was compared with that of the untreated cerium. To avoid effects due to changes in counter characteristics, both the separated and unseparated samples were always counted and their ratios computed. (Ratio: $R=(x-b)/(y-b)$ where x is the counting rate of the separated sample, y is the counting rate of the unseparated sample, and b is the background rate.) These ratios have been plotted in Fig. 3, each point

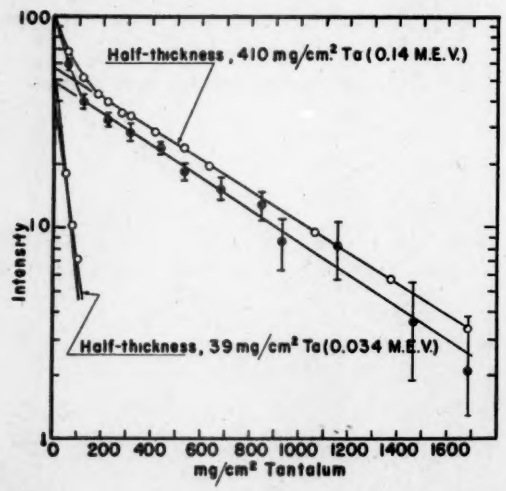

FIG. 2. Absorption curve of cerium photons in tantalum. ○—203 days after end of irradiation (sample *A*). ⊕—363 days after end of irradiation (sample *A*). [270 mg/cm² of Al in front of counter to stop electrons.]

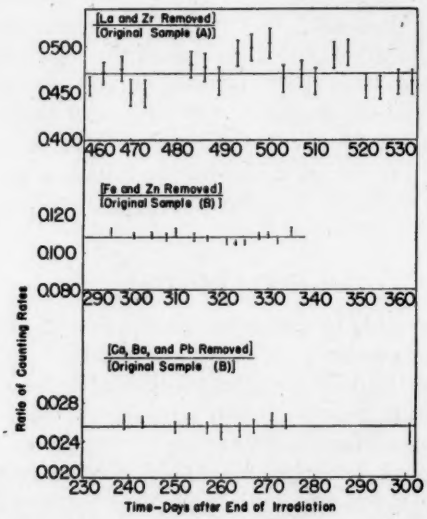

FIG. 3. Ratios of photon counting rates of separated and unseparated cerium samples.

with a width 2σ.

$$\sigma=[(\partial R/\partial x)^2\sigma_x^2+(\partial R/\partial y)^2\sigma_y^2+(\partial R/\partial b)^2\sigma_b^2]^{\frac{1}{2}}.$$

A chi-square determination of the data showed that the ratios did not deviate from a constant value by more

[7a] In the first series the La carrier was separated from Ce by the method of Boldridge and Hume (AECD-2531-C). In this procedure the Ce was oxidized to the tetravalent state and precipitated as $Ce(IO_3)_4$. The La was subsequently precipitated as the oxalate. In the second series Ce was separated from Pb, Ca, and Ba carriers which should also have carried Sr and Ra. Lead was first precipitated as PbI_2. Cerium was precipitated with NH_3 in the presence of NH_4Cl and finally the alkaline earths were precipitated as sulfates. In the third series Fe and Zn carriers were separated from the cerium. Ferric iron was separated by 10 extractions into ether-HCl solution. After evaporation of the solvent, it was precipitated with ammonia, redissolved in HF, and finally precipitated again by ammonia after the removal of HF. Zn was separated by precipitation with H_2S from mixed citrate and formate buffers [H. A. Fales and G. M. Ware, J. Am. Chem. Soc. 41, 487 (1919).].

than would reasonably be expected from statistical fluctuations.

It was estimated from Fig. 1 that at 240 days after irradiation the long-lived activity contributed about one-fourth of the total gamma-count. Even if the chemical separations were only 50 percent efficient so that this contribution was reduced from one-fourth to one-eighth, it was calculated that the counting rate ratios should change by about 20 percent in two months. The absence of such variations in any of the three samples was considered as proof that the long-lived activity was not carried by any of the other elements and must therefore be associated with a cerium isotope.

The evidence for the presence of Ce^{139} consists in: (1) The existence of a half-life of greater than 120 days in the photon component of the irradiated cerium, (2) the greater contributions of soft radiation corresponding to x-rays following K capture in this activity, and (3) the impossibility of separating the activity chemically from cerium, by removal of the most likely impurities.

III. ESTIMATE OF CROSS SECTION RATIO

An estimate of the ratio of cross sections of (Ce^{138}/Ce^{140}) should now be possible from the fact mentioned above, that at 240 days after a 30-day irradiation the counting activity of the long-lived gammas was one-third of that for the short-lived activity which Shepard estimated to occur in 70 percent of the disintegrations of Ce^{141}. Then, estimating the counting efficiency for Ce^{139} radiation to be twice as great as that for Ce^{141} because of the larger fraction of x-rays of about 30 kev energy,[8] the ratio of the disintegration rates 139/141 at this time would be 0.12. Using the half-life values of 140 and 28 days this ratio would have been 1.1×10^{-3} at the end of irradiation. For a 30-day bombardment, and using the isotopic abundances of 0.250 and 88.48 percent given by Ingham, Hayden, and Hess,[9] the ratio of the cross sections was calculated to be: $\sigma(138)/\sigma(140)\approx1.4$.

[8] H. Maier-Liebnitz, Zeits. f. Naturforsch. 1, 243 (1946).
[9] Ingham, Hayden, and Hess, Phys. Rev. 72, 967 (1947).

PHYSICAL REVIEW VOLUME 79, NUMBER 3 AUGUST 1, 1950

Variational Principles for Scattering Processes. I

B. A. LIPPMANN
Nucleonics Division, Naval Research Laboratory, Washington, D. C.

AND

JULIAN SCHWINGER
Harvard University, Cambridge, Massachusetts

(Received April 10, 1950)

A systematic treatment is presented of the application of variational principles to the quantum theory of scattering.

Starting from the time-dependent theory, a pair of variational principles is provided for the approximate calculation of the unitary (collision) operator that describes the connection between the initial and final states of the system. An equivalent formulation of the theory is obtained by expressing the collision operator in terms of an Hermitian (reaction) operator; variational principles for the reaction operator follow. The time-independent theory, including variational principles for the operators now used to describe transitions, emerges from the time-dependent theory by restricting the discusson to stationary states. Specialization to the case of scattering by a central force field establishes the connection with the conventional phase shift analysis and results in a variational principle for the phase shift.

As an illustration, the results of Fermi and Breit on the scattering of slow neutrons by bound protons are deduced by variational methods.

I. INTRODUCTION

ALTHOUGH variational methods have long been applied to eigenvalue problems in many fields of physics, no systematic use had been made of variational procedures in connection with scattering processes until the period 1942–1946 when variational techniques, among others, were extensively employed in the solution of electromagnetic wave guide problems.[1] Variational formulations have also been devised for the treatment of neutron diffusion,[2] acoustical and optical diffraction,[3] and quantum-mechanical scattering problems.[4] Indeed,

[1] "Notes on Lectures by Julian Schwinger: Discontinuities in Waveguides," prepared by David S. Saxon, MIT Radiation Laboratory Report, February 1945.

[2] J. Schwinger, unpublished; R. E. Marshak, Phys. Rev. 71, 688 (1947).

[3] H. Levine and J. Schwinger, Phys. Rev. 74, 958 (1948); 75, 1423 (1949).

[4] J. Schwinger, "Lectures on Nuclear Physics," Harvard University, 1947; J. Schwinger, Phys. Rev. 72, 742 (1947); J. M. Blatt, Phys. Rev. 74, 92 (1948); W. Kohn, Phys. Rev. 74, 1763 (1948); J. M. Blatt and J. D. Jackson, Phys. Rev. 76, 18 (1949). Variational principles for scattering problems have also been independently developed by L. Hulthén, see Mott and Massey, *The Theory of Atomic Collisions* (Oxford University Press, London, 1949), 2nd ed., p. 128, and I. Tamm, J. Exp. Theor. Phys. USSR 18, 337 (1948); 19, 74 (1949).

such methods are applicable in any branch of physics where the fundamental equations can be derived from an extremum principle.

It is the purpose of this paper to describe the quantum mechanical time-dependent scattering theory and its variational reformulation. As a simple illustration of these methods, we consider the scattering of slow neutrons by protons bound in a molecule. This was first discussed by Fermi[5] in terms of an equivalent potential used in conjunction with the Born approximation. A more exact integral equation treatment was given by Breit,[6] with quite small ensuing corrections[7] to Fermi's theory. We shall show that the results of Fermi and Breit are easily derived from a variational treatment. Although one could consider, without difficulty, the scattering by any number of nuclei, the discussion will be restricted to the spin-dependent scattering by a single proton in an otherwise inert molecule of arbitrary mass. An extension to two protons, and in particular to the hydrogen molecule, is contained in an accompanying paper by one of us. Also included is an estimate of the error in the para-hydrogen scattering cross section calculated by Fermi's method.

II. TIME-DEPENDENT SCATTERING THEORY

We are concerned with the development in time of a system consisting of two interacting parts, which are such that the interaction energy approaches zero as the two parts are separated spatially. Correspondingly, the Hamiltonian is decomposed into the unperturbed Hamiltonian H_0, describing the two independent parts, and H_1, the energy of interaction. Since the problem is to describe the effect of H_1, it is convenient to remove the time dependence associated with H_0 from the Schrodinger equation

$$i\hbar[\partial\Psi'(t)/\partial t]=(H_0+H_1)\Psi'(t). \tag{1.1}$$

This is accomplished by the unitary transformation

$$\Psi'(t)=\exp(-iH_0t/\hbar)\Psi(t) \tag{1.2}$$

which yields

$$\begin{aligned} &i\hbar[\partial\Psi(t)/\partial t]=H_1(t)\Psi(t), \\ &H_1(t)=\exp(iH_0t/\hbar)H_1\exp(-iH_0t/\hbar). \end{aligned} \tag{1.3}$$

The initially non-interacting parts of the system are characterized by the state vector $\Psi(-\infty)$. On following the course of the interaction and the eventual separation of the two parts, we are led to the state vector $\Psi(+\infty)$, representing the final state of the system. This description can be made independent of the particular initial state by regarding the time development as the unfolding of a unitary transformation:

$$\Psi(t)=U_+(t)\Psi(-\infty), \tag{1.4}$$

In particular,

$$\Psi(\infty)=S\Psi(-\infty), \quad S=U_+(\infty) \tag{1.5}$$

defines the collision operator, which generates the final state of the system from an arbitrary initial state. The operator $U_+(t)$ is to be obtained as the solution of the differential equation

$$i\hbar[\partial U_+(t)/\partial t]=H_1(t)U_+(t) \tag{1.6}$$

subject to the boundary condition

$$U_+(-\infty)=1. \tag{1.7}$$

It is also useful to introduce a unitary operator $U_-(t)$, which generates the state vector $\Psi(t)$ from the final state $\Psi(\infty)$,

$$\Psi(t)=U_-(t)\Psi(\infty)=U_-(t)S\Psi(-\infty). \tag{1.8}$$

Since the two operators are related by

$$U_+(t)=U_-(t)S \tag{1.9}$$

the operator $U_-(t)$ is evidently the solution of the equations

$$i\hbar[\partial U_-(t)/\partial t]=H_1(t)U_-(t), \quad U_-(\infty)=1. \tag{1.10}$$

Furthermore,

$$U_-(-\infty)=S^{-1} \tag{1.11}$$

which is the operator generating the initial state vector from the final state vector.

The differential equation for $U_+(t)$ can be replaced by the integral equation

$$\begin{aligned} U_+(t)&=1-(i/\hbar)\int_{-\infty}^{t}H_1(t')U_+(t')dt' \\ &=1-(i/\hbar)\int_{-\infty}^{\infty}\eta(t-t')H_1(t')U_+(t')dt' \end{aligned} \tag{1.12}$$

which incorporates the boundary condition (1.7). Here

$$\begin{aligned} \eta(t-t')&=1; \quad t>t'. \\ &=0; \quad t<t'. \end{aligned} \tag{1.13}$$

Similarly, $U_-(t)$ obeys the integral equation

$$\begin{aligned} U_-(t)&=1+(i/\hbar)\int_{t}^{\infty}H_1(t')U_-(t')dt' \\ &=1+(i/\hbar)\int_{-\infty}^{\infty}dt'H_1(t')U_-(t')\eta(t'-t). \end{aligned} \tag{1.14}$$

By considering the limit as $t\to\infty$ in (1.12) and $t\to-\infty$ in (1.14), we obtain

$$S=1-(i/\hbar)\int_{-\infty}^{\infty}H_1(t)U_+(t)dt \tag{1.15}$$

[5] E. Fermi, Ricerca Scient. VII-II, 13 (1936).
[6] G. Breit, Phys. Rev. 71, 215 (1947).
[7] G. Breit and P. R. Zilsel, Phys. Rev. 71, 232, 240 (1947); Breit, Zilsel, and Darling, Phys. Rev. 72, 576 (1947).

and

$$S^{-1}=1+(i/\hbar)\int_{-\infty}^{\infty}H_1(t)U_-(t)dt \qquad (1.16)$$

which are, of course, connected by (1.9).

The differential and integral equations characterizing $U_+(t)$ and $U_-(t)$ will now be replaced by equivalent variational principles from which the fundamental equations are obtained as conditions expressing the stationary property of a suitable expression. Furthermore, the stationary value of this quantity is just S, the collision operator. Hence the variational formulation of the problem also yields a practical means of approximate calculation, since errors in the construction of S will be minimized by employing a stationary expression.

We first consider

$$'S'=U_+(\infty)-\int_{-\infty}^{\infty}U_-{}^+(t)\left(\frac{\partial}{\partial t}+\frac{i}{\hbar}H_1(t)\right)U_+(t)dt, \qquad (1.17)$$

which is regarded as a function of the operator $U_+(t)$, subject only to the restriction (1.7), and of the Hermitian conjugate of the arbitrary operator $U_-(t)$. The change induced in $'S'$ by small, independent, variations of U_+ and U_- is

$$\begin{aligned}\delta'S'=&(1-U_-(\infty))^+\delta U_+(\infty)\\&-\int_{-\infty}^{\infty}\delta U_-{}^+(t)\left(\frac{\partial}{\partial t}+\frac{i}{\hbar}H_1(t)\right)U_+(t)dt\\&+\int_{-\infty}^{\infty}\left[\left(\frac{\partial}{\partial t}+\frac{i}{\hbar}H_1(t)\right)U_-(t)\right]^+\delta U_+(t)dt. \qquad (1.18)\end{aligned}$$

The requirement that $'S'$ be stationary with respect to arbitrary variations of U_+ and U_-, apart from the restriction (1.7), thus leads to the differential equations (1.6), (1.10) and the boundary condition (1.10) for $U_-(t)$. It is also evident from (1.17) that the stationary value of $'S'$ is the collision operator S, according to (1.5). A somewhat more symmetrical version of (1.17) is

$$\begin{aligned}'S'=&\tfrac{1}{2}(U_+(\infty)+U_-{}^+(-\infty))\\&-\int_{-\infty}^{\infty}\left[\frac{1}{2}U_-{}^+(t)\frac{\partial U_+(t)}{\partial t}-\frac{1}{2}\frac{\partial U_-{}^+(t)}{\partial t}U_+(t)\right.\\&\left.+\frac{i}{\hbar}U_-{}^+(t)H_1(t)U_+(t)\right]dt \qquad (1.19)\end{aligned}$$

subject to the restrictions

$$U_+(-\infty)=U_-(\infty)=1. \qquad (1.20)$$

It is easily verified that $'S'$ is stationary with respect to variations of U_+ and U_- about the solutions of the differential equations (1.6) and (1.10), subject to the boundary conditions (1.20), and that the stationary value of $'S'$ is S.

A variational basis for the integral equations (1.12) and (1.14) is provided by the expression

$$\begin{aligned}'S'=&1-\frac{i}{\hbar}\int_{-\infty}^{\infty}[U_-{}^+(t)H_1(t)+H_1(t)U_+(t)]dt\\&+\frac{i}{\hbar}\int_{-\infty}^{\infty}U_-{}^+(t)H_1(t)U_+(t)dt\\&+\left(\frac{i}{\hbar}\right)^2\int_{-\infty}^{\infty}\int_{-\infty}^{\infty}U_-{}^+(t)H_1(t)\eta(t-t')\\&\times H_1(t')U_+(t')dtdt'. \qquad (1.21)\end{aligned}$$

Thus,

$$\begin{aligned}\delta'S'=&\frac{i}{\hbar}\int_{-\infty}^{\infty}dt\delta U_-{}^+(t)H_1(t)\left[U_+(t)-1\right.\\&\left.+\frac{i}{\hbar}\int_{-\infty}^{\infty}\eta(t-t')H_1(t')U_+(t')dt'\right]\\&+\frac{i}{\hbar}\int_{-\infty}^{\infty}dt\left[U_-(t)-1-\frac{i}{\hbar}\int_{-\infty}^{\infty}dt'H_1(t')\right.\\&\left.\times U_-(t')\eta(t'-t)\right]^+H_1(t)\delta U_+(t), \qquad (1.22)\end{aligned}$$

which is indeed zero if U_+ and U_- satisfy their defining integral equations. It is also evident that the stationary value of $'S'$ is just the collision operator, in the form (1.15).

This variational principle differs from (1.17), or (1.19), in that no restrictions are imposed on U_+ and U_-, and that every integral contains the interaction operator H_1. The latter property implies that an adequate approximation to U_+ and U_- is required only during the actual process of interaction. Furthermore, the second type of variational principle will yield more accurate results than the first if the same approximate operators U_+ and U_- are employed. This is indicated by the results of inserting the simple but crude approximation

$$U_+(t)=U_-(t)=1 \qquad (1.23)$$

in (1.17) and (1.21). The former yields

$$S\simeq 1-(i/\hbar)\int_{-\infty}^{\infty}H_1(t)dt \qquad (1.24)$$

which is equivalent to the first Born approximation, while (1.21) gives

$$\begin{aligned}S\simeq&1-(i/\hbar)\int_{-\infty}^{\infty}H_1(t)dt+(i/\hbar)^2\int_{-\infty}^{\infty}\int_{-\infty}^{\infty}H_1(t)\\&\times\eta(t-t')H_1(t')dtdt' \qquad (1.25)\end{aligned}$$

the second Born approximation.

These approximate expressions for S illustrate a disadvantage of the variational principles thus far discussed; the unitary property is not guaranteed for an inexact S. It follows from (1.24), for example, that

$$S^+S \simeq 1+(1/\hbar^2)\left(\int_{-\infty}^{\infty} H_1(t)dt\right)^2. \tag{1.26}$$

A version of the theory that meets this objection is obtained on replacing the unitary operators $U_+(t)$ and $U_-(t)$ by

$$V(t)=U_+(t)2/(1+S)=U_-(t)2/(1+S^{-1}). \tag{1.27}$$

Note that

$$\begin{aligned} V(-\infty)&=2/(1+S);\\ V(\infty)&=2/(1+S^{-1})=2S/(1+S), \end{aligned} \tag{1.28}$$

whence

$$\tfrac{1}{2}(V(\infty)+V(-\infty))=1 \tag{1.29}$$

and

$$V(\infty)=V^+(-\infty). \tag{1.30}$$

The property (1.29) leads us to write

$$V(\infty)=1-\tfrac{1}{2}iK; \quad V(-\infty)=1+\tfrac{1}{2}iK \tag{1.31}$$

while (1.30) supplies the information

$$K^+=K \tag{1.32}$$

the so-called reaction operator K is Hermitian. On remarking that

$$S=V(\infty)/V(-\infty) \tag{1.33}$$

we obtain

$$S=(1-\tfrac{1}{2}iK)/(1+\tfrac{1}{2}iK) \tag{1.34}$$

which represents the unitary S in terms of the Hermitian K. We shall now construct a variational principle for K in which the Hermitian property is assured.

Consider the operator $'K'$, defined by

$$\begin{aligned} 'K'=-\frac{i}{2}\int_{-\infty}^{\infty}&\left(V^+(t)\frac{\partial V(t)}{\partial t}-\frac{\partial V^+(t)}{\partial t}V(t)\right)dt\\ &+\frac{1}{\hbar}\int_{-\infty}^{\infty}V^+(t)H_1(t)V(t)dt\\ &+\frac{i}{2}[(V(\infty)-V(-\infty))\\ &-(V^+(\infty)-V^+(-\infty))] \end{aligned} \tag{1.35}$$

which is evidently Hermitian for arbitrary $V(t)$. The effect of a small variation in $V(t)$ and $V^+(t)$ is indicated by

$$\begin{aligned} \delta'K'=-\frac{1}{\hbar}\int_{-\infty}^{\infty}&\left[\delta V^+(t)\left(i\hbar\frac{\partial}{\partial t}-H_1(t)\right)V(t)\right.\\ &\left.+\left[\left(i\hbar\frac{\partial}{\partial t}-H_1(t)\right)V(t)\right]^+\delta V(t)\right]dt\\ &-\frac{i}{2}\left[(V^+(\infty)-V^+(-\infty))\delta\left(\frac{V(\infty)+V(-\infty)}{2}\right)\right.\\ &+\left(\frac{V^+(\infty)+V^+(-\infty)}{2}-1\right)\delta(V(\infty)-V(-\infty))\\ &-\delta\left(\frac{V^+(\infty)+V^+(-\infty)}{2}\right)(V(\infty)-V(-\infty))\\ &-\delta(V^+(\infty)-V^+(-\infty))\\ &\left.\times\left(\frac{V(\infty)+V(-\infty)}{2}-1\right)\right]. \end{aligned} \tag{1.36}$$

If, therefore, $V(t)$ is restricted by the mixed boundary condition (1.29), $'K'$ is stationary with respect to variations about the solution of the differential equation

$$\left(i\hbar\frac{\partial}{\partial t}-H_1(t)\right)V(t)=0 \tag{1.37}$$

and the stationary value of $'K'$ equals K, according to (1.31) and (1.32).

The integral equation satisfied by $V(t)$ can be constructed from that obeyed by $U_+(t)$, or directly in the following manner. On integrating the differential equation (1.37) from $-\infty$ to t, and from ∞ to t, we obtain

$$\begin{aligned} V(t)&=V(-\infty)-\frac{i}{\hbar}\int_{-\infty}^{t}H_1(t')V(t')dt',\\ V(t)&=V(\infty)+\frac{i}{\hbar}\int_{t}^{\infty}H_1(t')V(t')dt' \end{aligned} \tag{1.38}$$

The addition of these equations yields, in consequence of the boundary condition (1.29),

$$V(t)=1-\frac{i}{2\hbar}\int_{-\infty}^{\infty}\epsilon(t-t')H_1(t')V(t')dt' \tag{1.39}$$

where

$$\begin{aligned} \epsilon(t-t')&=1; \quad t>t'.\\ &=-1; \quad t<t'. \end{aligned} \tag{1.40}$$

Conversely, the differential equation and boundary condition obeyed by $V(t)$ can be deduced from the integral equation. Note also that

$$K=i(V(\infty)-V(-\infty))=\frac{1}{\hbar}\int_{-\infty}^{\infty}H_1(t)V(t)dt. \tag{1.41}$$

A variational principal formulation of this integral equation is provided by the expression

$$'K'=\frac{1}{h}\int_{-\infty}^{\infty}(H_1(t)V(t)+V^+(t)H_1(t))dt$$
$$-\frac{1}{h}\int_{-\infty}^{\infty}V^+(t)H_1(t)V(t)dt$$
$$-\frac{i}{2h^2}\int_{-\infty}^{\infty}\int_{-\infty}^{\infty}V^+(t)H_1(t)\epsilon(t-t')H_1(t')\times V(t')dtdt' \quad (1.42)$$

which is obviously Hermitian for arbitrary $V(t)$. Now

$$\delta'K'=-\frac{1}{h}\int_{-\infty}^{\infty}\delta V^+(t)H_1(t)\Big[V(t)-1$$
$$+\frac{i}{2h}\int_{-\infty}^{\infty}\epsilon(t-t')H_1(t')V(t')dt'\Big]dt$$
$$-\frac{1}{h}\int_{-\infty}^{\infty}\Big[V(t)-1+\frac{i}{2h}\int_{-\infty}^{\infty}\epsilon(t-t')H_1(t')\times V(t')dt'\Big]+H_1(t)\delta V(t)dt \quad (1.43)$$

which is indeed zero if $V(t)$ satisfies the integral equation (1.39). Furthermore, the stationary value of $'K'$ is just (1.41), the correct reactor operator.

The abstract theory thus far developed can be made more explicit by introducing eigenfunctions, Φ_a, for the separated parts of the system, which will describe the initial and final states. Thus, since $S\Phi_a$ is the final state that emergies from the initial state Φ_a, the probability that the system will be found eventually in the particular state Φ_b, is

$$W_{ba}=|(\Phi_b, S\Phi_a)|^2=|S_{ba}|^2. \quad (1.44)$$

It is slightly more convenient to deal with the operator

$$T=S-1, \quad (1.45)$$

which generates the change in the state vector produced by the interaction process. The unitary property of S implies that

$$T^+T=-(T+T^+) \quad (1.46)$$

and the probability that the system will be found in a particular final state differing from the initial one is

$$b\neq a; \quad W_{ba}=|T_{ba}|^2. \quad (1.47)$$

Now, according to (1.15),

$$T_{ba}=-(i/\hbar)\int_{-\infty}^{\infty}dt(\Phi_b, H_1(t)U_+(t)\Phi_a),$$
$$=-(i/\hbar)\int_{-\infty}^{\infty}dt(\Phi_b, \exp(iH_0t/\hbar)H_1\times\exp(-iH_0t/\hbar)U_+(t)\Phi_a). \quad (1.48)$$

It should be noted that Φ_b cannot be an exact eigenfunction of H_0, since a superposition of momentum states (wave packet) is required to produce the spatial localizability involved in the definite separation of the two parts of the system. An equivalent description is obtained, however, by introducing eigenfunctions of H_0,

$$H_0\Phi_b=E_b\Phi_b \quad (1.49)$$

and simulating the cessation of interaction, arising from the separation of the component parts of the system, by an adiabatic decrease in the interaction strength as $t\to\pm\infty$. The latter can be represented by the factor $\exp(-\epsilon|t|/\hbar)$ where ϵ is arbitrarily small. Accordingly, (1.48) becomes

$$T_{ba}=-(i/\hbar)(\Phi_b, H_1\Psi_a^{(+)}(E_b)) \quad (1.50)$$

where

$$\Psi_a^{(+)}(E)=\int_{-\infty}^{\infty}dt\exp(i(E-H_0)t/\hbar)\times\exp(-\epsilon|t|/\hbar)U_+(t)\Phi_a. \quad (1.51)$$

Formula (1.16) for $S^{-1}-1=T^+$ leads, in a similar way, to

$$(T^+)_{ba}=(i/\hbar)(\Phi_b, H_1\Psi_a^{(-)}(E_b)) \quad (1.52)$$

or equivalently,

$$T_{ab}=-(i/\hbar)(\Psi_a^{(-)}(E_b), H_1\Phi_b) \quad (1.53)$$

in which

$$\Psi_a^{(-)}(E)=\int_{-\infty}^{\infty}dt\exp(i(E-H_0)t/\hbar)\times\exp(-\epsilon|t|/\hbar)U_-(t)\Phi_a. \quad (1.54)$$

Determining equations for $\Psi_a^{(+)}(E)$ and $\Psi_a^{(-)}(E)$ can be obtained from (1.12) and (1.14), the integral equations for $U_+(t)$ and $U_-(t)$. Thus

$$\Psi_a^{(+)}(E)=\int_{-\infty}^{\infty}dt\exp(i(E-E_a)t/\hbar)\exp(-\epsilon|t|/\hbar)\Phi_a$$
$$-(i/\hbar)\int_0^{\infty}d\tau\exp(i(E-H_0)\tau/\hbar)\times\exp(-\epsilon\tau/\hbar)H_1\Psi_a^{(+)}(E) \quad (1.55)$$

and

$$\Psi_a^{(-)}(E)=\int_{-\infty}^{\infty}dt\exp(i(E-E_a)t/\hbar)\exp(-\epsilon|t|/\hbar)\Phi_a$$
$$+(i/\hbar)\int_0^{\infty}d\tau\exp(-i(E-H_0)\tau/\hbar)\times\exp(-\epsilon\tau/\hbar)H_1\Psi_a^{(-)}(E), \quad (1.56)$$

where $\tau=|t-t'|$. Now

$$\mp\frac{i}{\hbar}\int_0^\infty d\tau\,\exp(\pm i(E-H_0)\tau/\hbar)\exp(-\epsilon\tau/\hbar)$$

$$=\frac{1}{E\pm i\epsilon-H_0}=\frac{E-H_0}{(E-H_0)^2+\epsilon^2}\mp i\frac{\epsilon}{(E-H_0)^2+\epsilon^2}$$

$$=P\frac{1}{E-H_0}\mp i\pi\delta(E-H_0). \quad (1.57)$$

The last expression is a symbolic statement of the following integral properties possessed by the real and imaginary parts of (1.57) in the limit as $\epsilon\to 0$.

$$\begin{aligned}\operatorname*{Lim}_{\epsilon\to 0}\int_{-\infty}^{\infty}\frac{x}{x^2+\epsilon^2}f(x)dx&=P\int_{-\infty}^{\infty}\frac{f(x)}{x}dx,\\ \operatorname*{Lim}_{\epsilon\to 0}\frac{1}{\pi}\int_{-\infty}^{\infty}\frac{\epsilon}{x^2+\epsilon^2}f(x)dx&=f(0),\end{aligned} \quad (1.58)$$

where P denotes the principal part of the integral and $f(x)$ is an arbitrary function. Therefore

$$\Psi_a^{(\pm)}(E)=2\pi\hbar\delta(E-E_a)\Phi_a+\frac{1}{E\pm i\epsilon-H_0}H_1\Psi_a^{(\pm)}(E) \quad (1.59)$$

and, on writing

$$\Psi_a^{(\pm)}(E)=2\pi\hbar\delta(E-E_a)\Psi_a^{(\pm)} \quad (1.60)$$

we obtain

$$\Psi_a^{(\pm)}=\Phi_a+\frac{1}{E_a\pm i\epsilon-H_0}H_1\Psi_a^{(\pm)}. \quad (1.61)$$

These equations provide a time-independent formulation of the scattering problem, in which the small positive or negative imaginary addition to the energy serves to select, automatically, outgoing or incoming scattered waves.

A matrix element of the operator T can now be expressed as

$$T_{ba}=-2\pi i\delta(E_a-E_b)\mathbf{T}_{ba} \quad (1.62)$$

where

$$\mathbf{T}_{ba}=(\Phi_b, H_1\Psi_a^{(+)})=(\Psi_b^{(-)}, H_1\Phi_a) \quad (1.63)$$

are equivalent forms for an element of the association matrix $\mathbf{T}$, which is defined only for states of equal energy. The resulting formula for the transition probability,

$$W_{ba}=4\pi^2[\delta(E_a-E_b)]^2|\mathbf{T}_{ba}|^2 \quad (1.64)$$

is to be interpreted by replacing one factor, $\delta(E_a-E_b)$, by its defining time integral

$$\delta(E_a-E_b)=\frac{1}{2\pi\hbar}\int_{-\infty}^{\infty}\exp(i/(E_a-E_b)t/\hbar)\times\exp(-\epsilon|t|/\hbar)dt;\quad \epsilon\to 0 \quad (1.65)$$

in which E_a-E_b must be placed equal to zero, in view of the second delta-function factor. The expression thus obtained

$$W_{ba}=\frac{2\pi}{\hbar}\delta(E_a-E_b)|\mathbf{T}_{ba}|^2\int_{-\infty}^{\infty}dt, \quad (1.66)$$

evidently describes the fact that transitions occur only between states of equal energy for the separated system, and with an intensity proportional to the total time of effective interaction. In the idealized limit $\epsilon\to 0$, the latter is infinitely large. However, we infer from (1.66) that the rate at which the transition probability increases is

$$w_{ba}=(2\pi/\hbar)\delta(E_a-E_b)|\mathbf{T}_{ba}|^2. \quad (1.67)$$

A somewhat more satisfactory derivation of this result follows from the evaluation of

$$w_{ba}=\frac{\partial}{\partial t}|(\Phi_b, U_+(t)\Phi_a)|^2 \quad (1.68)$$

which expresses the increase, per unit time, of the probability that the system, known to be initially in the state a, will be found at time t in the state b. Now

$$w_{ba}=\frac{i}{\hbar}(H_1(t)U_+(t)\Phi_a, \Phi_b)\times(\Phi_b, U_+(t)\Phi_a)+\text{complex conjugate}$$

$$=\frac{1}{\hbar^2}\int_{-\infty}^{t}dt'(\exp(i/(E_b-H_0)t/\hbar)U_+(t)\Phi_a, H_1\Phi_b)\times(\Phi_b, H_1\exp(i(E_b-H_0)t'/\hbar)\times U_+(t')\Phi_a)+\text{c.c.} \quad (1.69)$$

in which we have employed (1.12), and assumed that $b\neq a$. This can be simplified by noting that (1.51) and (1.60),

$$\int_{-\infty}^{\infty}dt\,\exp(i(E-H_0)t/\hbar)\exp(-\epsilon|t|/\hbar)U_+(t)\Phi_a=2\pi\hbar\delta(E-E_a)\Psi_a^{(+)} \quad (1.70)$$

imply that

$$\exp(-iH_0t/\hbar)U_+(t)\Phi_a=\exp(-iE_at/\hbar)\Psi_a^{(+)} \quad (1.71)$$

which is just the state vector, in the Schrödinger representation, of our idealized stationary state. Hence

$$w_{ba}=\frac{1}{\hbar^2}|\mathbf{T}_{ba}|^2\int_{-\infty}^{t}\exp(i(E_a-E_b)(t-t')/\hbar)dt'+\text{c.c.}$$

$$=\frac{2\pi}{\hbar}|\mathbf{T}_{ba}|^2\delta(E_a-E_b). \quad (1.72)$$

A simple expression for the total rate of transition from the initial state follows from the general property

of the operator T contained in (1.46). On writing a matrix element of this operator relation and substituting (1.62), we obtain

$$4\pi^2 \sum_b \delta(E_a-E_b)\mathbf{T}_{ba}{}^*\delta(E_b-E_c)\mathbf{T}_{bc} = 2\pi i\delta(E_a-E_c)(\mathbf{T}_{ac}-\mathbf{T}_{ca}{}^*). \quad (1.73)$$

The factor $\delta(E_a-E_c)$ can be canceled and (1.73) then yields, for the special situation, $c=a$,

$$4\pi^2 \sum_b \delta(E_a-E_b)|\mathbf{T}_{ba}|^2 = -4\pi Im(\mathbf{T}_{aa}) \quad (1.74)$$

or

$$\sum_b w_{ba} = -(2/\hbar)\, Im(\mathbf{T}_{aa}). \quad (1.75)$$

The left side of this formula is not exactly the total rate of transition out of the state a, since $b=a$ is included in the summation. However, a single state makes no contribution to such a summation; a group of states is required. A relation of the type (75) is characteristic of a wave theory, in which the reduction in intensity of a plane wave passing through a scattering medium is accounted for by destructive interference between the original wave and the secondary waves scattered in the direction of propagation.

A variational formulation of Eq. (1.61) by means of a stationary expression for $\mathbf{T}_{ba}$ can be obtained from the variational principle (1.21). A matrix element of this operator equation reads

$$\begin{aligned}
{}'T'_{ba} = &-\frac{i}{\hbar}\int_{-\infty}^{\infty} dt[(\exp(i(E_a-H_0)t/\hbar)U_-(t)\Phi_b, H_1\Phi_a) \\
&+(\Phi_b, H_1\exp(i(E_b-H_0)t/\hbar)U_+(t)\Phi_a)] \\
&+\frac{i}{\hbar}\int_{-\infty}^{\infty} dt(\exp(-iH_0t/\hbar)U_-(t)\Phi_b, \\
&\qquad \times H_1\exp(-iH_0t/\hbar)U_+(t)\Phi_a) \\
&+\left(\frac{i}{\hbar}\right)^2\int_{-\infty}^{\infty} dt\int_{-\infty}^{t} dt'(\exp(-iH_0t/\hbar)U_-(t)\Phi_b, \\
&\times H_1\exp(-iH_0(t-t')/\hbar) \\
&\qquad \times H_1\exp(-iH_0t'/\hbar)U_+(t')\Phi_a) \quad (1.76)
\end{aligned}$$

in which the adiabatic reduction of H_1 for large $|t|$ has not been indicated explicitly. We now restrict ourselves to the class of stationary states, according to the assumption

$$\exp(-iH_0t/\hbar)U_\pm(t)\Phi_a = \exp(-iE_at/\hbar)\Psi_a{}^{(\pm)}. \quad (1.77)$$

The result of performing the time integrations is expressed by

$$\begin{aligned}
{}'\mathbf{T}'_{ba} = &(\Psi_b{}^{(-)}, H_1\Phi_a)+(\Phi_b, H_1\Psi_a{}^{(+)}) \\
&-(\Psi_b{}^{(-)}, H_1\Psi_a{}^{(+)}) \\
&+\left(\Psi_b{}^{(-)}, H_1\frac{1}{E+i\epsilon-H_0}H_1\Psi_a{}^{(+)}\right), \quad (1.78)
\end{aligned}$$

where E is the common energy of states a and b. We shall verify directly that (1.78) has the required properties. Thus

$$\begin{aligned}
\delta{}'\mathbf{T}'_{ba} = &\left(\delta\Psi_b{}^{(-)}, H_1\left(\Phi_a+\frac{1}{E+i\epsilon-H_0}H_1\Psi_a{}^{(+)}\right.\right. \\
&\left.\left.-\Psi_a{}^{(+)}\right)\right)+\left(\left(\Phi_b+\frac{1}{E-i\epsilon-H_0}H_1\Psi_b{}^{(-)}\right.\right. \\
&\left.\left.-\Psi_b{}^{(-)}\right), H_1\delta\Psi_a{}^{(+)}\right) \quad (1.79)
\end{aligned}$$

which is indeed zero for variations about the solutions of (1.61). Furthermore, it is a consequence of the latter equations that

$$\begin{aligned}
&(\Psi_b{}^{(-)}, H_1\Psi_a{}^{(+)})-\left(\Psi_b{}^{(-)}, H_1\frac{1}{E+i\epsilon-H_0}H_1\Psi_a{}^{(+)}\right) \\
&\qquad = (\Psi_b{}^{(-)}, H_1\Phi_a) = (\Phi_b, H_1\Psi_a{}^{(+)}) \quad (1.80)
\end{aligned}$$

so that the stationary value of ${}'\mathbf{T}'_{ba}$ is $\mathbf{T}_{ba}$, according to (1.63).

A similar theory can be developed for the matrix elements of the operator K. It is easily shown that

$$K_{ba} = 2\pi\delta(E_a-E_b)\mathbf{K}_{ba}, \quad (1.81)$$

where

$$\mathbf{K}_{ba} = (\Phi_b, H_1\Psi_a{}^{(1)}) = (\Psi_b{}^{(1)}, H_1\Phi_a). \quad (1.82)$$

The time-independent state vector $\Psi_a{}^{(1)}$ describes a stationary state, according to the relation

$$\exp(-iH_0t/\hbar)V(t)\Phi_a = \exp(-iE_at/\hbar)\Psi_a{}^{(1)} \quad (1.83)$$

and obeys the equation

$$\Psi_a{}^{(1)} = \Phi_a+P\left(\frac{1}{E_a-H_0}\right)H_1\Psi_a{}^{(1)}. \quad (1.84)$$

A variational basis for (1.82) and (1.84) is provided by

$$\begin{aligned}
{}'K'_{ba} = {}'K'_{ab}{}^* = &(\Psi_b{}^{(1)}, H_1\Phi_a) \\
&+(\Phi_b, H_1\Psi_a{}^{(1)})-(\Psi_b{}^{(1)}, H_1\Psi_a{}^{(1)}) \\
&+\left(\Psi_b{}^{(1)}, H_1P\left(\frac{1}{E-H_0}\right)H_1\Psi_a{}^{(1)}\right). \quad (1.85)
\end{aligned}$$

The connection between the matrices $\mathbf{T}$ and $\mathbf{K}$ is obtained from

$$T = S-1 = -iK/(1+\tfrac{1}{2}iK) \quad (1.86)$$

on rewriting the latter as

$$T+\tfrac{1}{2}iKT = -iK. \quad (1.87)$$

Non-vanishing matrix elements of this operator relation are restricted to states of equal energy, according to

(1.62) and (1.81), whence

$$\mathbf{T}_{ba}+i\pi\sum_c \mathbf{K}_{bc}\delta(E_c-E)\mathbf{T}_{ca}=\mathbf{K}_{ba}, \quad (1.88)$$

where E is the common energy states a and b. An effective way to solve this equation is to construct the eigenfunctions of $\mathbf{K}$, which are defined by the eigenvalue equation

$$\sum_a \mathbf{K}_{ba}\delta(E_a-E)f_{aA}=\mathbf{K}_A f_{bA}. \quad (1.89)$$

Since $\mathbf{K}$ is an Hermitian matrix, the eigenvalues $\mathbf{K}_A$ are real, the eigenfunctions f_{aA} are orthogonal, and may be normalized according to

$$\sum_a f_{aA}{}^*\delta(E_a-E)f_{aB}=\delta_{AB}. \quad (1.90)$$

The matrix elements of $\mathbf{K}$ can be exhibited in terms of the eigenfunctions and eigenvalues of $\mathbf{K}$

$$\mathbf{K}_{ba}=\sum_A f_{bA}\mathbf{K}_A f_{aA}{}^*. \quad (1.91)$$

Equation (1.88) for $\mathbf{T}$ will then be satisfied by

$$\mathbf{T}_{ba}=\sum_A f_{bA}\mathbf{T}_A f_{aA}{}^*, \quad (1.92)$$

where

$$\mathbf{T}_A+i\pi\mathbf{K}_A\mathbf{T}_A=\mathbf{K}_A \quad (1.93)$$

or

$$\mathbf{T}_A=\mathbf{K}_A/(1+i\pi\mathbf{K}_A). \quad (1.94)$$

This is only to say that $\mathbf{T}$ is a function of $\mathbf{K}$ and therefore possesses the same eigenfunctions, while its eigenvalues are determined by those of $\mathbf{K}$. These eigenvalues can be conveniently expressed by introducing the real angles δ_A, according to

$$\mathbf{K}_A=-(1/\pi)\tan\delta_A \quad (1.95)$$

so that

$$\mathbf{T}_A=-(1/\pi)\sin\delta_A e^{i\delta_A}. \quad (1.96)$$

The resulting expression for the transition probability per unit time is

$$w_{ba}=(2/\pi\hbar)|\sum_A \sin\delta_A e^{i\delta_A}f_{bA}f_{aA}{}^*|^2\delta(E_a-E_b) \quad (1.97)$$

and the total probability per unit time for transitions from a particular state is given by

$$\sum_b w_{ba}=(2/\pi\hbar)\sum_A \sin^2\delta_A|f_{aA}|^2 \quad (1.98)$$

according to (1.97) or (1.75). Finally, the sum of the total transition probability per unit time over all initial states of the same energy is expressed by

$$\sum_{b,a} w_{ba}\delta(E_a-E)=(2/\pi\hbar)\sum_A \sin^2\delta_A. \quad (1.99)$$

These results are generalizations of familiar formulas obtained in the conventional phase shift analysis of the scattering of a particle by a central field of force. In the latter situation, the eigenfunctions of $\mathbf{K}$ are evident from symmetry considerations, namely the invariance of $\mathbf{K}_{ba}$ under a simultaneous rotation of $\mathbf{k}_a$ and $\mathbf{k}_b$, the propagation vectors that define the initial and final states. It may be inferred that the f_{aA} are spherical harmonics, considered as a function of the angles that define the direction of $\mathbf{k}_a$,

$$f_{aA}=CY_l{}^m(\mathbf{k}_a);\quad A\equiv l, m, \quad (1.100)$$

and that the eigenvalues of $\mathbf{K}$ depend only upon the order of the spherical harmonics, i.e., $\delta_A\equiv\delta_l$. The constant C is fixed by the normalization convention contained in (1.90), which now reads,

$$|C|^2\int Y_l{}^{m*}(\mathbf{k})Y_{l'}{}^{m'}(\mathbf{k})\rho d\Omega=\delta_{ll'}\delta_{mm'}. \quad (1.101)$$

Here $\rho d\Omega$ is the number of states, per unit energy range, associated with motion within the solid angle $d\Omega$. This occurs as a weight factor in a summation over states with equal energy, replacing the summation over all states as restricted by the factor $\delta(E_a-E)$. Explicitly,

$$\rho=\frac{p^2dp}{8\pi^3\hbar^3dE}=\frac{1}{8\pi^3\hbar}\frac{k^2}{v}, \quad (1.102)$$

if we consider a unit spatial volume. The second form in (1.102) expresses ρ in terms of the wave number k and v, the speed of the particle. With spherical harmonics that are normalized on a unit sphere (1.101) requires that

$$|C|^2=1/\rho=8\pi^3\hbar v/k^2. \quad (1.103)$$

We may now compute from (1.97) the probability, per unit time, that the particle is scattered from the direction of $\mathbf{k}_a$ into the solid angle $d\Omega$ around the direction of $\mathbf{k}_b$,

$$w=(2/\pi\hbar)|\sum_{l,m}\sin\delta_l e^{i\delta_l}|C|^2Y_l{}^m(\mathbf{k}_b)Y_l{}^{m*}(\mathbf{k}_a)|^2\rho d\Omega. \quad (1.104)$$

We then obtain the well-known expression of the differential cross section for scattering through an angle ϑ,

$$d\sigma(\vartheta)=(1/k^2)|\sum_l(2l+1)\sin\delta_l e^{i\delta_l}P_l(\cos\vartheta)|^2d\Omega \quad (1.105)$$

on dividing w by v, which measures the flux of incident particles, and employing the spherical harmonics addition theorem,

$$\sum_{m=-l}^{l} Y_l{}^m(\mathbf{k}_b)Y_l{}^{m*}(\mathbf{k}_a)=[(2l+1)/4\pi]P_l(\cos\vartheta), \quad (1.106)$$

where the Legendre polynomial $P_l(\cos\vartheta)$ is a function of ϑ, the angle between $\mathbf{k}_a$ and $\mathbf{k}_b$. The total scattering cross section is obtained from (1.98),

$$\sigma=(2/\pi\hbar v)\sum_{l,m}\sin^2\delta_l|C|^2|Y_l{}^m(\mathbf{k}_a)|^2$$

$$=(4\pi/k^2)\sum_l(2l+1)\sin^2\delta_l \quad (1.107)$$

in consequence of

$$\sum_m |Y_l^m(\mathbf{k}_a)|^2=(2l+1)/4\pi. \tag{1.108}$$

Since the total cross section is independent of the incidence direction, the same result follows immediately from (1.99).

We consider finally, the variational formulation of problems possessing the general character of the scattering by a central force field; namely, those in which the eigenfunctions of $\mathbf{K}$ are determined by symmetry considerations, and the basic question is to obtain the eigenvalues $\mathbf{K}_A$, or the phase angles δ_A. For this purpose, we notice that the inverse of (1.91) is

$$\sum_{b,a} f_{bB}^*\delta(E_b-E)\mathbf{K}_{ba}f_{aA}\delta(E_a-E)=\mathbf{K}_A\delta_{AB}. \tag{1.109}$$

On introducing the state vectors

$$\sum_a \Phi_a f_{aA}\delta(E_a-E)=\Phi_A, \tag{1.110}$$

and

$$\sum_a \Psi_a^{(1)} f_{aA}\delta(E_a-E)=\Psi_A^{(1)}, \tag{1.111}$$

the variational principle (1.85) becomes

$$\begin{aligned}-\frac{1}{\pi}\tan\delta'_A\delta_{AB}&=(\Psi_B^{(1)}, H_1\Phi_A)\\&+(\Phi_B, H_1\Psi_A^{(1)})-(\Psi_B^{(1)}, H_1\Psi_A^{(1)})\\&+\left(\Psi_B^{(1)}, H_1P\left(\frac{1}{E-H_0}\right)H_1\Psi_A^{(1)}\right).\end{aligned} \tag{1.112}$$

Note that Φ_A, or more exactly written $\Phi_{A,E}$, has the following orthogonality-normalization property:

$$\begin{aligned}(\Phi_{A,E}, \Phi_{B,E'})&=\sum_a f_{aA}^*\delta(E_a-E)f_{AB}\delta(E_a-E')\\&=\delta(E-E')\sum_a f_{aA}^*\delta(E_a-E)f_{aB}\\&=\delta_{AB}\delta(E-E')\end{aligned} \tag{1.113}$$

and that the inverses of (1.110), (1.111) are

$$\Phi_a=\sum_A f_{aA}^*\Phi_A, \quad \Psi_a^{(1)}=\sum_A f_{aA}^*\Psi_A^{(1)} \tag{1.114}$$

which are expansions of these state vectors in eigenvectors of $\mathbf{K}$.

III. NEUTRON SCATTERING BY A BOUND PROTON

As an application of the variational methods discussed in the first section, we consider the scattering of slow neutrons by a proton bound in an otherwise inert molecule. If the momentum associated with the center of gravity of the whole system is assumed to be zero, the unperturbed Hamiltonian consists of two parts, one describing the relative motion of the neutron and the molecular center of gravity, the other being the Hamiltonian of the internal molecular motion,

$$H_0=(\mathbf{p}_n^2/2\mu)+H_m. \tag{2.1}$$

Here

$$\mu=AM/(A+1) \tag{2.2}$$

is the reduced mass for relative motion of the neutron and molecule, while A is the molecular mass in units of M, the mass of the neutron. The perturbation is the neutron-proton interaction energy,

$$H_1=V(\mathbf{r}_n-\mathbf{r}_p) \tag{2.3}$$

which also depends upon the spin operators of neutron and proton, $\boldsymbol{\sigma}_n$ and $\boldsymbol{\sigma}_p$. The simplifying feature in this problem arises from the short range and large magnitude of the nuclear potential contrasted with the long range, weak molecular forces. The variational principle (1.78) requires a knowledge of the wave function representing the state vector only within the region of nuclear interaction, where the molecular force on the proton is negligible. Thus, the basic problem is the scattering of a neutron by a free proton, with essentially zero energy of relative motion. We therefore first consider some properties of the latter system.

The unperturbed Hamiltonian for a neutron and a free proton, in the system in which the center of gravity is at rest, is

$$\mathcal{H}_0=\mathbf{p}^2/M, \tag{2.4}$$

where $\mathbf{p}$ is the relative momentum of the particles. If we temporarily omit the spin coordinates, the wave function φ, representing the unperturbed state vector Φ_a, is simply a constant in the limit of zero energy. This constant can be chosen as unity, corresponding to a unit spatial volume. The wave function representing the state vectors $\Psi_a^{(+)}$ and $\Psi_a^{(-)}$ will be denoted by $\psi(\mathbf{r})$. There is no distinction between outgoing and incoming waves in the limit of zero energy. Since the scattering is necessarily isotropic, $\mathbf{T}_{ba}$ is simply a constant, denoted by $\mathbf{t}$. According to (1.63), $\mathbf{t}$ is given by

$$\mathbf{t}=(\varphi, V\psi)=\int V(\mathbf{r})\psi(\mathbf{r})d\mathbf{r}, \tag{2.5}$$

where ψ obeys the integral equation (1.61).

$$\psi+(1/\mathcal{H}_0)V\psi=\varphi. \tag{2.6}$$

The connection between $\mathbf{t}$ and the S phase shift is obtained from (1.92) and (1.96),

$$\mathbf{t}=-|f|^2ka/\pi, \tag{2.7}$$

in which we have employed the zero energy limiting form,

$$\sin\delta\rightarrow ka; \quad k\rightarrow 0 \tag{2.8}$$

thereby introducing the scattering amplitude a. The constant f is fixed by the normalization condition (1.90),

$$|f|^2 4\pi\rho=1 \tag{2.9}$$

where, (1.102),

$$4\pi\rho=k^2/2\pi^2\hbar v=kM/4\pi^2\hbar^2. \tag{2.10}$$

The second form of (2.10) follows from $\hbar k=\frac{1}{2}Mv$, the relation between the relative momentum and the relative velocity. Finally,

$$\mathbf{t}=-4\pi\hbar^2a/M. \tag{2.11}$$

If the neutron-proton interaction operator is spin-dependent, $\mathbf{t}$ must be replaced by a matrix in the spin quantum numbers. The eigenfunctions of this spin matrix are those of the triplet and singlet states of resultant spin angular momentum. The associated eigenvalues of $\mathbf{t}$ are related to the triplet and singlet scattering amplitudes,

$$\mathbf{t}_{1,0}=-4\pi\hbar^2 a_{1,0}/M. \tag{2.12}$$

As in (1.92), the matrix $\mathbf{t}$ can be constructed as a linear combination of its eigenvalues, multiplied by coefficients which are the matrix elements of projection operators for the corresponding eigenvalues. The projection operators for the triplet and singlet states are well known to be

$$P_1=\tfrac{1}{4}(3+\boldsymbol{\sigma}_n\cdot\boldsymbol{\sigma}_p), \quad P_0=\tfrac{1}{4}(1-\boldsymbol{\sigma}_n\cdot\boldsymbol{\sigma}_p). \tag{2.13}$$

Hence, to include spin dependent interactions it is sufficient to regard $\mathbf{t}$ in (2.11) as a spin operator, with

$$a=a_1P_1+a_0P_0=\tfrac{1}{4}(3a_1+a_0)+\tfrac{1}{4}(a_1-a_0)\boldsymbol{\sigma}_n\cdot\boldsymbol{\sigma}_p. \tag{2.14}$$

We shall now perform an approximate but highly accurate evaluation of $\mathbf{T}_{ba}$, which describes the scattering of a neutron by a bound proton. For this purpose, (1.78) is written

$$\begin{aligned}{}'\mathbf{T}'_{ba}=&(\Psi_b^{(-)},\ V\Phi_a)+(\Phi_b,\ V\Psi_a^{(+)})\\&-(\Psi_b^{(-)},\ V\Psi_a^{(+)})-\left(\Psi_b^{(-)},\ V\frac{1}{\mathfrak{H}_0}V\Psi_a^{(+)}\right)\\&+\left(\Psi_b^{(-)},\ V\left(\frac{1}{E+i\epsilon-H_0}+\frac{1}{\mathfrak{H}_0}\right)V\Psi_a^{(+)}\right),\end{aligned} \tag{2.15}$$

In treating the spin dependent interactions, it is convenient to suppress spin functions and thus regard $\mathbf{T}_{ba}$ as a spin operator. The first approximation to be introduced concerns the wave function representing the state vector Φ_a, say $\Phi_a(\mathbf{r}_n, \mathbf{r})$. Here $\mathbf{r}_n$ is the neutron coordinate relative to the molecular center of gravity, while $\mathbf{r}$ symbolizes the set of internal molecular coordinates, including $\mathbf{r}_p$, the proton position vector relative to the molecular center of gravity. This wave function, describing the independent motion of the neutron and molecule, will have the form

$$\Phi_a(\mathbf{r}_n, \mathbf{r})=\exp(i\mathbf{k}_a\cdot\mathbf{r}_n)\cdot\chi_a(\mathbf{r}) \tag{2.16}$$

in which $\chi_a(\mathbf{r})$ is an internal molecular wave function. Now $\Phi_a(\mathbf{r}_n, \mathbf{r})$ in (2.15), only occurs multiplied by the short range nuclear potential $V(\mathbf{r}_n-\mathbf{r}_p)$. We shall therefore replace $\Phi_a(\mathbf{r}_n, \mathbf{r})$ by

$$\Phi_a(\mathbf{r}_p, \mathbf{r})=F_a(\mathbf{r}). \tag{2.17}$$

The error thereby incurred is of the order $(kr_0)^2$, where r_0 is a measure of the nuclear force range. Since the influence of molecular binding is only of interest for slow neutrons, $(kr_0)^2\gtrsim 10^{-6}$, and we need not introduce a correction to compensate for this replacement.

A second approximation involves the last term of (2.15), which is small in comparison with the other terms, since molecular energies are negligible in comparison with the practically equal kinetic energies of neutron and proton during the nuclear interaction process. If we initially ignore the last term of (2.15) the latter reads

$$\begin{aligned}{}'\mathbf{T}'_{ba}=&(\Psi_b^{(-)},\ VF_a)+(F_b,\ V\Psi_a^{(+)})\\&-(\Psi_b^{(-)},\ V\Psi_a^{(+)})-\left(\Psi_b^{(-)},\ V\frac{1}{\mathfrak{H}_0}V\Psi_a^{(+)}\right).\end{aligned} \tag{2.18}$$

The condition that ${}'\mathbf{T}'_{ba}$ be stationary is that $\Psi_a^{(\pm)}$ satisfy the relation

$$\Psi_a^{(\pm)}+(1/\mathfrak{H}_0)V\Psi_a^{(\pm)}=F_a(\mathbf{r}). \tag{2.19}$$

On comparison with (2.6), it is evident that

$$\Psi_a^{(\pm)}=\psi(\mathbf{r}_n-\mathbf{r}_p)F_a(\mathbf{r}) \tag{2.20}$$

and the stationary value of ${}'\mathbf{T}'_{ba}$, an approximation to the correct $\mathbf{T}_{ba}$, is given by

$$\begin{aligned}\mathbf{T}_{ba}\simeq&(F_b,\ V\Psi_a^{(+)})=(F_b,\ V\psi F_a)\\&=\mathbf{t}\int F_b^*(\mathbf{r})F_a(\mathbf{r})d\mathbf{r}\end{aligned} \tag{2.21}$$

according to (2.5). This result,

$$\begin{aligned}\mathbf{T}_{ba}\simeq-\frac{4\pi\hbar^2}{M}a\int&\exp[i(\mathbf{k}_a-\mathbf{k}_b)\cdot\mathbf{r}_p]\cdot\\&\times\chi_b^*(\mathbf{r})\chi_a(\mathbf{r})d\mathbf{r}\end{aligned} \tag{2.22}$$

is the Fermi approximation.

To include the last term in (2.15), we observe that it may be written, in terms of wave functions, as

$$\begin{aligned}\int&\Psi_b^{(-)*}(\mathbf{r}_n, \mathbf{r})V(\mathbf{r}_n-\mathbf{r}_p)\\&\times\left(\mathbf{r}_n, \mathbf{r}\left|\frac{1}{E+i\epsilon-H_0}+\frac{1}{\mathfrak{H}_0}\right|\mathbf{r}_n', \mathbf{r}'\right)V(\mathbf{r}_n'-\mathbf{r}_p')\\&\times\Psi_a^{(+)}(\mathbf{r}_n', \mathbf{r}')d\mathbf{r}_n d\mathbf{r} d\mathbf{r}_n' d\mathbf{r}'.\end{aligned} \tag{2.23}$$

We shall again introduce an approximation which exploits the short range of V in comparison with molecular dimensions, namely, the replacement of (2.23) by

$$\begin{aligned}\int&\Psi_b^{(-)*}(\mathbf{r}_n, \mathbf{r})V(\mathbf{r}_n-\mathbf{r}_p)K^{(+)}(\mathbf{r}, \mathbf{r}')V(\mathbf{r}_n'-\mathbf{r}_p')\\&\times\Psi_a^{(+)}(\mathbf{r}_n', \mathbf{r}')d\mathbf{r}_n d\mathbf{r} d\mathbf{r}_n' d\mathbf{r}',\end{aligned} \tag{2.24}$$

where

$$K^{(\pm)}(\mathbf{r}, \mathbf{r}')=\left(\mathbf{r}_p, \mathbf{r}\left|\frac{1}{E\pm i\epsilon-H_0}+\frac{1}{\mathfrak{H}_0}\right|\mathbf{r}_p', \mathbf{r}'\right). \tag{2.25}$$

The conditions that $'\mathbf{T}'_{ba}$ be stationary are then expressed by

$$\Psi_a^{(\pm)}+\frac{1}{\mathfrak{IC}_0}V\Psi_a^{(\pm)}=F_a(\mathbf{r})+\int K^{(\pm)}(\mathbf{r},\mathbf{r}')\times V(\mathbf{r}_n'-\mathbf{r}_p')\Psi_a^{(\pm)}(\mathbf{r}_n',\mathbf{r}')d\mathbf{r}_n'd\mathbf{r}' \quad (2.26)$$

which, in virtue of (2.5) and (2.6), imply that

$$\Psi_a^{(\pm)}=\psi(\mathbf{r}_n-\mathbf{r}_p)G_a^{(\pm)}(\mathbf{r}) \quad (2.27)$$

where $G_a^{(\pm)}(\mathbf{r})$ obeys the integral equation

$$G_a^{(\pm)}(\mathbf{r})-\mathbf{t}\int K^{(\pm)}(\mathbf{r},\mathbf{r}')G_a^{(\pm)}(\mathbf{r}')d\mathbf{r}'=F_a(\mathbf{r}). \quad (2.28)$$

This is a generalization of the integral equation obtained by Breit.

The stationary value of $'\mathbf{T}'_{ba}$ is given by

$$\mathbf{T}_{ba}\simeq(F_b, V\Psi_a^{(+)})=\mathbf{t}\int F_b^*(\mathbf{r})G_a^{(+)}(\mathbf{r})d\mathbf{r}. \quad (2.29)$$

The integral equation for $G_a^{(+)}(\mathbf{r})$ can be solved by successive substitutions,

$$G_a^{(+)}(\mathbf{r})=F_a(\mathbf{r})+\mathbf{t}\int K^{(+)}(\mathbf{r},\mathbf{r}')F_a(\mathbf{r}')d\mathbf{r}'+\mathbf{t}^2\int K^{(+)}(\mathbf{r},\mathbf{r}')K^{(+)}(\mathbf{r}',\mathbf{r}'')\times F_a(\mathbf{r}'')d\mathbf{r}'d\mathbf{r}''+\cdots, \quad (2.30)$$

which is evidently a power series expansion in a/l, where l is a characteristic molecular dimension. Since $a/l\sim10^{-3}$, the series converges rapidly and it is quite sufficient to retain only the first term beyond $F_a(\mathbf{r})$ to obtain an accurate estimate of the correction to Fermi's approximation. Therefore,

$$\mathbf{T}_{ba}\simeq\mathbf{t}\int F_b^*(\mathbf{r})F_a(\mathbf{r})d\mathbf{r}+\mathbf{t}^2\int F_b^*(\mathbf{r})K^{(+)}(\mathbf{r},\mathbf{r}')F_a(\mathbf{r}')\times d\mathbf{r}d\mathbf{r}'. \quad (2.31)$$

To construct $K^{(+)}(\mathbf{r},\mathbf{r}')$, we observe that

$$\left(\mathbf{r}_n,\mathbf{r}\left|\frac{1}{E+i\epsilon-H_0}\right|\mathbf{r}_n',\mathbf{r}'\right)=\sum_c\Phi_c(\mathbf{r}_n,\mathbf{r})\frac{1}{E+i\epsilon-E_a}\Phi_c^*(\mathbf{r}_n',\mathbf{r}')=\sum_\gamma\int\frac{d\mathbf{k}}{(2\pi)^3}\exp(i\mathbf{k}\cdot\mathbf{r}_n)\cdot\chi_\gamma(\mathbf{r})\times\frac{1}{E+i\epsilon-(\hbar^2k^2/2\mu)-W_\gamma}\times\exp(-i\mathbf{k}\cdot\mathbf{r}_n')\chi_\gamma^*(\mathbf{r}'). \quad (2.32)$$

In the second version, the summation over the states of the system molecule plus free neutron is explicitly performed over the independent states of the molecule and of the neutron. For the evaluation of the corresponding matrix element of $1/\mathfrak{IC}_0$, it must be realized that the latter operator refers to the relative motion of neutron and proton only. Thus

$$\left(\mathbf{r}_n,\mathbf{r}\left|\frac{1}{\mathfrak{IC}_0}\right|\mathbf{r}_n',\mathbf{r}'\right)=\int\frac{d\mathbf{k}}{(2\pi)^3}\exp(i\mathbf{k}\cdot(\mathbf{r}_n-\mathbf{r}_p)\left(\frac{M}{\hbar^2k^2}\right)\times\exp(i\mathbf{k}\cdot(\mathbf{r}_n'-\mathbf{r}_p'))\times\delta\left(\frac{\mathbf{r}_n+\mathbf{r}_p}{2}-\frac{\mathbf{r}_n'+\mathbf{r}_p'}{2}\right)\delta(\mathbf{s}-\mathbf{s}'), \quad (2.33)$$

where $\mathbf{s}$ symbolizes the set of internal molecular coordinates, omitting $\mathbf{r}_p$. We are actually interested in (2.33) as $\mathbf{r}_n\to\mathbf{r}_p$ and $\mathbf{r}_n'\to\mathbf{r}_p'$. In this limit, $\delta(\mathbf{r}_n+\mathbf{r}_p/2-\mathbf{r}_n'+\mathbf{r}_p'/2)$ becomes $\delta(\mathbf{r}_p-\mathbf{r}_p')$ and we may employ the completeness relation for the molecular eigenfunctions,

$$\delta(\mathbf{r}_p-\mathbf{r}_p')\delta(\mathbf{s}-\mathbf{s}')=\delta(\mathbf{r}-\mathbf{r}')=\sum_\gamma\chi_\gamma(\mathbf{r})\chi_\gamma^*(\mathbf{r}'). \quad (2.34)$$

One can now combine (2.32) and (2.33) to form

$$K^{(+)}(\mathbf{r},\mathbf{r}')=\sum_\gamma\int\frac{d\mathbf{k}}{(2\pi)^3}\exp(i\mathbf{k}\cdot\mathbf{r}_p)\chi_\gamma(\mathbf{r})\times\left[\frac{1}{E+i\epsilon-(\hbar^2k^2/2\mu)-W_\gamma}+\frac{1}{(\hbar^2k^2/M)}\right]\times\exp(-i\mathbf{k}\cdot\mathbf{r}_p')\chi_\gamma^*(\mathbf{r}')=\frac{M}{\hbar^2}\sum_\gamma\int\frac{d\mathbf{k}}{(2\pi)^3}\exp(i\mathbf{k}\cdot(\mathbf{r}_p-\mathbf{r}_p')\times\left[\frac{2\mu/M}{k_\gamma^2+i\eta-k^2}+\frac{1}{k^2}\right]\chi_\gamma(\mathbf{r})\chi_\gamma^*(\mathbf{r}'). \quad (2.35)$$

Here

$$k_\gamma^2=(2\mu/\hbar^2)(E-W_\gamma) \quad (2.36)$$

and $\eta=(2\mu/\hbar^2)\epsilon$. The $\mathbf{k}$ integration in (2.35) involves the well-known integrals

$$\int\frac{d\mathbf{k}}{(2\pi)^3}\frac{\exp(i\mathbf{k}\cdot(\mathbf{r}_p-\mathbf{r}_p'))}{\kappa^2-k_\gamma^2-i\eta}=\frac{\exp(ik_\gamma|\mathbf{r}_p-\mathbf{r}_p'|)}{4\pi|\mathbf{r}_p-\mathbf{r}_p'|} \quad (2.37)$$

and

$$\int\frac{d\mathbf{k}}{(2\pi)^3}\frac{\exp(i\mathbf{k}\cdot(\mathbf{r}_p-\mathbf{r}_p'))}{k^2}=\frac{1}{4\pi|\mathbf{r}_p-\mathbf{r}_p'|}, \quad (2.38)$$

where

$$k_\gamma = +\left(\frac{2\mu}{\hbar^2}(E-W_\gamma)\right)^{\frac{1}{2}}; \quad W_\gamma < E$$

$$= +i\left(\frac{2\mu}{\hbar^2}(W_\gamma - E)\right)^{\frac{1}{2}}; \quad W_\gamma > E \qquad (2.39)$$

the propagating or attenuating nature of the spherical wave corresponding to whether or not the excitation of the molecular state γ is energetically possible. Finally, then

$$K^{(+)}(\mathbf{r}, \mathbf{r}') = -\frac{M}{4\pi\hbar^2}\sum_\gamma \chi_\gamma(\mathbf{r})\chi_\gamma^*(\mathbf{r}') \times \frac{2\mu}{M}\frac{\exp(ik_\gamma|\mathbf{r}_p-\mathbf{r}_p'|)-1}{|\mathbf{r}_p-\mathbf{r}_p'|} \qquad (2.40)$$

and

$$\mathbf{T}_{ba} \simeq -\frac{4\pi\hbar^2}{M}a\Big[\int F_b^*(\mathbf{r})F_a(\mathbf{r})d\mathbf{r} + a\sum_\gamma \int F_b^*(\mathbf{r})\chi_\gamma(\mathbf{r})\chi_\gamma^*(\mathbf{r}') \times \frac{(2\mu/M)\exp(ik_\gamma|\mathbf{r}_p-\mathbf{r}_p'|)-1}{|\mathbf{r}_p-\mathbf{r}_p'|}F_a(\mathbf{r}')d\mathbf{r}d\mathbf{r}'\Big]. \qquad (2.41)$$

The ratio $2\mu/M$ ranges from unity, referring to a free proton, to 2, which applies to a proton bound in an infinitely heavy molecule. Our results for these situations are in agreement with those of Breit. In particular, for a free proton $k_\gamma = k$, since there is no internal molecular motion, and (2.41) reduces to

$$\mathbf{T}_{ba} = \mathbf{t}' = -\frac{4\pi\hbar^2}{M}a(1+ika). \qquad (2.42)$$

This is simply the exact version of (2.7)

$$\mathbf{t}' = -\frac{1}{\pi}|f|^2\sin\delta e^{i\delta} = -\frac{4\pi\hbar^2}{M}\frac{1}{k}\frac{\tan\delta}{1-i\tan\delta} \qquad (2.43)$$

with $\tan\delta$ replaced by ka, the low energy limiting form, but retaining the complex factor $1/(1-i\tan\delta) \simeq 1+ika$. The latter has a negligible effect on transition probabilities in the energy range of interest, but is necessary to preserve the general conservation theorem (1.74). We shall, indeed, verify (1.74) for the more general expression (2.41). It is most evident from (2.31) and (2.32) that

$$-\frac{1}{\pi}Im\mathbf{T}_{aa} = \mathbf{t}^2\sum_c \int F_a^*(\mathbf{r})F_c(\mathbf{r})\delta(E-E_c) \times F_c^*(\mathbf{r}')F_a(\mathbf{r}')d\mathbf{r}d\mathbf{r}' = \sum_c |\mathbf{T}_{ca}|^2\delta(E-E_c) \qquad (2.44)$$

in which $\mathbf{T}_{ca}$ on the right side is computed from the Fermi approximation. This is in accordance with the approximate nature of (2.41).

Variational Principles for Scattering Processes. II. Scattering of Slow Neutrons by Para-Hydrogen*

B. A. LIPPMANN
Nucleonics Division, Naval Research Laboratory, Washington, D. C.
(Received April 10, 1950)

Continuing the illustrative example of the preceding paper, the scattering of slow neutrons by two protons bound to a molecule is treated by variational methods. A numerical evaluation indicates that the Fermi approximation to the para-hydrogen cross section is reliable to about 0.3 percent.

I. INTRODUCTION

THE variational principles described in the preceding paper,[1] applied there to the scattering of slow neutrons by a single proton bound to a molecule, will be adapted here to describe the situation in which the neutrons interact with two protons in the molecule. Although the discussion will be kept general in the early stages, where it serves to indicate the straightforward nature of the extension to many nuclei, the molecule will eventually be considered to be hydrogen and the results will then be evaluated numerically to show that the Fermi approximation to the para-hydrogen cross section is reliable to about 0.3 percent.

The argument, and the notation, are continued from the preceding paper, references to which are indicated by (A).

II. NEUTRON SCATTERING BY TWO BOUND PROTONS

As in Sec. III of reference 1, the center of mass of the system neutron plus molecule is assumed to be at rest, and the unperturbed Hamiltonian falls into two parts, one referring to the motion of the neutron relative to the center of mass of the molecule, and the other describing the internal molecular motion [A(2.1), (2.2)]. The perturbation is the sum of the separate energies of interaction of the neutron with each of the two protons,

$$H_1 = V_1 + V_2 = V(\mathbf{r}_n - \mathbf{r}_{p1}) + V(\mathbf{r}_n - \mathbf{r}_{p2}), \qquad (1)$$

where the dependence on the spin operators of the neutron and the two protons, $\boldsymbol{\sigma}_n, \boldsymbol{\sigma}_I, \boldsymbol{\sigma}_{II}$, is implicit, and the interaction has the same form for each of the two protons.

The total scattering will now be composed of the scattering produced by each proton acting alone plus interference terms, as may be seen directly by substituting (1) in [A(1.78)]. Without the interference terms, the result is just the sum of two terms of the form [A(2.15)],

$$\mathbf{T}'_{ba} \simeq \mathbf{T}'_{ba}{}^{I} + \mathbf{T}'_{ba}{}^{II} \qquad (2)$$

where

$$\mathbf{T}'_{ba}{}^{I,II} = (\Psi_b^{(-)}, V_{1,2}\Phi_a) + (\Phi_b, V_{1,2}\Psi_a^{(+)}) - (\Psi_b^{(-)}, V_{1,2}\Psi_a^{(+)}) - \left(\Psi_b^{(-)}, V_{1,2}\frac{1}{\mathcal{K}_0}V_{1,2}\Psi_a^{(+)}\right) + \left(\Psi_b^{(-)}, V_{1,2}\left(\frac{1}{E+i\epsilon-H_0}+\frac{1}{\mathcal{K}_0}\right)V_{1,2}\Psi_a^{(+)}\right). \qquad (3)$$

From [A(1.78)], the interference terms that must be added to (2) are

$$(\Psi_b^{(-)}, V_1\mathcal{K}^{(+)}V_2\Psi_a^{(+)}) + (\Psi_b^{(-)}, V_2\mathcal{K}^{(+)}V_1\Psi_a^{(+)}) \qquad (4)$$

where

$$\mathcal{K}^{(\pm)} = 1/(E \pm i\epsilon - H_0). \qquad (5)$$

The evaluation of each term in (2) proceeds exactly as in [A], except that the notation must be extended slightly since the $\mathbf{r}_p$ used there will now be $\mathbf{r}_{p1}$ or $\mathbf{r}_{p2}$, depending on whether the position of proton 1 or proton 2 relative to the molecular center of mass is involved. Thus, the approximation of [A(2.16)] by [A(2.17)] becomes, in the present problem, the replacement of [A(2.16)] by

$$\Phi_a(\mathbf{r}_{p1}, \mathbf{r}) = F_a^{(1)}(\mathbf{r}) \qquad (6)$$

if the neutron is in the neighborhood of proton 1, with 1→2 for the case where the neutron is near proton 2. The justification for the approximation is the same as in [A]. The notation $\Psi_a^{(+)}(1)$, $\Psi_a^{(+)}(2)$, will also be used to indicate that the wave function representing the state vector $\Psi_a^{(+)}$ is to be evaluated for $\mathbf{r}_n \to \mathbf{r}_{p1}$, $\mathbf{r}_n \to \mathbf{r}_{p2}$, respectively. Finally, [A(2.25)] becomes

$$K_1^{(\pm)}(\mathbf{r}, \mathbf{r}') = \left(\mathbf{r}_{p1}, \mathbf{r}\left|\frac{1}{E\pm i\epsilon-H_0}+\frac{1}{\mathcal{K}_0}\right|\mathbf{r}_{p1}', \mathbf{r}'\right), \qquad (7)$$

if the $\mathbf{r}_p$ in [A(2.25)] refers to proton 1, with an analogous convention when the $\mathbf{r}_p$ in [A(2.25)] refers to proton 2.

To summarize, the generalization of [A(2.15)] to two scattering centers, obtained by adding the inter-

* Taken in part from a thesis submitted to Harvard University in partial fulfillment of the requirements for the degree of Doctor of Philosophy.

[1] B. A. Lippmann and J. Schwinger, Phys. Rev. **78**, 469 (1950).

ference terms (4) to (2), is

$$\begin{aligned}{}'\mathbf{T}'_{ba}\simeq&\{(\Psi_b^{(-)}, V_1F_a^{(1)})+(F_b^{(1)}, V_1\Psi_a^{(+)})\\&-(\Psi_b^{(-)}, V_1\Psi_a^{(+)})-(\Psi_b^{(-)}, V_1(1/\mathfrak{K}_0)V_1\Psi_a^{(+)})\\&+(\Psi_b^{(-)}, V_1K_1^{(+)}V_1\Psi_a^{(+)})\}+\{(\Psi_b^{(-)}, V_2F_a^{(2)})\\&+(F_b^{(2)}, V_2\Psi_a^{(+)})-(\Psi_b^{(-)}, V_2\Psi_a^{(+)})\\&-(\Psi_b^{(-)}, V_2(1/\mathfrak{K}_0)V_2\Psi_a^{(+)})\\&+(\Psi_b^{(-)}, V_2K_2^{(+)}V_2\Psi_a^{(+)})\}\\&+(\Psi_b^{(-)}, V_1\mathfrak{K}^{(+)}V_2\Psi_a^{(+)})\\&+(\Psi_b^{(-)}, V_2\mathfrak{K}^{(+)}V_1\Psi_a^{(+)}).\end{aligned}\tag{8}$$

The stationary property of ${}'\mathbf{T}'_{ba}$ now requires that:

$$\begin{aligned}&\Psi_a^{(\pm)}(1)+\frac{1}{\mathfrak{K}_0}V_1\Psi_a^{(\pm)}(1)\\&\quad=F_a^{(1)}+K_1^{(\pm)}V_1\Psi_a^{(\pm)}(1)+\mathfrak{K}^{(\pm)}V_2\Psi_a^{(\pm)}(2),\\&\Psi_a^{(\pm)}(2)+\frac{1}{\mathfrak{K}_0}V_2\Psi_a^{(\pm)}(2)\\&\quad=F_a^{(2)}+K_2^{(\pm)}V_2\Psi_a^{(\pm)}(2)+\mathfrak{K}^{(\pm)}V_1\Psi_a^{(\pm)}(1).\end{aligned}\tag{9}$$

These equations differ from [A(2.26)] by the coupling terms on the extreme right, which express the effect of the interference between the waves scattered by each of the protons, but the procedure followed in [A(2.27)–(2.31)] obviously requires only slight generalization. We first generalize [A(2.5)] to

$$\mathbf{t}^{I,II}=(\varphi, V_{1,2}\psi)=\int V_{1,2}(\mathbf{r})\psi(\mathbf{r})d\mathbf{r}\tag{10}$$

where, from [A(2.11)],

$$\mathbf{t}^{I,II}=-(4\pi\hbar^2/M)a^{I,II}\tag{11}$$

with $a^{I,II}$ given by

$$a^{I,II}=\tfrac{1}{4}(3a_1+a_0)+\tfrac{1}{4}(a_1-a_0)\boldsymbol{\sigma}_n\cdot\boldsymbol{\sigma}_{I,II}\tag{12}$$

as is clearly required by [A(2.14)].

With ψ a solution of [A(2.6)], the pair of Eqs. (9) will be satisfied by

$$\Psi_a^{(\pm)}(1,2)=\psi(\mathbf{r}_n-\mathbf{r}_{p1,2})G_a^{(\pm)}(1,2)\tag{13}$$

provided that:

$$\begin{aligned}G_a^{(\pm)}(1)&=F_a^{(1)}+\mathbf{t}^IK_1^{(\pm)}G_a^{(\pm)}(1)+\mathbf{t}^{II}\mathfrak{K}^{(\pm)}G_a^{(\pm)}(2),\\G_a^{(\pm)}(2)&=F_a^{(2)}+\mathbf{t}^{II}K_2^{(\pm)}G_a^{(\pm)}(2)+\mathbf{t}^I\mathfrak{K}^{(\pm)}G_a^{(\pm)}(1).\end{aligned}\tag{14}$$

The stationary value of (8) is

$$\begin{aligned}\mathbf{T}_{ba}\simeq&(F_b^{(1)}, V_1\Psi_a^{(+)}(1))+(F_b^{(2)}, V_2\Psi_a^{(+)}(2))\\&=\mathbf{t}^I(F_b^{(1)}, G_a^{(+)}(1))+\mathbf{t}^{II}(F_b^{(2)}, G_a^{(+)}(2))\end{aligned}\tag{15}$$

and the Fermi approximation corresponds to neglecting the terms after the first on the right-hand side of (14) and substituting the result into (15). We are interested, however, in a more exact calculation of $\mathbf{T}_{ba}$. Using the argument following [A(2.30)], a solution of (14), sufficiently accurate to estimate the correction to the Fermi approximation, is

$$\begin{aligned}G_a^{(+)}(1,2)\simeq&F_a^{(1,2)}+\mathbf{t}^{I,II}K_{1,2}^{(+)}F_a^{(1,2)}\\&+\mathbf{t}^{II,I}\mathfrak{K}^{(+)}F_a^{(2,1)}\end{aligned}\tag{16}$$

so that

$$\begin{aligned}\mathbf{T}_{ba}\simeq&\mathbf{t}^I(F_b^{(1)}, F_a^{(1)})+\mathbf{t}^{II}(F_b^{(2)}, F_a^{(2)})\\&+(\mathbf{t}^I)^2(F_b^{(1)}, K_1^{(+)}F_a^{(1)})+(\mathbf{t}^{II})^2(F_b^{(2)}, K_2^{(+)}F_a^{(2)})\\&+\mathbf{t}^I\mathbf{t}^{II}(F_b^{(1)}, \mathfrak{K}^{(+)}F_a^{(2)})+\mathbf{t}^{II}\mathbf{t}^I(F_b^{(2)}, \mathfrak{K}^{(+)}F_a^{(1)}).\end{aligned}\tag{17}$$

The various integrals in (17) occur in pairs, differing from one another only in that $\mathbf{r}_{p1}$ and $\mathbf{r}_{p2}$ are alternately substituted for the neutron position vector, $\mathbf{r}_n$. The terms of each pair may be combined by interchanging the positions of protons 1 and 2 in one member of the pair. Thus, from [A(2.16)], (6),

$$(F_b^{(2)}, F_a^{(2)})=\pm(F_b^{(1)}, F_a^{(1)}),\tag{18}$$

where the (+) sign applies if states "a" and "b" have the same parity, and the (−) sign if they are of opposite parity. With this observation, (17) becomes

$$\begin{aligned}\mathbf{T}_{ba}\simeq&[\mathbf{t}^I\pm\mathbf{t}^{II}](F_b^{(1)}, F_a^{(1)})\\&+[(\mathbf{t}^I)^2\pm(\mathbf{t}^{II})^2](F_b^{(1)}, K_1^{(+)}F_a^{(1)})\\&+[\mathbf{t}^I\mathbf{t}^{II}\pm\mathbf{t}^{II}\mathbf{t}^I](F_b^{(1)}, \mathfrak{K}^{(+)}F_a^{(2)}).\end{aligned}\tag{19}$$

Here, by virtue of the Pauli principle, the correct combination of spin operators is automatically selected when taking spin matrix elements, the upper sign for initial and final spin states of the same spin symmetry and the lower sign for states of opposite spin symmetry. The first term of (19) represents the scattering of zero energy neutrons by each of two free protons independently (Fermi approximation), the second term corrects for non-zero neutron energy and molecular binding, and the third term contributes the interference effects.

The general conservation theorem [A(1.74)] may be verified by remarking from (5) and (7), that $K^{(+)}$ and $K^{(-)}$ differ only in their real parts so that the imaginary part of (17) leads to:

$$\begin{aligned}-\frac{1}{\pi}Im\mathbf{T}_{aa}=-\frac{1}{\pi}Im(&[\mathbf{t}^IF_a^{(1)}+\mathbf{t}^{II}F_a^{(2)}],\\&\times\mathfrak{K}^{(+)}[\mathbf{t}^IF_a^{(1)}+\mathbf{t}^{II}F_a^{(2)}]).\end{aligned}\tag{20}$$

Using [A(2.32)] and (15), [A(1.74)] follows.

III. PARA-PARA SCATTERING

Equation (19) may be adapted to the hydrogen molecule by introducing the position vector of proton

1 relative to proton 2 for the internal coordinate $\mathbf{r}$:

$$\mathbf{r}_{p1}=\tfrac{1}{2}\mathbf{r};\quad \mathbf{r}_{p2}=-\tfrac{1}{2}\mathbf{r}. \tag{21}$$

For the first term of (19), we find, by (6) and (21),

$$(F_b^{(1)}, F_a^{(1)})=\int \Phi_b^*(\tfrac{1}{2}\mathbf{r}, \mathbf{r})\Phi_a(\tfrac{1}{2}\mathbf{r}, \mathbf{r})d\mathbf{r}. \tag{22}$$

To construct the second term, we first note, from (7), (21), and [A(2.25)], that $K_1^{(+)}$ as defined by (7) is given by replacing $\mathbf{r}_p$ by $\frac{1}{2}\mathbf{r}$ and $\mathbf{r}_p'$ by $\frac{1}{2}\mathbf{r}'$ in [A(2.40)]. Combining this with [A(2.2)], which shows that $\mu M=\frac{2}{3}$,

$$\begin{aligned}&(F_b^{(1)}, K_1^{(+)}F_a^{(1)})\\&=-(M/4\pi\hbar^2)\int \Phi_b^*(\tfrac{1}{2}\mathbf{r}, \mathbf{r})\textstyle\sum_\gamma \chi_\gamma(\mathbf{r})\chi_\gamma^*(\mathbf{r}')\\&\times\frac{(4/3)\exp[ik_\gamma|\frac{1}{2}(\mathbf{r}-\mathbf{r}')|]-1}{|\frac{1}{2}(\mathbf{r}+\mathbf{r}')|}\Phi_a(\tfrac{1}{2}\mathbf{r}', \mathbf{r}')d\mathbf{r}d\mathbf{r}'.\end{aligned} \tag{23}$$

Finally, for the last term of (19), we require:

$$\begin{aligned}(F_b^{(1)}, \mathcal{K}^{(+)}F_a^{(2)})&=\int \Phi_b^*(\tfrac{1}{2}\mathbf{r}, \mathbf{r})(\tfrac{1}{2}\mathbf{r}, \mathbf{r}|\,\mathcal{K}^{(+)}|-\tfrac{1}{2}\mathbf{r}', \mathbf{r}')\\&\quad\times\Phi_a(-\tfrac{1}{2}\mathbf{r}', \mathbf{r}')d\mathbf{r}d\mathbf{r}'.\end{aligned} \tag{24}$$

Comparing (5) with [A(2.32)],

$$\begin{aligned}&(F_b^{(1)}, \mathcal{K}^{(+)}F_a^{(2)})\\&=-(M/4\pi\hbar^2)\int \Phi_b^*(\tfrac{1}{2}\mathbf{r}, \mathbf{r})\textstyle\sum_\gamma \chi_\gamma(\mathbf{r})\chi_\gamma^*(\mathbf{r}')\\&\quad\times\frac{(4/3)\exp[ik_\gamma|\frac{1}{2}(\mathbf{r}+\mathbf{r}')|]}{|\frac{1}{2}(\mathbf{r}-\mathbf{r}')|}\Phi_a(-\tfrac{1}{2}\mathbf{r}', \mathbf{r}')d\mathbf{r}d\mathbf{r}\\&=-(M/4\pi\hbar^2)\int \Phi_b^*(\tfrac{1}{2}\mathbf{r}, \mathbf{r})\textstyle\sum_\gamma \chi_\gamma(\mathbf{r})\chi_\gamma^*(-\mathbf{r}')\\&\quad\times\frac{(4/3)\exp[ik_\gamma|\frac{1}{2}(\mathbf{r}-\mathbf{r}')|]}{|\frac{1}{2}(\mathbf{r}-\mathbf{r}')|}\Phi_a(\tfrac{1}{2}\mathbf{r}', -\mathbf{r}')d\mathbf{r}d\mathbf{r}'\end{aligned} \tag{25}$$

in which the second expression differs from the first by reversal of the sign of $\mathbf{r}'$.

For the scattering of slow neutrons by hydrogen, (19) is therefore reduced to:

$$\begin{aligned}\frac{\mathrm{T}_{ba}}{(-4\pi\hbar^2/M)}&=[a^I\pm a^{II}]\int \Phi_b^*(\tfrac{1}{2}\mathbf{r}, \mathbf{r})\Phi_a(\tfrac{1}{2}\mathbf{r}, \mathbf{r})d\mathbf{r}\\&+[(a^I)^2\pm(a^{II})^2]\int \Phi_b^*(\tfrac{1}{2}\mathbf{r}, \mathbf{r})\textstyle\sum_\gamma \chi_\gamma(\mathbf{r})\chi_\gamma^*(\mathbf{r}')\\&\times\frac{(4/3)\exp[ik_\gamma|\frac{1}{2}(\mathbf{r}-\mathbf{r}')|]-1}{|\frac{1}{2}(\mathbf{r}-\mathbf{r}')|}\Phi_a(\tfrac{1}{2}\mathbf{r}', \mathbf{r}')d\mathbf{r}d\mathbf{r}'\\&+[a^Ia^{II}\pm a^{II}a^I]\int \Phi_b^*(\tfrac{1}{2}\mathbf{r}, \mathbf{r})\textstyle\sum_\gamma \chi_\gamma(\mathbf{r})\chi_\gamma^*(-\mathbf{r}')\\&\times\frac{(4/3)\exp[ik_\gamma|\frac{1}{2}(\mathbf{r}-\mathbf{r}')|]}{|\frac{1}{2}(\mathbf{r}-\mathbf{r}')|}\Phi_a(\tfrac{1}{2}\mathbf{r}', -\mathbf{r}')d\mathbf{r}d\mathbf{r}',\end{aligned} \tag{26}$$

where we have made use of (11) to introduce the spin operators defined by (12). Initial and final state spin functions may now be applied to (26) to obtain the complete matrix element for the transition $a\rightarrow b$.

The range of the neutron-proton interaction, as conventionally determined, is a sensitive function of the para-para cross section for slow neutrons, the measured value of which is interpreted by a theoretical analysis based on the first term of (26). The remaining terms of (26) permit us to estimate the reliability of this analysis.

Specializing (26) to the case of para-para scattering, both initial and final state spin functions refer to singlet states and the (+) sign is automatically selected in each term. The spin operators of (26) have, for their matrix elements that are diagonal in the singlet state of the molecule,

$$\begin{aligned}[a^I+a^{II}]_{0,0}&=\tfrac{1}{2}(3a_1+a_0),\\[(a^I)^2+(a^{II})^2]_{0,0}&=\tfrac{1}{8}[(3a_1+a_0)^2+3(a_1-a_0)^2],\\[a^Ia^{II}+a^{II}a^I]_{0,0}&=\tfrac{1}{8}[(3a_1+a_0)^2-3(a_1-a_0)^2].\end{aligned} \tag{27}$$

In the evaluation of Eq. (26), we shall consider only zero-energy neutrons and shall approximate the molecule by a rigid rotator. The molecular wave functions thereby become normalized spherical harmonics multiplied by a radial delta function centered about r_e, the equilibrium separation of the protons,

$$\chi_\gamma(\mathbf{r})\equiv\chi_{l,m}(r, \vartheta, \varphi)=[\delta(r-r_e)/r^2]^{\frac{1}{2}}Y_l^m(\vartheta, \varphi) \tag{28}$$

while, from [A(2.16)],

$$\Phi_a(\mathbf{r}_n, \mathbf{r})=\chi_a(\mathbf{r})\equiv\chi_{0,0}(r, \vartheta, \varphi)=[\delta(r-r_e)/4\pi r^2]^{\frac{1}{2}}. \tag{29}$$

By reason of the definition of k_γ, [A(2.39)], the exponential factors in (26) correspond to attenuated waves,

$$k_\gamma\equiv k_l=i(4MW_l/3\hbar^2)^{\frac{1}{2}}=i[4l(l+1)/3r_e^2]^{\frac{1}{2}}. \tag{30}$$

Using the spherical harmonic addition theorem, [A(1.106)], the integrals appearing in (26) become:

$$\begin{aligned}r_eI_1&=r_e\int \Phi_b^*(\tfrac{1}{2}\mathbf{r}, \mathbf{r})\textstyle\sum_\gamma \chi_\gamma(\mathbf{r})\chi_\gamma^*(\mathbf{r}')\\&\quad\times\frac{(4/3)\exp[ik_\gamma|\frac{1}{2}(\mathbf{r}-\mathbf{r}')|]-1}{|\frac{1}{2}(\mathbf{r}-\mathbf{r}')|}\\&\qquad\times\Phi_a(\tfrac{1}{2}\mathbf{r}', \mathbf{r}')d\mathbf{r}d\mathbf{r}'\\&=\int_{-1}^{1}d(\cos\phi)\sum_{l=0}^{\infty}(l+\tfrac{1}{2})P_l(\cos\phi)\\&\quad\times\frac{[(4/3)\exp[-((4/3)l(l+1))^{\frac{1}{2}}\sin\phi/2]-1}{\sin\phi/2}\end{aligned} \tag{31}$$

and

$$r_e I_2 = r_e \int \Phi_b^*(\tfrac{1}{2}\mathbf{r}, \mathbf{r}) \sum_\gamma \chi_\gamma(\mathbf{r}) \chi_\gamma^*(-\mathbf{r}') \times \frac{(4/3)\exp[ik_\gamma|\tfrac{1}{2}(\mathbf{r}-\mathbf{r}')|]}{|\tfrac{1}{2}(\mathbf{r}-\mathbf{r}')|} \times \Phi_a(\tfrac{1}{2}\mathbf{r}', -\mathbf{r}') d\mathbf{r} d\mathbf{r}'$$

$$= \int_{-1}^{1} d(\cos\phi) \sum_{l=0}^{\infty} (-)^l (l+\tfrac{1}{2}) P_l(\cos\phi) \times \frac{(4/3)\exp[-((4/3)l(l+1))^{\frac{1}{2}} \sin\phi/2]}{\sin\phi/2}, \quad (32)$$

where P_l is the Legendre polynomial of degree l and ϕ is the angle between the vectors $\mathbf{r}$ and $\mathbf{r}'$.

Finally, collecting our formulae, the total para cross section, σ, is proportional to

$$\sigma \sim (3a_1+a_0)^2 \left[1 + \frac{1}{2(3a_1+a_0)} \{ [(3a_1+a_0)^2 + 3(a_1-a_0)^2] I_1 + [(3a_1+a_0)^2 - 3(a_1-a_0)^2] I_2 \} \right]. \quad (33)$$

IV. NUMERICAL EVALUATION

It is convenient to evaluate I_1 in two steps:

$$r_e I_1 = \int_{-1}^{1} d(\cos\phi) \sum_{l=0}^{\infty} (l+\tfrac{1}{2}) P_l(\cos\phi) \times \frac{(4/3)\exp[-(2/\sqrt{3})(l+\tfrac{1}{2})\sin\phi/2] - 1}{\sin\phi/2}$$

$$+ \frac{4}{3} \int_{-1}^{1} d(\cos\phi) \sum_{l=0}^{\infty} (l+\tfrac{1}{2}) P_l(\cos\phi) \times \frac{\exp[-((4/3)l(l+1))^{\frac{1}{2}} \sin\phi/2] - \exp[-(2/\sqrt{3})(l+\tfrac{1}{2})\sin\phi/2]}{\sin\phi/2}$$

$$= I_1' + I_1''. \quad (34)$$

In the Appendix, we show that

$$-I_1' = \frac{24\sqrt{3}}{\pi} \int_0^1 \frac{dt}{(t)^{\frac{1}{2}}} \int_0^\infty \frac{d\varphi}{\varphi} \frac{\left[\frac{\sin\varphi - \varphi\cos\varphi}{\varphi^2}\right]\left[1 - (1-t)\frac{\sin^2\varphi}{\varphi^2}\right]}{[3+(1-t)(\sin^2\varphi/\varphi^2)]^3} > 0. \quad (35)$$

Replacing $(1-t)(\sin^2\varphi)/\varphi^2$ successively by zero and $(1-t)$,

$$0.182 < -I_1' < 0.770. \quad (36)$$

In the limit of large l, $P_l(\cos\phi)$ approaches the Bessel function of order zero:

$$P_l(\cos\phi) \to J_0(l\phi). \quad (37)$$

As $l \to \infty$, a typical term of I_1'' therefore becomes

$$\frac{8}{3} \int_0^\pi d\phi \cos\phi/2 \cdot l J_0(l\phi) \exp\left(-\frac{2l}{\sqrt{3}} \sin\phi/2\right) \times \left(\exp\left(\frac{\sin\phi/2}{4\sqrt{3}l}\right) - 1 \right) \to \frac{1}{3\sqrt{3}l^2} \int_0^\infty d\phi l^2 \phi J_0(l\phi) \times \exp(-l\phi/\sqrt{3}) = \frac{1}{8\sqrt{3}} \frac{1}{l^2}, \quad (38)$$

and the series converges like $1/l^2$. Using Watson's definitions of the Bessel functions of purely imaginary argument,

$$I_{n+\frac{1}{2}}(x) = i^{-(n+\frac{1}{2})} J_{n+\frac{1}{2}}(ix),$$

$$K_{n+\frac{1}{2}}(x) = i \frac{\pi}{2} i^{(n+\frac{1}{2})} H_{n+\frac{1}{2}}^{(1)}(ix),$$

where $H^{(1)}$ is the Hankel function of the first kind,

$$\frac{\exp(-\kappa|r_> - r_<|)}{|r_> - r_<|} = \sum_{l=0}^{\infty} \frac{(2l+1)}{(|r_<||r_>|)^{\frac{1}{2}}} I_{l+\frac{1}{2}}(\kappa r_<) \times K_{l+\frac{1}{2}}(\kappa r_>) P_l(\cos \mathbf{r}_< \cdot \mathbf{r}_>), \quad (39)$$

and I_1'' may be expressed as an infinite series:

$$I_1'' = \frac{8}{3} \sum_{l=0}^{\infty} (2l+1) \left\{ I_{l+\frac{1}{2}}\left[\left(\frac{l(l+1)}{3}\right)^{\frac{1}{2}}\right] \times K_{l+\frac{1}{2}}\left[\left(\frac{l(l+1)}{3}\right)^{\frac{1}{2}}\right] - I_{l+\frac{1}{2}}\left(\frac{l+\frac{1}{2}}{\sqrt{3}}\right) K_{l+\frac{1}{2}}\left(\frac{l+\frac{1}{2}}{\sqrt{3}}\right) \right\}. \quad (40)$$

The $l=5$ term in (40) differs from its asymptotic form by 0.0005. The first six terms of the series were computed and the remaining terms, which contribute about $1\frac{1}{2}$ percent of the total, $I_1''=0.708$, were replaced by their asymptotic form.

The second integral, I_2, may be written

$$r_e I_2 = \frac{8}{3} \sum_{l=0}^{\infty} (-)^l (2l+1) I_{l+\frac{1}{2}} \times \left[\left(\frac{l(l+1)}{3}\right)^{\frac{1}{2}}\right] K_{l+\frac{1}{2}}\left[\left(\frac{l(l+1)}{3}\right)^{\frac{1}{2}}\right]. \quad (41)$$

Following the procedure used for I_1'', one finds that the asymptotic form of a typical term of this series is

$(-)^l 4/\sqrt{3}$, and direct computation shows that the asymptotic form is practically attained by $l=5$. We have summed exactly from $l=0$ to $l=5$ and then used $\sum_{l=6}^{\infty}(-)^l=\frac{1}{2}$, with the result

$$r_e I_2 = 1.531. \tag{42}$$

Combining these numerical results with the experimental values[2] of a_1, a_0, and r_e, the first-order correction, as computed from (33), is,

$$\sigma \sim (3a_1+a_0)^2(1-\alpha); \quad 0.002<\alpha<0.003. \tag{43}$$

I am deeply indebted to Professor Julian Schwinger, who suggested this problem, and who patiently and generously guided me towards its solution.

APPENDIX

To show that (35) follows from (34), we use

$$\frac{e^{-\kappa r}}{r}=\frac{1}{2(\pi)^{\frac{1}{2}}}\int_0^\infty \frac{d\tau}{\tau^{\frac{1}{2}}}\exp\left(-\frac{r^2}{4\tau}-\kappa^2\tau\right)$$

to put (34) in the form:

$$I_1'=\frac{2}{3(\pi)^{\frac{1}{2}}}\int_0^\infty \frac{d\tau}{\tau^{\frac{1}{2}}}\left[\int_0^\pi d\phi\,\sin\phi\exp\left(-\frac{\sin^2\phi/2}{4\tau}\right)\right.$$
$$\left.\times\sum_{l=0}^{\infty}\exp\left(-\frac{4\tau}{3}(l+\tfrac{1}{2})^2\right)(l+\tfrac{1}{2})P_l(\cos\phi)-\tfrac{3}{4}\right].$$

Now introduce the representation:

$$\exp\left(-\frac{4\tau}{3}(l+\tfrac{1}{2})^2\right)$$
$$=\frac{\sqrt{3}}{4(\pi)^{\frac{1}{2}}}\int_{-\infty}^{\infty}\frac{d\xi}{\tau^{\frac{1}{2}}}\exp\left(-\frac{3\xi^2}{16\tau}+i\xi(l+\tfrac{1}{2})\right).$$

Integrate the right-hand side by parts. Since only the real part is different from zero,

$$\sum_{l=0}^{\infty}(l+\tfrac{1}{2})\exp\left(-\frac{4}{3}\tau(l+\tfrac{1}{2})^2\right)P_l(\cos\phi)$$
$$=Re\frac{-i3\sqrt{3}}{16(\pi)^{\frac{1}{2}}}\sum_{l=0}^{\infty}\int_0^\infty\frac{d\xi}{\tau^{\frac{1}{2}}}\xi\exp\left(-\frac{3\xi^2}{16\tau}+i\xi(l+\tfrac{1}{2})\right)P_l(\cos\phi).$$

We observe that, since $\xi\geqslant 0$,

$$Re(-i)\sum_{l=0}^{\infty}\exp(i\xi(l+\tfrac{1}{2}))P_l(\cos\phi)=Re\frac{1}{[2(\cos\phi-\cos\xi)]^{\frac{1}{2}}}$$
$$=\left\{\int_\phi^\pi d\theta+\int_\pi^{2\pi-\phi}d\theta\right\}\sum_{n=0}^{\infty}\frac{\delta(\theta-\xi+2\pi n)}{[2(\cos\phi-\cos\theta)]^{\frac{1}{2}}},$$
$$(n=0,1,2,\cdots).$$

[2] Sutton, Hall, Anderson, Bridge, DeWire, Lavatelli, Long, Snyder, and Williams, Phys. Rev. 72, 1147 (1947).

Using these results,

$$I_1'=\frac{(3/2)^{\frac{1}{2}}}{8\pi}\int_0^\infty\frac{d\tau}{\tau^3}\int_0^\pi d\phi\,\sin\phi\exp\left(-\frac{\sin^2\phi/2}{4\tau}\right)$$
$$\times\left\{\int_\phi^\pi d\theta+\int_\pi^{2\pi-\phi}d\theta\right\}\int_0^\infty\frac{d\xi\xi\exp(-3\xi^2/16\tau)}{(\cos\phi-\cos\theta)^{\frac{1}{2}}}$$
$$\times\sum_{n=0}^{\infty}\delta(\theta-\xi+2\pi n)-\frac{1}{2(\pi)^{\frac{1}{2}}}\int_0^\infty\frac{d\tau}{\tau^{\frac{1}{2}}}.$$

Replace θ by $2\pi-\theta$ in the second ingeral over θ:

$$I_1'=\frac{(3/2)^{\frac{1}{2}}}{8\pi}\int_0^\infty\frac{d\tau}{\tau^3}\int_0^\pi d\phi\,\sin\phi\exp\left(-\frac{\sin^2\phi/2}{4\tau}\right)$$
$$\times\int_\phi^\pi\frac{d\theta}{(\cos\phi-\cos\theta)^{\frac{1}{2}}}\int_0^\infty d\xi\xi\exp(-3\xi^2/16\tau)$$
$$\times\sum_{n=0}^{\infty}\{\delta(\theta-\xi+2\pi n)+\delta(-\theta-\xi+2\pi(n+1))\}$$
$$-\frac{1}{2(\pi)^{\frac{1}{2}}}\int_0^\infty\frac{d\tau}{\tau^{\frac{1}{2}}}.$$

Invert the order of the θ and ϕ integrations, and replace ϕ by t through the relation

$$\cos\phi=\cos\theta+(1-\cos\theta)t.$$

$$I_1'=\frac{(3/2)^{\frac{1}{2}}}{8\pi}\int_0^\infty\frac{d\tau}{\tau^3}\int_0^\pi d\theta\int_0^1\frac{dt}{(t)^{\frac{1}{2}}}$$
$$\times\exp\left(-\frac{(1-t)}{4\tau}\sin^2\theta/2\right)(1-\cos\theta)^{\frac{1}{2}}$$
$$\times\int_0^\infty d\xi\xi\exp(-3\xi^2/16\tau)\sum_{n=0}^{\infty}\{\delta(\theta-\xi+2\pi n)$$
$$+\delta(-\theta-\xi+2\pi(n+1))\}-\frac{1}{2(\pi)^{\frac{1}{2}}}\int_0^\infty\frac{d\tau}{\tau^{\frac{1}{2}}}.$$

We can make the replacement

$$\int_0^\pi d\theta\sum_{n=0}^{\infty}\{\delta(\theta-\xi+2\pi n)+\delta(-\theta-\xi+2\pi(n+1))\}$$
$$=\int_0^\infty d\theta\delta(\theta-\xi)$$

so that

$$I_1'=\frac{\sqrt{3}}{8\pi}\int_0^\infty\frac{d\tau}{\tau^{\frac{1}{2}}}\left[\int_0^\infty\frac{d\theta}{\tau^{\frac{1}{2}}}\theta\sin\theta/2\exp(-3\theta^2/16\tau)\right.$$
$$\left.\times\int_0^1\frac{dt}{(t)^{\frac{1}{2}}}\exp\left(-\frac{(1-t)}{4\tau}\sin^2\theta/2\right)\right]-\frac{1}{2(\pi)^{\frac{1}{2}}}\int_0^\infty\frac{d\tau}{\tau^{\frac{1}{2}}}.$$

Integrating the second τ integral, and the first τ integral by parts, the singularities cancel leaving

$$I_1'=\frac{\sqrt{3}}{4\pi}\int_0^\infty \frac{d\tau}{(\tau)^{\frac{1}{2}}}\frac{\partial}{\partial\tau}\int_0^\infty \frac{d\theta}{\tau^{\frac{1}{2}}}\theta\sin\theta/2\int_0^1\frac{dt}{(t)^{\frac{1}{2}}} \times\exp(-[\tfrac{3}{4}\theta^2+(1-t)\sin^2\theta/2]/4\tau).$$

We now replace τ by $\zeta=1/\tau$, θ by 2θ, and carry out the operation $\partial/\partial\zeta$ that appears under the integral sign:

$$I_1'=\frac{-3\sqrt{3}}{2\pi}\int_0^\infty d\zeta\zeta\int_0^\infty d\theta\theta\sin\theta\int_0^1\frac{dt}{(t)^{\frac{1}{2}}} \times\exp\left(-\frac{\zeta\theta^2}{4}\left[3+(1-t)\frac{\sin^2\theta}{\theta^2}\right]\right) -\frac{\sqrt{3}}{\pi}\int_0^\infty d\zeta\zeta^2\frac{\partial}{\partial\zeta}\int_0^\infty d\theta\theta\sin\theta\int_0^1\frac{dt}{(t)^{\frac{1}{2}}} \times\exp\left(-\frac{\zeta\theta^2}{4}\left[3+(1-t)\frac{\sin^2\theta}{\theta^2}\right]\right).$$

We integrate the second term by parts. The ζ integration is from $\zeta=0$ to $\zeta=L$, where we shall ultimately take the limit $L\to\infty$:

$$I_1'=-\frac{\sqrt{3}}{\pi}L^2\int_0^\infty d\theta\theta^2\int_0^1\frac{dt}{(t)^{\frac{1}{2}}}\exp\left(-\frac{L\theta^2}{4}(4-t)\right) +\frac{\sqrt{3}}{2\pi}\int_0^L d\zeta\zeta\int_0^\infty d\theta\theta\sin\theta\int_0^1\frac{dt}{(t)^{\frac{1}{2}}} \times\exp\left(-\frac{\zeta\theta^2}{4}\left[3+(1-t)\frac{\sin^2\theta}{\theta^2}\right]\right)$$

$$=-2\left(\frac{3L}{\pi}\right)^{\frac{1}{2}}\int_0^1\frac{dt}{(t)^{\frac{1}{2}}(4-t)^{\frac{1}{2}}}-\frac{2\sqrt{3}L}{\pi}\int_0^\infty d\theta \times\int_0^1\frac{dt}{(t)^{\frac{1}{2}}}\frac{\exp\left(-\frac{L\theta^2}{4}(4-t)\right)}{(4-t)} +\frac{2\sqrt{3}}{\pi}\int_0^L d\zeta\int_0^\infty d\theta\frac{\sin\theta}{\theta}\int_0^1\frac{dt}{(t)^{\frac{1}{2}}} \times\frac{\exp\left(-\frac{\zeta\theta^2}{4}\left[3+(1-t)\frac{\sin^2\theta}{\theta^2}\right]\right)}{\left[3+(1-t)\frac{\sin^2\theta}{\theta^2}\right]}$$

$$=-4\left(\frac{3L}{\pi}\right)^{\frac{1}{2}}\int_0^1\frac{dt}{(t)^{\frac{1}{2}}(4-t)^{\frac{1}{2}}}-\frac{8\sqrt{3}}{\pi}\int_0^\infty\frac{d\theta}{\theta^2} \times\int_0^1\frac{dt}{(t)^{\frac{1}{2}}}\frac{\exp\left(-\frac{L\theta^2}{4}(4-t)\right)}{(4-t)^2}+\frac{8\sqrt{3}}{\pi}\int_0^\infty\frac{d\theta}{\theta^2} \times\int_0^1\frac{dt}{(t)^{\frac{1}{2}}}\frac{\sin\theta/\theta}{[3+(1-t)\sin^2\theta/\theta^2]^{\frac{1}{2}}}.$$

Upon integrating the last two terms by parts, the terms containing L vanish and we find

$$I_1'=\frac{8\sqrt{3}}{\pi}\int_0^\infty\frac{d\theta}{\theta}\int_0^1\frac{dt}{(t)^{\frac{1}{2}}}\frac{\partial}{\partial\theta}\frac{\sin\theta/\theta}{[3+(1-t)\sin^2\theta/\theta^2]^{\frac{1}{2}}}$$

from which (35) follows.

Isomerism in Co^{58}

KARL STRAUCH
Radiation Laboratory and Department of Physics, University of California, Berkeley, California
(Received April 28, 1950)

An isomer of Co^{58} has been identified which decays with a half-life of 8.8 hours by emission of a 24.9±1.0 kev γ-ray. The ratio of the K and L conversion coefficients was 1.9±0.2. The relative cross section for formation of the isomeric and ground state of Co^{58} by α-particle bombardment of manganese was found to be 1.7. The conversion coefficient of the 805 kev γ-ray of Fe^{58} was 2.5×10^{-4}. Possible decay schemes are presented.

I. INTRODUCTION

WHEN a manganese metal target was bombarded with 40-Mev α-particles from the 60-inch cyclotron, a weak 8.8 hour activity appeared in the chemically separated cobalt fraction, in addition to the expected long half-lives of Co^{56} (72 days), Co^{57} (270 days) and Co^{58} (72 days). A similar period was found in cobalt fractions from nickel and cobalt bombarded with 18 Mev deuterons and fast neutrons, and from copper placed in the circulating deuteron beam of the 184-inch cyclotron. These cobalt samples were followed with a 3.2 mg/cm² end window Victoreen counter. When a 71 mg/cm² aluminum absorber was placed between the counter and the samples, no 8.8 hour activity could be detected; when a 210 mg/cm² absorber was used, the samples grew with a half-life of approximately 9 hours. The results of the investigation reported here show this new period to be associated with an isomer of Co^{58}. The main part of the work was carried out with a magnetic lens spectrometer of the type described by Siegbahn,[1] calibrated with annihilation radiation.

II. ISOTOPIC ASSIGNMENT

The α-particle bombardment of manganese was found to be the most convenient method of production of the unknown activity; the only other period of comparable half-life formed in this case was the 2.6 hour Mn^{56}. The low measured intensity of the 8.8 hour activity made formation from target impurities suspect. A thorough chemical investigation (see the Appendix) therefore had to be carried out, and different manganese compounds in addition to the metal were used as targets. The bulk of the 8.8 hour activity under investigation followed the cobalt fractions and we can conclude that the new period belongs to that element.

The isotopic assignment is made by considering the momentum spectrum of the cobalt fraction obtained from manganese bombarded with 40 Mev α-particles. This spectrum showed the characteristic radiations[2] of Co^{58}, Co^{57}, and Co^{56} formed by (α, n), $(\alpha, 2n)$ and $(\alpha, 3n)$ reactions. In addition a conversion line was found at 530 gauss-cm which decayed with an 8.8 hour half-life; this corresponds to electrons whose range is only slightly larger than the 0.4 mg/cm² thickness of the nylon counter window. As will be seen in the next section, this line is due to L electrons, the K electrons being absorbed in the counter window. At the same time part of the continuous spectrum grew, and an analysis showed the characteristic β^+-continuum of Co^{58} to be responsible for the growth. The activity associated with the conversion line thus decayed to Co^{58}.

Verification of this assignment was accomplished by reducing the α-energy to 17 Mev with aluminum absorbers, so that Co^{57} and Co^{56} [formed by $(\alpha, 2n)$ and $(\alpha, 3n)$ reactions] were not present. The resulting spectrum is shown in Fig. 1. At low values of $H\rho$ are two peaks due to K and L conversion electrons as obtained with a thin zapon window (Section III). In the center can be seen the continuous β^+-spectrum of Co^{58} that grew as the two low energy conversion peaks decayed (Section IV); the insert at high values of $H\rho$ magnifies the conversion electrons of the 805 kev γ-ray of Fe^{58} (Section V). Any possible contamination by products of an $(\alpha, 2n)$ reaction would have been noticed as conversion electrons of the 117 kev and 130 kev γ-rays emitted in the decay of Co^{57}: no such lines were observed. These results show the existence of an 8.8 hour isomer of Co^{58} decaying to the 72-day ground state.

III. PROPERTIES OF THE ISOMER

In order to study the conversion electrons associated with the new isomer, a thin counter window was constructed with a single zapon film supported by a wire grid. With the counter connected to a 2 liter reservoir, leakage was small enough so the counting characteristics did not change appreciably over 3 hour periods. This fact was checked by taking frequent counts with a standard. The cobalt sulfide sample, prepared from manganese bombarded with 17 Mev α-particles, was placed on a thin zapon film and was estimated to have less than 0.1 mg/cm² thickness. The observed K and L conversion peaks are shown in Fig. 1. The width at half-maximum checks the known resolution of the spectrometer and the two lines are well separated. Possible M conversion electrons could not be resolved and are included under the L peak.

Since any small permanent value of $H\rho$ in the spec-

[1] K. Siegbahn, Phil. Mag. **37**, 162 (1946).
[2] G. T. Seaborg and I. Perlman, Rev. Mod. Phys. **20**, 585 (1948).

trometer is important at the low energies involved here, Auger electrons of Cd^{111} were used to check the calibration of the machine in this region. Values of 17.0 kev and 24.1 kev were obtained for the energies of the K and L cobalt conversion electrons; the $E_L - E_K$ difference of 7.1 kev agrees within the expected error with the cobalt value of 6.9 kev, and the energy of the isomeric transition is given as 24.9 kev. The position of the L line was also measured by reversing the current and taking the average of the two values. The result was 24.2 kev. The energy with estimated uncertainty of the isomeric transition is thus given as 24.9 ± 1.0 kev. Considering this energy value and the half-life of 8.8 hours, a $\Lambda = 4$ transition is indicated, according to Axel and Dancoff.[3]

The ratio of the K to L conversion coefficients has been obtained by comparison of the intensities of the two lines. Lawson and Cork[4] have shown that the ratio of the experimental peak heights (before division of the counting rate by $H\rho$) should be equal to the ratio of the normalized areas (after division of the counting rate by $H\rho$). Experimental values given by these two methods are shown in Table I. The close agreement indicates that self-absorption and back-scattering in the source, if not negligible, at least affect both peaks equally. That the thickness of the counter window did not appreciably influence the ratio was shown by placing zapon films prepared from the same solution as the window over the source. With one film covering the sample a decrease of 2 percent in the relative peak height was observed; with two films this decrease amounted to 7 percent. The contribution of M electrons to the L peak is unknown but is believed to be small. Table I also lists theoretical values for a $\Lambda = 4$ transition obtained from the paper by Hebb and Nelson.[5] The isomeric transition thus appears to be caused by a mixture of magnetic 2^3 and electric 2^4 pole radiation.

The 72-day decay of the ground state of Co^{58} has been investigated by Deutsch and co-workers.[6,7] They have

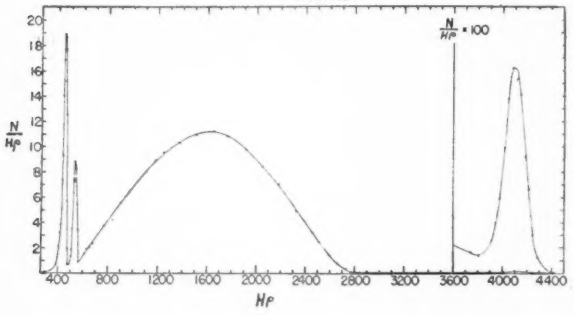

FIG. 1. Momentum distribution of beta-rays of Co^{58} showing internal conversion lines of the Co^{58} isomer and of Fe^{58}.

TABLE I. Experimental and theoretical values for a $\Lambda = 4$ transition of the ratio of the conversion coefficients in the K and L shells for the 24.9 kev γ-ray of Co^{58}.

Experiment		Magnetic 2^3 pole	Electric 2^4 pole
from peak heights	from area		
1.93 ± 0.10	1.89 ± 0.19	6.6	0.41

shown that the decay proceeds 14.5 percent by β^+-emission and 85.5 percent by K-capture to an excited state of Fe^{58} from which the ground state is reached by emission of an 805 kev γ-ray. The β^+-spectrum has an end point of 0.47 Mev. It is concluded that the β^+-transition occurs with an angular momentum change of unity or zero, with the parity change undetermined. No decay to the ground state of Fe^{58} was observed by these investigators, which means that this transition must be at least twice forbidden by comparison with Co^{56} whose decay has this degree of forbiddennesss according to Konopinski.[8]

No evidence for the decay of the isomer of Co^{58} to the ground state of Fe^{58} was found. This would have appeared as high energy β^+-particles decaying with the 8.8 hour half-life. Transitions from the isomer to the excited state of Fe^{58} would have been hard to detect due to the small energy difference between the two states of Co^{58}; however, such transitions must be very rare as indicated in the following section.

IV. RELATIVE CROSS SECTION

During the bombardment of a thick manganese target with 17 Mev α-particles both 8.8 hour isomeric and 72-day ground state of Co^{58} are formed. The continuous β^+-spectrum grows therefore as the isomer decays after the sample is introduced into the spectrometer. This was observed by following the activity at the $H\rho = 1500$ gauss-cm point with time; since the length and intensity variation of the bombardment is known, the ratio of the cross section for the formation of the isomer σ_1 to the cross section for formation of the ground state σ_2 can be calculated and a value of $\sigma_1/\sigma_2 = 1.7$ is obtained. The result would be in serious error if an appreciable number of transitions occurred between the isomer and the excited state of Fe^{58}. This is highly improbable since even if such a transition were of the allowed or first forbidden type it would have a partial half-life comparable to the 72 days of the ground state; however possible spin assignments discussed in Section VI make such a decay very highly forbidden.

V. CONVERSION COEFFICIENT OF THE Fe^{58} γ-RAY

The conversion electrons of the 805 kev γ-ray emitted following β^+-emission by the ground state of Co^{58} are shown in the insert of Fig. 1. A relatively thick source of about 1 mg/cm^2 and a 0.4 mg/cm^2 Nylon counter window were used to measure the β^+-continuum and

[3] P. Axel and S. M. Dancoff, Phys. Rev. **76**, 892 (1949).
[4] J. L. Lawson and J. M. Cork, Phys. Rev. **57**, 982 (1940).
[5] M. H. Hebb and E. Nelson, Phys. Rev. **58**, 486 (1940).
[6] M. Deutsch and L. G. Elliot, Phys. Rev. **65**, 211 (1944).
[7] Good, Peaslee, and Deutsch, Phys. Rev. **69**, 313 (1946).
[8] E. J. Konopinski, Rev. Mod. Phys. **15**, 209 (1943).

TABLE II. Experimental and theoretical values of the interna conversion coefficient in the K shell for the 805 kev γ-ray of Fe^{58}: $\alpha_K \times 10^4$.

Experiment	Electric pole 2^1	Electric pole 2^2	Magnetic pole 2^1	Magnetic pole 2^2
2.5	1.3	3.4	2.4	5.9

the high energy conversion line in order to obtain large enough counting rates. The continuous background between the end of the β^+-spectrum and the 805 kev line was probably due to Compton electrons from the source and parts of the spectrometer. The width at the half-intensity point of the line agrees with the known 4 percent resolution of the spectrometer; however the maximum counting rate on the peak was only twice the normal counter background. This makes the result sensitive to the inevitable background variations. The contribution from photo-electrons produced in the sample should amount to only a few percent. To check on this possible source of error a 2.8 mg/cm² nickel foil was placed over the source and no significant change in peak height observed.

To obtain the desired conversion coefficient the ratio of the area under the line to 6.9 times the area under the continuous β^+-spectrum must be taken. The latter is distorted below 150 kev by scattering in the sample and counter window. Above this energy a Fermi plot gives a straight line. This line was extrapolated to zero momentum and the result used to obtain the area under the β^+-spectrum. The conversion peak contains both K and L electrons. According to Hebb and Nelson[8] the latter amount to 8 percent of the total number. This correction was applied to the observed area under the line. Thus the value quoted in Table II is obtained.

This table also lists theoretical values of the conversion coefficient as interpolated from recent calculations by M. E. Rose.[9] Comparison with the experimental result indicates a magnetic dipole transition, although the estimated accuracy of the measurement is not such as to exclude electric quadrupole radiation. In either case the transition occurs with no change in parity.

VI. DISCUSSION

Figure 2 represents a decay scheme of Co^{58} which is possible on the basis of the results of Deutsch *et al.*,[6,7] summarized in Section III, and the work reported in this paper. The spin of the ground state of Fe^{58}, an even-even nucleus, is undoubtedly zero and the parity was taken as positive on the basis of the shell model. The spin and parity assignments in Fig. 2 are made by assuming the β^+-decay of Co^{58} to be of the allowed type and appear to be the only possible ones if the excited Fe^{58} state decays by magnetic dipole radiation. If electric quadrupole radiation is responsible for this transition, then the assignments for the 0.805 Mev, 1.785 Mev, and 1.810 Mev levels could be 2+, 2+, and 5+, or 2+, 3+, and 6+, respectively. Values of 2+, 3−, and 6− for these levels appear probable if a first forbidden transition is responsible for the β^+-spectrum. In any case the isomeric state has a higher spin value than the ground state.

This is verified by the measured relative cross sections for formation of the two states of cobalt. According to the statistical theory this is given by

$$\sigma_1/\sigma_2=(2I_1+1)/(2I_2+1),$$

where σ_1 and σ_2 are the cross sections for the formation and I_1 and I_2, the spin values of the isomeric and ground states respectively. This formula is only expected to apply to the case of high excitation energy and heavy nuclei as discussed by Segrè and Helmholz.[10] As was just seen, two sets of choices for I_1 and I_2 appear possible. These give theoretical values for the relative cross section of 2.20 and 1.86. These are close to the experimental result of $\sigma_1/\sigma_2=1.7$.

It is of interest to compare the properties of the isomers of Co^{58} and Co^{60}. The latter has been investigated by Deutsch, Elliot, and Roberts[11] and more recent work is quoted by Axel and Dancoff.[3] From these the following conclusions can be drawn.

(1) The Co^{60} isomer decays to the ground state by emission of a mixture of 2^3 magnetic and 2^4 electric pole radiation; this is similar to Co^{58} as shown in Section III. Thus the same spin difference exists between the two levels of each isotope.

(2) The spin I_1 of the isomeric state in Co^{60} is lower than the spin I_2 of the ground state; the opposite is true for Co^{58}. It is possible that corresponding spin values are the same for the two isotopes, but this cannot be ascertained from the available data. The reversal of the spin order might indicate a crossing of energy levels as two neutrons are added to Co^{58}.

The writer is greatly indebted to Professor A. C. Helmholz for his continued interest and many helpful suggestions during the course of this work. The β-ray spectrometer was constructed by Dr. R. W. Hayward and its use is much appreciated. Mrs. D. Stewart sug-

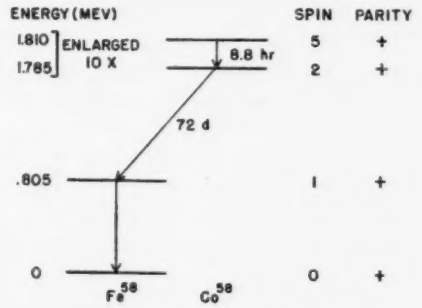

FIG. 2. Proposed decay scheme of Co^{58}.

[8] M. E. Rose *et al.* (private communication).

[10] E. Segrè and A. C. Helmholz, Rev. Mod. Phys. **21**, 271 (1949).
[11] Deutsch, Elliot, and Roberts, Phys. Rev. **68**, 193 (1945).

gested several of the chemical separations. Thanks are also due Mr. Bernie Rossi and the 60-inch cyclotron crew for carrying out the bombardments.

APPENDIX. CHEMICAL PROCEDURE

To the solution of Mn in HCl 10 mg amounts of Co, Cu, Fe, Ni, Zn carriers were added. The 1*N* solution was saturated with $(NH_4)_3SCN$ and shaken with a 50 percent mixture of diethyl ether and amyl alcohol. After several washings the alcohol-ether extract was found to be free of Mn. The remaining metals were removed from the extract by shaking with an ammoniacal solution, the copper precipitated as sulfide in 0.3*N* acid solution, the nickel separated as the dimethyl glyoxime, the zinc obtained as sulfide in nearly neutral solution, the iron precipitated as the hydroxide and finally the cobalt separated as sulfide in a basic solution or precipitated by nitroso-β-naphthol. This procedure in parts or as a whole was repeated several times. After the assignment to the element had been established, 1 mg amounts of Co carrier were extracted from a solution of the manganese target with the alcohol-ether mixture, and directly precipitated as the sulfide from an ammoniacal solution.

PHYSICAL REVIEW VOLUME 79, NUMBER 3 AUGUST 1, 1950

Decay Constants of K^{40}

G. A. SAWYER AND M. L. WIEDENBECK
Randall Laboratory of Physics, University of Michigan, Ann Arbor, Michigan
(Received April 14, 1950)

New measurements have been made of the decay constants of K^{40} for beta-ray emission and for electron capture, and a decay scheme is proposed on the basis of these measurements and the previous data. Special counters adapted to the measurement of low levels of activity were developed for making the measurements. The results obtained were 28.3±1.0 beta-rays per gram of K per sec. and 13.5±4.0 electron captures per 100 beta-rays, corresponding to a total half-life of $12.7\pm0.5\times10^8$ yr., with 88 percent of the decays by beta-ray emission and 12 percent by electron capture. A previous measurement of the gamma-ray intensity in K^{40}, by the present authors, gave 3.6±0.3 gamma-rays per gram of K per sec., or about 12.7 gamma-rays per 100 beta-rays. Since the numbers of gamma-rays and of electron captures in the decay of K^{40} are essentially the same, and since previous measurements indicate that the gamma-energy is greater than the beta-energy, it is proposed that the gamma-ray be associated with the electron-capture decay, a gamma-ray following each electron capture.

I. INTRODUCTION

POTASSIUM 40 is known to decay by beta- and gamma-ray emission and by electron capture, but recent measurements of the decay constants have been in rather poor agreement. The most reliable recent measurements[1–6] of the beta-half-life have given values ranging from 12.0 to 17.8×10^8 yr., with an average value of about 14.4×10^8 yr. The most ingenious method was that of Stout,[4] who mixed into his potassium sources an accurately known activity of Na^{24}, which has nearly the same beta-energy as K^{40}, and measured the ratio of K^{40} to Na^{24} counting rates. Knowing the specific activity of the Na^{24}, he was then able to determine the K^{40} activity directly, without corrections, and obtained 13.1×10^8 yr.

There is even more disparity between the recent estimates of electron-capture intensity, the values ranging from 5 to 190 electron captures per 100 beta-rays. The discrepancies here can be attributed to the uncertainties inherent in the methods used in making the measurements. The measurement of Bleuler and Gabriel[7] was made with a counter arranged to admit gaseous absorbers to absorb selectively the x-rays resulting from the electron-capture decay. Most of the counting rate was due to beta-rays from K^{40}, and the reduction in counting rate when the absorber was introduced was only about two percent. Scattering of the beta-rays in the gaseous absorber may have caused a large part of the two percent change in their counting rate, and the result of 190 electron captures per 100 beta-rays is probably considerably too large. The other determinations[2,8,9] of electron-capture intensity were made from the amount of argon trapped in potassium-bearing minerals, on the assumption that the argon had been produced by decaying potassium. The most refined of these measurements was that of Aldrich and Nier,[10] who used the mass spectrograph to analyze the ratio of A^{40} to A^{36} in minerals. They found that A^{40} was relatively more abundant in potassium-bearing minerals than in present-day atmospheric argon, and from their data they estimated that there are about 10 electron captures per 100 beta-rays in K^{40}.

New measurements of the decay constants for beta-ray emission and for electron capture were undertaken.

[1] T. Gráf, Phys. Rev. **74**, 831 (1948).
[2] L. B. Borst and J. J. Floyd, Phys. Rev. **74**, 989 (1948).
[3] O. Hirzel and H. Wäffler, Phys. Rev. **74**, 1553 (1948).
[4] R. W. Stout, Phys. Rev. **75**, 1107 (1949).
[5] J. J. Floyd and L. B. Borst, Phys. Rev. **75**, 1106 (1949)
[6] F. W. Spiers, Nature **165**, 356 (1950).
[7] E. Bleuler and M. Gabriel, Helv. Phys. Acta **20**, 67 (1947).
[8] L. H. Ahrens and R. D. Evans, Phys. Rev. **74**, 279 (1948).
[9] H. E. Suess, Phys. Rev. **73**, 1209 (1948).
[10] L. T. Aldrich and A. O. Nier, Phys. Rev. **74**, 876 (1948).

A measurement of the gamma-ray intensity, yielding a value of 3.6±0.3 gamma-rays per gram of K per sec. has already been reported.[11]

II. BETA-RAY MEASUREMENTS

A. The Beta-Counter

Measuring the beta-activity of K^{40} is difficult because the activities of available sources are weak, and sources of large area must be used to achieve measurable counting rates. Obviously, the best possible arrangement for measuring the weak activity of K^{40} would be one in which a source of large area could be placed inside a counter in such a manner that every beta-ray leaving the source would be counted. To this end, a special counter was constructed (Fig. 1), using an adaptation of the cell counters developed by Beyster and Wiedenbeck.[12] The counter uses two independent, pancake-like cell-sections. Basically, each section is a short brass cylinder, 6 in. in diameter and $1\frac{1}{4}$ in. high, closed at both ends. The anode wire of each section is a 10-mil tungsten wire, bent into a ring 3 in. in diameter and supported in the center of the section by glass rods which are sealed through the wall of the cylinder. The two cells are placed together, with a common cathode surface between them, and operated as a single counter. This common cathode surface is a thin aluminum-foil disk on which the source of K^{40} is mounted. The counter is so arranged that, for background measurements, the source-bearing foil can be replaced by a blank foil without breaking the vacuum seal of the counter. The two aluminum foils, one blank, and the other bearing the source, are mounted on a tray which can be moved back and forth by a rack-and-pinion arrangement. Thus either foil can be centered in the counter while the other foil moves out into one of the wings of the counter.

This beta-counter, because of the geometrical arrangement, has the advantages over conventional counters that sources of considerable area can be used (about 120 cm^2) and that every beta-ray which leaves the source enters the sensitive volume of the counter.

B. Performance of the Beta-Counter

Before a counter of such unconventional design could be used to measure the absolute number of disintegrations in a sample, it was necessary to prove that it had the proper characteristics, namely, that it actually counted every beta-ray leaving the source and that it added no additional spurious counts itself. Accordingly, tests were made of its plateau, sensitivity, and efficiency.

The counter was filled to 10 cm pressure with a mixture of 90 percent argon and 10 percent alcohol.

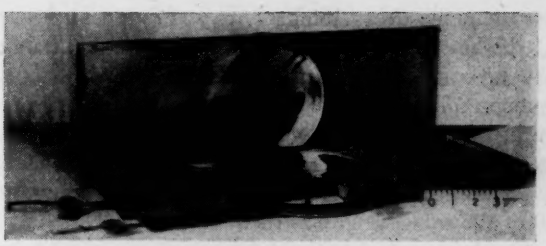

FIG. 1. View of the beta-counter disassembled.

Although the counter was self-quenching, an auxiliary quench circuit was used, because with it the plateau was flattened considerably. The plateau of the counter was about 125 volts long, and the rise in counting rate along it was about three percent per 100 volts.

The sensitivity of the counter was tested by placing a point souce of Tl^{204}, a pure beta-emitter, on the sliding tray inside the counter and measuring the counting rate as the source was moved in $\frac{1}{4}$-in. steps across the diameter. The counter was found to be uniformly sensitive except near the walls and in the exact center, where a small dip was observed in the sensitivity. This dip is not surprising, because a particle leaving the source at the center and passing vertically upward through the counter travels through a region of zero field. A correction of two percent was made to the measured activity of K^{40} to allow for the lack of uniform sensitivity.

The efficiency of the counter was measured by the coincidence method and was found to be greater than 98 percent. Calculations based on the known specific ionization caused in argon by beta-particles[13] indicated that the efficiency of the counter was about 99 percent. Accordingly, a one percent correction was made to the K^{40} data for counter inefficiency.

The tests just described demonstrated that the counter had a flat plateau, high efficiency, and nearly uniform sensitivity and that it was, therefore, suitable for use in measuring the activity of K^{40}.

C. Measurements with Ordinary Potassium

For the measurements on ordinary potassium, sources of chemically pure KCl were used. A saturated solution of KCl in water was sprayed onto aluminum-foil blanks in a fine mist. Any desired thickness could be deposited; the amount deposited was determined by accurate weighings of the blank, both before and after spraying.

Twenty sources were made, of thickness varying from 0.5 to 13 mg/cm^2, and on three weights of aluminum-foil backing: 0.18, 2.67, and 5.43 mg/cm^2. Each of these sources was placed in the counter, together with a blank foil identical with the source-carrying foil, and counting runs were made, alternating source and background

[11] G. A. Sawyer and M. L. Wiedenbeck, Phys. Rev. **76**, 1535 (1949).

[12] J. R. Beyster and M. L. Wiedenbeck, Rev. Sci. Inst. **19**, 819 (1948).

[13] S. A. Korff, *Electron and Nuclear Counters* (D. Van Nostrand Company, Inc., New York, 1946), p. 70.

measurements every 1000 sec. It was found in practice that if the sources were not covered with an aluminum foil, the counting-rate in the counter section faced by the open source increased until the counter went into a continuous discharge. The cause, apparently, was an electrical charging of the insulating surface of KCl. Accordingly, all sources were covered with aluminum foil of the same weight as the backing foil.

From the data obtained with various source- and backing-thicknesses, it was possible to extrapolate the measured activity of the K^{40} beta-rays to zero source-thickness and zero backing-thickness, and this extrapolated value was found to be 28.3 disintegrations per gram of K per sec. This specific activity corresponds to a half-life of 14.2×10^8 yr. for beta-decay in K^{40}, using the recent value[14] of Nier, 0.0119 ± 0.0001 percent, as the isotopic abundance of K^{40} in ordinary potassium.

The statistical counting errors in the experiment are less than one percent except for the thinnest sources. An indication that the statistical errors are small is the fact that in extrapolating the activity to zero source-thickness, when a straight line was drawn through the plotted data, only one point fell more than one percent off the line. Systematic errors, such as those caused by counter inefficiency, are probably not more than two or three percent. The value for the half-life, therefore, is given as $14.2\pm0.5\times10^8$ yr.

D. Measurements with an Enriched Source

A small sample of KCl containing K^{40} enriched to isotopic abundance 0.40 ± 0.02 percent was obtained from the Carbide and Carbon Chemicals Corporation, Oak Ridge, Tennessee, and a source was made from this sample by evaporating the KCl from a tungsten filament onto a silvered zapon film. Source- and backing-thickness were both about 0.1 mg/cm². A measurement of the beta-half-life was made with this source, in the special beta-counter. The measured half-life was $13.0\pm0.7\times10^8$ yr., the largest contribution to the error being in the isotopic abundance of K^{40} in the source. This value barely agrees, within the probable errors, with the measurements made with ordinary potassium. Since only a single measurement was made and the uncertainties are greater, this value is less reliable than the measurements with ordinary KCl sources and, therefore, was not used; the half-life was taken as 14.2×10^8 yr., as measured with the ordinary KCl sources.

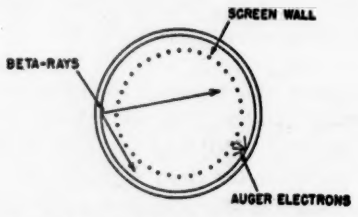

FIG. 2. End view of the electron-capture counter showing paths of beta-rays and Auger electrons.

[14] A. O. Nier, Phys. Rev. 77, 789 (1950).

III. ELECTRON-CAPTURE MEASUREMENTS

A. The Electron-Capture Counter

The electron-capture decay in K^{40} can be positively identified through the characteristic x-rays emitted by the daughter nucleus, A^{40}, as the vacancy in its K shell is refilled. However, in the case of argon, 88 percent of the x-rays are converted to Auger electrons of 2.9-kev energy,[15] and these Auger electrons can be used, instead, as a measure of the electron capture.

The chief problem in measuring the electron-capture intensity with a Geiger counter is to distinguish between the Auger-electron counts and the beta-ray counts which also come from K^{40}. To investigate this problem, a screen-wall counter was constructed. The counter is contained in a cylindrical steel shell, $1\frac{1}{4}$ in. in diameter and 6 in. long. The counter cathode is a cylindrical screen, 1 in. in diameter, placed inside the steel shell and insulated from it, while the anode of the counter is a 12-mil tungsten wire placed axially in the center of the counter. The special screen-cathode was made by winding a "squirrel-cage," or cylindrical grid, of 10-mil copper wire, on a frame consisting of two copper rings, 1 in. in diameter, spaced 5 in. apart and supported by tungsten rods sealed through the end plate of the steel shell. A small bias voltage can be applied between the screen and the shell of the counter. The radioactive source was mounted in a thin layer on the inside surface of the counter shell.

This counter arrangement permitted the Auger electrons to be distinguished from the beta-rays in the counter. The range of the Auger electrons in the counter gas is only a few millimeters and so they were stopped between the shell of the counter and the screen cathode and did not get into the sensitive region of the counter; the beta-rays from the source, on the other hand, are much more energetic, and they were able to pass through the screen into the sensitive region of the counter to be counted. Now, if a bias voltage is applied between the screen and the counter shell so that the screen is negative, the secondary electrons produced by the Auger electrons in ionizing the counter gas between the shell and the screen will be drawn to the shell of the counter and will not be counted. But if the bias voltage is reversed, so that the screen is positive with respect to the shell, the secondary electrons produced by the Auger electrons are drawn through the screen into the sensitive region of the counter and are therefore counted.

The small bias voltage applied (30 volts) has no effect on the trajectory of the high energy beta-rays, and one might, at first thought, expect the beta-ray

[15] A. H. Compton and S. K. Allison, *X-Rays in Theory and Experiment* (D. Van Nostrand Company, Inc., New York, 1935), p. 488.

counting rate to be independent of it. However, applying the positive bias to the screen does increase the number of beta-ray counts, because some of the beta-rays leave the source in such a direction that they do not pass through the screen into the counting region, as can be readily seen from the end view of the counter in Fig. 2. When the screen is made positive, the secondary electrons produced by these beta-rays are drawn through it and are counted, while with the screen negative, they are not counted. Thus, the beta-rays which do not enter the sensitive part of the counter produce exactly the same effect as the Auger electrons, and they must, therefore, be taken into account.

B. Performance of the Counter

Figure 3 shows the counting rate of the counter as a function of bias voltage between shell and screen. It can be seen that at both positive and negative 30-volt bias—the bias voltage used in the measurements with the counter—the counting rate is independent of the bias. This fact indicates that with the screen at 30 volts negative, all secondary electrons formed between shell and screen are prevented from entering the sensitive region of the counter, and that with the screen at 30 volts positive, all secondary electrons formed between shell and screen are drawn into the sensitive region and are therefore counted.

Two beta-ray emitting sources, Na^{24} and K^{42}, were tried in the counter to determine exactly how much the counting rate for beta-rays changed as the screen-bias voltage was switched from negative to positive. The ratio of screen-positive to screen-negative counting rates for the two beta-ray sources was 71.9 and 70.0 percent, respectively. In other words, approximately 71 percent of the beta-rays pass into the sensitive part of the counter.

To determine the characteristics of the counter for Auger electrons, a source of Cr^{51} was used. Cr^{51} decays by electron capture,[16] with 97 percent of the disintegrations going directly to the ground state of V^{51}. The other three percent are by electron capture to excited states of the V nucleus, with emission of gamma-rays as the V falls to its ground state. In the case of V, about 75 percent of the x-rays are converted to Auger electrons,[15] a smaller number than in the case of A^{40} because V has a higher atomic number. The ratio of screen-negative to screen-positive counts for Cr^{51} in the counter was found to be seven percent—vastly different from the ratio for beta-rays. For pure Auger electrons, the ratio should be zero, if all the electrons are stopped in the gas before reaching the screen. The seven percent remaining here is attributed to the V x-rays emitted following 25 percent of the disintegrations.

To establish that all of the Auger electrons were stopped in the gas before reaching the screen, the ratio of screen-negative, to screen-positive counts was determined as a function of gas pressure in the counter. The counting rate with screen-positive was independent of pressure, as would be expected, but the counting rate with screen-negative increased if the gas pressure was reduced below 13 cm Hg. This increase was clearly caused by Auger electrons whose range, at the lower gas pressure, was sufficient to enable them to reach the screen and the sensitive counting region of the counter. The ratio of screen-negative to screen-positive counts as a function of gas pressure is shown in Fig. 4. It is clear that 13 cm of gas pressure is sufficient to stop the Auger electrons from V, which have an energy of 5 kev, and it is therefore adequate to stop the 2.9-kev Auger electrons from A. Accordingly, this was the gas pressure used in the experiments with the K^{40} source.

C. Measurements on K^{40}

For the determination of the electron capture in K^{40}, an extremely thin source of KCl, enriched in K^{40} to isotopic abundance 0.40 percent, was prepared by evaporating the KCl, in a vacuum, from a tungsten filament onto an aluminum-foil blank. The average thickness of this source was about 10 $\mu g/cm^2$, which was approximately one-sixth the range of the Auger electrons from A. The real counts from this source were about half the background counting rate. Several long runs were made with this source, alternated with

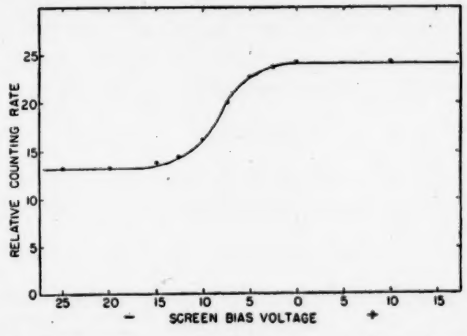

FIG. 3. Counting rate as a function of screen-bias voltage in the electron-capture counter.

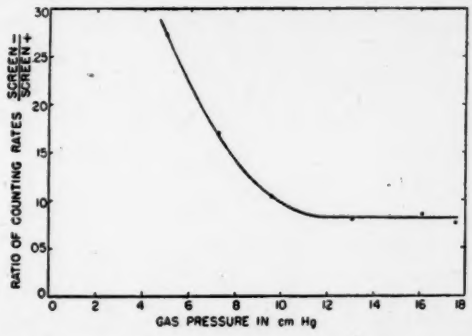

FIG. 4. Ratio of negative-screen to positive-screen counting rate as a function of gas pressure in the electron-capture counter.

[16] Bradt, Gugelot, Huber, Medicus, Preiswerk, and Scherrer, Helv. Phys. Acta 18, 259 (1945).

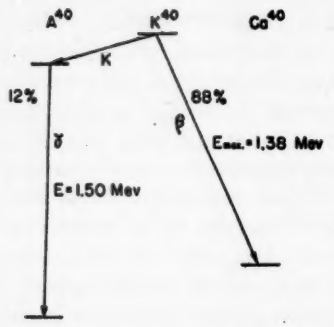

FIG. 5. Proposed decay scheme for K^{40}.

background runs, and a ratio of screen-negative to screen-positive counting rates of 64.4 percent was obtained. This ratio is to be compared with the values of 71.9 percent and 70.0 percent found for the two beta-ray emitters. It is clear that the ratio is slightly lower for K^{40} than for pure beta-ray emitters, a fact which indicates that Auger electrons are present. The number of Auger electrons calculated from these data is 12/100 beta-rays. Since, in addition, x-rays are emitted in 12 percent of the electron-capture decays and these are not detected, the actual number of electron captures is about 13.5/100 beta-rays.

Because of the uncertainty in the corrections for backscattering from the counter wall and for self-absorption in the source, the error in this value is fairly large, possibly as much as 30 percent, and it should not be regarded as exact. It does show, however, that electron capture actually takes place in K^{40}, and in about the same amount as the gamma-ray emission, there being, according to our previous measurement,[11] about 12.7 ± 1.1 gamma-ray per 100 beta-rays.

This result is consistent with the findings of Suess[9] and Aldrich and Nier.[10] The value of Bleuler and Gabriel[7] (190 electron captures per 100 beta-rays), however, is definitely ruled out, since such a large number of electron captures would mean a ratio of screen-negative to screen-positive counts of 30 percent in the present experiment.

III. CONCLUSIONS

When the decay constants of K^{40} for beta-decay (28.3 beta-rays per gram of K per sec.) and electron capture (13.5 electron captures per 100 beta-rays) are combined, the total half-life of K^{40} is calculated to be $12.7\pm0.6\times10^8$ yr.

A decay scheme for K^{40}, shown in Fig. 5, is proposed, which associates the gamma-ray with the electron-capture disintegration to A^{40}, rather than with the beta-decay to Ca^{40}. The reasons for this association are: (1) The most reliable measurements of the beta-ray[5,17–21] and gamma-ray[17,22–24] energies indicate that the gamma-ray energy is greater than the maximum beta-ray energy, and since there are many more beta-rays than gamma-rays in the decay of K^{40}, the gamma-ray cannot easily be fitted into a scheme placing it in cascade with a beta-ray. If the gamma-rays were associated with the beta-ray disintegrations, it would be necessary for part of the beta-decay to be to an excited state of Ca^{40}, followed by gamma-rays to the ground state of Ca^{40}, while the rest of the beta-decay would be directly to the ground state of Ca^{40}. These parallel processes are clearly impossible if no beta-rays have more energy than the gamma-rays. (2) The numbers of electron captures and gamma-ray emissions in K^{40} decay are equal, within the experimental errors, a fact which indicates that there is one gamma-ray for each electron-capture disintegration and that all electron-capture disintegrations are to an excited state of A^{40}, with a gamma-ray following.

[17] O. Hirzel and H. Wäffler, Helv. Phys. Acta **19**, 216 (1946).
[18] Dželepow, Kopjava, and Vorobjov, Phys. Rev. **69**, 538 (1946).
[19] W. J. Henderson, Phys. Rev. **71**, 323 (1947).
[20] D. Alburger, Phys. Rev. **75**, 1442 (1949).
[21] Bell, Weaver, and Cassidy, Phys. Rev. **77**, 399 (1950).
[22] E. Gleditsch and T. Graf, Phys. Rev. **72**, 640 (1947).
[23] P. R. Bell and J. M. Cassidy, Phys. Rev. **77**, 409 (1950).
[24] Pringle, Standil, and Roulston, Phys. Rev. **77**, 841 (1950).

Reflection Properties of Spin ½ Fields and a Universal Fermi-Type Interaction

C. N. YANG
Institute for Advanced Study, Princeton, New Jersey

AND

J. TIOMNO*
Palmer Physical Laboratory, Princeton University, Princeton, New Jersey

(Received March 22, 1950)

It is pointed out that four different transformations are possible under an inversion for fields of spin ½. The consequences are discussed, and the bearing on the possibility of a universal Fermi-type interaction is analyzed.

I. INTRODUCTION

THE transformation property under an inversion of the space coordinates of the wave function of a particle of spin zero (or one) leads to the differentiation between scalar and pseudoscalar (or vector and pseudovector) particles. It is the purpose of the present note to point out that there is also a similar differentiation of the various spin ½ particles. In contrast to the case of integral spin, however, there are for spin ½ particles *four* different types of transformation properties under an inversion.

The types of transformation properties to which the various known spin ½ fields belong are physical observables and could in principle be determined experimentally from their mutual interactions and their interactions with fields of integral spin. In practice this is, of course, very difficult. This problem is discussed in Section III in connection with β-decay and with the symmetry properties of the π-mesons.

In the final section, an attempt is made to see if by properly assigning the various known fields of spin ½ to the four types one could have a universal Fermi-type interaction that would account for the experimental information accumulated in recent years about the interactions between spin ½ fields.

II. GENERAL THEORY

We consider first the transformation property of a *single* particle under an orthochronous proper Lorentz transformation[1] (i.e., a Lorentz transformation involving neither time reversal nor space reflection). The wave function ψ undergoes[2] the following transformation

$$\psi' = S\psi. \tag{1}$$

The matrix S is defined only up to a $(\pm)$ sign. In particular, the identity transformation is represented by

$$S_0 = \pm I, \quad I = \text{unit matrix}. \tag{2}$$

This ambiguity of sign is *necessary* because a rotation through 360° about any axis always brings about a change of sign of the wave function of a spin ½ particle.

The space inversion P is usually represented[2] by the transformation

$$\psi' = \pm\gamma_4\psi. \tag{3}$$

With this definition one might say that there is only *one* double-valued representation of the orthochronous Lorentz group for particles of spin ½. This, however, leads to *two* different possibilities when the transformation properties of two different fields ψ_A and ψ_B are considered at the same time:

$$\begin{cases} \psi_A' = S\psi_A, \quad \psi_B' = S\psi_B & \text{for } L \text{ (orthochronous proper Lorentz transformation)} \\ \psi_A' = \pm\gamma_4\psi_A, \quad \psi_B' = \pm\gamma_4\psi_B & \text{for } P \text{ (space inversion)} \end{cases} \tag{4}$$

or

$$\begin{cases} \psi_A' = S\psi_A, \quad \psi_B' = S\psi_B & \text{for } L \\ \psi_A' = \pm\gamma_4\psi_A, \quad \psi_B' = \mp\gamma_4\psi_B & \text{for } P. \end{cases} \tag{5}$$

If case (4) holds, the fields A and B behave exactly alike under all orthochronous Lorentz transformations. This is customarily accepted as true for all spin ½ fields. We see now that there is also possible the other case (5) in which the two fields A and B *always differ by a rotation of 360° under a space reflection.*

Racah[3] has pointed out that for the space inversion of a single particle it is also possible to have instead of Eq. (3),

$$\psi' = i\gamma_4\psi. \tag{6}$$

This introduces two other possible transformations for a spin ½ field under a space inversion. Altogether, we would have four kinds of fields of spin ½ that behave differently under an inversion. Denoting by ψ_A, ψ_B, ψ_C, and ψ_D four such fields one has under a space inversion

$$\begin{pmatrix} \psi_A' \\ \psi_B' \\ \psi_C' \\ \psi_D' \end{pmatrix} = \pm \begin{pmatrix} \gamma_4 & & & 0 \\ & -\gamma_4 & & \\ & & i\gamma_4 & \\ 0 & & & -i\gamma_4 \end{pmatrix} \begin{pmatrix} \psi_A \\ \psi_B \\ \psi_C \\ \psi_D \end{pmatrix}. \tag{7}$$

It is important to notice that with the simultaneous existence of the fields A, B with C, D the representation

* Rockefeller Foundation fellow of the University of São Paulo, Brazil.

[1] This nomenclature is due to H. J. Bhabha, Rev. Mod. Phys. **21**, 451 (1949).

[2] W. Pauli, *Handbuch der Physik*, Vol. 24/1, pp. 220–227.

[3] G. Racah, Nuovo Cimento **14**, 322 (1937).

becomes four-valued. For example, the identity transformation corresponds now to

$$\begin{pmatrix}\psi_A'\\ \psi_B'\\ \psi_C'\\ \psi_D'\end{pmatrix}=\pm\begin{pmatrix}\psi_A\\ \psi_B\\ \psi_C\\ \psi_D\end{pmatrix}\quad\text{or}\quad\pm\begin{pmatrix}\psi_A\\ \psi_B\\ -\psi_C\\ -\psi_D\end{pmatrix}. \tag{8}$$

The necessity of the two latter possibilities arises from the fact that if the inversion (7) is applied twice one gets a representation of the identify transformation with a relative change of sign of the fields ψ_A, ψ_B and ψ_C, ψ_D.

It is also important to notice that there is no *intrinsic* difference between the A-type fields (i.e., fields with the transformation property of ψ_A) and the B-type fields, or between the C- and D-type fields. The difference is only relative, and is there only if both types of fields exist. If, for example, only C- (or D-) type fields exist, it is impossible to tell whether it is the C-type or the D-type. Further, it would not be appropriate, for example, to call the A-type fields "fields" and the B-type fields "pseudofields." This is to be contrasted with the case of fields with integral spin, for which there is an *intrinsic* difference between fields and pseudofields.

It is easy to show that the charge conjugate field of an A-type field is B-type, and *vice versa*. On the other hand, the charge conjugate field of a C-type field (D-type) is also C-type (D-type). This fact is summarized in Table I.

TABLE I. Field type of charge conjugate field.

Field (particle)	A	B	C	D
Charge conjugate field (antiparticle)	B	A	C	D

It should be remarked that the fact that the C- and D-type fields have the same transformation properties as their charge conjugate fields has led Racah[3] to the proposal that all spin $\frac{1}{2}$ fields transform like C-type fields.

With the Majorana theory, since the field and the charge conjugate field are identical, the C- and D-type transformations are the only possibilities.

III. APPLICATIONS TO ELECTRON AND MESON FIELDS

The five densities $\phi^*\gamma_4\psi$, $\phi^*\gamma_4\gamma_\mu\psi$, $\phi^*\gamma_4(\gamma_\mu\gamma_\nu-\gamma_\nu\gamma_\mu)\psi$, $\phi^*\gamma_1\gamma_2\gamma_3\gamma_\mu\psi$ and $\phi^*\gamma_1\gamma_2\gamma_3\psi$ are usually referred to as scalar, vector, tensor, pseudovector, and pseudoscalar quantities.[4] This is evidently correct if $\phi=\psi$, whatever type of field ψ is. However, if ϕ and ψ are two different fields, and if they belong to different types, it is not correct, for example, to call $\phi^*\gamma_4\psi$ a scalar quantity. In fact, if ψ is an A-type field, while ϕ is a B-type field, then $\phi^*\gamma_4\psi$ is a pseudoscalar.

[4] See, for example, H. A. Bethe and R. F. Bacher, Rev. Mod. Phys. 8, 190 (1936). We use the same notation for the α-, β-, and γ_μ-matrices as these authors.

In the β-decay theory, the following five interactions

$$\psi_P^*\beta\psi_N\psi_e^*\beta\gamma_5\psi_\nu, \tag{9}$$

$$\psi_P^*\psi_N\psi_e^*\gamma_5\psi_\nu-\psi_P^*\alpha\psi_N\psi_e^*\sigma\psi_\nu, \tag{10}$$

$$\psi_P^*\beta\sigma\psi_N\psi_e^*\beta\alpha\psi_\nu+\psi_P^*\beta\alpha\psi_N\psi_e^*\beta\sigma\psi_\nu, \tag{11}$$

$$\psi_P^*\gamma_5\psi_N\psi_e^*\psi_\nu-\psi_P^*\sigma\psi_N\psi_e^*\alpha\psi_\nu, \tag{12}$$

$$\psi_P^*\beta\gamma_5\psi_N\psi_e^*\beta\psi_\nu, \tag{13}$$

are usually rejected on the ground that they are not invariant under a space inversion. We see now that this is not justifiable in view of the fact that the types of fields to which ψ_P, ψ_N, ψ_e, and ψ_ν belong are not known. If it turns out that protons, neutrons, and electrons are all of type A, while the neutrino is of type B, then these five interactions are the invariant ones instead of the usual five.

If the mass of the neutrino is not zero, the interactions (9) to (13) lead to β-spectra different from that predicted by the ordinary interactions, especially near the upper end of the electron spectra. Also, the angular correlation between the electron and the neutrino would be different.

On the other hand, if the mass of the neutrino is zero, it is experimentally impossible to differentiate between the five possibilities (9) to (13) and the usual five (unless one could measure the neutrino spin). This is so because when the square of the matrix element of the interaction Hamiltonian is summed over the spin of the neutrino, the result for (9), for example, is the same as the result for the ordinary scalar-type of Fermi interaction, provided the mass of the neutrino is zero.

It is interesting to notice that the original proposal of Fermi[5] is identical with the interaction (10), rather than with the usual vector interaction. Hence, Fermi's spectrum is different from that of later authors for the case in which the mass of the neutrino is not zero, a fact already pointed out by Konopinski and Uhlenbeck.[6]

The usual statements about the meson theory of nuclear forces need to be understood in a new light now that, for example, $\psi_P^*\beta\psi_N$ can be a pseudoscalar. In particular, contrary to the usually accepted concept, a *scalar* meson *can* have a "pseudoscalar" and a "pseudovector" interaction with the nucleons:

$$iF\psi_P^*\gamma_4\gamma_5\psi_N\phi+iG\psi_P^*\gamma_4\gamma_5\gamma_\mu\psi_N(\partial\phi/\partial\chi_\mu).$$

It is also to be remarked that if the process

$$P\rightarrow N+\pi$$

occurs, it is impossible that the proton field be of type A or B, while the neutron field be of type C or D, or *vice versa*. This fact will be used later in Section IV.

IV. A UNIVERSAL FERMI-TYPE INTERACTION

An analysis of the phenomena of:

$$\beta\text{-decay}: N\rightarrow P+e+\nu, \tag{14}$$

[5] E. Fermi, Zeits. f. Physik. 88, 161 (1934).

[6] E. J. Konopinski and G. Uhlenbeck, Phys. Rev. 48, 7 (1935).

$$\mu\text{-capture}:^{7,8}\ P+\mu^-\rightarrow N+\nu, \tag{15}$$

and

$$\mu\text{-decay}:^{8,9}\ \mu\rightarrow e+2\nu \tag{16}$$

by assuming that the charged μ-meson[10] has spin $\frac{1}{2}$, and that the interactions which lead to these processes are of the Fermi-type, gives values of the coupling constants in the three interactions of the same order of magnitude.[11] This suggests the possibility of the existence of a universal interaction of the Fermi-type between *all* particles of spin $\frac{1}{2}$,[11] provided the requirement of conservation of charge is satisfied. The difficulty immediately arises that such a universal interaction would lead to processes inconsistent with experience, such as

$$N+P\rightarrow e+\nu \quad \text{or} \quad N\rightarrow e^+ +\mu^- +\nu. \tag{17}$$

To rule out these processes, one might propose[12] that some additional conservation laws other than the conservation of charge must be fulfilled. Indeed, with the proper assignment of the spin $\frac{1}{2}$ fields to the four types discussed in Section II, one might expect to obtain such conservation laws as consequences of the principle of invariance under a space inversion.

We have attempted to carry this out but have not succeeded in finding a completely satisfactory assignment. It turns out that some additional rather arbitrary tules will still have to be introduced. In the following, a brief account of our attempt is given, together with the results obtained.

A. The Universal Interaction

To make the proposal of a universal interaction quite definite, one has to choose a definite form of Fermi interaction. We have chosen the Wigner-Critchfield interaction[13]

$$H_{rstu}=g\int d^3\mathbf{x}\sum_{\alpha\beta\gamma\delta}\epsilon_{\alpha\beta\gamma\delta}\psi_\alpha{}^r(\mathbf{x})\psi_\beta{}^s(\mathbf{x})\psi_\gamma{}^t(\mathbf{x})\psi_\delta{}^u(\mathbf{x}), \tag{18}$$

where $\epsilon_{\alpha\beta\gamma\delta}=\pm 1$ is antisymmetric with respect to its four indices, and $\psi_\alpha{}^r(\mathbf{x})$ is the α-component of the q-number spinor wave function of the rth field. To avoid taking into account the explicit occurrence of the complex conjugate of the wave functions in the interaction, we consider a field and its charge conjugate field as *two separate* fields. The reason that the Wigner-Critchfield interaction is chosen is that it is the *only* interaction that is symmetrical with respect to the four fields.[14] It is also evidently invariant under an orthochronous proper Lorentz transformation.

The universal interaction is formulated thus: *Between any four fields r, s, t, u, the interaction (18) exists with the same constant g provided it is consistent with charge conservation and is invariant under a space inversion, in the sense discussed in Section I.*[14a]

This last requirement we use to eliminate the undesired interactions, such as (17). For example, the term H_{rstu} would be absent in the Hamiltonian if the fields r, s, t are of type A and u of type B, C, or D, because in any of these cases H_{rstu} is not invariant under a space inversion.

B. Restrictions on the Assignments of Spin $\frac{1}{2}$ Fields to the Different Types

We want to allow the process

$$N\rightarrow P+e+\nu \tag{19}$$

which amounts to the same thing as

$$P\rightarrow N+\bar{e}+\bar{\nu} \tag{20}$$

where the bar over e and ν means the antiparticle. At the same time we want to forbid the process

$$N+P\rightarrow\bar{e}+\bar{\nu} \quad \text{or} \quad P\rightarrow\bar{N}+\bar{e}+\bar{\nu}. \tag{21}$$

This is only possible if N and $\bar{N}$ have different transformation properties, and from Table I we conclude that the neutron field is of type A or B. Similar reasoning, with the additional requirement that we want to forbid the process

$$N+P\rightarrow\bar{e}+\nu \quad \text{or} \quad P\rightarrow\bar{N}+\bar{e}+\nu, \tag{22}$$

leads to the conclusion that the neutrino is of type C or D. Now it is generally accepted that the π-meson has integral spin and interacts with the $N-P$ field. Therefore, the proton field, like the neutron field, must be of type A or B (see Section III). Consequently, from (19) one concludes that the electron is a C- or D-type field.

From an analogous analysis of the μ-capture, we conclude that μ also belongs to the C- or D-type field.

These assignments lead immediately to a *conservation law of heavy particles* which has been noticed by many physicists.

Another feature of this assignment is that it is consistent with the double β-decay,[15] with Majorana's theory of the neutrino,[16] and with the experiments[8] on μ-decay and π-decay.

C. Results

By writing down all the Fermi-type interactions consistent with charge conservation and continuing the

[7] B. Pontecorvo, Phys. Rev. **72**, 246 (1947).
[8] For more complete references to the literature see J. Tiomno and J. A. Wheeler, Rev. Mod. Phys. **21**, 144–153 (1949). See also, Taketani, Nakamura, Ono, and Sasaki, Phys. Rev. **76**, 60 (1949), and L. Michel, Nature **163**, 959 (1949). Proc. Phys. Soc. London (to be published).
[9] Leighton, Anderson, and Seriff, Phys. Rev. **76**, 159 (1949).
[10] J. Tiomno, Phys. Rev. **76**, 858 (1949).
[11] J. Tiomno and J. A. Wheeler, reference 8; Lee, Rosenbluth, and Yang, Phys. Rev. **75**, 905 (1949).
[12] This was pointed out by Professor E. Fermi in a seminar of about a year ago.
[13] C. L. Critchfield, Phys. Rev. **63**, 416 (1943).
[14] This is so because two spin $\frac{1}{2}$ fields which are not charge conjugate to each other anticommute.
[14a] One notices that the interaction Hamiltonian consistent with this proposal is Hermitian.
[15] E. L. Fireman, Phys. Rev. **75**, 323 (1949).
[16] E. Majorana, Nuovo Cimento **14**, 171 (1937).

above analysis it is found that unless some additional conditions are imposed one cannot eliminate all the undesired interactions (in particular, those indicated in footnotes 17 and 18). To be more definite, the conclusion is as follows:

The only two possible assignments are

$$(\alpha) \quad P, N \epsilon A, \quad \mu, e, \nu \epsilon C \tag{23}$$

where ϵ reads "belong to type." Notice that this assignment is identical, for example, with the assignment

$$P, N \epsilon B, \quad \mu, e, \nu \epsilon C. \tag{24}$$

(Compare Section II.) Or

$$(\beta) \quad P \epsilon A, \quad N \epsilon B, \quad \nu \epsilon C \quad \text{and} \quad \mu, e \epsilon D. \tag{25}$$

But the additional restrictions will have to be imposed that (a) all terms in which a field and its charge conjugate field appear,[17] and (b) all terms in which four identical fields appear[18] are to be excluded from the Hamiltonian.

If experimental results should show the existence of another neutral spin $\frac{1}{2}$ particle μ_0 such as in[8]

$$P+\mu^- \rightarrow N+\mu_0, \tag{26}$$

and[8,9]

$$\mu \rightarrow e+\mu_0+\nu, \tag{27}$$

it would be straightforward to include μ_0 in the present scheme of considerations.

The authors wish to thank Professor J. R. Oppenheimer, Professor E. P. Wigner, and Dr. A. Wightman for helpful discussions.

[17] This is to forbid such processes as $P+\mu \rightarrow P+e$ which contradicts the experimental result that no electrons are emitted in the capture of the μ^--meson by heavy nuclei.

[18] This is to forbid such processes as $N+N \rightarrow \bar{N}+\bar{N}$ which would lead to the instability of complex nuclei.

PHYSICAL REVIEW VOLUME 79, NUMBER 3 AUGUST 1, 1950

The Origin of Cosmic Rays

EDWIN M. McMILLAN
Radiation Laboratory, Department of Physics, University of California, Berkeley, California

(Received January 31, 1950)

The original idea of Menzel and Salisbury concerning the origin of cosmic rays has been extended and some of its possible consequences worked out in more detail. It is concluded that low frequency electromagnetic waves (a few cycles per second) may exist in limited regions near the outer edge of the solar corona, and could accelerate ions to cosmic-ray energies. An attempt is made to explain both the "ordinary" cosmic rays and the intensity increases following solar flares in terms of the action of these waves.

I. INTRODUCTION

IN a very interesting paper Menzel and Salisbury[1] have proposed a mechanism for the origin of cosmic rays, in which the active agent is assumed to be low frequency electromagnetic radiation from the sun. These waves, with frequencies of a few cycles per second, would probably be difficult to detect at the earth's surface because of their nearly total reflection by the ionosphere; there is also some difficulty concerning their propagation through interplanetary space. This comes from the fact that the refractive index of a medium containing N free particles of charge e and mass m per cubic centimeter, traversed by a wave of angular frequency ω, is equal to $(1-4\pi Ne^2/m\omega^2)^{\frac{1}{2}}$. If the usual assumption is made that interplanetary space contains at least one free electron per cubic centimeter, one finds that the refractive index becomes imaginary, leading to total reflection of the waves, for frequencies less than 9 kilocycles per second.

This situation is not improved by relativistic effects; the results of Section II of this paper show that electrons starting from rest move so that the relation between their displacement and the phase of the wave is identical with that given by classical laws, so that the refractive index formula requires no relativistic correction, except for that imposed by the initial velocities of the electrons which will not change the order of magnitude of the low frequency transmission limit.

In spite of these difficulties, it seems worth while to examine the possibilities of this type of mechanism in more detail. The initial problem is to find the relativistic motion of ions under the influence of such waves, which is done in the following section.

II. MOTION OF IONS IN A PLANE WAVE

It is desired to find the motion of a charged particle in a plane polarized electromagnetic wave. (The more general case of arbitrary polarization with different time variations of the components leads to a very similar solution; since it does not alter any of the conclusions, this extra complication has been omitted.) Let the wave be moving in the positive x-direction with the electric vector in the y-direction, and let the electric field at a fixed point vary with time like $(1/e)F(t)$, where e is the charge on the particle. The field com-

[1] D. H. Menzel and W. W. Salisbury, Nucleonics **2**, No. 4, 67 (1948).

ponents (in Gaussian units) are then given by:

$$E_y=H_z=F(\theta)/e, \quad \theta=t-(x/c). \tag{1}$$

The dynamical equations are (neglecting radiation reaction):

$$dW/dt=ev_yE_y=v_yF(\theta), \tag{2}$$

$$dp_x/dt=ev_yH_z/c=v_yF(\theta)/c, \tag{3}$$

$$dp_y/dt=eE_y-ev_xH_z/c=[1-(v_x/c)]F(\theta), \tag{4}$$

$$dp_z/dt=0. \tag{5}$$

In the above, W represents the particle energy, which we shall understand to mean the total relativistic energy, p represents the momentum, and v the velocity.

In order to solve these, we must eliminate the time. Dividing (2) by (3) gives $dW=cdp_x$, so that $W-cp_x$ is a constant of the motion. We also have the relativistic relation $cp_x/W=v_x/c$, and the kinematic relation $d\theta/dt=1-v_x/c$. Therefore, letting M be an arbitrary constant determined by the initial conditions,

$$W-cp_x=W[1-(v_x/c)]=W(d\theta/dt)=\text{const.}\equiv Mc^2. \tag{6}$$

With the help of this we find that the components of momentum can be written:

$$p_x=(W/c^2)v_x=(W/c^2)(dx/d\theta)(d\theta/dt)=M(dx/d\theta), \quad p_y=M(dy/d\theta), \quad p_z=M(dz/d\theta). \tag{7}$$

Now since $d/dt=[1-(v_x/c)]d/d\theta$, Eqs. (4) and (5) become:

$$M(d^2y/d\theta^2)=F(\theta), \quad d^2z/d\theta^2=0, \tag{8}$$

which are identical (except for θ replacing t) with the classical equations of motion of a particle of mass M moving under the y-force $F(t)$. Then (2) and (3) can be written:

$$dW/d\theta=F(\theta)(dy/d\theta)=M(d^2y/d\theta^2)(dy/d\theta)=(M/2)(d/d\theta)(dy/d\theta)^2, \tag{9}$$

$$d^2x/d\theta^2=(1/Mc)F(\theta)(dy/d\theta)=(1/2c)(d/d\theta)(dy/d\theta)^2. \tag{10}$$

Thus the energy change is related to $dy/d\theta$ as it is classically to dy/dt, again letting M play the part of an equivalent mass. The procedure in making a solution is now obvious; y, z, and W are found from Eqs. (8) and (9) which are like the classical ones, and x from the integral of (10); then θ can be eliminated to find the path. If the time relations are desired, the relation between t and θ is found from the integral of $dt=d\theta+dx/c$.

As an illustration, consider the case of a particle starting from rest, for which M is the rest mass m_0, and:

$$\left.\begin{aligned} dy/d\theta&=1/m_0\int_0^\theta F(\theta)d\theta \\ W-m_0c^2&=\tfrac{1}{2}m_0(dy/d\theta)^2 \\ dx/d\theta&=(1/2c)(dy/d\theta)^2 \\ dt/d\theta&=1+(1/2c^2)(dy/d\theta)^2 \end{aligned}\right\}. \tag{11}$$

An interesting corollary of these relations is that $dy/dx=[2m_0c^2/(W-m_0c^2)]^{\frac{1}{2}}$, so that a particle accelerated from rest to a kinetic energy large compared with its rest energy moves nearly parallel to the direction of propagation of the wave, rather than at right angles to that direction; the sense of this motion is always positive.

As a still further specialization, consider the wave described by $F=eE_0\sin(2\pi c\theta/\lambda)$, with the particle starting at $\theta=0$, $x=0$, $y=0$. The integrations are elementary and will not be written down. One cycle of the path is a monotonic S-shaped curve, something like half of a curly bracket, with the initial motion in the y-direction. At the end of the cycle $x=\frac{3}{4}k^2\lambda$, $y=k\lambda$, and the elapsed time is $(1+\frac{3}{4}k^2)\lambda/c$, where $k=eE_0\lambda/2\pi m_0c^2$. The time interval is longer than the period of the wave because the particle tends to follow the wave crest. The kinetic energy reaches its maximum value of $2k^2m_0c^2$ at the middle of the cycle, and returns to zero at the end. The next cycle will repeat this motion from the new starting point. Thus the energy is oscillatory, while the displacements are cumulative. A similar treatment with arbitrary starting phase shows that the path is always made of "curly bracket" segments, the energy is always oscillatory and the x-displacement always cumulative, while the y-displacement is cumulative except in the singular cases of starting phase $\pm 90°$. The mean velocity of progression in the x-direction ranges from $\frac{1}{4}k^2c/(1+\frac{1}{4}k^2)$ to $\frac{3}{4}k^2c/(1+\frac{3}{4}k^2)$. This continued displacement is not to be described as an effect of "radiation pressure" in the usual sense; the latter has in fact been left out by the omission of radiation reaction terms from the equations of motion.

III. ORIGIN AND PROPAGATION OF THE WAVES

It is clear that low frequency waves cannot propagate through the solar corona. This is a highly ionized medium in which mass motions of matter, currents, and magnetic fields are linked together by magneto-hydrodynamic laws. It is probable that the motions have a high degree of turbulence, driven by the turbulent motion of the sun's surface. The outer boundary of such a medium would then be expected to radiate at frequencies corresponding to the fluctuation frequencies of the currents; it is therefore postulated that the Menzel-Salisbury waves originate in the extreme outer parts of the solar corona. Their further fate is hard to predict. They may simply be totally reflected by electrons in the immediately adjacent region of space, but there is another possibility. The results of Section II show that charged particles will be rapidly driven along by the waves, and if this rate of removal exceeds the rate of escape from the corona, which is probably limited by the static magnetic fields accompanying the coronal matter, the waves may be able to clear a path for themselves by sweeping out all the ions in their way. This process could conceivably proceed to the extent of clearing the ions out of a large part of inter-

planetary space. The latter however seems unlikely, and we shall tentatively suppose that the waves gain only an occasional temporary victory over the electrons in local regions of high solar activity. According to this idea, sometimes there will be a sufficient long wave intensity over some part of the coronal surface that electrons and ions will be pushed out of a region many wave-lengths in extent. The front of this region will still be totally reflecting, but since the boundary is not likely to be flat the reflected waves will not be expected to retrace the path of the incident waves, and therefore there can be an appreciable volume occupied by traveling waves. In the following, such regions will be treated as the accelerating agents of cosmic rays; for convenience they will be called "wave bubbles."

Some justification should be made for invoking a mechanism which is at first sight rather strange, and may turn out to be impossible when the physical circumstances at the edge of the corona are better understood. One reason is that it does not seem possible to generate a sufficiently high electric field strength in the presence of the normal concentration of free electrons; another is that standing waves in regions of total reflection are not as effective as traveling waves in accelerating particles to relativistic velocities. The correct treatment of the situation at the coronal edge, involving the transition from a magneto-hydrodynamic region to one of relatively free ion motion, is beyond the author's competence but it may be a rewarding field for investigation. If it should turn out that "wave bubbles" cannot be formed, the idea of cosmic-ray acceleration by electromagnetic waves may have to be abandoned. There would still remain the possibility that the non-radiative fields (chiefly magnetic) associated with the turbulent motion of the corona could accelerate cosmic rays by a mechanism similar to that suggested by Fermi[2] for interstellar fields.

IV. DIRECT ACCELERATION OF COSMIC RAYS

The recent observations of large temporary increases in cosmic-ray intensity following solar flares suggest that in these cases at least one is dealing with a direct production of cosmic rays by the sun. The following connection is proposed. The flare initiates a large magnetic disturbance at the sun's surface; this is propagated through the corona, and when it reaches the surface of the latter a "wave bubble" is formed. Then ions are accelerated by the mechanism of Section II. Assuming, for example, a sinusoidal wave of frequency 10 cycles per second and peak electric field of 10 volts per cm acting on protons, and applying the formulas of the last paragraph of Section II, it is found that an energy of 5×10^{10} ev can be imparted to the protons. They would move forward 9.4 wave-lengths during their acceleration, which would take place in a half-cycle of wave phase as seen by the particle. Electrons in the same wave field would tend to acquire still higher energies, but would move forward so far that the finite size of the bubble would be a limiting factor. Thus if the wave field is terminated at 10 wave-lengths, electrons starting at the most favorable phase (maximum field) would pick up only about 6×10^{9} ev. On the other hand, multiply charged heavy ions would acquire great energy; a completely stripped iron nucleus would be accelerated to a maximum of 6×10^{11} ev by the same field.

The above figures show that no extreme assumptions regarding field strength or frequency are necessary to account for acceleration to energies sufficient to penetrate the earth's magnetic field. The question of escape from the sun's general magnetic field must be left open since so little is known about its magnitude at present. No "prediction" of particle energies can be made since the intensities and frequencies of the waves, as well as the dimensions of the bubbles, are not known. However it is suggested that the energy spectrum and composition of the "solar flare" cosmic rays may be rather different from that of the "ordinary" cosmic rays; in particular, the very highest energies (Auger showers) may be lacking, and some primary electrons may be present.

V. SOURCE OF THE "ORDINARY" COSMIC RAYS

The steady flux of cosmic rays can hardly be accounted for by the direct action of the process discussed, the most compelling argument against this being the contrast between the constancy of cosmic radiation and the variability of solar activity. Various mechanisms involving cumulative acceleration have been proposed, such as the theories of Fermi,[2] Richtmyer and Teller,[3] and Alfvén.[4] In the first of these, the acceleration is assumed to occur in interstellar space; in the other two, the ions are assumed to be confined to the solar system by a weak but very extended magnetic field. In this paper the second assumption will be made. (It should be pointed out that the process of Section IV could serve as an injector for the Fermi acceleration mechanism, but this does not remove all the difficulties of that mechanism in accelerating the heaviest ions.) The source of the trapping magnetic field is rather obscure, but an extremely small unbalanced rotation of the interplanetary positive ions and electrons would be capable of producing a field having suitable magnitude and configuration, and the general rotation of the solar system may be capable of exciting such a motion.

It is clear that in the presence of a trapping field, ions will continue to circulate in the solar system until removed by collisions or perhaps by escape from some orbits that extend very far out. If this situation exists, a very small average rate of "injection" from the sun would be sufficient to account for the observed cosmic-ray flux, and therefore it is suggested that the process of Section IV, even though it may occur infrequently, is the

[2] E. Fermi, Phys. Rev. **75**, 1169 (1949).
[3] H. D. Richtmyer and E. Teller, Phys. Rev. **75**, 1729 (1949).
[4] H. Alfvén, Phys. Rev. **75**, 1732 (1949); **77**, 375 (1950).

primary source of all cosmic radiation. The particles of the cosmic rays would then represent a sample of ions taken from the edge of the solar corona, and since even relatively heavy elements exist there in a highly ionized state these heavy particles would be accelerated as effectively as protons.

Accepting tentatively the assumption that trapping of ions takes place, one can then proceed in two ways. One can suppose that no further acceleration takes place, and that the observed steady flux represents an average of all the "solar flare" particles emitted for the past few million years, with the electrons removed by radiative losses and by the inverse Compton effect. This would imply that some flares cause waves intense enough to accelerate the highest energy particles observed. (If the orbits are distributed uniformly throughout a sphere of radius 50 times the earth-sun distance, the mean life for capture by the planets is about 6 million years. Capture by the sun, if allowed by the solar magnetic field, would reduce this by a factor of 50. Capture by meteoritic matter, because of the large cross section per unit mass of finely divided material, could be even more important but is hard to estimate.)

The second possibility is that the circulating ions receive further acceleration by subsequent passages through "wave bubbles." One bubble with a diameter of 10 wave-lengths of 10-cycle radiation would have a cross section about twice that of the combined planets. The frequency of occurrence of bubbles cannot be inferred from the observed cosmic-ray intensity increases, since they may not all contain waves intense enough to cause such increases, and may not all eject particles in a suitable direction for observation at the earth. Therefore a reasonable estimate of the chance for an ion to undergo repeated traversals through strongly accelerating regions, with an average cumulative gain in energy, cannot be made. Nevertheless a cumulative process for the production of the very highest energies is attractive, and if the regions of strong acceleration are not sufficiently numerous, another source of cumulative acceleration may be found in the action of the nonradiative magnetic fields of the solar corona.

PHYSICAL REVIEW VOLUME 79, NUMBER 3 AUGUST 1, 1950

The Extraordinary Increase of Cosmic-Ray Intensity on November 19, 1949

SCOTT E. FORBUSH
Department of Terrestrial Magnetism, Carnegie Institution of Washington, Washington, D. C.
AND
THOMAS B. STINCHCOMB AND MARCEL SCHEIN
Department of Physics, University of Chicago, Chicago, Illinois
(Received April 20, 1950)

Four sudden increases in cosmic-ray intensity associated with solar flares or chromospheric eruptions have so far been observed during more than a decade of continuous registration of cosmic-ray intensity. The last and largest of these increases occurred on November 19, 1949, when such an effect was recorded for the first time at a mountain station at Climax, Colorado. Here the intensity increased to about 200 percent above normal in half an hour. At the sea-level station at Cheltenham, Maryland, the increase was about 43 percent. No increase occurred at the equator. From the increase in the effect with altitude and latitude, it is concluded that the increase was due to the nucleonic component produced by relatively low energy primary charged particles probably accelerated by some solar mechanism.

THE sudden increase in cosmic-ray intensity which began at 10^h45^m GMT, November 19, 1949, was the largest yet recorded during more than a decade of continuous registration of cosmic-ray ionization at several stations (see Table I). Only three other unusual increases had been previously recorded.[1] These occurred on February 28, 1942, March 7, 1942, and July 25, 1946. All were registered with Compton-Bennett ionization chambers completely shielded with 12-cm Pb. Three of the increases began during intense chromospheric eruptions or solar flares.[1] While no solar flare was actually observed during the increase of cosmic-ray intensity on March 7, 1942, a radio fadeout occurred very near the time the increase in cosmic-ray intensity began. The fadeout, which occurred only on the daylight side of the earth, quite definitely indicates the existence of a solar flare.

The terrestrial-magnetic effect of such solar flares is

TABLE I. Location and elevation of Compton-Bennett cosmic-ray meters.[a]

Station	Latitude (degrees)	Longitude (degrees)	Geomagnetic latitude (degrees)	Elevation (meters)	Operation began
Godhavn, Greenland	69.2 N	53.5 W	79.9 N	9	October, 1938
Cheltenham, Maryland	38.7 N	76.8 W	50.1 N	72	March, 1935
Climax, Colorado	39.4 N	106.2 W	48.1 N	3500	
Teoloyucan, Mexico	19.2 N	99.2 W	29.7 N	2285	February, 1937[b]
Huancayo, Peru	12.0 S	75.3 W	0.6 S	3350	June, 1936
Christchurch, New Zealand	43.5 S	172.6 E	48.6 S	8	June, 1936

[a] 12-cm Pb shield around all meters, except that the meter at Climax had, in addition, a slab of Fe 16.5 cm thick directly over the meter.
[b] Not operating after 1945.

[1] S. E. Forbush, Phys. Rev. **70**, 771 (1946).

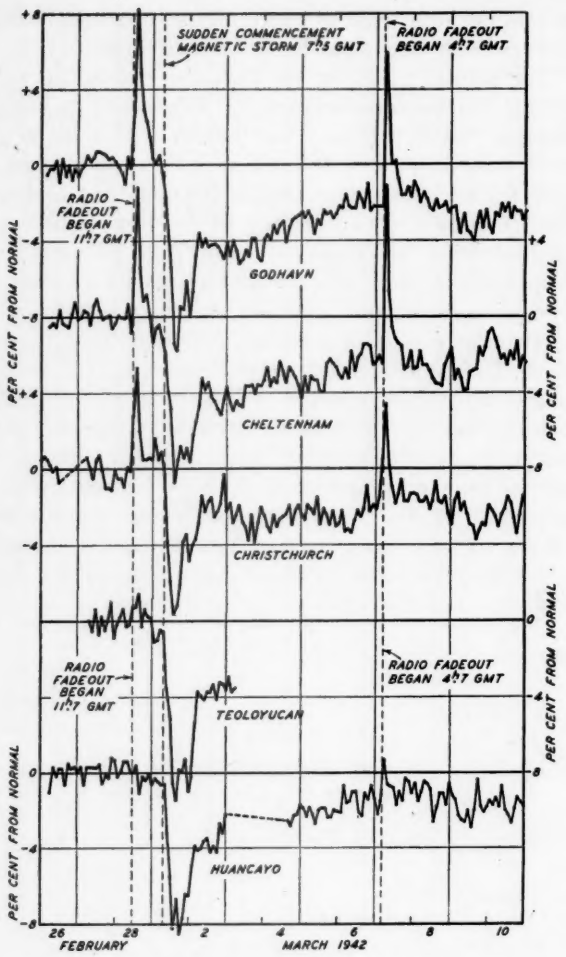

FIG. 1. Increases of cosmic-ray intensity, February 28 and March 7, 1942.

an increase, on the daylight side of the earth, in the normal diurnal variation in the earth's field.[2] The known small diurnal variation[3] in cosmic-ray intensity excludes the possibility that the increases were due to changes in the earth's external magnetic field resulting from an augmentation of the magnetic diurnal variation. The evidence thus indicates[1] that the four increases in cosmic-ray intensity were probably due to charged particles accelerated by some mechanism[4] on the sun. Unless the particles responsible for the increases were charged, it would be difficult to explain either the simultaneous occurrence of the increases on both the daylight and dark hemispheres or the absence of the increases at the equator.

The sudden increases in cosmic-ray intensity on February 28 and March 7, 1942, are shown in Fig. 1, in which the curves are drawn through the bihourly means, after correcting these to constant barometric pressure. It is evident that neither increase occurred at

[2] A. G. McNish, Terr. Mag. 42, 109 (1937).
[3] S. E. Forbush, Terr. Mag. 42, 1 (1937).
[4] Forbush, Gill, and Vallarta, Rev. Mod. Phys. **21**, 44 (1949).

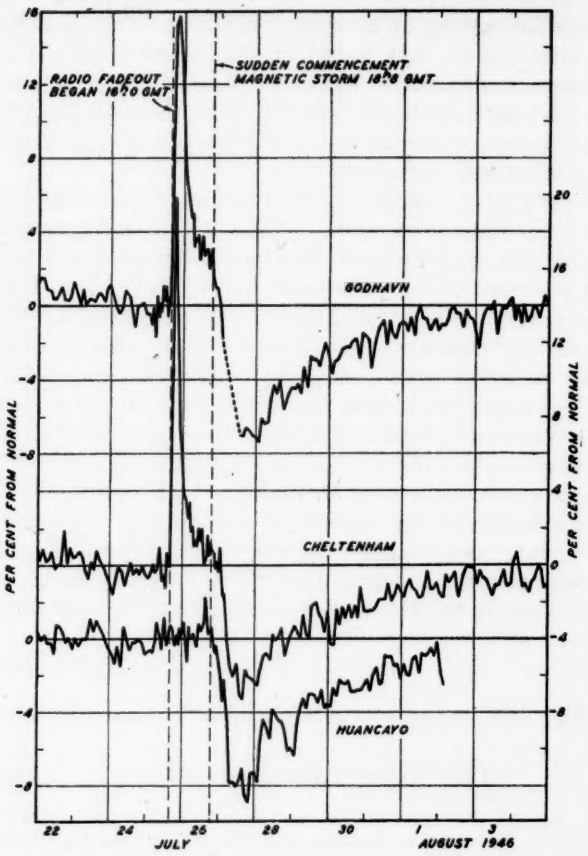

FIG. 2. Increase of cosmic-ray intensity, July 25, 1946.

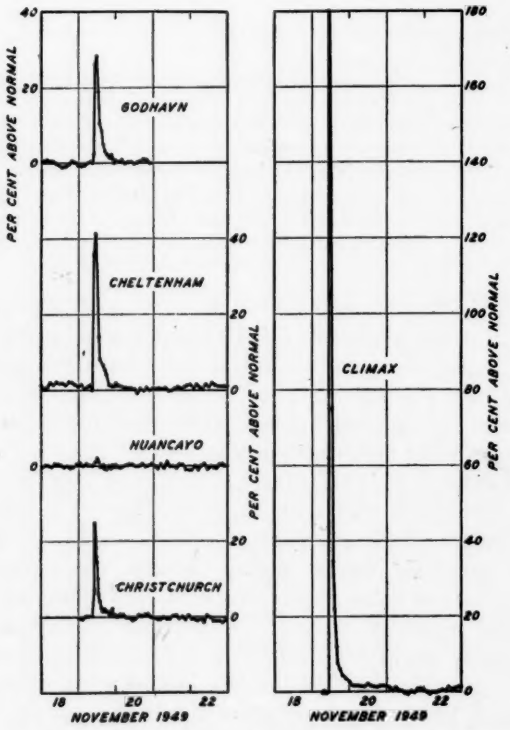

FIG. 3. Increase of cosmic-ray intensity, November 19, 1949.

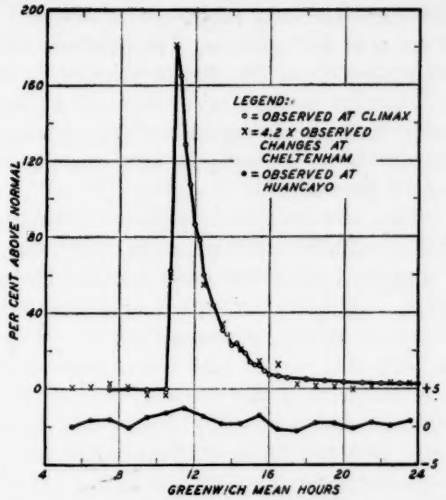
LEGEND:
○ = OBSERVED AT CLIMAX
× = 4.2 × OBSERVED CHANGES AT CHELTENHAM
• = OBSERVED AT HUANCAYO
PER CENT ABOVE NORMAL
GREENWICH MEAN HOURS

FIG. 4. Cosmic-ray intensity, November 19, 1949.

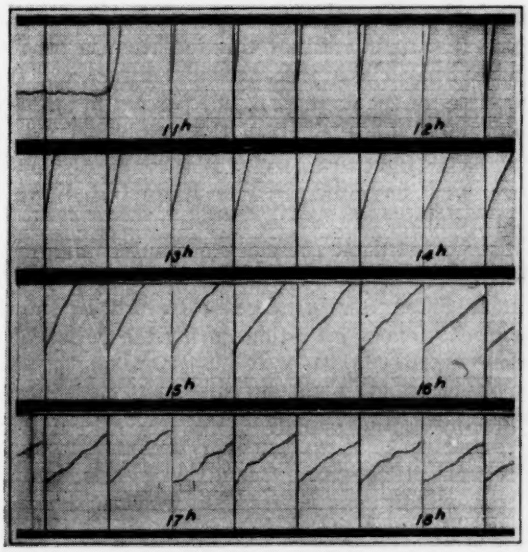

FIG. 5. Cosmic-ray records for Climax, Colorado, showing increase beginning at 10 hr. 45 min. GMT, November 19, 1949.

Huancayo and that the increase on February 28 did not occur at Teoloyucan. The decrease in cosmic-ray intensity during the magnetic storm following the sudden commencement on March 1 is evident at all the stations. The sudden increase in cosmic-ray intensity on July 25, 1946, is shown in Fig. 2. No data for this period were available from the other stations in Table I. Again, no increase occurred at Huancayo although the decrease during the subsequent magnetic storm is evident there.

The sudden increase in cosmic-ray intensity at the time of the solar flare on November 19, 1949, is shown in Fig. 3. This is the first instance when an increase in bosmic-ray intensity accompanying a solar flare has ceen recorded at a mountain station and at sea-level stations. The increase, in percent of the total cosmic-ray ionization, is obviously very much greater at Climax than at Cheltenham. In fact, if the ordinates on the curve showing the increase at Cheltenham are multiplied by 4.2, the resulting points, shown in Fig. 4, lie on the curve for Climax. It may also be noted in Fig. 3 that the increase on November 19 was not followed by a decrease in cosmic-ray intensity during the magnetic storm which began about 18^h GMT on November 19.

The rapid increase on November 19, 1949, is evident beginning at 10^h45^m GMT in Fig. 5, which is a reproduction of part of the cosmic-ray record for Climax on that date. The electrometer is grounded every 15 min. The large increase in intensity caused the image of the electrometer needle to go off scale during the first few minutes in several of the 15-min. intervals. Departures of cosmic-ray intensity from the balance-value (electrometer trace horizontal) in percent of the total intensity are obtained by multiplying the slope by 9.8.

Figures 6 and 7 permit more detailed comparison of the solar-flare effects observed at several stations than

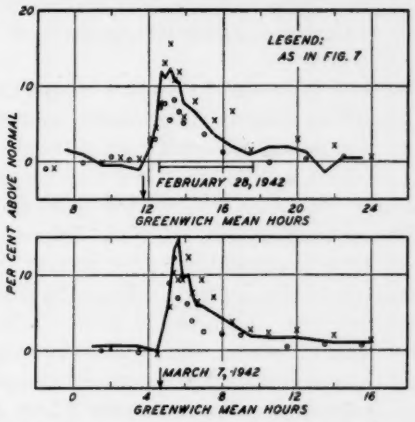

FIG. 6. Increases in cosmic-ray intensity during two solar flares, for different stations.

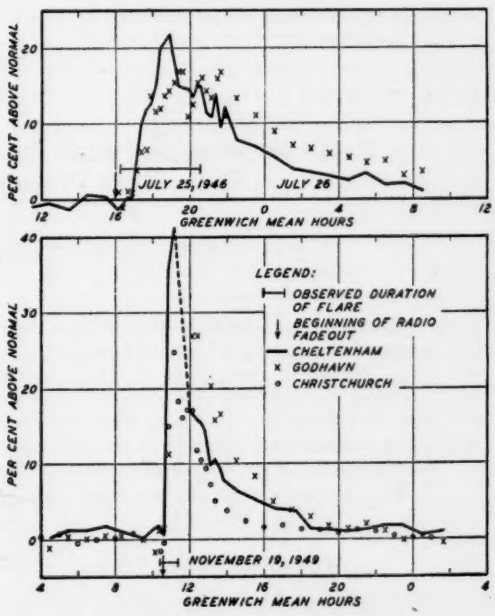

FIG. 7. Increases in cosmic-ray intensity during two solar flares, for different stations.

is possible in Figs. 1, 2, and 3. The observed durations of the solar flares are also indicated as well as the times of commencement of the radio fadeouts.

In addition to complete shielding by 12-cm Pb, the meter at Climax was under a rectangular iron shield 4 ft. long, 1 ft. wide, and 16.5 cm thick. The absorption mean free path for nucleons of medium energy in iron is approximately 240 g cm^{-2}. Taking the dimensions of the shield into account and figuring the zenith angle distribution for a radiation exponentially absorbed with an absorption coefficient of about 145 g cm^{-2}, it is estimated that the increase at Climax on November 19, 1949, would have been 15 percent greater without the iron shield. Thus it is estimated that the maximum of the increase on November 19 at Climax would have been about 207 percent without the iron shield, instead of the uncorrected 180 percent as shown in Figs. 3 and 4. This correction also results in a factor of 4.8 for the ratio of the percentage increase at Climax on November 19 relative to that at Cheltenham, instead of 4.2 as is indicated in Fig. 4.

Since the total ionization at Climax (under 12-cm Pb) is about 2.5 times that at Cheltenham, and since the percentage increase on November 19, 1949, was about 4.8 times that at Cheltenham, the actual magnitude of the increase on that date at Climax was about 12 times greater than at Cheltenham. Since the difference in the atmospheric layer is equivalent to 340 g cm^{-2}, the radiation responsible for the increase during the flare has an absorption coefficient of about 137 g cm^{-2}. This is just about the rate at which the nucleonic component, responsible for star production, increases with altitude.[5] The increase in total ionization under 12-cm Pb by a factor of 2.5 from Cheltenham to Climax is mainly due to mesons. It is thus evident that the magnitude of the flare effect increases too rapidly with altitude to be ascribed to ordinary mesons. The latitude effect in chambers under 12-cm Pb, due principally to mesons, is small, whereas the flare effect exhibits a strong dependence on latitude (being zero at the equator). This also indicates that ordinary mesons contribute negligibly to the flare effect.

The results of Conversi[6] and those of Simpson[7] on the latitude variation of the proton and neutron intensity suggested that the cross section for nucleon production relative to that for meson production decreases rapidly with increasing energy of primary particles. This is in accord with the conclusion that the increase in intensity during the solar flare of November 19, 1949, was due principally to the nucleonic component or to local radiations originating from it, and not to ordinary mesons.

At Climax, under 12-cm Pb, probably not more than about 10 percent of the total ionization is normally due to local radiation originating from the nucleonic component. If we assume that this radiation is produced entirely by particles in the same band of energy as those responsible for the increase of 207 percent in ionization on November 19, 1949, then the number of primary particles, reaching there per unit time, in that band of energy, must have increased to at least 20 times the normal value.

Three sets of triple coincidence counters and one set of fourfold coincidence counters, located above the meter at Climax and arranged to record air showers, were in continuous operation during the period of the increase in ionization on November 19, 1949. There was no evidence of any significant increase in the rate of air showers during this period.

[5] J. J. Lord and Marcel Schein, Phys. Rev. **75**, 1956 (1949).

[6] Marcello Conversi, Phys. Rev. **76**, 444 (1949).

[7] J. A. Simpson, Jr., Phys. Rev. **76**, 569 (1949).

PHYSICAL REVIEW VOLUME 79, NUMBER 3 AUGUST 1, 1950

Ratio of Cross Sections for Electron Capture and Electron Loss by Proton Beams in Metals

THEODORE HALL
Institute for Nuclear Studies, University of Chicago, Chicago, Illinois
(Received March 2, 1950)

Measurements have been made of the ratio of the charged to the neutral component (protons to hydrogen atoms) in hydrogen ion beams of energies between 20 and 400 kv, passing through the metallic media beryllium, aluminum, silver, and gold. The data show that this ratio is the same, within the accuracy of the experiment, for the three lighter elements, but is slightly less in gold above 100 kv. The curves depicting this ratio as a function of ion speed cannot be fitted by a power law over the entire energy range, but the high energy end of the data can be fitted fairly well in this way. At 350 kv, the slopes correspond to a dependence on ion speed v of the form v^9 in the case of the lighter elements, and v^7 in the case of gold.

The cross sections for electron capture and electron loss are found to be equal at an ion energy of 26 kv. The ion then has a speed 0.95 times that of the hydrogen orbital electron ($e^2/\hbar$).

I. INTRODUCTION

FOR several reasons there is interest in the capture and loss of electrons by light ions as they pass through matter: the phenomena themselves are fundamental atomic processes; the charge of these ions influences their slowing down; and furthermore, in the case of the light ions it is possible to test present ideas about electron capture and loss which apply to the

stopping of fission fragments, where charge of the fragment plays a major role.

An incomplete listing of previous work on this subject is given.[1–15] References 1 to 4 deal with experimental work on hydrogen canal rays, 5 to 9 with experimental work on alpha-rays, 10 and 11 with the classical theory of electron capture, 12 and 13 with the quantum-mechanical theory of capture, and 14 and 15 with general surveys on the field. The article by Bohr,[15] offers simple ideas for handling the difficult problem of electron capture under a wide range of conditions, and the present data will be considered largely in the light of these ideas.

In studying the average charge of fast ions, these specific questions are of the greatest interest: how does the state of charge depend on the speed of the ion, how does it depend on the stopping medium, and at what ion speed is it equally likely for a given electron orbit to be filled or unfilled? An experimental answer to these questions is most instructive in the case of hydrogen ions, for which the theory is simplest. It is also desirable to investigate light ions of speeds near the speed $v_0=e^2/\hbar$, because capture and loss cross sections are then nearly equal. Data for hydrogen ions of such speeds has not previously been available, since the experimental studies cited use either alpha-rays from radioactive sources, or low speed hydrogen canal rays.

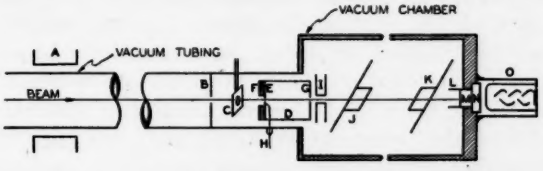

FIG. 1. Apparatus, schematic.

The present work is a study of hydrogen ions, of speeds between v_0 and $4v_0$ (energies between 20 and 400 kv), provided by the University of Chicago Cockcroft-Walton accelerator.[16] Thin metallic foils were placed in the path of the ion beam, and the emerging beam, whose energy was accurately known, was analyzed into neutral and charged components. In order to study the dependence of the charge state upon the atomic number of the foil material, foils of beryllium, aluminum, silver, and gold were used. Since the beam quickly comes to a state of charge equilibrium in the foils, the data do not give information about the absolute size of the cross sections for electron capture and loss. The results reported here are in the form of ratios of the loss to the capture cross section, as a function of hydrogen ion speed and stopping medium.

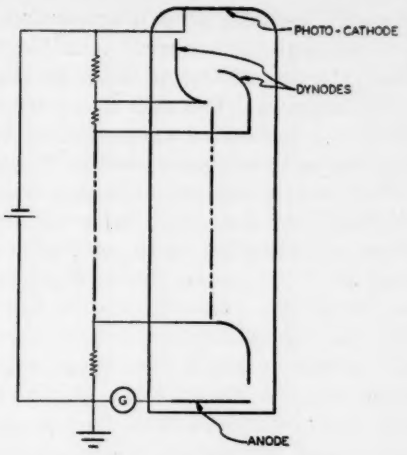

FIG. 2. Photo-multiplier circuit.

II. EXPERIMENTAL ARRANGEMENT

The apparatus is shown schematically in Fig. 1. Everything shown there is kept at high vacuum except the photo-multiplier tube, 0. The energy of the beam is obtained by measuring the current through a resistor stack placed between ground potential and the high voltage end of the accelerator. As the beam leaves the accelerating tube, it is analyzed magnetically at A; the selected component, either H^+ or H_2^+, then travels down a 50-in. tube to B, where a 3/16-in. hole improves its definition. It then strikes the foil under study, mounted over a circular hole in a thin brass frame, C, which can be moved into or out of the beam by means of a Wilson seal. After emerging from the foil, the beam has the charge composition characteristic of the foil material and the energy of the emerging beam. Beam particles which have not undergone excessive Rutherford scattering can then pass through a 6-in. collimating tube, D, which has collimating holes (No. 70 drill size) in its brass end plates, E and G. After collimation the beam travels 20 in. to a potassium iodide (thallium enriched) crystal, M; light from the crystal leaves the vacuum chamber through a glass window, N, and a galvanometer is used to record the anode current produced by this light in the adjacent photo-multiplier tube, 0 (RCA Type 5819). Two electrodes at I, directly after collimation, can be used to apply a strong electric field to the beam. With this field turned off the multiplier current is proportional to the strength of the en-

[1] J. Konigsberger and J. Kutchewsky, Ann. d. Physik **37**, 195 (1912).
[2] E. Ruchardt, Ann. d. Physik **71**, 377 (1923).
[3] A. Ruttenauer, Zeits. f. Physik **4**, 267 (1921).
[4] H. Bartels, Ann. d. Physik **6**, 957 (1930).
[5] E. Rutherford, Phil. Mag. **47**, 277 (1924).
[6] P. Kapitza, Proc. Roy. Soc. **106**, 602 (1924).
[7] G. H. Henderson, Proc. Roy. Soc. **109**, 157 (1925).
[8] G. H. Briggs, Proc. Roy. Soc. **114**, 241 (1927).
[9] C. Gerthsen, Physik. Zeits. **31**, 948 (1930).
[10] R. H. Fowler, Phil. Mag. **47**, 416 (1924).
[11] L. H. Thomas, Proc. Roy. Soc. **114**, 561 (1927).
[12] J. R. Oppenheimer, Phys. Rev. **31**, 349 (1928).
[13] H. C. Brinkman and H. A. Kramers, Proc. Akad. Amsterdam **33**, 973 (1930).
[14] J. Knipp and E. Teller, Phys. Rev. **59**, 659 (1941).
[15] N. Bohr, *The Penetration of Atomic Particles through Matter* (Kgl. Danske Vid. Sels., 1948). This book can be obtained in America from Stechert and Company, New York.
[16] Allison, del Rosario, Hinton, and Wilcox, Phys. Rev. **71**, 139(A) (1947).

tire beam; with the field on it is proportional to the strength of the neutral component alone.[17] The difference between the two readings of course corresponds to the charged component. The data thus yield the ratio of the charged to the neutral component of the beam.

As to the further details shown in Fig. 1, J is a brass shutter which can be rotated through a Wilson seal to cut the beam off completely from the crystal, so that the background current of the multiplier tube can be corrected for. K is a similar shutter which is made of glass and swings into place directly in front of the crystal; its function is discussed below. L is a brass tube which serves to mount the crystal and also to shield it from stray radiation. F is a plastic cap which covers most of the insulated collimating plate E, leaving only a few square millimeters exposed to the beam, and H is a lead going from E to the outside through a Kovar seal. Since neutral and total beams are not measured simultaneously, correction is made for beam fluctuations by normalizing all multiplier readings to simultaneous readings of the current delivered through H. The collection of secondary electrons from the foil is avoided here by maintaining the plate E at a negative potential of approximately 200 v. The current to E ranges from 0.1 to 5 μa and is read with a d.c. amplifier or directly by galvanometer. One further feature should be mentioned: the photo-multiplier background is very sensitive to extraneous light and also to slight mechanical vibration. The background was kept low by fitting a Bakelite cylinder snugly onto the tube base and then sealing the Bakelite to the vacuum chamber with apiezon clay, an arrangement which is entirely opaque and avoids rigid mechanical coupling. The tube was supported with rubber-cushioned clamps.

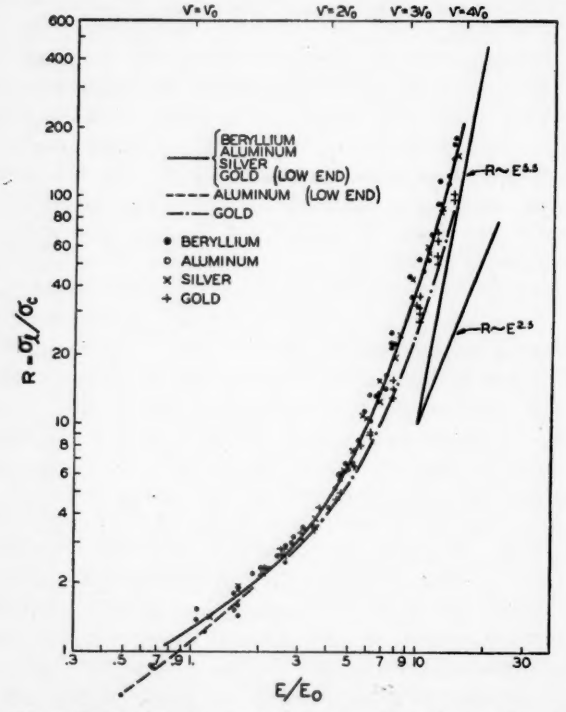

FIG. 3. Ratio of loss to capture cross section σ_I/σ_c as a function of ion energy E. At energy E_0 the ion speed $v=v_0=e^2/\hbar$. $E_0=24.8$ kev.

[17] The crystal response is the same to neutral and to charged particles because an ion changes its state of charge many times as soon as it enters the crystal.

The photo-multiplier circuit is shown in Fig. 2. Proper potentials between the tube electrodes are maintained by a regulated voltage supply feeding a set of bleeder resistances as shown. The first multiplication surface is the photo-cathode, which is a coating applied directly to the glass wall of the tube. The galvanometer is placed in the circuit as illustrated, between ground and anode.[18] The anode current never exceeded 15 μa during the measurements, while the tube is rated for a maximum of $\frac{3}{4}$ μa, so that linearity is assured.

At ion speeds where the total beam was of the order of 10 times the neutral component, the two were compared by shunting the galvanometer, in order to keep its deflection fairly constant. At higher ion speeds, the ratio of the total to the neutral component was found to be of the order of 100:1. Strongly shunting the galvanometer for these measurements was awkward for technical reasons, so an alternative procedure was adopted. A careful calibration curve was run for the multiplier tube, plotting current gain *vs.* tube voltage, and the very unequal total and neutral beams were then observed using different tube voltages. The calibration curve was run by admitting light into the vacuum chamber near point I (Fig. 1).

Calibrating the multiplier provides notable flexibility. Since the current gain of the tube changes by a factor of about 10^5 as tube voltage goes from 400 to 1400 v, the ratio of largest and smallest beams easily comparable by this method is of the order of one million to one.

III. THIN FOIL TECHNIQUE

The foils had to meet stringent requirements. In the first place, due to the severe collimation, Rutherford scattering in the foils eliminated most of the beam, so that any pinholes transmitting intense unscattered pencils would be intolerable. Second, the foils must have known uniform thickness so that the energy of the emergent beam may be well established.

Adequate foils were produced by covering the foil frames first with a very thin layer of Nylon or zapon (approximately 0.005 mg/cm^2) and then evaporating the metal onto this backing.[19] In use the beam is directed into the side with the backing, of course.

[18] In this arrangement, the voltage drop across the galvanometer subtracts from the voltage between the last dynode and the collecting electrode, so that the multiplier gain is slightly reduced as current increases. This effect was small enough to require no correction.

[19] We are grateful to Dr. Hugh Bradner of the University of California for supplying us with beryllium foil produced by a different evaporation technique. We used these foils before learning to make our own, and obtained the same results with both sets.

Foil thickness was measured by exposing half of an interferometer mirror placed adjacent to the foil frames during evaporation, and measuring displacement of the interference fringes. The energy loss was then calculated on the basis of the recent work in our laboratory on the slowing down of hydrogen ions of the same speeds in the same media.[20] No allowance was made for the Nylon or zapon backing in calculating this loss, since most of the backing undoubtedly burned off under the beam, leaving a negligible carbon deposit.

The foils ranged from $\frac{1}{4}$ to $\frac{1}{2}$ in. in diameter, and from 0.01 to 0.3 mg/cm^2 in thickness. The ions lost between 5 and 50 kv in crossing them. It was a pleasant surprise thot these foils stood up for hours without showing any damage under beams as strong as 3 μa concentrated on 0.2 cm^2. Only in the case of the very thin gold foils, 0.02 mg/cm^2, did such beams annihilate the foil, and this was presumably because the foil was so thin that it could not hold together once the backing was destroyed.

IV. EXPERIMENTAL PROCEDURE

During the actual runs the procedure was as follows. The ion beam was set to a particular energy and the foil placed in its path. Then readings of the multiplier current were taken, with the deflecting field first turned off and then turned on. The monitor current at point E (Fig. 1) was taken simultaneously with each reading. The field-off-field-on pairs were repeated two or more times to check the consistency of the readings and to reduce random errors. Then the shutter was placed in the way of the beam; background currents were observed; the accelerator was adjusted to a different beam energy and the cycle repeated. Since the beam area was much less than the foil area, the foil position could be changed several times in the course of a run, and foil uniformity was checked further by noting the stability of the multiplier current while moving the foil. Generally the beam could be passed over almost the entire foil with current fluctuations of only a few percent, and the results showed no dependence on foil position. Consistency was tested further by running the early and late points of a run at the same ion energies; results of this test were satisfactory except in the case of some of the gold runs, and the significance of this point is discussed below.

For the higher energy points it was feared that the very thin foils might not be thick enough to establish charge equilibrium. (Capture and loss cross sections decrease as energy increases, for ion speeds above v_0.) On the other hand, several reasons made very thin foils desirable for the lower energy points: for these points, straggling in the thicker foils and experimental uncertainty in the rate of energy loss lead to a serious percentage uncertainty in the final beam energy, and strong Rutherford scattering and weaker crystal response create a sensitivity problem. Consequently, for each element two or more foils of different thicknesses were used. By overlapping data taken with these foils, it was guaranteed that charge equilibrium was established in the foils.

It may be assumed that charge equilibrium was established in all of the observations, since no dependence on foil thickness was ever noted. Such dependence could probably have been observed, had the study of the very thin gold foil been extended to the highest energies available. Detection of this dependence would have provided approximate absolute values for the capture and loss cross sections. In the present data, the thin gold foil (0.028 mg/cm^2) was studied up to the ion energy of 132 kv (ion speed 2.3 v_0); the fact that charge equilibrium was still established means that the foil had a thickness of at least one mean free path at this energy, corresponding to a cross section of at least 10^{-17} cm^2. As is indicated in Section V, this figure refers strictly to the sum of capture and loss cross sections. Since the loss cross section is much the larger at this speed, it essentially provides a lower limit to the loss cross section.

V. EMPIRICAL MATHEMATICAL DESCRIPTION OF CAPTURE AND LOSS

To interpret the data, we need an elementary description of the beam's fate in the foil. Let N be the number of atoms per square centimeter in the foil, x the number of atoms per square centimeter from the front face of the foil to a variable position in the foil, σ_c and σ_l the cross sections per atom for electron capture and loss by the beam particles, and $f_1(x)$ and $f_0(x)$ the fractions of the beam which are singly charged and uncharged at x. The quantity measured in this experiment is then $f_1(N)/f_0(N)$. As the beam passes through a layer of foil dx, its change in composition is described by the equations

$$df_1=(-\sigma_c f_1+\sigma_l f_0)dx=-df_0. \quad (1)$$

The solution of these equations for constant σ_c and σ_l is

$$f_1=(\sigma_l/\sigma_t)+[f_1(0)-\sigma_l/\sigma_t]\cdot\exp(-\sigma_t x)$$
$$f_0=(\sigma_c/\sigma_t)+[f_0(0)-\sigma_c/\sigma_t]\cdot\exp(-\sigma_t x)=1-f_1, \quad (2)$$

with

$$\sigma_t\equiv\sigma_l+\sigma_c.$$

The concept of charge equilibrium is applicable if the cross sections change only slightly due to energy change as the beam travels the distance of a mean free path, $\delta x=\sigma_t^{-1}$. In this case, once the beam has traveled several mean free paths in the foil, its composition is described almost exactly, in consequence of Eq. (2), by

$$f_1(x)/f_0(x)=\sigma_l(x)/\sigma_c(x). \quad (3)$$

Thus the state of the beam is independent of its initial composition and only changes slowly with the changes in cross sections: a state of near-equilibrium is estab-

[20] S. D. Warshaw, Phys. Rev. **76**, 1759 (1949). Foil thickness in Warshaw's work was obtained by the same method.

TABLE I. Exponents "n" as a function of ion speed. The data are fitted in segments by equations $R \equiv \sigma_l/\sigma_c = (v/v_1)^n$. The "light" elements are Be, Al, and Ag.

Elements	Ion energy E, kev	v/v_0	n	v_1/v_0
Light	350	3.75	9.2	2.2
Au			7.0	1.9
Light	300	3.48	8.0	2.0
Au			7.0	1.9
Light	200	2.84	5.8	1.7
Au			4.9	1.6
Light	100	2.01	3.2	1.3
Au			2.6	1.2

lished. As the beam leaves the foil,

$$f_1(N)/f_0(N) = \sigma_l/\sigma_c, \tag{3a}$$

where the cross sections correspond to the energy of the emergent beam. Thus the beam composition gives directly the ratio of loss to capture cross section. Equation (3a) applies to all of the data in this paper.

VI. RESULTS

All of the results are contained in Fig. 3, which gives the ratios of electron loss to electron capture cross sections for the different ion speeds and media studied. Only one curve is drawn for the elements beryllium and silver, since the data do not reveal any difference in charge state for these media. The aluminum data too are indistinguishable from the solid curve over most of the energy range. However, at the lowest energies studied the beam seemed to be more neutral in aluminum, and these data are represented on a broken line. There is no explanation for this variation in aluminum, and it may not be real. It should be pointed out that experimental error increases at the low energies due to decreased detector sensitivity, but this error still should not exceed about eight percent at the very lowest points.

The gold curve is indistinguishable from the solid line at the lower energies, but for higher energies the beam is more neutral in gold. This is in line with theoretical ideas implying larger capture cross sections in the heavier elements. For the higher energies the gold curve (broken line) is drawn through the most neutral points, since the others are believed to have suffered from a systematic error. This point is discussed under the fourth of the systematic errors considered below.

Current theories generally predict that the capture and loss cross sections will vary with some power of the ion energy. For convenience in the discussion offered below, straight lines have been drawn in Fig. 3 corresponding to the exponents which occur in these theories. As regards the absolute size of the cross sections, these theories are generally very approximate; therefore the straight lines in Fig. 3 correspond to these theories in exponent only, and their location has no significance.

VII. SYSTEMATIC ERRORS

While the experiment described here is extremely simple in principle, a number of systematic errors may invalidate the results. Presumably some of these errors are connected with the great inconsistency between the different reports in this field. Therefore several possible errors will be discussed here in some detail.

(1) The beam produces some light by excitation of the residual gas in the vacuum chamber and this light acts like a neutral beam component. While a consideration of the mean free path for excitation indicates that this light should be negligible in amount, the ionic beam has always been quite visible at the end of the accelerator tube, so it was thought best to check this point experimentally. The glass shutter, part K in Fig. 1, was used for this purpose; with the beam striking the shutter much more light is produced in it than in all of the residual gas. The light produced even with this exaggerated effect was never more than barely detectable with the photo-multiplier.

There remains the possibility that such an effect could occur with ultraviolet light alone. However, at the higher energies the beam from the accelerator was observed to be overwhelmingly charged (as described in the next paragraph), proving that no specious neutral beam was produced. The ultraviolet light effect is not expected to be any stronger at lower ion energies.

(2) The electric field was able to eliminate the charged component of the beam quite completely, and the shield L prevented detection of any stray radiation produced by this component after it was deflected. This point was confirmed by measuring the composition of a high energy beam with no foil in the beam path; the observed ratio f_1/f_0 was more than two thousand.

(3) It is essential that the beam should not change composition between leaving the foil and entering the deflecting electric field. Such a change may occur from collisions with solid structures such as the collimator walls, or from collisions with the residual gas in the vacuum. The collimation geometry guarantees that there is no error for the first reason: to reach the crystal a particle must pass directly from one collimating hole to the other and can collide with no solid material after leaving the foil. Collisions with the residual gas must be prevented of course by an adequate vacuum. In this experiment the pressure at the vacuum gauge was about 4.10^{-5} mm.

Stability of the beam composition was tested by making measurements without the foil in the beam path; such beams should be very predominantly charged. As was pointed out, this was found to be the case for the higher energy beams, but the neutral component became steadily stronger as the energy de-

creased, until at the lowest energies used the ratio f_1/f_0 was only three or four times greater with the foil out than with it in. This effect is much stronger than one would expect from the residual gas with the vacuum stated above. Nevertheless, while the residual gas between magnetic analysis and electric deflection was evidently dense enough to affect the beam strongly at low energies, it still amounted to less than a mean free path for change of charge. Since the distance from foil to electric deflection was only one-seventh of that from magnetic selection to electric deflection, the former is only a very small fraction of a mean free path and the residual gas effect must be negligible.

(4) It is essential that the beam composition should not change at the surface of the foils because of the presence there of oxide layers or films of oil from the diffusion pumps. As to oxide layers, which form on beryllium and aluminum, they are much too thin to change the state of charge, and the results show anyway that the state of charge is probably the same in all elements of atomic numbers between those of beryllium and silver. Deposition of oil is a much more serious problem. All diffusion pumps used were well baffled and equipped with elaborate liquid air traps; nevertheless, oil has sporadically appeared on the targets and foils during experiments in our laboratory. However, in our experience the oil films always build up over a period of hours. Taking advantage of this, we did not expose the vacuum chamber even to liquid-air trapped diffusion pumps, until a few minutes before the start of each run, and then repeated the early points at the end of each run. The consistency of these points proves either that no oil deposited or that the oil layer did not change the beam's state of charge.

The initial and final points in each run were consistent for the three lighter elements studied, but not for gold. In three successive gold runs, the initial points fell on one curve and the later points were displaced toward the curve characteristic of lighter elements. In the last of these runs special care was taken to minimize the oil effect and the displacement of the later points was only slight, so that the data seemed to represent gold legitimately. At any rate there is no question that the beam has a larger neutral component in gold than in the lighter elements, and the oil effect, if significant at all, causes us to underestimate this difference.

It should be noted that oil films on targets and foils can usually be seen, especially after a beam carbonizes them. Visual observation confirms the conclusions stated, in that no oil was observed on the foils after almost all the runs with the three lighter elements. Oil was observed on two of the three thick gold foils.

(5) Another important question is that of the equality of response of the crystal to neutral and to charged particles. The sufficient condition for this equality, in the case of low energy beams, is that charged particles entering the crystal must pick up an electron before traveling an appreciable part of their range. Because of the large electron capture cross section, this condition is easily satisfied.

(6) Some systematic error is involved in the use of the multiplier gain curve for the higher energy points. Several measurements of this gain curve showed that over the region where the curve was needed (tube voltage varying from 400 to 900 v) the current gain was closely proportional to the eighth power of the tube voltage, with an uncertainty of about one percent in the exponent. For the highest energies studied, where the resulting error is the greatest, this corresponds to a systematic uncertainty of about two percent in the ratio σ_1/σ_c.

VIII. ACCURACY OF THE MEASUREMENTS

The two largest sources of error are the uncertainty in the energy of the beam as it leaves the foil, and the random fluctuations of the beam during the observations.

At the high energy end of the curves in Fig. 3, uncertainties in the measurement of the foil thicknesses and in the available figures for rates of energy loss lead to a probable error of approximately ± 1 kv in energy of the emergent beam. This is only about one-third of one percent of the beam energy, but appears as an error of about ± 1.5 percent in the ratio σ_1/σ_c, the increase being caused by the steepness of the curve. For the lower energies, at 30 kv, for example, the corresponding numbers are ± 1 kv or ± 3 percent in beam energy and ± 2 percent in σ_1/σ_c. Errors in the available data on rates of energy loss displace all the curves taken with a particular element, and errors in the measurement of thickness of a foil displace the curve taken with that foil, but such errors do not produce a random spread from point to point within any run. There is also a permanent uncertainty of about plus or minus one-third of one percent in the beam energy, corresponding to the precision with which the accelerating voltage is known; this last effect may simply translate all of the data *en masse* a small amount to the right or left in a log-log plot like Fig. 3.

Random fluctuations of the beam during the observations produce a spread from point to point. With the very strong collimation used, any slight change in the orientation of the beam, as well as any change in intensity, will strongly affect the current reaching the detector. While the monitoring arrangement described above successfully smooths out fluctuations in intensity, it does not respond well to changes in beam orientation. Judging from the fluctuations observed during runs and from the scatter of the points about a smooth curve, the ratio σ_1/σ_c seems to be obtained at each point with a probable error of approximately ± 4 percent. Since this error is random, the final smooth curve is not so strongly affected, and suffers from an uncertainty roughly between one and two percent because of these fluctuations.

A third significant uncertainty arises from use of the

multiplier tube gain curve, as discussed above. The three types of error compound to a probable error of about three percent over almost the entire range of Fig. 3.

In the case of gold, however, the greatest uncertainty is due to oil films. Because of these films, the ratio σ_l/σ_e may appear to be as much as 10 percent greater than its true value in gold.

IX. INTERPRETATION OF RESULTS

A. Qualitative Features

The general shape of the curves in Fig. 3 is not unreasonable. At ion speeds of v_0 or greater, the capture and loss cross sections and their ratio are strongly energy-dependent. As the ion speed is brought down to v_0 the cross sections both become large, but cannot much exceed the geometric cross section of the atom. Hence they are no longer as strongly energy dependent and the curve becomes flatter. Unfortunately it was not possible to extend the curves below the energies shown because of insufficient sensitivity. However, the canal-ray data of references 1 through 4, while too inconsistent to permit quantitative analysis, show that as the ion energy decreases still further, the loss cross section rapidly falls off and the beam becomes predominantly neutral.

As the energy increases, the ratio σ_l/σ_e is seen to become more and more energy-dependent. This is perhaps to be expected, since classical theory, which applies at lower speeds, predicts that σ_e will vary with the inverse sixth power of the ion velocity, while quantum theory, which is applicable to ions of much higher speed, suggests a twelfth power dependence.

B. Basis for Comparison with Theory

As will be brought out in the following discussion, the theory of the interaction between the fast ions and the medium is inadequate for the ion energies of the present data. Indeed, present theory is weakest in the interesting region of ion speeds near v_0. This prevents a really satisfactory study of the data beyond an empirical level. But in order to provide some link with present thought, an analytical procedure has been carried out.

The existing theories each indicate that the ratio of capture and loss cross sections will be proportional to some power of the ion speed. For the sake of comparison with these theories, the data have been analyzed to give values for this power "n" as a function of ion speed. Specifically, tangents were drawn to the log-log curves of Fig. 3 and the tangents were fitted by equations of the form $R=(v/v_1)^n$; the parameters "n" and "v_1" are tabulated in Table I. Experimentation with various ways of drawing the curves and tangents shows that each exponent is defined by the data with a leeway of approximately ± 0.2.

Since the slope changes considerably over the entire energy range in Fig. 3, it is clear that the entire curve cannot be described by a power law. However, where the slope is not rapidly changing, a power law applies fairly well to each limited part of the range, and the tangent in that region reveals its exponent.

C. Theory of Ionization

So far as ionization of the incident hydrogen beam is concerned, Bohr[15] divides the ionizing media into several classes. The lightest media are such that most orbital electrons remain generally a distance of a_0 or greater from their nuclei. (a_0 is the Bohr radius $\hbar^2/me^2$.) For such media, collisions with the incident system will either be so distant that the ionizing field is almost entirely screened and the ionizing effect is negligible, or else the incident electron will come close to some one particle in the medium, nucleus or electron, and will undergo a collision in which all other particles may be neglected. Thus for sufficiently light media one may simply sum over the ionizing effects of all particles in the medium, attributing a Coulomb field to each. In this case Bohr estimates a total ionization cross section

$$\sigma_l=4\pi a_0^2(Z^2+Z)(v_0/v)^2, \tag{4}$$

where Z is the atomic number of the stopping material. The term in Z^2 corresponds to ionization by the nucleus and that in Z to a sum over all the orbital electrons in each atom.

For somewhat heavier media the inner electrons are closer to the nuclei and the incident system encounters not separate Coulomb fields, but the screened fields of the nuclei. The situation is much more complicated and requires further analysis. Bohr defines the parameter ζ as an index of the degree of screening of the nuclear field: $\zeta\equiv b/a$, where b is the distance of closest approach to the unscreened nucleus, and a is the length characterizing the exponential decrease of the screened field. In the case of ionization of the hydrogen atom by the nuclear fields in the medium, $\zeta\cong 2Z^{4/3}(v_0/v)^2$. Bohr then shows that so long as ζ is approximately unity, the most important collisions occur in a region where the medium potential varies as r^{-2}, and furthermore that ionization occurs here only if the incident electron is deflected so strongly that classical mechanics may be correctly applied. On this basis he estimates the cross section σ_l to be

$$\sigma_l\sim\pi a_0^2 Z^{\frac{1}{3}}(v_0/v). \tag{5}$$

For the velocity range of this experiment, ζ is near one for a very limited range of elements from lithium through carbon, roughly speaking. Thus for aluminum and heavier elements, we are already dealing with cases of much stronger screening and different approximations are needed. As a matter of fact, neither classical mechanics nor the Born approximation can properly be applied in these cases, but it will be worth while to note the conclusions suggested by each of these approximations.

In the classical picture, for larger Z and stronger

screening, the distance of closest approach is only slightly increased, but the field inside $r=a$ becomes so strong that incident electrons moving towards this region are almost certainty ionized. The cross section σ_l therefore comes to depend on v even less strongly than the first power, and remains of the order $\sigma_l \sim \pi a^2$.*

According to the Born approximation, for very strong screening the scattering of the incident electron by the nuclear field approaches spherical symmetry in the center-of-mass system, and the total scattering cross section becomes independent of the relative velocities.† The ionization cross section will then depend, roughly speaking, only on the size of the critical angle at which energy transfer is great enough to free the electron. This again implies a very weak dependence on velocity, weaker than the first power. The analysis is not really applicable because, for the present data, the incident waves are strongly perturbed by the collision, which invalidates the Born approximation.

However, both classical and simple quantum-mechanical analysis imply that σ_l becomes less dependent on velocity as Z increases. Furthermore, with still larger values of Z and very strong screening, the field is so strong within a region of radius approximately a_0 that ionization must occur, and the cross section is then almost independent of velocity.

To summarize, we may expect the following behavior of the cross section for ionization of hydrogen atoms in the beam:

For very light media, up to beryllium:

$$\sigma_l \sim 4\pi a_0^2 (Z^2+Z)(v_0/v)^2. \tag{4}$$

From beryllium, through carbon:

$$\sigma_l \sim \pi a_0^2 Z^{\frac{1}{2}} (v_0/v). \tag{5}$$

From carbon on: the dependence on v should be weaker than the first power. It should be progressively weaker in aluminum, silver, and gold, and amost non-existent in gold.

The equations above become completely inapplicable below some ion speed of the order of v_0, since σ_l then decreases as v decreases. This speed should coincide roughly with the maxima in the proton stopping curves, which occur near $v=2v_0$.

The equations above are consistent with some previous experiments. Jacobsen's experiments on fast alpha-particles in hydrogen agree with Eq. (4), and Rutherford's data on fast alpha-particles in air with Eq. (5). In Rutherford's work the parameter ζ is nearly unity, so that Eq. (5) properly applies.

Earlier work also shows how well these ideas may be applied to ion speeds as low as $2v_0$ to $4v_0$. No direct measurements of σ_l are available in this velocity range. However, data on the energy loss of ions also provide information about ionization; as Fano has shown, this energy loss is proportional to the ionization of the stopping medium.[21] On this basis, Warshaw's stopping data indicate that the power law most suitable for the ionization of the medium is between $v^{-0.5}$ and v^{-1} for $2v_0<v<4v_0$, while Bohr's analyses lead to a form v^{-1}.

TABLE II. Exponents for the velocity dependence of $R \equiv \sigma_l/\sigma_c$, σ_l, and σ_c.

Element	n_R (observed)	n_l (estimated)	n_c (n_l-n_R)
Be	9.2	−1.5	−11
Al	9.2	−0.5	−10
Ag	9.2	0	− 9
Au	7.0	0	− 7

It may be concluded reliably then that in the present experiments the velocity dependence of the ionization cross section varies between v^{-2} and v^0, in a manner which is fairly well understood. At any rate, the suitable exponent should never be unknown to an extent greater than ± 0.5. On the other hand, the capture cross section depends very strongly on v and there is no complete theory for it. The present data will therefore be considered chiefly as descriptive of the capture cross section.

D. Theory of Capture

To provide some theoretical basis for considering the velocity dependence of σ_c, Bohr divides stopping media into two classes. In the first, none of the electrons in the medium have speeds as great as v. Capture must then occur by a double process; first an electron gains energy from the incident particle and then, in a second collision with its own nucleus, it is set into a direction which makes capture possible. For such a process the classical calculation by Thomas indicates a probability varying as $v^{-5.5}$; the classical theory, however, does not apply to ions as fast as v_0 or faster. The corresponding quantum theory calculation, while it cannot be described by means of the orbital picture, also reveals the process to be very strongly velocity dependent; the calculation of Brinkman and Kramers[13] indicates a dependence on v^{-12}. The quantum-mechanical calculation also cannot be expected to apply well to the present data, since it is based on the Born approximation and assumes that $v \gg v_0$.

For heavier media, however, Bohr proposes a very different mechanism of capture; since some of the electrons in the medium already have a speed as large as v, these may be given the same speed and direction as the incident ion, and then captured, as a result of just one collision. A statistical estimate of such collisions leads Bohr‡ to the equation

$$\sigma_c \sim 4\pi a_0^2 Z^{\frac{1}{2}} (v_0/v)^6 \tag{6}$$

for such cases.

These estimates may now be compared with the present data. Table I shows the observed behavior of the

* See reference 15, p. 31.
† See reference 15, Eq. (1.4.5).

[21] U. Fano, Phys. Rev. **70**, 44 (1946).
‡ See reference 15, Eq. (4.3.5).

ratio σ_l/σ_c. From the previous discussion we may assign reasonable exponents, for the behavior of σ_l alone. Combining the two sets of exponents, one finds the behavior of σ_c alone. This procedure is carried out in Table II, for the ions with an energy of 350 kv.

Thus the capture cross section is more dependent on velocity than is suggested by the process Bohr proposes, in which capture is a single collision process involving electrons of orbital speeds near v. As the ion speed increases, the velocity dependence continues to become stronger for the lighter media, suggesting an approach to the quantum-mechanical approximation of Brinkman and Kramers. However, the dependence on velocity becomes progressively less as Z increases, and in the case of gold it is almost as predicted by Bohr's one-collision process.

E. Dependence of the Charge State on the Medium

One of the most remarkable features of the data is that the composition of the beam is found to be almost the same, for all speeds studied, in the media beryllium, silver, gold, and aluminum. This indifference of the beam composition to the medium has been noted previously by the experimenters referred to: Henderson,[7] Briggs,[8] and Gerthsen[9] could find no difference between the charge composition of alpha-ray beams in aluminum, mica, copper, silver, and gold, and Kapitza[6] even found the same charge composition in air and in hydrogen for alphas of speeds between $2v_0$ and $3v_0$. Rutherford reported that alpha-beams were very slightly more neutral in gold than in mica, and Jacobsen observed that quite fast alphas (speed around $8v_0$) are definitely less neutralized in hydrogen than in air. In the hydrogen canal-ray experiments, observers have reported different charge compositions in oxygen, nitrogen, and air, but inconsistencies in these data show that these results may be due to experimental errors. The over-all evidence is that the charge composition is independent of the medium over a wide range of values of Z, from beryllium through silver at least, and remains almost the same in gold.

Theoretically it is expected that σ_l and σ_c will both be almost independent of Z for the heavier elements. However, there is no explanation at present for the uniformity of beam composition from beryllium through silver.

F. Ion Speed for Which $\sigma_l = \sigma_c$

For calculations of the stopping of fission fragments, it is important to know the ion speed for which $\sigma_l = \sigma_c$. The data were carried down through this point in the case of aluminum, and the speed is found to be $0.95 \pm 0.05 v_0$. This speed is somewhat lower than the value of $1.1v_0$ given by Bartels for canal rays in air. The fact is once again confirmed that capture and loss probabilities are about equal for ionic orbits of speeds near the speed of the ion.

X. CONCLUSIONS

The ratio of the loss to the capture cross section for proton beams of speeds v_0 to $4v_0$ in various metals behaves qualitatively as one might expect from present theory. Quantitatively, in beryllium, aluminum, and silver, the capture cross section depends on the velocity more strongly than one would expect on the assumption that capture is mainly of electrons with speed near v. In beryllium, this dependence becomes greater as the ion speed increases, and at an ion speed of $4v_0$ it is almost as great as that predicted by the quantum-mechanical theory of Brinkman and Kramers. However, in gold the velocity dependence of the capture cross section is almost as predicted on the assumption that the captured electrons have speeds near v (Bohr's crude statistical model).

For the four media studied, the beam composition is almost identical, being indistinguishable in the three lighter media and slightly more neutral in gold at ion speeds greater than two v_0. Existing theory offers no explanation for this lack of dependence on medium.

The capture and loss cross sections are observed to be equal for hydrogen ions of speed $v = 0.95v_0$.

The ratio σ_l/σ_c is also useful for corrections to the stopping theory for light nuclei. For this purpose it is convenient to note these approximate values for hydrogen beams in metals: $\sigma_l/\sigma_c = 10$ at $v = 2.5v_0$ and $\sigma_l/\sigma_c = 100$ at $v = 3.2v_0$.

I wish to thank S. K. Allison for proposing this work and for his help during its progress, A. J. Dempster for suggestions in connection with the design of the vacuum chamber, S. D. Warshaw for his very close collaboration in the design and initial testing of the apparatus, and David Bushnell for sharing the work in constructing parts and taking the measurements.

The Nuclear Quadrupole Moment of N^{14} and the Structure of Nitrogen Trifluoride from Microwave Spectra*

JOHN SHERIDAN** AND WALTER GORDY
Department of Physics, Duke University, Durham, North Carolina
(Received April 10, 1950)

Measurements of the $J=1\rightarrow2$ rotational transitions of $N^{14}F_3$ and $N^{15}F_3$ yield the following molecular and nuclear properties. For $N^{14}F_3$, $B_0=10{,}680.96$ Mc/sec., $I_B=78.5475\times10^{-40}$ g cm²; for $N^{15}F_3$, $B_0=10{,}629.35$ Mc/sec., $I_B=78.9291\times10^{-40}$ g cm². The molecular dimensions are: $d_{NF}=1.371$A and $\angle FNF=102°\,9'$. The nuclear quadrupole coupling of N^{14} is -7.07 Mc/sec. This yields $+0.01\times10^{-24}$ cm² as the most probable value of the nuclear quadrupole moment of N^{14}.

I. INTRODUCTION

PREVIOUS workers have proposed various molecular configurations for the pyramidal molecule nitrogen trifluoride, NF_3. The infra-red spectrum[1] is reported to indicate an angle FNF of 110° or more, and the distance, d_{NF}, of 1.45A is suggested by the application of Badger's rule to the observed NF stretching force-constant. An equally large FNF angle has also been favored on account of the small electric dipole moment found for the molecule.[2] A recent electron diffraction study,[3] on the other hand, indicates an angle FNF of only $102.5°\pm1.5°$ and a distance d_{NF} of 1.37 ± 0.02A.

We have measured the $J=1\rightarrow2$ transitions in the pure rotation spectra of $N^{14}F_3$ and $N^{15}F_3$. The moments of inertia prove that the molecule has a structure very close to that found by the electron diffraction method. The nuclear quadrupole coupling of N^{14} has also been obtained from the hyperfine structure of the $N^{14}F_3$ spectrum, and provides additional evidence of the nature of the bonding. A new evaluation of the nuclear quadrupole moment of N^{14} has been made.

II. EXPERIMENTAL METHOD AND RESULTS

Nitrogen trifluoride was prepared by the electrolysis of fused ammonium bifluoride[4] using an anode of carbon impregnated with copper, which did not polarize readily. The nitrogen trifluoride, which was formed in a yield of only some 10 to 15 percent of that expected from the electrical charge passed, was purified by distillation at -150°C.

The $N^{15}F_3$ (7.5 atom percent N^{15}) was prepared by condensation of anhydrous ammonia into the required amount of anhydrous hydrogen fluoride at -78°C with subsequent electrolysis of the fused product in the same copper vessel.

The experimental measurements on the microwave spectra were made using methods previously described.[5]

Table I lists the frequencies found for the unperturbed rotational absorptions, and also the B_0 and I_B values. Table II summarizes the molecular dimensions obtained by substitution of the appropriate I_B and mass values into the relationship

$$I_B=1.6599\left[\frac{3}{2}M_F d_{NF}^2\sin^2\beta+d_{NF}^2\cos^2\beta\left(M_N-\frac{M_N^2}{3M_F+M_N}\right)\right],$$

where $\sin\beta=(2/3^{\frac{1}{2}})\sin(\frac{1}{2}\angle FNF)$. Table III gives the calculated and observed hyperfine structure of the $J=1\rightarrow2$ transition of $N^{14}F_3$.

III. DISCUSSION OF MOLECULAR STRUCTURE

The distance d_{NF} is close to that predicted by the Schomaker-Stevenson rule[6] for a single N—F bond with partial ionic character. This would be in accord with the assumption that structure I and three structures of type II are the main contributing states:

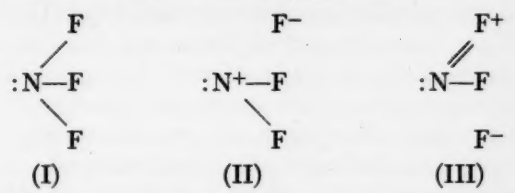

The electronegativity difference[7] of N and F, indicates that the NF link will be about 20 percent ionic, and accordingly it is reasonable to regard the three forms of type II as the most important. Three structures of type III may also contribute to some extent without greatly changing the nuclear separations. Any marked contribution of forms III, however, might be expected

* The research reported in this document has been made possible through support and sponsorship extended by the Geophysical Research Directorate of the Air Force Cambridge Research Laboratories under Contract No. W19-122-ac-35. It is published for technical information only and does not represent recommendations or conclusions of the sponsoring agency.

** On leave from Department of Chemistry, University of Birmingham, Birmingham, England.

[1] Bailey, Hale, and Thompson, J. Chem. Phys. **5**, 275 (1937).

[2] K. L. Ramaswamy, Proc. Ind. Acad. Sci. **2A**, 364 (1934).

[3] C-S. Lu and V. Schomaker, quoted by P. W. Allen and L. E. Sutton, Acta Crys. **3**, 65 (1950).

[4] O. Ruff *et al.*, Zeits. f. anorg. allgem. Chemie **172**, 417 (1928).

[5] Gordy, Simmons, and Smith, Phys. Rev. **74**, 243 (1948).

[6] V. Schomaker and D. P. Stevenson, J. Am. Chem. Soc. **63**, 37 (1941).

[7] L. Pauling, *The Nature of the Chemical Bond* (Cornell University Press, 1940), p. 70.

TABLE I. Molecular constants.

Molecule	Unperturbed frequency for $J=1\rightarrow2$ Mc/sec.	B_0 Mc/sec.	D_{JK} Mc/sec.	I_B* g cm²
$N^{14}F_3$	42,723.84±0.10	10,680.96	−0.025	78.5475×10^{-40}
$N^{15}F_3$	42,517.38±0.10	10,629.35		78.9291×10^{-40}

* Calculated by taking Planck's constant as 6.6242×10^{-27} erg/sec.

TABLE II. Molecular dimensions.*

Molecule	d_{NF}	∠FNF
NF_3	1.371A	102° 9′

* Taking $M_F=19.00452$ a.m.u., $M_N=14.0075$ a.m.u. and 15.00489 a.m.u., from M. S. Livingston and H. A. Bethe, Rev. Mod. Phys. 9, 373 (1937).

to cause d_{NF} to become shorter than the Schomaker-Stevenson rule predicts, since similar resonance has been thought to be the cause of the abnormally short CF distance in fluorocarbons.[8] The contribution of forms of the type of III thus appears to be less in NF_3 than in analogous carbon fluorides.

The angle FNF of 102° 9′ is significantly less than tetrahedral and indicates that the NF bonds have more than 75 percent p-character. This is important in connection with the discussion of the nuclear quadrupole coupling in the molecule (below).

The only serious difficulty encountered by the above theory is in accounting for the smallness of the electric dipole moment, 0.21 D, reported for the molecule[2] by the gas-temperature method. The observed intensities of the rotational absorptions also suggest that the moment is not much greater than this. With the observed valency angle, the predominance of forms of type II and the bond-moments predicted approximately from electronegativity differences[9] would be expected to give rise to a larger moment. This effect would not be offset by contributions of I and III unless these are larger than has been supposed. It is probable that a reduction in moment results from dipole interactions such as have been postulated in other cases of a similar nature. In view of the position, however, we propose to redetermine the dipole moment of the molecule using Stark modulation of the microwave spectrum.

IV. NUCLEAR COUPLING AND QUADRUPOLE MOMENT OF N^{14}

Table IV summarizes the calculated nuclear constants of N^{14}. The N^{14} nuclear quadrupole coupling in NF_3, −7.07 Mc/sec., is much larger than that found for N^{14} in any other molecule. Its magnitude is 73 percent greater than that, 4.10 Mc/sec., in the similar NH_3 molecule. This coupling can be accounted for by assuming about 17 percent s-character for each of the bonding orbitals, so that the non-bonding orbital would have about 50 percent p-character. In this calculation we have neglected distortion effects and have assumed structures of type II to be the most important ones. However, sizeable contributions from I or III would not significantly affect the results. We have assumed[10] 10 Mc/sec. coupling per unbalanced p-electron, and have multiplied by a factor of 1.25 to correct for the positive formal charge on N in structure II. The resulting hybridization is in good agreement with the observed bond angles.

Except for N_2O, in which the bonding is extremely complex and the observed coupling is so small that it could be caused almost entirely by distortion effects, Townes and Dailey were able to account satisfactorily for all of the N^{14} couplings then measured, by assuming either 10 Mc/sec. or 24 Mc/sec. coupling per unbalanced p-electron, and by postulating different kinds of sp-hybridization. This situation causes large uncertainties in the value, $+0.02\times10^{-24}$ cm², which they estimated for the N^{14} quadrupole moment. The higher value, 24 Mc/sec., can be ruled out by the NF_3 coupling. Less than 10 percent s-character in bonding orbitals would be required to account for the observed coupling, whereas the observed bond angles indicate that the bonding orbitals have 15 to 20 percent s-character. Hence, it appears that the lower value 10 Mc/sec. is closer to the correct one. We accordingly assign $+0.01\times10^{-24}$ cm² as the most probable value for the nuclear quadrupole moment of N^{14}.

The value of 10 Mc per unbalanced p electron would

TABLE III. Observed and calculated hyperfine structure of the $J=1\rightarrow2$ transition of $N^{14}F_3$.

K	$F\rightarrow F'$	Frequency (Mc/sec.) Calculated*	Frequency (Mc/sec.) Observed	Relative intensity Calculated	Relative intensity Observed
0	1→1	42,727.39	42,727.39	18	15
1	0→1	42,726.61	42,726.60	18	20
1	2→3	42,724.39	42,724.36	75	70
0	2→3	42,724.00	42,723.94	100	150
0	1→2	42,723.85		54	
1	2→2	42,723.25	42,723.28	13	18
1	1→2	42,722.18	42,722.16	40	75
0	0→1	42,722.08		24	
0	2→2	42,721.73	42,721.73	18	20

* Calculated by using $eQ(\partial^2V/\partial z^2)=-7.07$ Mc/sec. and $D_{JK}=-0.025$ Mc/sec.

[8] L. O. Brockway, J. Phys. Chem. 41, 747 (1937).
[9] L. Pauling, reference 7, p. 68.
[10] The 10 Mc/sec. per unbalanced electron is the lower value employed by Townes and Dailey, J. Chem. Phys. 17, 782 (1949). The factor 1.25 is that used by these authors to correct for a positive formal charge of one unit.

require the σ-bond wave function of multiple bonded N to be $(1/\sqrt{2})\psi_s+(1/\sqrt{2})\psi_p$ rather than[10] $\frac{1}{2}\psi_s+(\sqrt{3}/2)\psi_p$, and would favor structures of the type

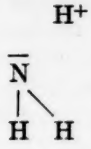

for ammonia rather than that written $N\equiv H_3$ by Townes and Dailey.

TABLE IV. Nuclear constants of N^{14}.

Nucleus	Spin	Coupling in NF_3 $eQ(\partial^2V/\partial z^2)$	Quadrupole moment
N^{14}	1	-7.07 ± 0.10 Mc/sec.	0.01×10^{-24} cm^2

PHYSICAL REVIEW VOLUME 79, NUMBER 3 AUGUST 1, 1950

An Application of the W.K.B. Method to the Cohesive Energy of Monovalent Metals

T. S. KUHN*
Harvard University, Cambridge, Massachusetts
(Received March 2, 1950)

A new method is developed which, within the limits of the spherical cell approximation first presented by Wigner and Seitz, will permit the evaluation of the cohesive energy, lattice constant, and compressibility of a monovalent metallic solid without the explicit computation of a central field for the atom. Analytic formulas for approximate solid state wave functions are produced in the region outside the atomic core by utilizing Imai's form of the W.K.B. method with the phase constant determined explicitly in terms of the known quantum defect of the free atom. These wave functions are applied to the determination of the minimum ground state energy in the alkali metals and of the sphere radius at which this occurs as functions of the quantum defects of the free atoms. These functions, when applied to Fröhlich's semi-empirical formula, yield a rapid and accurate method for the computation of the ground-state energy as a function of sphere radius.

I. Introduction: A previous paper[1] has developed the "function matching method" which permits computation of solid state wave functions to be undertaken without a knowledge of the potential function of the atomic core. Before the discovery of that technique an attempt had been made to achieve the same result with wave functions of the W.K.B. type. This proved to be feasible only in theory, for the region in which the wave functions are of physical interest lies near the outer turning point of the wave equation where the W.K.B. approximation tends to break down. Even Langer's[2] W.K.B. formalism yielded significant errors in this region, so the attempt was abandoned in favor of the function matching technique.

Recently Imai[3] has suggested a revision of the W.K.B. method which materially improves the approximation near the turning point. His formalism is applied in the present paper to the computation of wave functions for the solid state and, in a sample specialization, yields numerical results almost identical with those computed by more exact methods. Because the computations involved are less arduous and because this revised W.K.B. technique proves less critically sensitive to small changes in the experimental data, it is presented here as an improvement on our earlier method. No attempt has been made, however, to duplicate the computations made in the earlier paper (A), for there is every evidence that the two formalisms will yield almost identical results.

The objectives and the physical presuppositions of this paper are identical with those discussed in (A). Readers acquainted with (A) will note that the general solution of the radial wave equation, there produced as an arbitrary linear combination of Whittaker's two solutions of the confluent hypergeometric equation, is here replaced by Imai's W.K.B. solution with an undetermined phase constant. The condition that the wave function be zero at the origin is then seen to determine explicitly the phase constant used in the W.K.B. expansion about the inner turning point, so that the phase constant to be used about the outer turning point can be determined as a function of the quantum defect of the atom by an obvious modification of the usual phase-integral quantum condition. This procedure serves to determine the wave functions for the solid without the computation of the logarithmic derivative function required by the earlier, function matching procedure.

II. The Imai Procedure for the Solid State: Imai has shown that a differential equation,

$$d^2U/(dx^2)+k^2P(x)U=0, \qquad (1)$$

* Junior Fellow, Society of Fellows.
[1] T. S. Kuhn and J. H. Van Vleck, Phys. Rev., **79**, 382 (1950). This paper will be referred to as (A).
[2] R. E. Langer, Phys. Rev. **51**, 669 (1937).
[3] I. Imai, Phys. Rev. **74**, 113 (1948).

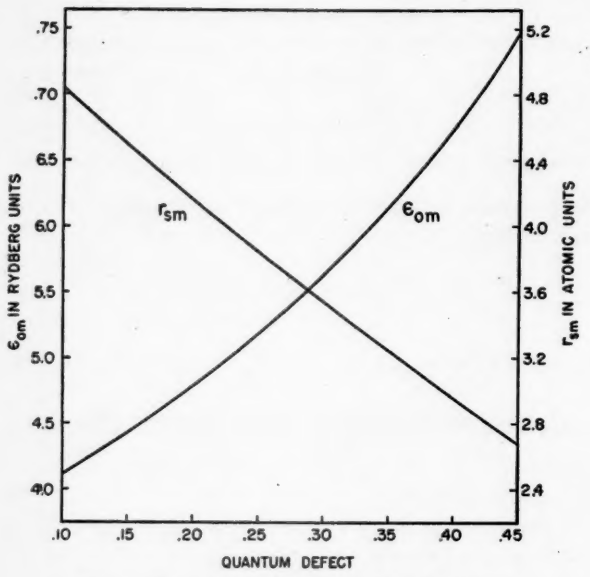

FIG. 1. Curves of ϵ_{om} and r_{sm} as functions of δ.

possesses, in the vicinity of its ith turning point x_i, an approximate general solution of the form

$$U=z^{1/6}\xi^{\frac{1}{2}}P^{-\frac{1}{4}}[\cos(\tfrac{1}{3}\pi+\eta_i)J_{1/3}(\tfrac{1}{3}\kappa\xi^{\frac{3}{2}}) +\cos(\tfrac{1}{3}\pi-\eta_i)J_{-1/3}(\tfrac{1}{3}\kappa\xi^{\frac{3}{2}})], \quad (2)$$

in which an arbitrary amplitude factor has been omitted, η_i is an arbitrary constant, and

$$z=\int_{x_i}^{x}[P(x)]^{\frac{1}{2}}dx, \quad \xi=(3z)^{\frac{2}{3}}+\lambda\kappa^{-2}. \quad (3)$$

Here it has been supposed that in the vicinity of the turning point, x_1, $P(x)$ can be expressed in the form

$$P(x)=\sum_{m=1}^{\infty}a_m(x-x_i)^m, \quad (4)$$

so that the constants κ and λ are then defined in terms of the first four coefficients, a_m, of (4) by

$$\kappa^2=k^2-(4/75)(14a_2^3-35a_1a_2a_3+25a_1^2a_4)a_1^{-4},$$
$$\lambda=(12/35)(3a_2^2-5a_1a_3)(2a_1^2)^{-4/3}. \quad (5)$$

The family of functions (2) are shown by Imai to be exact solutions of that differential equation which is gained by dropping all but the first four terms of the expansion of $P(x)$ in (1). They are therefore excellent approximate solutions at and near the turning point.

The particular utility of the form (2) is, however, a consequence of its asymptotic behavior, for if k is large enough so that $k^2\sim\kappa^2$ in (5), the functions (2), at large distances from the turning point, reduce to

$$U\sim P^{-\frac{1}{4}}\cos(kz-\tfrac{1}{4}\pi+\eta_i) \quad \text{for } P>0, \quad (6a)$$

$$U\sim P^{-\frac{1}{4}}[2\sin\eta_i e^{|kz|}+\cos\eta_i e^{-|kz|}] \quad \text{for } P<0, \quad (6b)$$

and, since large k corresponds to large absolute values of the energy in the wave equation, these formulas are seen to be precisely the normal W.K.B. expansions. It follows that the functions (2) are good approximate solutions at distances between but not too near the turning points. Since (6a) and (6b) join smoothly to (2) at opposite sides of the turning point x_i, they are seen to contain the usual connection formulas.

This is the formalism to be applied to the wave equation (A-1) of concern in the theory of solids. By means of the substitutions

$$\theta=-\epsilon r, \quad \gamma=(-\epsilon)^{\frac{1}{2}}, \quad (7)$$

this normal radial wave equation can be written in the more manageable form

$$\frac{d^2U^{(l)}}{d\theta^2}+\frac{1}{\gamma^2}\left[-1-V(\theta)-\frac{l(l+1)}{\theta^2}\right]U^{(l)}=0, \quad (8)$$

which will be termed "the standard equation" in this development. Now Langer has pointed out that the standard equation (8) is not suitable for application of the W.K.B. method, because with any physical potential function, $V(\theta)$, its inner turning point, θ_1, will be too near the origin ($\theta=0$) to permit application of the asymptotic form (6b) anywhere in the region $0\leq\theta\leq\theta_1$. This deficiency he remedies by introducing the further substitutions

$$\theta=e^x, \quad U^{(l)}(x)=e^{\frac{1}{2}x}u(x), \quad (9)$$

and so transforming (8) to the more suitable form

$$\frac{d^2u}{dx^2}+\frac{1}{\gamma^2}[-e^{2x}-e^{2x}V(e^x)-(l+\tfrac{1}{2})^2\gamma^2]u=0, \quad (10)$$

which will be called the "transformed" wave equation.

Approximate solutions of (10) in the form (2) or (6) cannot normally be produced without an explicit knowledge of the potential function $V(e^x)$, and this information is not generally available except in the region well outside the atomic core (say for all $x\geq X$) where the potential function is known to be hydrogenic, i.e., where $V(e^x)=-2e^{-x}$. The quantity X, which marks the effective boundary of the hydrogenic region, may be expected to lie between the two turning points of (8) or (10), for physically (see the discussion in (A)) the valence electron wave function takes its maximum values in the hydrogenic region, and mathematically these maxima are first attained in the region between the turning points, where the wave functions exhibit sinusoidal behavior.

It follows that for all $x\geq X$ the W.K.B. wave functions are completely defined, except for the phase constant η_2, by an expansion of the form (2) or (6) about the outer turning point, x_2, of the wave equation (10). In this expansion $k^2P(x)$ is given by

$$k^2P_h(x)=\gamma^{-2}[-e^{2x}+2e^x-(l+\tfrac{1}{2})^2\gamma^2], \quad (11)$$

where the subscript h denotes the hydrogenic form of $P(x)$, and the outer turning point, x_2, to be substituted

for x_i in (3), is given by

$$x_2=\ln\{1+[1-(l+\tfrac{1}{2})^2\gamma^2]^{\frac{1}{2}}\}. \quad (12)$$

These formulas permit explicit analytic definitions of z, ξ, λ, and κ, so that the production of explicit approximate wave functions in the hydrogenic region is limited only by our ability to determine the phase constant η_2.

Now for any value of the energy parameter γ the phase constant η_2 is completely determined by the condition that the wave function $e^{\frac{1}{2}x}u(x)$ be zero at the origin. This is equivalent to the condition that the phase constant η_1, used in the expansion (6) about the inner turning point, be zero. For as $x\rightarrow-\infty$, the potential function $V(e^x)$ must behave as $-2Ze^{-x}$, so it follows from (3) and (10) that the term $e^{|kx|}$ in (6b) must carry the wave function to infinity at the origin unless $\eta_1=\sin\eta_1=0$.

Between the two turning points the wave function can be expressed as an expansion about either turning point, and since η_1 is now known, the value of η_2 is completely determined by the condition that the two expansions yield identical results in the region where Eq. (6a) is valid. This leads, in the usual fashion, to an explicit definition of η_2 by the formula

$$\eta_2=(m+\tfrac{1}{2})\pi-k\int_{x_1}^{x_2}[P(x)]^{\frac{1}{2}}dx, \quad (13)$$

where m is any integer or zero, and $P(x)$ is γ^{-2} times the square bracket in (10).

Equation (13) cannot, of course, be integrated explicitly unless $V(e^x)$ is known, for it is only near the outer turning point, x_2, that $P(x)$ reduces to the hydrogenic form $P_h(x)$ defined by (11). But a slight modification of a device utilized by Bohr[4] in deriving the Rydberg law makes it possible, from (13), to give values of η_2 in terms of the measured values of the quantum defect. For define δ by the equation

$$\pi\delta=k\int_{x_1}^{x_2}[P(x)]^{\frac{1}{2}}dx-k\int_{x_1'}^{x_2}[P_h(x)]^{\frac{1}{2}}dx, \quad (14)$$

where x_1' is the inner turning point of the hydrogenic form of (10), and the other quantities are those previously defined. Then, as discussed by Kemble,[4] the quantity δ must be virtually independent of the energy parameter γ. For examine the integrands in (14): the quantity $k[P(x)]^{\frac{1}{2}}dx$ may be rewritten

$$k[P(x)]^{\frac{1}{2}}dx=[\epsilon-V(r)+(l+\tfrac{1}{2})^2r^{-2}]dr, \quad (15)$$

and $k[P_h(x)]^{\frac{1}{2}}dx$ has the same form with $V(r)=-2/r$. Now at the upper limit of integration $P(x)=P_h(x)$, for x_2 is in the hydrogenic region; throughout most of the region in which $P(x)\neq P_h(x)$, $|V|\gg|\epsilon|$, so that changes in ϵ do not appreciably influence the integrand; and, finally, the position of the lower limits, x_1 and x_1', are almost independent of ϵ. From all of which it follows that the difference between the integrals can show little dependence on the energy.

The second integration in (14) can now be carried through explicitly, so that (13) and (14) combine to yield

$$\eta_2=n\pi-\delta\pi-\gamma^{-1}\pi, \quad (16)$$

in which n $(=m+l+1)$ is an arbitrary integer greater than l. Equation (16) permits δ to be identified physically, for the atomic wave functions $U^{(l)}$ are just those functions (2) which go to zero both at the origin and at infinity, and the functions which go to zero at infinity are those for which $\eta_2=0$. But if $\eta_2=0$, (16) can be rewritten as

$$\epsilon=-(n-\delta)^{-2}, \quad (17)$$

which is just Rydberg's Law, so that δ is the quantum defect of the atom.

Conversely, if δ is known from spectroscopic data, η_2 can be computed from (16), and the wave functions (2) and (6b) can be produced explicitly, for any value of energy, everywhere in the hydrogenic region. These wave functions may be used, precisely as in (A), to compute the three solid state parameters normally treated by the Wigner-Seitz method.

III. An Application to the Ground-State Energy of Monovalent Metals: The accuracy of these W.K.B. wave functions can be tested by a sample application to the computation of the minimum ground state energy, ϵ_{om}, of monovalent metals, and this application will incidentally provide an extremely rapid and compara-

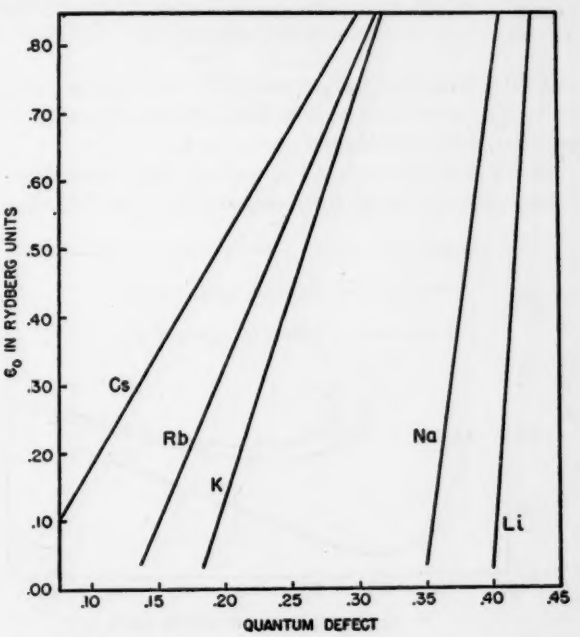

FIG. 2. Quantum defects for the s-wave functions of the alkali metals as a function of energy. From the experimental values in Bacher and Goudsmit.

[4] N. Bohr, Proc. London Phil. Soc. 35, 296 (1923). See also E. C. Kemble, *Fundamental Principles of Quantum Mechanics* (McGraw-Hill Book Company, Inc., New York, 1937), p. 478 ff.

tively accurate means of computing the curve $\epsilon_o(r_s)$ for any monovalent metal for which the quantum defect is known.

For the ground state wave function $U^{(0)}(\theta)$ of the valence electron of a monovalent metallic solid is just that solution of the standard equation (8) which satisfies the Wigner-Seitz boundary condition (A-2) at $\theta=\theta_s$. In terms of the function u and the variable x of of the "transformed equation," this boundary condition may be rewritten as

$$u'(x_s)-\tfrac{1}{2}u(x_s)=0, \tag{18}$$

and this condition, in conjunction with the explicit wave functions given by (2) and (16), must, for a given δ, define the energy parameter γ as a function of the sphere radius variable x_s.

By defining two new functions

$$\begin{aligned} g_\gamma(x)&=z^{1/6}\xi^{\frac{1}{2}}P_h^{-\frac{1}{2}}J_{1/3}(\tfrac{1}{3}\kappa\xi^{\frac{3}{2}})\\ h_\gamma(x)&=z^{1/6}\xi^{\frac{1}{2}}P_h^{-\frac{1}{2}}J_{-1/3}(\tfrac{1}{3}\kappa\xi^{\frac{3}{2}}),\end{aligned} \tag{19}$$

the approximate solution (2) of the "transformed equation" (10) can, with the aid of (16), be written as

$$\begin{aligned} u(x)=&\cos(\tfrac{1}{3}-\delta-\gamma^{-1})\pi g_\gamma(x)\\ &+\cos(\tfrac{1}{3}+\delta+\gamma^{-1})\pi h_\gamma(x),\end{aligned} \tag{20}$$

so that the boundary condition (18) becomes

$$\delta=\frac{1}{\pi}\tan^{-1}\left[(3)^{-\frac{1}{2}}\frac{F_\gamma(x_s)+1}{F_\gamma(x_s)-1}\right]-\frac{1}{\gamma}, \tag{21}$$

with the new function $F_\gamma(x)$ defined by

$$F_\gamma(x)=-\frac{h'_\gamma(x)-\tfrac{1}{2}h_\gamma(x)}{g'_\gamma(x)-\tfrac{1}{2}g_\gamma(x)}. \tag{22}$$

With δ determined experimentally (21) can be solved for γ as a function of x_s, and this relationship, with (7) and (9), yields the desired curve for $\epsilon_o(r_s)$.

Such a computation may be usefully and conveniently illustrated at the outer turning point, θ_2, of the "standard equation" (8), for as Fröhlich[5] has shown, at this point the ground-state energy ϵ_o must take its minimum value, ϵ_{om}. With $l=0$ and $V(\theta)=-2/\theta$ in Eq. (8), Fröhlich's theorem states that the minimum sphere ground-state energy, ϵ_{om}, always occurs at a sphere radius r_{sm} to which it is related by the equation

$$\epsilon_{om}=-2/r_{sm} \quad \text{or} \quad \theta_{sm}=2. \tag{23}$$

In terms of the new variable x_s of the transformed equation, (23) states that the minimum ground-state energy must occur at a point x_{sm} given by

$$x_{sm}=\ln 2, \tag{24}$$

a point which lies near but not at the outer turning point $x_2(=\ln[1+(1-\frac{1}{4}\gamma^2)^{\frac{1}{2}}])$ of the "transformed equation."

At distances near the outer turning point x_2, the functions $f_\gamma(x)$, $g_\gamma(x)$, and $F_\gamma(x)$ are conveniently expanded in terms of the variable $x-x_2$, and at the point $x=x_{sm}(x_{sm}(\gamma))$ these expansions yield $F_\gamma(x_{sm})$ as a function of the energy parameter alone. This procedure has been carried through, and a long and extremely arduous manipulation yields the series

$$\begin{aligned} F_{\epsilon_{om}}(x_{sm})=(\tfrac{3}{2})^{\frac{1}{3}}\frac{\Gamma(\frac{4}{3})}{\Gamma(\frac{2}{3})}(-\epsilon_{om})^{\frac{1}{3}}\Big[&\frac{4}{5}-\frac{5{,}583}{98{,}000}\epsilon_{om}\\ &+\frac{21{,}918{,}107}{6{,}585{,}600{,}000}\epsilon_{om}{}^2+\cdots\Big],\end{aligned} \tag{25}$$

in which ϵ_{om} has been inserted for $-\gamma^2$.

Equation (25) in conjunction with (21) determines the minimum ground-state energy as a function of the observed quantum defect; the radius r_{sm} at which this minimum occurs can also be found as a function of δ by use of (23). These functions, $\epsilon_{om}(\delta)$ and $r_{sm}(\delta)$, are displayed graphically in Fig. 1. The values of δ are there restricted to the interval $0\leq\delta\leq 1$, since integral changes in δ do not affect the solution of (21). These curves are conveniently utilized in conjunction with experimentally derived curves of $\delta(\epsilon_o)$, and such curves for the five alkali metals are shown in Fig. 2.

From these curves values of ϵ_{om} and r_{sm} can be computed, for if one starts with a trial value of ϵ_{om}, a value of δ can be found from Fig. 2, and this value can be used to find a more accurate ϵ_{om} from Fig. 1. Two or three applications of the procedure suffice to determine ϵ_{om} to three-figure accuracy. Final values of ϵ_{om} and r_{sm} gained by this procedure are compared with the results of other computations in Table I. It will be observed that the agreement is, throughout, well within the limits of computational accuracy.

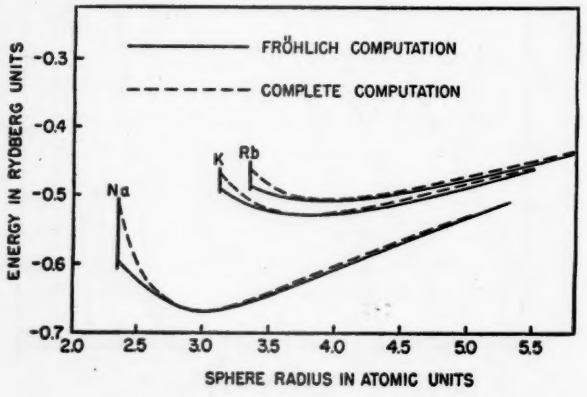

FIG. 3. Ground-state energy as a function of sphere radius for Na, K, and Rb: comparison of Fröhlich's formula with the complete computations of (A).

IV. Application to Fröhlich's Formula: Equation (21) can be used to compute values of ϵ_0 for values of $x_s\neq x_{sm}$, but this computation would be laborious and

[5] H. Fröhlich, Proc. Roy. Soc. **A158**, 97 (1937).

seems unnecessary in view of the accuracy of the approximate procedure which follows.

Fröhlich[6] has shown that, to a good approximation, the ground-state energy, ϵ_0, may be represented by

$$\epsilon_o=(a/r_s^3)-(3/r_s), \tag{26}$$

a formula which takes as its minimum value, $\epsilon_o=-2/r_{sm}$, with $r_{sm}=(a)^{\frac{1}{3}}$. Equation (26) may therefore be rewritten in terms of the results of Section II in the form

$$\epsilon_o=\frac{[r_{sm}(\delta)]^2}{r_s^3}-\frac{3}{r_s}. \tag{27}$$

This equation can be used with the values of r_{sm} listed in Table I, and curves of $\epsilon_o(r_s)$ derived from (27) are compared with those derived by the complete computations of (A) in Fig. 3. It is immediately indicated that the results of this abridged computation are sufficiently accurate to render the lengthy computation superfluous. Equation (27) can also be used in conjunction with the usual approximate formula for the Fermi energy, $\epsilon_F=2.21/r_s^2$, in an approximate computation of binding energy as a function of sphere radius. This computation should yield results substantially identical with those of the "plane wave" ($\alpha=1$) computation in (A), so they have not been carried out here.

V. Comments: The W.K.B. wave functions developed in Section II permit a direct computation of approximate wave functions for the solid state. The application provided in Section III indicates that these wave functions compare favorably with those produced by exact solutions of the wave equation, so we conclude that these functions could be employed for the "complete computation" carried through in (A) by the function matching method.

[6] H. Fröhlich, reference 5. A better derivation is given by J. Bardeen, J. Chem. Phys. **6**, 372 (1938). Bardeen's treatment does not, however, develop the exact relationship (23).

TABLE I. Theoretical values of ϵ_{om} and r_{sm}.

Element	ϵ_{om}(Ry.)		r_{sm}(a.u.)	
	W.K.B.	Other[a]	W.K.B.	Other[a]
Li	0.706	0.700	2.84	2.87
Na	0.667	0.668	3.00	2.97
K	0.530	0.530	3.78	3.75
Rb	0.508	0.506	3.92	3.87
Cs	0.468		4.28	

[a] The values for Li are taken from F. Seitz, Phys. Rev. **47**, 400 (1935). The values for the other elements are taken from (A).

This method of producing wave functions shares with the function matching method the advantage that no explicit formula for $V(r)$ is required. It surpasses the function matching method by its less critical dependence upon experimental data, for although no adequate theoretical explanation of the fact has been found, the extrapolations of Fig. 2 turn out to be "safer" than those of $\phi_R^{(l)}(\epsilon_0)$ in (A). Also, except in those ranges of the parameter l, and r for which the coefficients $\bar{W}_k^{(l)}(r)$ and $\tilde{W}_k^{(l)}(r)$ of (A-12) have been *previously* computed, the computations involved in the W.K.B. approach are simpler than those required for function matching. In any case, for the computation of the ground-state energy, the accuracy of Fröhlich's formula taken in conjunction with the curves of Fig. 1 and Fig. 2 seems to obviate the necessity of any more complete computation procedure.

It should, however, be noted explicitly that the practicability of W.K.B. wave functions in this application is completely dependent upon the revision of the method provided by Imai, for the previous W.K.B. formalisms are too inaccurate near the point r_{sm}. In particular, an attempt to apply Langer's formulas to the computations carried out in Section III, above, produced values of ϵ_{om} and r_{sm} which differed by ten to twenty percent from those listed in Table I.

Quantum Field Theory*

HARTLAND S. SNYDER
Brookhaven National Laboratory, Upton, Long Island, New York
(Received January 30, 1950)

It is usually contended that the quantum theory of fields is intrinsically divergent. The present paper attempts to show that this divergence is due to the perturbation theory generally employed and not to the field theory itself. By means of a minor modification in the perturbation calculations, the divergent integrals may be given appropriate finite values. Although there are many apparent ambiguities in field theory, these are ambiguities of representation, and not ambiguities in physical content. The self-energy and stress of particles are zero. The expectation value of the energy momentum tensor for the true vacuum state is zero. From this point of view the polarization of the vacuum and charge renormalization seem to be factitious.

I. INTRODUCTION

IT has been long believed that the quantum theory of interacting fields is inherently divergent.[1] This belief has persisted in spite of the remarkable success of quantum electrodynamics in accounting for the Lamb-Retherford shift[2] and the anomalous magnetic moment[3] of the electron, in addition to its success in all predictions involving only the lowest order of perturbation theory for a given process. The origin of this belief lies in the fact that the application of ordinary perturbation theory gives rise to divergent integrals in terms which represent the zero-point energy of the vacuum, the self-energy of particles, polarization of the vacuum, and other phenomena. The so-called covariant formulations[4,5] of field theory have not changed this situation, nor could they have changed this situation since they are entirely equivalent[6] to earlier formulations[7] of field theory. These divergences of field theory are entirely fictitious: they are the result of the specialized way in which perturbation theory has been applied.

The quantum theory of fields is based on certain dynamical variables called fields which are supposed to be defined at all points in space-time. Equations of motion connect these field quantities in such a manner that the specification of the values of any selected complete set of field quantities at one instant of time should determine the expectation values of any other complete set of field quantities at any other instant of time. Other quantities, such as the energy and momentum, can be defined in terms of the field referring to a particular instant of time. The various field variables, and other variables defined in terms of them, satisfy certain algebraic relations which are conventionally cast in the form of commutation, or anticommutation relations.

It is the major task of quantum mechanics to find representations for these field quantities and for other physically significant quantities which are defined in terms of them. Although representations are known, these representations have been defective in certain respects. In those known representations in which the momentum is diagonal, the Hamiltonian has been cast in such a form that when it is applied to a state vector it maps the state vector into a vector of infinite length. In some representations the Hamiltonian is arranged to have finite matrix elements; in others not even this condition is met. It is the major purpose of this work to find representations for which the Hamiltonian maps finite state vectors into finite state vectors.

Although in this paper only the coupled equations of the Dirac-Maxwell theory are treated, the method used and the essential results obtained can be applied to all other cases as well. The method used is the construction, by means of suitable limiting processes, of a unitary transformation which transforms the original Hamiltonian into a new form in which there are no coupling matrix elements between different states of the system, unless these are states with at least two particles present. This transformation accomplishes the following objectives: (a) If the transformed Hamiltonian operates on the vacuum state eigenvector (no particles present), one obtains the null vector; (b) if the transformed Hamiltonian is applied to a state vector representing the presence of just one particle, one obtains this same state vector multiplied by the energy of the particle.

There are infinitely many distinct unitary transformations which accomplish objectives (a) and (b), and thus one finds that the interaction terms of the transformed Hamiltonian can appear in infinitely many forms. Considerable use may be made of this last fact since it enables one to select convenient forms for the Hamiltonian, in accordance with the problem to be solved. These various forms of the Hamiltonian are, of course, physically equivalent one to another, since they can be transformed into each other by means of a unitary transformation. It should be noted that the Hamiltonian of the system is not the only operator of physical interest which is transformed by the unitary operator.

* Research carried out at Brookhaven National Laboratory, under the auspices of the AEC.

[1] G. Wentzel, *Quantum Theory of Fields* (Interscience Publishers, Inc., New York, 1949), p. 212.
[2] W. E. Lamb, Jr. and R. C. Retherford, Phys. Rev. **72**, 241 (1947); **75**, 1325 (1949).
[3] P. Kusch and H. M. Foley, Phys. Rev. **74**, 250 (1948).
[4] S. Tomonaga, Prog. Theor. Phys. **1**, 27 (1946).
[5] Julian Schwinger, Phys. Rev. **74**, 1439 (1948); **75**, 651 (1949).
[6] S. T. Ma, Phys. Rev. **75**, 535 (1949).
[7] G. Wentzel, *Quantum Theory of Fields* (Interscience Publishers, Inc., New York, 1949).

One must also consider other operators, such as the charge and current densities, the energy momentum tensor, the momentum and angular momentum, and the operators generating infinitesimal Lorentz transformations.

A unitary transformation which accomplishes objectives (a) and (b) does not exist in the conventional sense of having finite matrix elements which satisfy the unitary condition. Rather, it must be regarded as the limit of a sequence of finite unitary transformations. This sequence of unitary transformations has the property that the limiting matrix element of the sequence of unitary transformations is zero. This last fact makes it abundantly clear that it is necessary to compute the matrix elements of the various operators as they are transformed by each member of the sequence of finite unitary transformations, and then pass to the limit. It is the major purpose of this work to show that a sequence of finite unitary transformations may be chosen so as to satisfy both (a) and (b), and so that the sequences of transformed operators approach finite limits. It is only by insuring that the sequences of transformed operators approach finite limits that it can be asserted that the commutation rules originally satisfied by these operators remain still satisfied by their transforms.

In the conventional treatments of field theory by perturbation theory, the unitary transformation is expanded in a power series in the coupling constant. Actually, only the first term in this expansion remains finite. In most treatments no consideration is given to the limiting process which must be used. Even in those cases when the limiting process has been considered, unfortunate choices of the forms of the successive terms in the expansion have prevented the convergence of terms in the expansion of the transforms of the various operators.

Since the treatment given here also involves an expansion of the unitary transformation in a power series in the coupling constants, certain limitations on the general arguments concerning the sequence of unitary transformations are evident. The transforms of the various operators are then expanded in a power series in the coupling constant for each member of the sequence of unitary transformations. The algebraic relations, such as commutation relations, which were satisfied by the original operators, will still be satisfied by their transforms as formal power series in the coupling constants. In general, the convergence of the power series defining the transforms is not proved even for finite unitary transformations. However, in the transforms of the various operators, those parts which are expressed as divergent integrals in usual perturbation theory will here be given finite values and, furthermore, the unitary transformations can be arranged so that the power series resulting from divergent integrals will converge. In particular, the power series expressing the particle self-energy parts of the transformed Hamiltonian can be made to converge to any desired value. The same is true to the polarization terms in the transformed charge and current densities. The reason for this apparent paradox is the fact that regular methods can always be found which will sum a divergent integral to any preassigned value. On the other hand, absolutely convergent integrals do not have their values changed, and, therefore, must be computed. These integrals are quite complicated and consequently the convergence of power series composed of absolutely convergent integrals has not yet been proved.

In this work all the operators concerned are expressed in terms of a complete set of dynamical variables which refer to the physical state at a particular instant of time. The operators in terms of which all other operators are expressed are the annihilation and creation operators of photons, electrons, and positrons. Since we use operators which refer only to a particular instant of time, the question of whether we are using the Heisenberg, Schrödinger, or interaction representation to connect operators referring to different instants of time or different Lorentz frames does not enter into the problem.

II. RELATIVISTIC AND GAUGE INVARIANCE

It has long been known that field theories derived from Lorentz invariant and gauge invariant Lagrangians give rise to covariant and gauge invariant field equations. It is further known that the canonical commutation relations[8] satisfied by the fields are maintained under Lorentz and gauge transformations. Other dynamical variables of importance are the total energy, the momentum, the total angular momentum, and the infinitesimal generators of the Lorentz transformations. These last ten quantities satisfy certain commutation relations,[9] which are necessary in order that a theory shall be relatistically invariant. If H denotes the Hamiltonian of the system, P_x, P_y, and P_z the components of the momentum, L_x, L_y, and L_z the components of the angular momentum, and M_x, M_y, and M_z the components of generators of Lorentz transformations, then their commutation rules are:

$$\begin{aligned}
&[H, P_x]=0; \quad [P_x, P_y]=0; \quad \text{etc.}\\
&[L_x, L_y]=[M_y, M_z]=iL_z; \quad \text{etc.}\\
&[M_x, L_y]=[L_x, M_y]=iM_z; \quad \text{etc.}\\
&[M_x, L_x]=[P_x, L_x]=0; \quad \text{etc.}\\
&[L_x, H]=0; \quad \text{etc.}\\
&[M_x, H]=iP_x; \quad \text{etc.}\\
&[M_x, P_x]=iH; \quad \text{etc.}\\
&[L_x, P_x]=iP_y; \quad \text{etc.}\\
&[M_x, P_y]=[M_y, P_x]=0; \quad \text{etc.}
\end{aligned} \tag{1}$$

Explicit expressions for these operators are given by

[8] See reference 7, Chapter I, Section 4.
[9] P. A. M. Dirac, Rev. Mod. Phys. 21, 392 (1949).

Wentzel.[10] It can also be shown that if these operators are obtained for field theories derivable from a Lorentz invariant Lagrangian they will, in fact, satisfy Eqs. (1). Because P_x, P_y, and P_z commute with H and with each other, it is possible to use a representation in which the linear momenta are diagonal. In this representation $\mathbf{P}$ is given as the sum of momenta of the particles which are present. In this special representation the angular momentum operators are represented in a simple form as the sum of the angular momenta of the particles. The expressions for H and M_x, M_y, and M_z are, however, complicated and all of them involve interaction terms between the fields.

An essential feature of the development is: "A unitary transformation does not alter the physical content of a theory; it simply expresses that physical content in a different form." In particular, the values of all commutators of dynamical variables are left unaltered by a unitary transformation. Of course, if the unitary transformation happens to be of such a nature that the matrix elements of the transformed dynamical operators do not exist, then the above statements become essentially meaningless. With respect to the appearance of non-covariant and non-gauge invariant expressions in the terms of the power series expansions for the transformed operators, it may be stated that it is of course possible to use a transformation which depends upon gauge or Lorentz frame and that these expressions must cancel when all terms in the expansion are summed.

One does not have to consider explicitly the unitary transforms of M_x, M_y, and M_z since these are intimately linked to the unitary transform of H by virtue of the relations $[M_x, P_x]=iH$, etc. Since a diagonal representation for P is used and the form of H is known, these equations may be solved for M_x, M_y, and M_z. The solution is not unique: the lack of uniqueness being essentially associated with the location of the point in coordinate space about which the infinitesimal homogeneous Lorentz transformation is taken. Since only unitary transformations which commute with the momentum and angular momentum operators will be used, it can be shown that a unitary transformation, which eliminates the vacuum state and one particle state coupling terms from H, will also eliminate these same coupling terms from M_x, M_y, and M_z. This means, of course, that the vacuum state in one Lorentz frame is the vacuum state of all Lorentz frames. The same is true of single particle states.

III. THE UNITARY TRANSFORMATION

In order to give the ideas stated in the previous sections explicit form, consider the case of the coupled Dirac-Maxwell fields. The Hamiltonian of this system is

$$H=H_0+H_1+H_2, \tag{2}$$

with

$$H_0=\int e_{ps}(\alpha_{ps}{}^{+}\alpha_{p's'})\delta(\mathbf{p}-\mathbf{p}')d\mathbf{p}d\mathbf{p}'$$

$$=\int K a_{\lambda\mathbf{K}}{}^{+}a_{\lambda\mathbf{K}'}\delta(\mathbf{K}-\mathbf{K}')d\mathbf{K}d\mathbf{K}', \tag{3}$$

$$H_1=-\frac{e}{2\pi}\int\frac{d\mathbf{p}d\mathbf{p}'d\mathbf{K}}{K^{\frac{1}{2}}}\delta(\mathbf{p}-\mathbf{p}'-\mathbf{K})$$
$$\times\{(\alpha_{ps}{}^{+}\alpha_{p's'})a_{\lambda\mathbf{K}}(\mathbf{p}s|\,\boldsymbol{\alpha}_\lambda|\,\mathbf{p}'s')$$
$$+(\alpha_{p's'}{}^{+}\alpha_{ps})a_{\lambda\mathbf{K}}{}^{+}(\mathbf{p}'s'|\,\boldsymbol{\alpha}_\lambda|\,\mathbf{p}s)\}, \tag{4}$$

$$H_2=\frac{e^2}{(2\pi)^2}\int\frac{d\mathbf{p}d\mathbf{p}'d\mathbf{p}''d\mathbf{p}'''}{|\mathbf{p}-\mathbf{p}'|^2}\delta(\mathbf{p}-\mathbf{p}'+\mathbf{p}''-\mathbf{p}''')$$
$$\times(\alpha_{ps}{}^{+}\alpha_{p's'}\alpha_{p''s''}{}^{+}\alpha_{p'''s'''})$$
$$\times(\mathbf{p}s|1|\mathbf{p}'s')(\mathbf{p}''s''|1|\mathbf{p}'''s'''). \tag{5}$$

Since the notation used in Eqs. (3)–(5) is the same as in a previous paper,[11] the definitions of the various quantities used will not be repeated here, except that $\boldsymbol{\varepsilon}_{\lambda\mathbf{K}}\cdot\boldsymbol{\alpha}$ is replaced by $\boldsymbol{\alpha}_\lambda$. It should also be noted that the vacuum and electron self-energies have been omitted from the Coulomb energy as it is given by (5). It can be shown independently that this does not interfere with the satisfying of relations (1).

The unitary transformations are used in such a way that they effect a canonical transformation. To see this, consider the expectation value of some operator A for the state vector ψ.

$$(\psi, A\psi)=(UU^{+}\psi, AUU^{+}\psi)=(U^{+}\psi, U^{+}AUU^{+}\psi), \tag{6}$$

with U a unitary operator. If one defines

$$A'=U^{+}AU \tag{7}$$

and

$$\psi'=U^{+}\psi \tag{8}$$

then

$$(\psi', A'\psi')=(\psi, A\psi). \tag{9}$$

All operators such as A and U are expressed in terms of the annihilation and creation operators $\alpha_{ps}{}^{+}$, α_{ps}, $a_{\lambda\mathbf{K}}{}^{+}$, and $a_{\lambda\mathbf{K}}$. If the transformed operators are expressed in terms of the same annihilation and creation operators, then the unitary transformation effects a canonical transformation. Also, the effect of the annihilation and creation operators on a state vector is simple only if state vectors are expressed as linear combinations of basis vectors which diagonalize the occupation number operators $\alpha_{ps}{}^{+}\alpha_{ps}$ and $a_{\lambda\mathbf{K}}{}^{+}a_{\lambda\mathbf{K}}$. Thus, a new set of basis vectors is used for ψ when a unitary transformation is used to effect a canonical transformation. This new set of basis vectors is labeled with the same occupation numbers as was the old set of basis vectors. How-

[10] See reference 7, Chapter I, p. 10.

[11] H. S. Snyder, Phys. Rev. 78, 98 (1950).

ever, the physical content is quite different and must be established by considering the expectation values of the appropriate transformed dynamical variables.

For all field theories it is very convenient to use the symmetrical energy momentum tensor to establish the physical content of a given state. In electrodynamics one must also use the charge and current densities, because the invariance of the Lagrangian under gauge transformations gives rise to the additional differential charge and current conservation law. Because of (9) the differential conservation laws may now be written

$$(\partial/\partial x_\mu)(\psi', T_{\mu\nu}'\psi')=0 \quad (\mu, \nu=1, 2, 3, 4) \tag{10}$$

with $x_4=it$ in which $T_{\mu\nu}'$ is the transform of the energy momentum tensor. Also,

$$(\partial/\partial x^\mu)(\psi', J_\mu'(x, t)\psi')=0 \tag{11}$$

in which iJ_4 is the charge density and the other components are the current densities. It is quite obvious that (10) and (11) are covariant relations. It is also evident that these relations do not depend on the unitary transformation U or its dependence on time, or upon whether the Heisenberg, Schrödinger, or interaction representation is used for ψ'.

The Hamiltonian (2) is now transformed by means of a finite unitary transformation of the form $U(\epsilon)=\exp[iS(\epsilon)]$ in which $S(\epsilon)$ is a finite Hermitian operator for all finite ϵ. The parameter ϵ is used to specify which particular finite unitary transformation of the previously mentioned sequence of finite unitary transformations is under consideration. The transformed Hamiltonian then becomes

$$\begin{aligned} H'(\epsilon)&=\exp[-iS(\epsilon)]H\exp[iS(\epsilon)] \\ &=H-i[S(\epsilon), H]-\tfrac{1}{2}[S(\epsilon), [S(\epsilon), H]]+\cdots. \end{aligned} \tag{12}$$

The operator $S(\epsilon)$ is expanded in a power series in the electronic charge

$$S(\epsilon)=S_1(\epsilon)+S_2(\epsilon)+S_3(\epsilon)+\cdots, \tag{13}$$

in which $S_k(\epsilon)$ is of the order e^k. Using (2), (12), and (13) and collecting in powers of e, one obtains

$$\begin{aligned} H'(\epsilon)=H_0+\{H_1-i[S_1(\epsilon), H_0]\}+\{H_2-i[S_1(\epsilon), H_1] \\ -\tfrac{1}{2}[S_1(\epsilon), [S_1(\epsilon), H_0]]-i[S_2(\epsilon), H_0]\}+\cdots. \end{aligned} \tag{14}$$

In the conventional treatments by perturbation theory the operator S_1 is chosen so that the term of order e in (14) is zero. This is not a well-defined process, because the length of the vector $S_1\psi$ is infinite for all the basis vectors of the Hilbert space. It is precisely at this point that the present treatment differs from earlier treatments of the problem. $S_1(\epsilon)$ is written here

$$\begin{aligned} S_1(\epsilon)=-\frac{ie}{2\pi}\int \frac{dpdp'd\mathbf{K}\delta(\mathbf{p}-\mathbf{p}'-\mathbf{K})}{K^{\frac{1}{2}}(e_{ps}-e_{p's'}-K)} g_1(ps|p's'|\epsilon) \\ \times\{(\alpha_{ps}{}^+\alpha_{p's'})a_{\lambda\mathbf{K}}(ps|\alpha_\lambda|p's') \\ -(\alpha_{p's'}{}^+\alpha_{ps})a_{\lambda\mathbf{K}}{}^+(p's'|\alpha_\lambda|ps)\}. \end{aligned} \tag{15}$$

In (15) the convergence producing function $g_1(ps|p's'|\epsilon)$ is taken so that, for all finite ϵ, $S_1(\epsilon)$ is a finite Hermitian operator. The appearance of the δ-function in the integrand of (a) insures that $S_1(\epsilon)$ will commute with the linear momentum operators. If, in addition, $g_1(ps|p's'|\epsilon)$ is invariant under rigid rotations of the vectors $\mathbf{p}$ and $\mathbf{p}'$ and is independent of the direction of the spins of the electrons and positrons and the polarization of the quanta, then $S_1(\epsilon)$ will commute with the angular momentum operators. Thus, $g_1(ps|p's'|\epsilon)$ depends only on the relative orientation and the magnitudes of the vectors $\mathbf{p}$ and $\mathbf{p}'$ and on whether the spin indices s, s' refer to positive and negative frequency states. Therefore, insofar as the function $g_1(ps|p's'|\epsilon)$ is concerned, its spin dependence is determined by using plus or minus signs for s and s' according to whether the state referred to is an electron or positron state.

By further limiting $S_1(\epsilon)$ to be charge symmetrical, the $g_1(ps|p's'|\epsilon)$ must satisfy the relations

$$\begin{aligned} g_1(\mathbf{p}, +|\mathbf{p}', +|\epsilon)&=g(-\mathbf{p}', -|-\mathbf{p}, -|\epsilon), \\ g_1(\mathbf{p}, +|\mathbf{p}', -|\epsilon)&=g(-\mathbf{p}', -|-\mathbf{p}, +|\epsilon), \\ g_1(\mathbf{p}, -|\mathbf{p}', +|\epsilon)&=g(-\mathbf{p}', +|-\mathbf{p}, -|\epsilon). \end{aligned} \tag{16}$$

To eliminate the terms of order e, one must take

$$\operatorname*{Lim}_{\epsilon\to\infty} g_1(ps|p's'|\epsilon)=1$$

although not uniformly in $\mathbf{p}$ and $\mathbf{p}'$ since otherwise $S_1(\epsilon)$ would not be finite for all finite ϵ. Also, the functions $g_1(ps|p's'|\epsilon)$ need not be everywhere positive. It is this possibility which permits the elimination of what would otherwise be positive or negative definite divergences. By inspection of (14) one sees that to order e^2 the usual divergent integrals for the electron and photon and zero-point self-energies have their integrands multiplied by a combination of linear and bilinear functions of the g_1's and may thus be given any desired value, in particular the value zero. In this particular case, the electron and photon self-energies may be made zero even if positive g_1's are used.[11] In other cases, for example, the case of the coupled equations of the charged scalar field with the electromagnetic field, one must use general g-functions in order to obtain finite self-energies for the charged particles. This completes the discussion of self-energy effects to order e^2.

To extend the above argument to all orders in the coupling constant the form of $H'(\epsilon)$ must first be examined. It must first be noted that the term of order e^0 in $H'(\epsilon)$ involves the product of an annihilation operator by a creation operator, with the annihilation operator written to the right of a creation operator. The product of a number of annihilation operators by a number of creation operators will be regarded to be in standard order whenever the annihilation operators are written to the right of the creation operators. The power of a particular term is defined as the sum of the number of annihilation plus creation operators which it contains, when these are written in the standard

order. Thus, the terms of order e are of the third power because of the choice of $S_1(\epsilon)$. The terms of order e^2 not involving $S_2(\epsilon)$ are of the fourth, second, and zeroth powers. The latter two types of terms give particle and zero-point self-energies. If $S_2(\epsilon)$ is chosen to be composed of fourth- and second-power terms, then all terms of order e^2 will be of fourth, second, and zeroth powers. In general, $S_n(\epsilon)$ will be chosen to be composed of terms of $(n+2)$th power, nth power, etc. It will then be found that the term of order e^n in $H'(\epsilon)$ will be composed of terms of the powers $n+2$, n, $n-2$, etc.

Terms may further be grouped into two classes which will be called "real" and "virtual" terms. A real term is a term which does not couple the vacuum or single particle states to other states; all other terms are virtual. It should be noted that all terms of first and third power are virtual. Terms of zero power are real. Terms of second power are real if they contain one creation and one annihilation operator; they are virtual if they contain two creation or two annihilation operators. Terms of fourth power or higher are real if they contain at least two creation and two annihilation operators; otherwise, they are virtual.

Returning to the question of the choice of $S_2(\epsilon)$, $S_3(\epsilon)$, etc., the operator $S_2(\epsilon)$ is now chosen so that in the limit $\epsilon\longrightarrow\infty$ all virtual terms of order e^2 are eliminated. In general, $S_n(\epsilon)$ is chosen so that all virtual terms of order e^n are eliminated in the limit $\epsilon\longrightarrow\infty$. As was the case with $S_1(\epsilon)$, the definition of $S_n(\epsilon)$ includes convergence producing functions $g_n(\mathbf{ps}|\mathbf{p's'}|\cdots|\mathbf{K\lambda}|\cdots|\epsilon)$ which enable one to evaluate all independent divergent integrals to any chosen value. A way to see that integrals may be evaluated as desired comes from the fact that the commutator of $S_n(\epsilon)$ with H_1 introduces into the terms of order e^{n+1} divergent integrals linear in the $g_n's$ which may be combined with the other divergent integrals which arise from lower order $S_{n'}(\epsilon)$ $n'<n$, and which might be positive or negative definite. It is now noted that for all terms of order e^2 or greater, the terms of $H'(\epsilon)$ of powers zero, one, two, and three are given by divergent integrals and may thus be made to vanish. It can be observed further that terms of power two are of a mass-like character, so that the elimination of the virtual terms of power two automatically eliminates the real terms of power two. Thus, the particle self-energy terms must be made to vanish if conditions (a) and (b) are to be met. Terms of power one and three, being entirely virtual, may as well be eliminated at each step of a perturbation calculation. The real terms of power zero may also be eliminated. It has now been shown that the objectives (a) and (b) can be accomplished by means of an appropriate unitary transformation, and that when this is accomplished the self-energies of all particles are exactly zero. The demonstration is constructive in that it tells one how to find such transformations.

The vacuum polarization problem is handled in essentially the same manner as the self-energy problem. The terms of order e^n in the transformed charge and current density are of the power $n+1$, $n-1$, etc. The terms of power one, i.e., terms linear in the annihilation and creation operators for photons, are expressed as divergent integrals and may, therefore, be evaluated to be zero. The terms of power two are also expressed as divergent integrals and may also, for n greater than two, be evaluated to be zero. By evaluating all these terms appropriately, it is insured that the integral over all space of the transformed charged density is the same as the transform of the total charge operator. If induced charge and current effects are to be eliminated, it is essential that g-functions, which take on negative as well as positive values, be used.

The lack of uniqueness of the transformed Hamiltonian arises formally because real terms of various powers may be introduced into the Hermitian operators $S_n(\epsilon)$, etc. It is to be noted that, because of the essential degeneracy of H_0 for two or more particle states, it is impossible to alter the values of the matrix elements of the interaction energy for which energy is conserved for any order in e by means of an S operator of that same order in e. It is this fact which insures that reaction or scattering cross sections calculated for maximal powers of the annihilation and creation operators at the lowest order in e at which the process occurs are unique.

It is observed that the vacuum state is unique. The specification of the momentum and type of particle present determines uniquely a one particle state. However, for multiple particle states the specification of the energy and momentum alone does not determine the state of the system. A further specification, using other dynamical variables, is required in order to specify multiple particle states uniquely. This specification is given by determining the expectation value of the energy momentum tensor and possibly other quantities. It should be noted that the expectation value of the transformed energy momentum tensor for the vacuum state is zero. Also, the expectation value of the transformed energy momentum tensor is just that of a single particle for a one particle state. These last two facts are most readily proved by using a relation due to Pais and Epstein,[12] given by their Eq. (5),

$$S(0)=\int\langle T_{11}\rangle dv=-\tfrac{1}{3}[\mu-m(\partial\mu/\partial m)], \qquad (17)$$

which holds for an electron at rest, in which μ is the electromagnetic self-energy of the electron, and in the case of the vacuum state μ is the zero-point energy of vacuum. In both these cases $\mu=0$ and thus $S(0)=0$. For single photon states a slight generalization of the relations used by Pais and Epstein will also show that the expectation value of the energy momentum tensor for a single photon state is correct. The expectation value of the transformed energy momentum tensor for

[12] A. Pais and S. T. Epstein, Rev. Mod. Phys. **21**, 445 (1949).

a state representing a single electron in motion is also correctly given, because single particle states are transformed into one another by infinitesimal Lorentz transformations.

A unitary transformation, which insures that states labeled as the vacuum state or a single particle state will have the properties of the vacuum state or a single particle state, does not insure that a state labeled as though it had two particles present actually corresponds to this labeling. However, one must restrict the unitary transformation so that the expectation value of the energy momentum tensor is just the sum of the expectation values of the energy momentum tensor of particles indicated as present by the labeling.

Actually, only the expectation value of the stress part of the energy momentum tensor need be considered. The T_{44}' component does not have the same expectation value for interacting systems as for non-interacting systems. On the other hand, the expectation values of the T_{4k}' ($k=1, 2, 3$) components are the same as those of non-interacting systems because the unitary transformation commutes with the linear momentum operator. The condition stated above on the stress part of the energy momentum tensor is clearly necessary. It is not evident that this condition is sufficient to establish uniquely the physical content of multiple particle states. There are, however, infinitely many other physical conditions which can be imposed. For example, one can require that the expectation value of $J_\mu'(x, t)J_{\mu'}'(x', t)$ shall be the same as for a non-interacting system. Further investigation is required to determine the necessary and sufficient conditions for the unitary transformation so that a state labeled as having certain particles present will have the appropriate physical properties.

As has been noted before, any divergent integral may be assigned any desired value. However, different divergent integrals arising from the transforms of different quantities may be so related that their values cannot be assigned independently. This condition arises whenever a linear combination of divergent integrals is a convergent integral. The relation (5) of Pais and Epstein[12] is an example of related divergent integrals. Another example of such related divergent integrals is found in the transforms of H, M_x, M_y, and M_z. In this case the related divergent integrals are identical, and for this reason the elimination of virtual terms from the transform of H also eliminates virtual terms from the transforms of M_x, M_y, and M_z.

IV. CONCLUSIONS

Quantum field theories of interacting particles are not inherently divergent. This conclusion is limited by the as yet unproved convergence of the power series expansions for the transformed dynamical variables. The usual difficulty, that even the individual terms in the power series expansions have been given infinite values, has been completely eliminated. Although many divergent integrals do appear in the expansions, it is suggested that these divergent integrals may be evaluated in such a manner that when states are occupied this corresponds to the physical presence of entities with particle-like properties. It is precisely the occurrence of divergent integrals which enables one to accomplish this desirable objective.

Although the only field theory for which explicit equations are given here in the Dirac-Maxwell field theory, it is clear that the general arguments used do not depend upon these particular formulas. The only essential features are the formal relativistic invariance of the field equations and the appearance of divergent integrals in terms representing particle self-energies, vacuum polarization and other allied phenomena. The general arguments given here must clearly be supplemented by detailed calculations to determine explicitly the physical predictions of quantum field theories.

Notes on the Theory of Dielectric Breakdown in Ionic Crystals

H. FRÖHLICH*
Department of Physics, Purdue University, Lafayette, Indiana
AND
F. SEITZ
Department of Physics, University of Illinois, Urbana, Illinois
(Received April 17, 1950)

A comparative discussion is given of the theories proposed by the authors on dielectric breakdown in ionic crystals.

IN the literature bearing on the subject of dielectric breakdown in crystals we have expressed somewhat different viewpoints concerning the details of the process.[1–3] This note is written with the intention of expressing these viewpoints in a somewhat coordinated manner.

I.

We both agree that in the range of velocity in which a free electron does not have sufficient energy to stimulate excitation waves or to ionize the atoms of the lattice, so that interaction with the lattice vibrations is the principal means by which the electron dissipates its energy, the interaction energy contains three prominent terms.

(a) An interaction with a dipole field which is described by treating the ions as if rigid, that is by neglecting any polarization or distortion of the electron shells. This interaction was first discussed by Fröhlich. It extends over a long range and is very large for longitudinal polarization waves of long wave-length.

(b) An interaction with the dipole component of the field arising from the distortion of the electron cloud. This component produces a long-range effect, very similar to the interaction (a) for long polar waves. If combined with (a) it decreases the influence of the latter. In the case of long polarization waves, the interaction resulting from the sum of (a) and (b) is similar in mathematical form to that derived for (a) alone, with the ionic charge replaced by an effective charge e^* of the form introduced by Lyddane, Sachs, and Teller.[4]

(c) An additional "short-range" interaction associated with electron distortion which excludes the dipole component (b). This component is the only one which occurs in metals and non-polar insulators.[5]

Interactions (a) and (b) are largest for long polar waves and decrease with decreasing wave-length. Both are small for acoustical waves of long wave-length and increase with decreasing wave-length.

Interaction (c) is negligible compared with the sum of (a) and (b) for long polar waves. On the other hand, (a) and (b) are negligible compared with (c) for long acoustical waves.

Fröhlich has, by definition, called interaction (a) the polar interaction. Although (b) is closely related to (a) for long polar waves, since the most important part of the electron polarization arises from the long-range electrostatic field associated with ionic displacement, Fröhlich believes that this interrelation between (a) and (b) ceases to be highly significant when the waves become short. For this reason, he believes it to be reasonable to regard (b) and (c) as a unit for purposes of discussion. Moreover, he believes that the sum of (b) and (c) will be relatively small for short waves since each will have opposite sign and nearly equal magnitude. As a result, (a) is the dominant term for short waves and it becomes permissible, for short waves, to treat the scattering with the use of Fröhlich's original theory in which electron polarization is neglected.

Seitz has called, by definition, the sum of (a) and (b) the polar interaction, and has termed (c) the non-polar interaction. He has assumed that the sum of (a) and (b) can be extrapolated to the range of short waves with the use of Fröhlich's equation for interaction (a) taken in the form in which the ionic charge is replaced by e^*. Interaction (c) was estimated with the use of equations developed for non-polar materials, and was assumed to dominate in the range of short waves.

These two viewpoints are not inconsistent with one another. In fact, both seem to lead to the same total interaction in the range of short waves which are of interest for the scattering of electrons with an energy of the order of several electron volts, which have wave number vectors lying close to the edge of a Brillouin zone.

To summarize, we have made different intuitive approaches to estimating the interaction for short waves and in these approaches have used different definitions of the polar interaction. Both approaches seem to lead to essentially the same conclusion, namely that the collision frequency of the conduction electrons

* On leave of absence from Department of Theoretical Physics, University of Liverpool, Liverpool, England.

[1] H. Fröhlich, Proc. Roy. Soc. **A160**, 230 (1937); Reports Prog. Phys. **6**, 411 (1939).
[2] H. Fröhlich, Proc. Roy. Soc. **A188**, 521, 532 (1937).
[3] F. Seitz, Phys. Rev. **76**, 1376 (1949).
[4] Lyddane, Sachs, and Teller, Phys. Rev. **59**, 673 (1941).
[5] F. Seitz, Phys. Rev. **73**, 550 (1948).

is high both when the electron has an energy of the order of $\hbar\omega$, where ω is 2π times the frequency of the longitudinal polar waves of long wave-length, and when the electron has an energy in the vicinity of the Brillouin zone.

Perturbation theory may be applied to obtain quantitative results only if $E<\hbar\omega$, and leads to the formula derived by Fröhlich and Mott[6] (modified according to Fröhlich, Pelzer, and Zienau[7] and by Callen[8]). The formal procedure of perturbation theory also converges in the region of higher energies, that is, when $E\gg\hbar\omega$, if applied to the form of the polar matrix components used in the low energy range. It then leads to the result

$$1/\tau=(\epsilon_\infty^{-1}-\epsilon^{-1})(\omega/ka_0)(1+2n_\omega) \qquad (1)$$

for the collision frequency, in which n_ω is the average number of vibrational quanta associated with an oscillator having frequency ω at temperature T, ϵ is the dielectric constant, ϵ_∞ is the square of the refractive index, $2\pi/k$ is the de Broglie wave-length of the electron, and a_0 is the Bohr radius. This equation can be obtained from Eq. (6.6) of reference 7 by replacing $2kT/\hbar\omega$ by $1+2n_\omega$. For energies near a Brillouin zone this equation yields a value of the collision frequency of $2\cdot10^{13}$ sec.$^{-1}$ in the case of NaCl at thc absolute zero of temperature. In this case $\omega\simeq5\cdot10^{13}$ sec.$^{-1}$, $\epsilon\simeq5.6$, $\epsilon_\infty=2.3$. Since application of the perturbation theory requires that $1/\tau>\omega/2\pi$, this is about the lowest energy in the high energy region for which the foregoing equation may be used.

We both believe, however, that the actual value of the collision frequency is higher than that given by Eq. (1). From Fröhlich's viewpoint, an approximation to the true value is to be computed by taking interaction (a) alone into account. The result is obtained by replacing (1) by an expression having similar form, but a larger coefficient [see Eq. (22) of reference 5]. Seitz has replaced (1) by an expression derived from a treatment of non-polar materials which takes into account the interaction (c) alone.

In this connection, Seitz desires to correct an ambiguity which appears in his paper[3] in the section following Eq. (22). The value of the collision frequency for an electron having an energy near the Brillouin zone which is given, namely $1.5\cdot10^{13}$ sec.$^{-1}$, is not computed from Eq. (22) which is the equation Fröhlich would employ to estimate the total collision frequency, but is obtained from the collision frequency ($4.3\cdot10^{14}$ sec.$^{-1}$) for electrons having energy in the range near $\hbar\omega$, given in a preceding paragraph, by multiplying by a factor $k(\hbar\omega)/k_s$ where $k(\hbar\omega)$ is the wave number associated with an electron having an energy $\hbar\omega$ and k_s is the wave number of an electron near the edge of the Brillouin zone. This multiplicative factor is suggested by the energy dependence contained in Eq. (22).

[6] H. Fröhlich and N. F. Mott, Proc. Roy. Soc. **A171**, 496 (1939).
[7] Fröhlich, Pelzer, and Zienau, Phil. Mag. **41** (March, 1950).
[8] H. Callen, Phys. Rev. **76**, 1394 (1949).

II.

We both agree that the increase in electrical conductivity in strong fields (but below breakdown strength) arises from a strongly fluctuating increase in the number of free electrons, and may be described in terms of avalanche formation. Seitz has related breakdown to the formation of avalanches by assuming that breakdown occurs when these avalanches exceed a certain size. He has adopted as a criterion for breakdown the condition that a primary produce 40 progeny in traversing the specimen. It was assumed that these progeny would produce further free electrons, so that $2^{40}=10^{12}$ electrons would result. This was regarded as a reasonable upper limit for the number required to induce changes that might be regarded as constituting breakdown.

The actual value of the breakdown field will depend upon the number of electrons required to bring about the onset of breakdown through the logarithm of this number and hence will not be highly sensitive to it.

We agree that considerations of the above type would lead to an upper theoretical limit for the breakdown strength, but that breakdown may occur through other processes connected with the existence of an increased number of free electrons. Experimentally, breakdown would then appear not as a continuation of pre-breakdown currents, but rather as a phenomenon abruptly interrupting the increase of pre-breakdown currents. Experimental work in this field is somewhat ambiguous; however it appears that von Hippel[9] has found this to be the case in his experiments on alkali halides. Fröhlich's low temperature theory[1] is based on the assumption of such an effect; in the high temperature theory[2] it follows as a consequence of the basic assumptions.

III.

Finally, Seitz wishes to thank Professor A. Nordsieck for indicating an error in connection with Section 8 of reference 3, which deals with excitons. Nordsieck has pointed out that a consistent treatment of the excitons with the use of the hydrogen-atom model requires, in analogy with the treatment of electron-positron states, that one identify the first exciton state with total quantum number $n=1$ instead of $n=2$, as was done in reference 3. This increases the ionization energy of the excitons by a factor 4, that is, changes the energy for diamond and sodium chloride from 0.049 and 0.30 ev to 0.20 and 1.2 ev, respectively. The change in the value for diamond does not alter the discussion appreciably: One still expects the excitons to be dissociated by the field near breakdown. On the other hand, the larger value for NaCl is in much closer agreement with Mott's value of about 1.7 ev discussed in the paper and makes it seem very dubious that the excitons are decomposed by fields as weak as the breakdown value in the alkali halides.

[9] A. von Hippel, Ergeb. d. exakt. Naturwiss. **14**, 79 (1935).

Letters to the Editor

PUBLICATION of brief reports of important discoveries in physics may be secured by addressing them to this department. The closing date for this department is five weeks prior to the date of issue. No proof will be sent to the authors. The Board of Editors does not hold itself responsible for the opinions expressed by the correspondents. Communications should not exceed 600 words in length.

Fission of Medium Weight Elements*

ROGER E. BATZEL AND GLENN T. SEABORG
Radiation Laboratory and Department of Chemistry, University of California, Berkeley, California
June 14, 1950

THE fission reaction has been observed with high energy accelerator projectiles for elements as light as tantalum[1] but has not been reported for medium weight elements. The present note presents evidence for the occurrence of reactions which are probably most properly described by the term "fission" and which seem to occur with very small yield throughout the region where this type of reaction is only slightly exoergic or even endoergic with respect to mass balance.

In the course of detailed investigation of the spallation of copper and the variation of the product yields with energy of the bombarding particle the threshold for formation of radioactive Cl^{38} (38 min. half-life) from elemental copper was studied. The energetically most economical way in which Cl^{38} might be formed by spallation reactions is by emission from the bombarded copper nucleus of nucleons in groups such as alpha-particles instead of single nucleons. The energetic requirements for the reaction $Cu^{63}(p, pn6\alpha)Cl^{38}$, in which the maximum number of alpha-particles are emitted, include (1) the mass difference between the reactants and the products and (2) the excitation energy which the alpha-particles must have in order to pass over the Coulombic barrier. Since the reaction is endoergic with respect to atomic masses, about 50 Mev must be supplied by the impinging proton to make up the mass difference. If the alpha-particles are considered as coming out consecutively, a value of about 50 Mev can be obtained for the Coulombic requirement and thus the threshold for this spallation reaction is roughly 100 Mev.

The production of Cl^{38} was definitely observed at proton bombardment energies beginning at about 60 to 70 Mev with a cross section of some 10^{-32} cm² which increased smoothly with energy to about 10^{-31} cm² at 100 Mev. The identification was made in all cases through chemical separation, measurement of half-life with a Geiger counter and observation of the sign of the beta-particles with a simple beta-ray spectrometer. The possibility that the observed activity might be due to impurities in the copper was eliminated through analysis by radioactivation methods for all possible impurities which might account for the observed yield of Cl^{38}. In order to explain the low threshold it must be assumed that substantially larger particles than alpha-particles are emitted and the reactions are therefore of a type which might more properly be termed fission. As an example, the extreme reaction $Cu^{63}+p\rightarrow Cl^{38}+Al^{25}+n$, which is energetically most economical but still endoergic, has a threshold of about 50 Mev as calculated by adding the amount of energy necessary to make up the mass difference to the excitation energy required for the potential barrier assuming that the fragments are spherical and tangent at the nuclear radii (taken as $1.48\times10^{-13}A^{\frac{1}{3}}$ cm). This calculated threshold is admittedly very rough, but illustrates that the threshold for this type of reaction is definitely lower than for the above described spallation reaction. The cross section is calculated on the basis of the single isotope observed and does not correspond to a total fission cross section, in the sense that the term is ordinarily used, where the yield of all the fission products is summed.

This result made it seem worth while to investigate other elements in the middle portion of the periodic system in order to see whether analogous reactions might occur as a general rule. Bromine was bombarded and the variation with energy of the yield of radioactive Sc^{44} (3.9 hr. isomer) was studied. The threshold for the reaction $Br^{79}(p, p7n7\alpha)Sc^{44}$ is about 180 Mev and that for $Br^{79}+p\rightarrow Sc^{44}+P^{34}+2n$ is about 80 Mev calculated as above. The Sc^{44} was observed with proton energies of 125 and 140 Mev with cross sections of about 10^{-32} cm², with the value at the higher energy several times that at the lower energy, and the yield was too small to measure at 70 Mev. Special purity ammonium bromide was synthesized and used in all bombardments.

The comparable reactions for silver, $Ag^{107}(p, p6n10\alpha)Co^{61}$ and $Ag^{107}+p\rightarrow Co^{61}+Sc^{45}+2n$, have calculated thresholds of about 210 and 60 Mev, respectively. In this case the fission reaction is exoergic by about ten Mev. The isotope Co^{61} (1.8 hours) was observed at an energy of 180 Mev with an approximate cross section of 10^{-32} cm² based on elemental silver, but the results must be termed borderline due to the difficulty in resolving the Co^{61} due to the silver from that formed by a small amount of copper impurity. Radioactivation methods were used to determine the amount of copper present. Unfortunately, the yield of Co^{61} from the copper impurity was about as much as that from the silver itself.

The formation of gallium isotopes from tin bombardment was also studied, and isolation of the gallium fraction showed the characteristic activities of Ga^{66} (about nine hours) and Ga^{72} (about 14 hours). The calculated threshold for $Sn^{118}(p, 7n10\alpha)Ga^{72}$ is about 230 Mev and that for the reaction $Sn^{118}+p\rightarrow Ga^{72}+Ca^{45}+2n$ is about 70 Mev; the fission reaction is exoergic by about ten Mev. The Ga^{66} and Ga^{72} were observed at energies of 150 and 180 Mev with cross sections based on elemental tin of about 10^{-32} cm² and with the values at the higher several times those at the lower energy; the yield at 100 Mev was too small to identify and no yield was detectable at 80 Mev.

Apparently, when the energy threshold requirements are met, large fragments are emitted among the competitive products of nuclear reactions throughout the entire range of atomic numbers of the elements. This is certainly not surprising and the measured yields reported here seem to be quite reasonable. It seems certain that the size of the fragments varies continuously from those (neutrons, protons, deuterons, alpha-particles, etc.) which accompany what we for convenience call spallation reactions, through intermediate sizes (for example,[2,3] Li^8, etc.), and on up to sizes such that the nucleus is split essentially into several pieces of comparable weight. Apparently a number of reactions in which there occurs the latter type of nuclear splitting have been observed in the present investigation and perhaps the term "fission" is as proper a name as any to apply to this process.

It should be emphasized again that the above cross sections are calculated on the basis of the single isotope observed and do not represent the total fission cross sections for the given elements in the sense that this term is ordinarily used. It should also be pointed out that the number of cases in which similar reactions can be studied at present is very limited due to the strict requirements on purity of the bombarded substance, the high factor of radioactive purification necessary, and the sensitivity needed in detecting the product isotope.

The bombardments were carried out on the 184-in. cyclotron, and the required energy was obtained by adjusting the distance of the target from the periphery of the tank. We wish to thank Mr. James T. Vale and the group operating the 184-in. cyclotron for the irradiations performed in the course of these studies.

* This work was performed under the auspices of the AEC.
[1] Perlman, Goeckermann, Templeton, and Howland, Phys. Rev. **72**, 352 (1947).
[2] S. Wright, Phys. Rev. **77**, 742(A) (1950).
[3] L. Marquez and I. Perlman, unpublished work (1950).

On the Nature of *V*-Centers in the Alkali Halides

FREDERICK SEITZ
Department of Physics, University of Illinois, Urbana, Illinois
June 5, 1950

ALEXANDER and Schneider[1] and Casler, Pringsheim and Yuster[2] have examined the production and bleaching of *V*-centers in alkali halide crystals darkened by x-rays and electron bombardment. The first investigators, studying NaCl, KCl and KBr, have found the following properties. (1) The number of *V*-centers is equal to the number of *F*-centers. (2) Irradiation with light in the *F*-band decreases the intensity of this band and also decreases the intensity of the *V*-band. (3) Irradiation in the *V*-band bleaches this band, but does not lead to any permanent removal, as is true at least in part for irradiation in the *F*-band, for the *V*-band returns to its original form in several days. (4) Light absorbed in the *F*-band is strongly effective in producing permanent bleaching if the crystal is irradiated either simultaneously or previously with light in the *V*-band, the total number of *F*-centers destroyed permanently in this efficient manner being equal to the number of *V*-centers which have been altered by irradiation in the *V*-band. (5) The *F*-band can be bleached with a strong electrostatic field during irradiation with light in the *F*-band, the centers wandering out of the crystal; however the *V*-centers cannot be removed in the same way.

The results of Casler, Pringsheim and Yuster on KCl and KBr differ from that of the previous work in the following important respects. (1) The *V*-band is somewhat weaker than the *F*-band; (2) when formed at room temperature, it is composed of two component bands (termed V_2 and V_3) which differ in relative intensity under different conditions of irradiation; (3) observations at liquid nitrogen temperature show that a new band (termed V_1) appears, having a peak at 3550A and 4100A in KCl and KBr, respectively. This may be bleached, along with part of the *F*-band, by irradiating with light in the V_1 band, or by warming. The V_2 band, which lies between V_1 and V_3, bleaches relatively slowly when the crystal is irradiated with light in the *F*-band, whereas V_3 is very difficult to bleach.

Alexander and Schneider have proposed an explanation of their results on the basis of a model suggested by the writer,[3] according to which the *V*-center formed at room temperature is represented by a hole trapped at an isolated positive-ion vacancy, which is the inverse of an *F*-center. They suggest that irradiation in the *V*-band frees a hole, and propose further that the hole possesses an exceedingly low mobility.

The writer would like to suggest an alternative explanation of the state of affairs, namely that the *V*-band as normally observed at room temperature arises from two centers which are composed of two positive ion vacancies to which one or two holes are attached respectively. Tentatively, these will be associated with the V_2 and V_3 bands of the Argonne group. Thus, the *V*-centers are the analog of the *R*-centers which are produced when *F*-centers are irradiated in such a way as to stimulate coagulation. This viewpoint is in accordance with the following facts.

(1) Mollwo[4] has found that the total number of *V*-centers formed in KBr and KI by additive means is proportional to the *first power* of the pressure of *diatomic* halogen molecules in the vapor.

(2) The positive ion vacancies are very mobile having a jump frequency of the order of unity or greater in KCl and NaCl at room temperature. As a result they may be expected to form the analog of the *R*-centers with ease at room temperature. In fact such centers will be the rule rather than the exception.

(3) It is reasonable to expect the first excited electronic level of a "diatomic" center either to join or cross the lowest electronic level for appropriate values of the configurational coordinates so that a hole is not automatically freed when the *V*-centers are excited. We may anticipate metastable states in which the excited hole is attached to the center. If we postulate that such states are formed when the *V*-band is bleached by irradiation in the *V*-band, it is unnecessary to assume that the hole has a very low mobility when free. In fact the experimental results of Mollwo on the electronic conductivity of KBr and KI containing excess halogen at elevated temperatures, which give experimental values of the product of the fraction of *V*-centers ionized and the mobility of holes (Figs. 10 and 11, reference 4), show, when extrapolated to infinite temperature where the fraction of ionized centers should be unity, that the mobility of holes is probably of the order of 1.0 cm²/volt-sec. This is a respectable value and about what one would anticipate from the theoretical calculations of the width of the filled band in the alkali halides.

(4) We might expect an activation energy to be required for capture of a free electron by the *V*-centers when in the ground state, particularly in the case of V_3 which is analogous to a halogen molecule, because the nuclear coordinates will have values different from those for an ionic state. As a result bleaching by irradiation in the *F*-band, which produces free electrons, is difficult.

According to this model, *V*-centers cannot be removed by a combination of irradiation with light in the *V*-band and a strong electrostatic field because *V*-centers do not become ionized when irradiated with light in the *V*-band. There do not appear to be experiments available concerning the presence or absence of photo-conductivity when a crystal containing *V*-centers is irradiated in the *V*-band. The picture presented here suggests that such photo-conductivity should be absent because the holes are not made free.

The observations on the bleaching of *V*- and *F*-bands can be explained in terms of this model in the following way.

(1) Irradiation in at least one of the *V*-bands (such as V_2) produces a metastable state in which the electronic configuration is associated with the first excited electronic level, which has crossed the ground state, much like the case which the writer[5] has proposed to explain the absence of luminenscence when the alkali halides are irradiated in the fundamental absorption band. The metastable state decays to the ground state in the course of several days.

(2) The configurational coordinates of the nuclei associated with at least one of the *V*-centers in its normol state (such as the V_3 center) are such that the holes cannot be annihilated by free electrons. On the other hand, the configurational coordinates associated with the metastable *V*-center, obtained by exciting the latter with light in the *V*-band, are such that the holes can be annihilated with free electrons.

(3) It is likely that the original *V*-center proposed by the writer occurs during irradiation at low temperatures and is responsible for the band observed at 3550A in KCl by the Argonne group. This center may be sufficiently mobile at room temperature that it vanishes by migration and combination.

The writer is indebted to Professor Pringsheim and Drs. Casler and Yuster for detailed discussions of their work.

[1] J. Alexander and E. E. Schneider, Nature **164**, 653 (1949).
[2] R. Casler, P. Pringsheim and P. Yuster, Quarterly Reports of Argonne National Laboratory, 1949. J. Chem. Phys. (to be published).
[3] F. Seitz, Rev. Mod. Phys. **18**, 384 (1946).
[4] E. Mollwo, Ann. d. Physik **29**, 394 (1937).
[5] F. Seitz, Trans. Faraday Soc. **35**, 74 (1939).

A Note on the Vapor Pressure of He^3, He^4 Solutions

JOHN E. KILPATRICK
Department of Chemistry, The Rice Institute, Houston, Texas
May 22, 1950

RECENTLY Gorter[1] has applied the concept of minimum free energy at equilibrium to the Tisza two fluid model of He^4. De Boer[2] and Gorter and De Boer[3] have extended this treatment to cover solutions of He^4 and He^3. The above authors have treated He^4, He^3 solutions on two bases, (1) that the equilibrium fraction of the He^4 in the normal state (y_s) is an internal property of He^4 and is independent of the mole fraction of He^3 (X), and (2) that

TABLE I. Data used in the calculations.

T°K	p_4^0 mm	p_3^0 mm	B_4 cc	B_3 cc
2.4	62.59	291	−136	− 98
2.3	50.19	254	−143	−102
2.2	39.55	213	−150	−106
2.1	30.85	181	−158	−111
2.0	23.38	150	−168	−116
1.9	17.25	125	−178	−121

TABLE II. Partial vapor pressures of He^3, He^4 solutions.

	Real gas			Ideal gas		
T°K	p_4	p_3	Z/X	p_4	p_3	Z/X
2.4	62.08	2.51	3.89	61.96	2.91	4.49
2.3	49.78	2.20	4.23	49.69	2.54	4.86
2.2	39.22	1.87	4.55	39.15	2.13	5.16
2.1	30.61	1.86	5.73	30.55	2.11	6.46
2.0	23.22	2.02	8.08	23.16	2.27	8.93
1.9	17.15	2.22	11.46	17.09	2.48	12.67

for a given composition of the liquid phase (He^3 mole fraction X) the mole fraction of the He^4 in the normal state adjusts itself to such a value ($\bar{y}_e$) that the free energy of the whole system is a minimum. The latter assumption seems the more reasonable to the writer and will be used here.

Gorter and De Boer[3] give equations for the partial pressures of He^3 and He^4 in equilibrium with a liquid solution. In this treatment they have used the vapor pressure of pure He^4 as a measure of the free energy of the liquid but have not included a correction for the gas imperfection of the vapor. This correction makes a considerable difference and must be included for consistency since the Keesom 1937 He^4 vapor pressure scale[4] below the lambda-point is consistent with the observed sixth-power variation of heat capacity with temperature and with the Sackur-Tetrode equation for the free energy of a monatomic gas including De Boer's[5] values for the second virial coefficient of He^4. This point is clearly shown by a plot of $\mu_{4v}^0(p_4^0, T)$, calculated statistically, both with and without the gas imperfection correction ($\mu_{\text{real}} - \mu_{\text{ideal, M.B.}} = p_4^0 B_4$), against T^7. Both plots are essentially straight lines but the latter has a slope corresponding to $S_\lambda = 0.55R$ while the former gives $S_\lambda = 0.80R$, the experimental value.

The second virial coefficient of a gaseous solution of He^3 and He^4 should be given by

$$B = N_3^2 B_3 + 2N_3 N_4 B_{34} + N_4^2 B_4,$$

where N_3 and N_4 are mole fractions, B_3 and B_4 the second virial coefficients of pure He^3 and He^4, and B_{34} the cross second virial coefficient. B_{34} should be calculated in the same way that De Boer and Michels[5] calculated B_4 but with the B.E. or F.D. term omitted, with all l-values allowed, and with the He^3, He^4 reduced mass. It should be intermediate between B_3 and B_4.

Lewis and Randall[6] propose that the ratio of the fugacity to the partial pressure of a component of a gaseous solution be taken to be the same as for that component pure, at the same temperature and total pressure. This is equivalent to assuming $B_{34} = \frac{1}{2}(B_3 + B_4)$. Lacking any direct knowledge of B_{34}, we will use that assumption here.

The chemical potentials of He^3 and He^4, vapor and liquid, can be shown to be in the form

$$\mu_{3v} = \mu_{3v}^0(T, P) + RT \ln Z, \quad (1)$$

$$\mu_3 = \mu_3^0(T) + RT \ln X_e, \quad (2)$$

$$\mu_{4v} = \mu_{4v}^0(T, P) + RT \ln(1-Z), \quad (3)$$

$$\mu_4 = \mu_4^0(T, y) + yRT \ln(1-X_e), \quad (4)$$

where ^{0} means pure component, $Z = p_3/P$, P is the total vapor pressure, $X_e = X/[X + y(1-X)]$, and y is the fraction of He^4 in the normal state. The chemical potential of pure liquid He^4 (below the lambda-point) can be taken in the form[1]

$$\mu_4^0(T, y) = E_0 - yTS_\lambda + (\sigma/\sigma+1) T_\lambda S_\lambda y^{(\sigma+1)/\sigma}. \quad (5)$$

We take $\sigma = 6$ and ignore the small effect of pressure on the entropy and free energy of the liquid. With this expression for μ_4^0 we have the equation for the equilibrium $\bar{y}_e$ at a He^3 concentration X:

$$\ln(1-X_e) + (S_\lambda/R)(\bar{y}_e^{1/6} y_e^{-1/6} - 1) = 0, \quad (6)$$

where $X_e = X/[X + \bar{y}_e(1-X)]$ and $y_e = (T/T_\lambda)$.[6]

Equations can now be written showing the equality of chemical potentials between liquid and vapor phases for He^4:

$$W + RT \ln p_4 + B_4 P = E_0 - \bar{y}_e TS_\lambda + (6/7) T_\lambda S_\lambda \bar{y}_e^{7/6} + \bar{y}_e RT \ln(1-X_e) \quad (7)$$

$$W + RT \ln p_4^0 + B_4 p_4^0 = E_0 - (1/7) y_e TS_\lambda \quad (8)$$

$$W = RT[7.282 - 3/2 \ln M_4 - 5/2 \ln T]. \quad (9)$$

We have then for He^4 (and the corresponding equation for He^3):

$$RT \ln p_4/p_4^0 + B_4(P - p_4^0) = \bar{y}_e RT \ln(1-X_e) + (6/7) T_\lambda S_\lambda \bar{y}_e^{7/6} - \bar{y}_e TS_\lambda + (1/7) y_e TS_\lambda \quad (10)$$

$$RT \ln p_3/p_3^0 + B_3(P - p_3^0) = RT \ln X_e. \quad (11)$$

These equations hold for $T \leqslant T_{\lambda x}$. For $T \geqslant T_\lambda$ the last three terms of Eq. (10) are dropped. For the case $X = 0.01$ ($T_{\lambda x} = 2.159$°K) we have obtained numerical solutions at several temperatures. The data used are shown in Table I and the results in Table II.

The values of p_4^0 are from Keesom,[4] p_3^0 from Sydoriak, Grilly, and Hammel[7] B_4 and B_3 from de Boer[5,8] as read from a smooth graph of $B_4 T^{3/2}$ and $B_3 T^{3/2}$ against T.

The Gorter-Taconis-de Boer theory shows very definitely a sharp rise in the relative concentration of He^3 in the vapor as compared with the liquid as the temperature is decreased below the lambda-point of the solution. The effect of gas imperfection is to decrease p_3 and Z/X by a considerable amount and to slightly increase p_4. An interesting minimum in p_3 occurs at about $T_{\lambda x} = 2.159$°K.

[1] C. J. Gorter, Physica **15**, 523 (1949).
[2] J. De Boer, Phys. Rev. **72**, 852 (1949).
[3] C. J. Gorter and J. de Boer, Phys. Rev. **77**, 569 (1950).
[4] W. H. Keesom, *Helium* (Elsevier Publishing Company, Inc., New York, 1942), p. 196.
[5] J. De Boer and A. Michels, Physica **6**, 409 (1939).
[6] G. N. Lewis and M. Randall, *Thermodynamics* (McGraw-Hill Book Company, Inc., New York, 1923), p. 226.
[7] Sydoriak, Grilly, and Hammel, Phys. Rev. **75**, 303 (1949).
[8] Van Kranendonk, Compaan, and de Boer, Phys. Rev. **76**, 1728 (1949).

The Isotopes of Americium*

K. STREET, JR., A. GHIORSO, AND G. T. SEABORG
Radiation Laboratory and Department of Chemistry, University of California, Berkeley, California

June 12, 1950

INTERMITTENT investigation of the isotopes of americium during the past two years has resulted in the production of three new americium activities and has also yielded some additional information about previously[1] reported activities. Since the work on americium is still in progress, this letter will give only a brief report of the new results obtained and a detailed description of the experiments will be deferred until a later date.

$Am^{238?}$.—Bombardment of Pu^{239} with 50-Mev deuterons in the 184-in. cyclotron results in the production of a new americium activity of *ca.* 1.2 hours half-life in addition to the previously reported 12- and 50-hour activities.[1] Differential counting with beryllium and lead absorbers indicates that the decay is accompanied by the emission of conversion electrons and x-rays. The same activity is produced in good yield with 17-Mev deuterons in the 60-in. cyclotron, thus its mass number is probably greater than 237, since there is good evidence[2,3] that even with the heavy elements the yield of the $(d, 4n)$ reaction is very small at 17 Mev. In view of its half-life, radiation characteristics, and method of formation, this activity is probably an orbital electron capturing isotope and is best assigned to Am^{238}.

Am^{239}.—The 12-hour orbital electron capturing Am^{239} has been previously reported to decay by alpha-particle emission of unknown energy to the extent of *ca.* 0.1 percent.[1] A re-determination of the alpha-branching ratio yielded the better value *ca.* 0.01 percent. The energy of the alpha-particle has been determined by means of a multichannel pulse analyzer to be 5.77 ± 0.05 Mev.

Am^{240}.—The 50-hour electron capturing americium activity was tentatively assigned[1] to Am^{240}. This assignment has been confirmed. The 50-hour activity is produced in good yield from the bombardment of Pu^{239} with 10-Mev deuterons and is not observed in the bombardment of Pu^{239} with 9-Mev protons (60-in. cyclotron) in which Am^{239} is produced in good yield. Since the yield of the $(d, 3n)$ reaction is low at 10 Mev and since (p, n) should be the principal reaction producing americium with 9-Mev protons, the 50-hour activity is best assigned to Am^{240}. No alpha-particles associated with the 50-hour americium have been observed. This is consistent with its assignment to Am^{240} since the systematics of alpha-radioactivity[4] predict for this odd-odd nucleus a partial half-life for alpha-decay of some 10^3 years.

Am^{241}.—The production of this isotope in milligram amounts by the neutron irradiation of plutonium[5] makes it possible to study the higher mass isotopes of americium produced by (n, γ) reactions and the results of such experiments are reported in the following paragraphs. Recent specific activity measurements by Cunningham, Thompson, and Lohr[6] give a somewhat shorter half-life for Am^{241} than that previously reported.[7] The new half-life is 475 years.

Am^{242}.—In addition to the 16-hour Am^{242m}, a long-lived Am^{242} produced by the (n, γ) reaction on Am^{241} has been reported;[1] alpha-decay of this isotope was demonstrated by separating the Np^{238} daughter and 0.5-Mev beta-particles in the americium fraction were also ascribed to Am^{242}. The fact that the observed beta-particles do belong to Am^{242} has now been demonstrated by observing the growth of Cm^{242} (half-life 162 days) in the purified pile neutron-bombarded americium in an amount corresponding to the number of beta-particles observed. Mass spectrographic analysis of this americium shows Am^{242} to be present to the extent of *ca.* 0.5 percent. This analysis together with the results from the above Cm^{242} growth experiment and the yield from a Np^{238} extraction allow both the alpha- and beta-decay half-lives of Am^{242} to be estimated. The partial half-life obtained for beta-particle emission is roughly 10^2 years and that for alpha-particle emission is *ca.* 10^4 years. O'Kelley, Crane, Barton, and Perlman,[8] using the beta-ray spectrometer in this laboratory, have determined the beta-particle energies of Am^{242} and Am^{242m} to be 0.575 ± 0.010 and 0.630 ± 0.005 Mev, respectively. The (n, γ) cross section for the formation of Am^{242} is very roughly 10^{-22} cm² but this may be off by a factor of several due to the many uncertainties involved, especially the neutron flux.

Am^{243}.—Neptunium separations from the americium fraction of an irradiation of Am^{241} with pile neutrons show the presence of equilibrium amounts of both Np^{238} and Np^{239}. The presence of Np^{239} proves the existence of the new isotope Am^{243} which is produced by two successive neutron capture processes in Am^{241} and decays by alpha-particle emission to Np^{239}. Mass spectrographic analysis of the americium of this bombardment showed Am^{243} present to the extent of *ca.* 0.5 percent. This together with the yield of Np^{239} determined in the chemical extraction experiments gives a partial half-life for alpha-particle emission for Am^{243} of roughly 10^4 years. Alpha-particle pulse analysis of americium from another irradiation (containing approximately ten percent Am^{243}) showed the alpha-particle energy to be 5.21 ± 0.03 Mev. This energy and half-life indicate that alpha-emission in this odd-even nucleus is not prohibited,[4] but like the case of the analogous nucleus Am^{241}, the measured alpha-particle energy may not represent the ground state transition. If one takes 5.89 Mev for the alpha-particle energy[9] of the ground state transition of Cm^{243} and closes a decay cycle using the measured alpha-particle energy of Am^{243} and 0.68 Mev for the beta-decay disintegration energy[10] of Np^{239}, one finds that Cm^{243} could be unstable with respect to electron capture by *ca.* 0.01 Mev. However, due to the uncertainties in the above energies (especially Np^{239}) it is entirely possible that Am^{243} is not beta-stable; the alpha-particle energy of Cm^{243} is also very uncertain and it is not known whether it corresponds to the ground state transition. In order to test this point curium was separated from an aged sample containing Am^{243} and no detectable Cm^{243} was found; this experiment places a lower limit of about 10^3 years on the partial half-life of Am^{243} for negative beta-emission. The cross section for the reaction $Am^{243}(n, \gamma)Am^{244}$ seems to be large, of the order of some 4×10^{-21} cm², a value which is subject to large error because of the uncertainty in the neutron flux.

Am^{244}?.—Irradiation of americium containing approximately ten percent of the isotope Am^{243} with thermal neutrons in the uranium-heavy water pile at the Argonne Laboratory produced a new americium activity of *ca.* 25-min. half-life at a yield corresponding to a cross section of roughly $\frac{1}{2}\times10^{-22}$ cm². This activity is probably caused by the beta-emitting isotope Am^{244}, formed by an (n, γ) reaction.

We would like to thank R. A. James and S. G. Thompson for their assistance in many of the experiments, and F. L. Reynolds for the mass spectrographic analysis of the americium samples. It is a pleasure to thank T. M. Putnam, Jr., G. B. Rossi, J. T. Vale, and the crews of the 60-in. and 184-in. cyclotrons for their cooperation in the bombardments with these machines, and also W. H. Zinn and the operating group of the Argonne Laboratory pile for their cooperation and help in neutron irradiation experiments.

* This work was performed under the auspices of the AEC.

[1] Seaborg, James, and Morgan, National Nuclear Energy Series, Plutonium Project Record, Vol. 14B, *The Transuranium Elements: Research Papers*, Paper 22.2 (McGraw-Hill Book Company, Inc., New York, 1949).
[2] James, Florin, Hopkins, and Ghiorso, National Nuclear Energy Series, Plutonium Project Record, Vol. 14B, *The Transuranium Elements: Research Papers*, Paper No. 22.8 (McGraw-Hill Book Company, Inc., New York, 1949).
[3] Magnusson, Thompson, and Seaborg, Phys. Rev. **78**, 363 (1950).
[4] Perlman, Ghiorso, and Seaborg, Phys. Rev. **77**, 26 (1950).
[5] Ghiorso, James, Morgan, and Seaborg, Phys. Rev. **78**, 472 (1950).
[6] Cunningham, Thompson, and Lohr, unpublished work (1949).
[7] B. B. Cunningham, National Nuclear Energy Series, Plutonium Project Record, Vol. 14B, *The Transuranium Elements: Research Papers*, Paper No. 19.2 (McGraw-Hill Book Company, Inc., New York, 1949).
[8] O'Kelley, Crane, Barton, and Perlman, unpublished work (1950).
[9] Thompson, Ghiorso, and Seaborg (to be published).
[10] G. T. Seaborg and I. Perlman, Rev. Mod. Phys. **20**, 585 (1948).

The Low Terms of Ti II

ABRAHAM MANY
Department of Physics, The Hebrew University, Jerusalem, Israel
May 29, 1950

THE Ti II spectrum has as its lowest levels a pair of terms of the same multiplicity and name, 860 cm^{-1} apart. These terms are a^4F and b^4F, one of which arises from the configuration $3d^24s$ and the other from $3d^3$. As they are very close together it is difficult to be sure which is which. Russell[1] concluded from the intensities of the combinations that a^4F arose from $3d^24s$, and b^4F from $3d^3$. From theoretical calculations of the low even terms the writer[2] proposed that the assignments should be interchanged. In a later paper[3] Russell concluded from considerations of the series limits of the higher even terms of Ti I that his original assignments were correct.

We thought it desirable to find a further criterion which would indicate the correct assignments independently of the position of the two terms. Using the formulas for the spin-orbit interaction integrals,[4] we calculated ζ_d from the intervals of the terms arising from $3d^24s$ and $3d^3$. We excluded the terms $3d^3a^2P$ and $3d^3a^4P$ as these terms are closed together and consequently the departure from (LS) coupling is considerable. Table I gives the calculated values of ζ_d. Excluding the ζ_d values of the two ^4F terms, it is seen that the mean value of ζ_d for $3d^24s$ is 113 and that for $3d^3$ is 91. By comparing these values with the values of ζ_d calculated

TABLE I. Calculated values of ζ_d from the multiplets of $3d^24s$ and $3d^3$.

	Term	ζ_d
	$a^4F_{3/2,5/2}$	112.73
	$a^4F_{5/2,7/2}$	112.74
	$a^4F_{7/2,9/2}$	111.83
	$b^4F_{3/2,5/2}$	91.01
	$b^4F_{5/2,7/2}$	88.64
	$b^4F_{7/2,9/2}$	85.58
$3d^24s$	a^2F	115.28
$3d^3$	a^2G	89.23
$3d^24s$	$b^4P_{1/2,3/2}$	115.74
	$b^4P_{3/2,5/2}$	112.80
$3d^3$	b^2D	82.15
$3d^3$	a^2H	88.93
$3d^24s$	b^2P	109.46
$3d^3$	b^2F	102.67

from the two ^4F terms we conclude that a^4F should be assigned to $3d^24s$ and b^4F to $3d^3$, in agreement with Russell's original assignments.

It is interesting to note that the levels of a^4F obey quite accurately Landè's interval rule, while those of b^4F deviate slightly from this rule. In order to see whether second-order effects can explain these deviations, the spin-orbit interactions were taken into account. By assuming that b^4F arises from $3d^3$, we found that the second-order effects brought about an improvement in the agreement with the interval rule, while by assuming that b^4F arises from $3d^24s$, the agreement becomes worse. This again verifies Russell's original assignments.

I am grateful to Professor G. Racah for suggesting the approach to the problem discussed in this paper.

[1] H. N. Russell, Astrophys. J. 66, 283 (1927).
[2] A. Many, Phys. Rev. 70, 511 (1946).
[3] H. N. Russell, Phys. Rev. 74, 689 (1948).
[4] E. U. Condon and G. H. Shortley, *Theory of Atomic Spectra* (Cambridge University Press, New York, 1935), Chapter 57; H. H. Marvin, Phys. Rev. 47, 521 (1935).

Remarks on the Variational Method for Scattering Problems

L. HULTHÉN AND P. O. OLSSON
Royal Institute of Technology, Stockholm, Sweden
May 31, 1950

IN a recent note[1] Huang has made an interesting analysis of the variational principle for continuous spectra.[2] The main point of his method is to replace the equation $\mathfrak{L}=0$ by

$$\partial\mathfrak{L}/\partial\lambda=k.$$

The last equation, involving derivatives of $\mathfrak{L}$ with respect to the phase parameter, is of the first degree in the parameters. By this means a system of solely linear equations is obtained, which greatly simplifies the numerical treatment. At the same time the ambiguity connected with the use of the quadratic equation $\mathfrak{L}=0$ is removed. It may be pointed out however that these inconveniences have been already overcome in a revised version of the principle,[3] which is more closely connected with familiar methods of the variational calculus.

As the condition $\mathfrak{L}=0$ has been given up in Huang's treatment the phase shift is *not stationary*. This may explain the somewhat poor agreement of Huang's numerical phase shifts with the earlier values. On the other hand, the expression $\mathfrak{L}-k\lambda$ is stationary, whence a first-order correction for λ can be obtained from the equation

$$\delta\mathfrak{L}=k\delta\lambda,$$

[see reference 3, Section 4]. For the exact solution we have $\mathfrak{L}=0$, hence $\delta\mathfrak{L}=\mathfrak{L}$ for the approximate solution and

$$\delta\lambda=(\mathfrak{L}/k).$$

Therefore, if λ is the value obtained from Huang's equations, then

$$\lambda_0=\lambda-(\mathfrak{L}/k)$$

TABLE I. Comparison of the procedures of Huang and of Hulthén. The values of the parameters have been recalculated and show good agreement with the values obtained by Huang.* For comparison the last row contains Huang's numerical phase shift values.

$k=0.8,\quad l=-1.5$

	c_1, c_2	c_1, c_3	c_1, c_2, c_3	c_1, c_3, c_4	c_1, c_2, c_3, c_4	Most probable value for η_0 (ref. 2)
c_1	1.13543	0.03493	0.59699	0.05206	0.02261	
c_2	−0.56617	—	−0.28911	—	0.01502	
c_3	—	0.90190	0.44074	0.89689	0.92092	
c_4	—	—	—	−0.06516	−0.06417	
λ	1.11888	1.10430	1.11190	1.11525	1.11469	
$\mathfrak{L}/k$	0.00998	−0.00460	0.00303	0.00623	0.00566	
λ_0	1.10890	1.10890	1.10887	1.10902	1.10903	
η_0	0.83699	0.83699	0.83698	0.83705	0.83705	0.83708
η_H	—	0.83492	0.83832	0.83982	0.83958	

$k=0.8,\quad l=-2.1$

	c_1, c_2	c_1, c_3	c_1, c_2, c_3	c_1, c_3, c_4	c_1, c_2, c_3, c_4	Most probable value for η_0 (ref. 2)
c_1	4.75407	0.52837	4.87421	0.65668	0.61438	
c_2	−2.17329	—	−2.23510	—	0.02157	
c_3	—	3.47191	−0.09840	3.45159	3.48610	
c_4	—	—	—	−0.49604	−0.49462	
λ	3.27890	3.22313	3.28046	3.31117	3.31036	
$\mathfrak{L}/k$	0.00655	−0.05128	0.00811	0.02972	0.02892	
λ_0	3.27235	3.27441	3.27235	3.28144	3.28145	
η_0	1.27422	1.27447	1.27422	1.27499	1.27499	1.27515
η_H	—	1.26996	1.27489	1.27749	1.27742	

* There are some minor divergencies, e.g. c_1, c_2, c_3 and c_1, c_2, c_3, c_4 for $l=-2.1$. However, the corrected phase shifts η_0 are quite insensitive to these variations.

should be a better value. To check this the values λ_0 corresponding to the λ-values obtained by Huang were calculated. For comparison the figures are tabulated in Table I. It is clear that the results thus obtained agree very well with the values of the original paper although trial functions containing powers or polynomials do not seem to be ideal for this problem. Moreover, this manner of correcting the phase shifts involves very little extra work, since the expression for $\mathfrak{L}$ can be shortened considerably by the use of Euler's theorem for homogeneous functions and the equations satisfied by the parameters [see reference 3, p. 9].

We are indebted to Mr. V. Grinvalds and Dr. H. Richter for skilled numerical assistance. Financial support from the Swedish Atomic Energy Committee is gratefully acknowledged.

[1] S. S. Huang, Phys. Rev. 76, 1878 (1949).
[2] L. Hulthén, Kungl. Fysiogr. Sällsk. i Lund Förhandl. 14, No. 21 (1944).
[3] L. Hulthén, Arkiv Mat. Astron. Fysik 35A, No. 25 (1948).

Photo-Fission of Bismuth*

NATHAN SUGARMAN
Institute for Nuclear Studies, University of Chicago, Chicago, Illinois
June 2, 1950

WE report here some features of the fission of bismuth from irradiation at the University of Chicago betatron. The betatron was constructed by the General Electric Company and its constructural and operational features are essentially those of the 100-Mev instrument described by Westendorp and Charlton.[1] The machine was operated at a maximum energy of 85 Mev and the operating intensity was about 600 roentgens per minute, 1 meter from the tungsten target.

The fission of bismuth with high energy *particles* from the 184-in. Berkeley cyclotron has been demonstrated both by radiochemical and physical measurements.[2] The nature of the fission process with 190-Mev deuterons has been studied in detail by Goeckermann and Perlman[3] by radiochemical techniques. They found that the fission products formed are, for the most part, β^--decaying species in the light group, and β^+-decaying or

TABLE I. Photo-fission yields of bismuth.

Fission product	Photo-fission yield, %	Deuteron-fission yield,[d] %	Predicted total mass yield,[d] %
12-hr. Ge^{77}	~0.3	1.5	1.9
40-hr. As^{77}	<0.4		
35-hr. Br^{82}	<0.5	1.0	3.0
2.4-hr. Br^{83}	1.2	1.7	3.2
33-min. Br^{84}	<1.4	—	3.4
9.7-hr. Sr^{91}	2.8[a]	4.4[e]	4.6
2.7-hr. Sr^{92}	2.8[a]	—	4.7
17-hr. Zr^{97}	3.0	—	5.0
4.5-hr. Ru^{105}	5.0[b]	3.1	4.9
13-hr. Pd^{109}	~6.4[c]	4.6	4.6
7.5-day Ag^{111}	~2.8	3.4	4.2
5.3-hr. Ag^{113}	3.0	[f]	4.0
54-min. I^{134}	<0.2	—	0.2
85-min. Ba^{139}	<0.1	—	0.07

[a] Yields of 2.7-hr. Sr^{92} and 9.7-hr. Sr^{91} assumed equal for analysis of complex decay curve.
[b] Assumed yield, other yields normalized to this value.
[c] Uncertain because of contribution of 21-hr. Pd^{113}.
[d] See reference 3.
[e] Measured yield of 57-day Y^{91}.
[f] Not observed because of high independent yield of 3.2-hr. Ag^{112}.

K-electron capture species in the heavy group. The yield-mass curve is symmetric around mass 99 and the maximum fission yield is about 5 percent.

Baldwin and Klaiber[4] studied photo-fission in heavy elements at the 100-Mev betatron at Schenectady, using a balanced ionization chamber and thin sources of uranium, thorium, bismuth, lead, and other elements. No fissions were observed in the elements tested other than uranium and thorium. On the basis of a maximum cross section of 5×10^{-26} cm^2 for the photo-fission of uranium, a maximum value of 10^{-29} cm^2 was set for the cross section for photo-fission of bismuth.

In the present experiments, samples of bismuth nitrate and bismuth metal of about 30 g were irradiated with high energy photons for about 4 hr., about 55 cm from the tungsten target. The samples were dissolved after the irradiation and radiochemical analyses were made for various elements regarded as probable fission products of bismuth. Analyses were made for germanium, arsenic, bromine, strontium, zirconium, ruthenium, palladium, silver, iodine, and barium by standard procedures.[5] The isolated samples contained the radioactivities expected for fission except that no activity of iodine or barium was observed. The counting rates of the products formed in high yield were about 100 c/min., where the chemical yield was about 50 percent and the geometric factor for counting with the standard end-window bell-shaped counter was about 25 percent.

Detailed studies were made in the case of one of the isolated products, 4.5-hr. Ru^{105}, to establish that the observed radioactivity originated in the fission of bismuth and not in the activation of impurities by photons. From irradiations of ruthenium, rhodium, palladium, silver, and cadmium, it was found that either the impurity level of any of these elements had to be many times that known to be present in the bismuth in order to give the observed counting rate, or the ruthenium activity isolated had radioactive properties different from those of 4.5-hr. Ru^{105}.

The results of the measurements are given in Table I, where the fission yields of the species are arbitrarily normalized to a yield of 5 percent for Ru^{105}. For comparison purposes the yield values of Goeckermann and Perlman[3] for fission with 190-Mev deuterons are also given (column 3), as well as their predicted total yield values for the mass numbers (column 4).

Comparison of the photo-yield data with those of 190-Mev deuterons indicates that the yield-mass curve for the photo-fission of bismuth is narrower than that of deuterons and that the primary fission products are probably neutron-excessive and decay by β^--emission. This conclusion is based on the relatively low yield of mass 77 to Ru^{105}, and the presence of 5.3-hr. Ag^{113} in high yield relative to 3.2-hr. Ag^{112} formed independently of its 21-hr. Pd^{113} parent.

The above results show that fission of bismuth occurs at the betatron. However, it still remains to be established definitely that the fission process studied at the betatron is not the result of secondary fast particles. Rough estimates indicate that the fission process is more likely photo-fission, but because of the absence of information on the number and energy of neutrons and protons emitted from bismuth, particle-fission cannot be excluded. In this respect it should be mentioned that the irradiation of bismuth produces bismuth activities in high yield of about the same half-lives as those reported[6] for Bi^{204} and Bi^{206}. This suggests that the emission of several neutrons from bismuth occurs in high probability.

A single experiment was performed on the fission of uranium by photons. Several fission products were isolated including 85-min. Ba^{139}. If a fission yield of 6 percent is taken for Ba^{139}, the integrated cross section under the resonance is about 1×10^{-24} cm^2 Mev, roughly five times that found by Baldwin and Klaiber,[4] and is in better agreement with the Goldhaber-Teller[7] resonance theory. The fission rate per gram of bismuth is about 1/1000 that of uranium.

The author gratefully acknowledges the assistance of Messrs. C. R. McKinney and B. C. Cook of the Betatron Group in these experiments.

* Assisted by the joint program of the ONR and AEC.
[1] W. F. Westendorp and E. E. Charlton, J. App. Phys. 16, 581 (1945).
[2] Perlman, Goeckermann, Templeton, and Howland, Phys. Rev. 72, 352 (1947); E. L. Kelly and C. Wiegand, Phys. Rev. 73, 1135 (1948).
[3] R. H. Goeckermann and I. Perlman, Phys. Rev. 76, 628 (1949).
[4] G. C. Baldwin and G. S. Klaiber, Phys. Rev. 71, 3 (1947).
[5] See papers of Part VI, Vol. 9, Div. IV, National Nuclear Energy Series, McGraw-Hill Book Company, Inc. New York (in preparation).
[6] I. Perlman and G. T. Seaborg, Rev. Mod. Phys. 20, 585 (1948).
[7] M. Goldhaber and E. Teller, Phys. Rev. 74, 1046 (1948).

Polaron States in Ionic Crystals*

HERBERT B. CALLEN
Randal Morgan Laboratory of Physics, University of Pennsylvania, Philadelphia, Pennsylvania
June 2, 1950

A CONDUCTION electron in a polar crystal induces an ionic polarization which, in turn, modifies the electronic wave function. The existence of this effect was first noted by von Hippel and Landau, and the contribution to the energy from this electron-ion interaction has been treated semiclassically by Pekar and by Markham and Seitz. Very recently Fröhlich, Pelzer, and Zienau[1] (F.P.Z.) have given a quantum-mechanical treatment of this energy and have also computed the effective mass of a polaron (electron plus surrounding ionic polarization). Despite the certain reality of the effect, however, no definite experimental observations have been correlated with it, and it would therefore seem desirable to survey the properties of polarons as they relate to experimental observability.

In a polar crystal the longitudinal optical phonons produce regions of positive and negative charge accumulation at alternate nodes. A conduction electron decreases its energy by concentrating its wave function at alternate nodes, thereby also altering the form and energy of the phonon; the net effect being a lowering of each of the states of the conduction band. As F.P.Z. have stressed, the polaron states are the only states in the conduction band; they are not additional states existing below the conduction band. Thus the usual proposal of observation of an infra-red absorption corresponding to optical excitation from polaron to conduction levels must necessarily fail. Furthermore, F.P.Z. have shown that the effective mass of a polaron is essentially equal to that of a conduction electron in a non-polar crystal, so that observations of mobility are not apt to be fruitful.

Consider the thermal excitation of an electron to the conduction band. After the excitation both electron and hole are surrounded by ionic polarization. If E_G is the gap width neglecting the polaron effect, and ΔE_t is the energy shift of an electron due to the polaron effect, the energy required for thermal excitation will thus be approximately $E_G-2\Delta E_t$. But ΔE_t, and hence the effective gap width, will depend upon temperature which is an effect which

may be observable in polar semiconductors. Unfortunately ΔE_t has been computed[1] only at $T=0°$, so that the form of the dependence of the effective gap width on temperature is not known.

The situation seems somewhat more hopeful in the case of optical excitation. The frequency of maximum absorption will be $\hbar\omega=E_G-2\Delta E_0$. It will be noted that the effective energy shift ΔE_0 here differs from ΔE_t, for the energy shift ΔE_t includes a contribution from the alteration of the form of the phonon; but, by the Franck-Condon principle, this contribution is absent in an optical process. Thus ΔE_0 must be computed by finding the change in energy of an electron in the field of a phonon, assuming the phonon states to be unaffected by the presence of the electron. Using the methods employed in the treatment of electrical breakdown in polar crystals,[2] we have computed[3] ΔE_0 as a function of temperature (ω_l is restrahl frequency, ϵ_0 and ϵ_s are optical and static dielectric constants):

$$(\Delta E_0)^3=\frac{me^4\omega_l^2}{2}\left(\frac{\epsilon_s}{\epsilon_0}\right)\left(\frac{1}{\epsilon_0}-\frac{1}{\epsilon_s}\right)^2\left(\exp\frac{\hbar\omega_l\epsilon_s^{\frac{1}{2}}}{kT\epsilon_0^{\frac{1}{2}}}+1\right)^2\left(\exp\frac{\hbar\omega_l\epsilon_s^{\frac{1}{2}}}{kT\epsilon_0^{\frac{1}{2}}}-1\right)^{-2}.$$

It may be hoped that the polaron effect can thus be observed as a dependence of the frequency of maximum absorption ω on T, and it is, in fact, observed that ω decreases with increasing T in polar crystals, but is virtually constant in non-polar crystals. Unfortunately there is a second effect which, in polar crystals, decreases the gap width with increasing temperature. This effect, which has been treated theoretically by Radkowsky,[4] arises from the fact that an electronic state subject to a collision frequency ν_c has a half-width $\frac{1}{2}\hbar\nu_c$, resulting in a decrease in gap width of approximately $\hbar\nu_c$. Recomputing Radkowsky's results in accordance with the methods of reference 2 one obtains

$$2\Delta E=\hbar\nu_c=\frac{2^{\frac{1}{2}}m^{\frac{1}{2}}e^3\omega_l^{\frac{1}{2}}\epsilon_s^{\frac{1}{2}}}{\hbar^{\frac{1}{2}}\epsilon_0^{\frac{1}{2}}}\left(\frac{1}{\epsilon_0}-\frac{1}{\epsilon_s}\right)\left(\exp\frac{\hbar\omega_l\epsilon_s^{\frac{1}{2}}}{kT\epsilon_0^{\frac{1}{2}}}-1\right)^{-1}.$$

These results may be compared with some experimental observations[4] which very likely represent the rate of shift of ω with T:

$(d\hbar\omega/dT)$ in 10^{-4} ev/°K	KI (296°)	KI (766°)	RbBr (360°)	RbBr (766°)
Observed	11.9	9.4	7.4	7.4
Polaron effect	4.4	3.3	5.0	4.0
Radkowsky effect	7.9	8.2	11.2	11.5

It would thus appear that the shift of optical absorption frequency with temperature allows, in principle, an observation of the polaron effect, but that experimental observations and theoretical treatments must be improved before truly quantitative conclusions can be drawn.

* This work was partially supported by the Bureau of Ships, U. S. Navy.

[1] Fröhlich, Pelzer and Zienau, Phil. Mag. **41**, 221 (1950).

[2] H. Callen, Phys. Rev. **76**, 1394 (1949).

[3] We had computed ΔE_0, ΔE_t and the effective mass prior to the appearance of reference 1, using conventional perturbation theory and the methods of reference 2. Our results for ΔE_t and effective mass agree with those of F.P.Z. except insofar as the results of those authors are improved by a novel variation of the perturbation technique. We have therefore recast the calculation of ΔE_0 so as to take advantage of this improvement in the perturbation method.

[4] A. Radkowsky, Phys. Rev. **73**, 749 (1948).

Paramagnetic Resonance and Hyperfine Structure in the Iron Transition Group

A. Abragam
Clarendon Laboratory, Oxford, England
May 23, 1950

In the paramagnetic ions of the iron group, the orbital angular momentum is generally quenched by the crystalline field, which makes the h.f.s. much narrower than in the free ion and thereby considerably increases the perturbing influence on this h.f.s. of excited states, with unpaired *s*-electrons and wide h.f.s.

This fact, and the great precision of paramagnetic resonance methods, make it necessary to know the electronic wave function with greater accuracy than is generally needed in the optical spectroscopy of the free atoms or ions. In fact the h.f.s. of the paramagnetic salts of divalent copper and manganese, calculated by assuming for Cu^{++} and Mn^{++} respectively the electronic configurations $3d^9\ ^2D$ and $3d^5\ ^6S$, suggested by the optical properties of these ions, disagree considerably with experiment.

The interaction between the electrons and the nuclear magnetic moment can be written $H=\mathbf{I}\cdot T\cdot\mathbf{S}$ where $\mathbf{I}$ is the nuclear spin ($\frac{3}{2}$ for Cu, 5/2 for Mn), $\mathbf{S}$ the total electronic spin ($\frac{1}{2}$ for Cu^{++}, 5/2 for Mn^{++}) and T is a tensor representing a generalized anisotopic h.f.s. interval. The principal values of the tensor T are (in 10^{-3} cm^{-1}):

Copper Tutton salts

Exper.[1] $|T_{11}|\simeq|T_{22}|$; $2<|T_{11}|<6$ according to the salt; $|T_{33}|\simeq 13$
Theoret.[2] $T_{11}\simeq T_{22}\simeq 13$; $T_{33}\simeq -6$

Copper fluosilicate

Exper.[3] $|T_{11}|\simeq|T_{22}|=2.1$; $|T_{33}|=2.8$
Theoret.[4] $T_{11}=T_{22}=T_{33}=7$

Manganese Tutton salts and fluosilicate

Exper.[5] $|T_{11}|\simeq|T_{22}|\simeq|T_{33}|\simeq 9$
Theoret. $T_{11}=T_{22}=T_{33}=0$.

These discrepancies can be explained by assuming that the electronic wave functions contain small admixtures of excited states with unpaired *s*-electrons, which are also respectively ^2D and ^6S states.

For Mn^{++} no state ^6S with unpaired 4*s*-electron can be constructed by exciting one or two 3*d*-electrons. For Cu^{++} the first excited state $3d^84s\ ^2D$ gives for T a positive isotropic correction ΔT which further increases the discrepancy.

As a working hypothesis we suggest the promotion of a 3*s*-electron to a 4*s*-orbital giving the excited configurations $3s3p^63d^94s\ ^2D$ and $3s3p^63d^54s\ ^6S$. Energetically these configurations are far above the ground state and their admixture in this state is small, but this is compensated by the fact that 3*s*-electron has a very wide h.f.s. For Mn^{++} the 3*s*-electron gives an isotropic h.f.s. of the right order of magnitude. For Cu^{++} it is possible to make the correction ΔT negative. If we take $\Delta T=-9$ we find the new theoretical values:

Copper Tutton salts

$T_{11}'\simeq T_{22}'\simeq 13-9=4$; $T_{33}'=-6-9=-15$

Copper fluosilicate

$T_{11}'\simeq T_{22}'\simeq T_{33}'=7-9=-2$

which agree reasonably with experiment.

Details of these calculations will be reported elsewhere.

[1] D. J. E. Ingram, Proc. Phys. Soc. London **A62**, 664 (1949).

[2] A. Abragam and M. H. L. Pryce, Nature **163**, 993 (1949).

[3] B. Bleaney and D. J. E. Ingram, Proc. Phys. Soc. London **A63**, 408 (1950).

[4] A. Abragam and M. H. L. Pryce, Proc. Phys. Soc. London **A63**, 409 (1950).

[5] B. Bleaney (to be published).

Properties of Tl^{209}

French Hagemann
Argonne National Laboratory, Chicago, Illinois
March 13, 1950

Previous investigations at this laboratory[1] of the decay products of U^{233} showed that Bi^{213} undergoes branching disintegrations, 98 percent decaying by beta-emission and two percent by alpha-emission. Canadian workers[2] who carried out parallel but independent studies also detected such alpha-branching. The product of alpha-disintegration of Bi^{213} would be Tl^{209} (neptunium C″) which, by analogy with the C″ products of the natural radioactive series, should be a beta-emitter with a half-life of only a few minutes. The amount of thallium activity formed by

decay of the milligram amounts of U^{233} used in the earlier investigations was too low to permit detection. However, gram quantities of U^{233} have since become available and with this larger amount of source material it has been possible to observe directly the Tl^{209} beta-particles.

The thallium was isolated by ether extraction from a solution of Ac^{225} obtained from a stock of U^{233} which had decayed for one year. The Ac^{225} was separated from the uranium by co-precipitation with lanthanum fluoride and was thoroughly purified by a procedure involving extraction of the Ac^{225} with a benzene solution of thenoyltrifluoracetone to separate from radium and thorium isotopes,[3] followed by addition of lead carrier and precipitation of lead sulfide to remove any extraneous lead, bismuth, or polonium activities.

Because of the short half-life of the thallium a method of rapid separation was necessary. The following procedure proved satisfactory. Ten milligrams of inactive thallium carrier and a small amount of bromine were added to 2 ml of 6*N* HCl containing the Ac^{225}. The solution was heated to oxidize the thallium to the extractable +3 state and the excess bromine boiled out. The solution was cooled, 2 ml of ether added and the mixture stirred for 30 sec. The ether phase was transferred to another vessel and stirred for several seconds with an equal volume of ether-saturated 6*N* HCl. After separation of the phases, the acid layer was drained through a stopcock and the washing repeated two or three times with fresh portions of acid. After the final wash the ether was transferred to a platinum dish and ignited. When the ether was consumed the platinum dish was rapidly cooled and placed immediately in the counter. The total time elapsed from start of the separation to start of counting was three to five minutes.

Decay of the thallium activity, which amounted to several thousand counts per minute initially, was followed at half-minute intervals. A small amount of long-lived activity, 20 to 30 counts/min. above the natural background, which remained after decay of the thallium was probably due to incomplete chemical separation. A typical decay curve is shown in Fig. 1. The half-life as determined by least-squares analysis of seven such decay curves was 2.20 min., with a probable error of ±0.07 min.

An aluminum absorption curve of the Tl^{209} beta-particles (Fig. 2) was obtained by isolating a series of samples and following the decay of each alternately with and without a given absorber. Each sample thus yielded one point on the absorption curve which was the ratio of the extrapolated counting rate at zero time with absorber to that without absorber. A Feather analysis[4] of the absorption curve, after subtraction of the hard component, gave a value of about 825 mg of aluminum for the range, corresponding to a maximum energy of 1.8 Mev. The half-thickness was about 80 mg Al/cm².

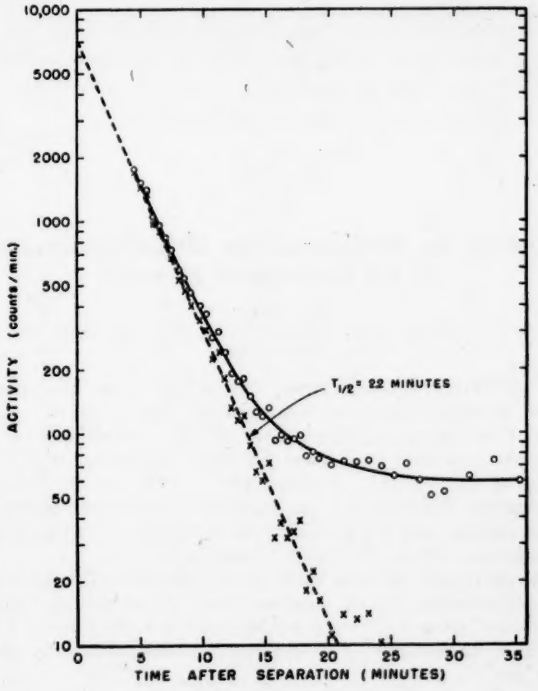

FIG. 1. Decay of Tl^{209}.

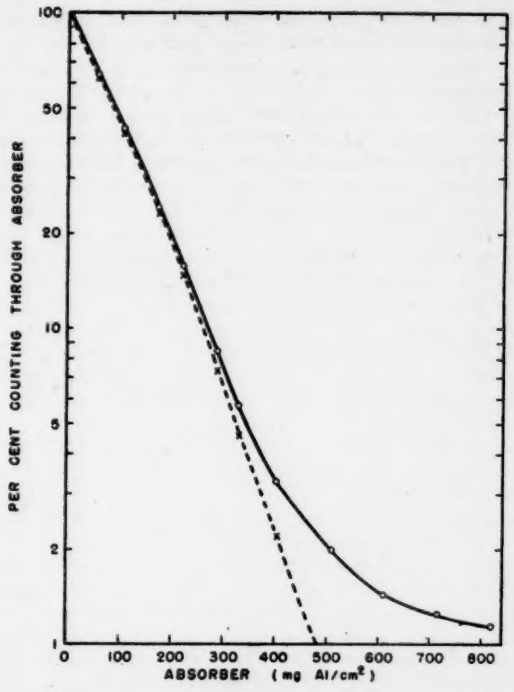

FIG. 2. Absorption of Tl^{209} beta-particles in aluminum. Feather range, ~825 mg Al/cm² corresponding to E_{max} = 1.8. Half-thickness ~80 mg Al/cm².

[1] Hagemann, Katzin, Studier, Seaborg, and Ghiorso, Phys. Rev. **72**, 252 (1947); Phys. Rev. **79**, 435 (1950), this issue.
[2] English, Cranshaw, Demers, Harvey, Hincks, Jelley, and May, Phys. Rev. **72**, 253 (1947).
[3] F. Hagemann, J. Am. Chem. Soc. **72**, 768 (1950).
[4] N. Feather, Proc. Camb. Phil. Soc. **34**, 599 (1938); L. E. Glendenin, Nucleonics **2**, 12 (1948).

Resistivity of Semiconductors Containing Both Acceptors and Donors*

C. S. HUNG AND V. A. JOHNSON
Purdue University, Lafayette, Indiana
June 8, 1950

THE resistivity of impurity semiconductors has previously been explained[1] by the addition of ρ_L, resistivity caused by scattering by lattice ions, and ρ_I, resistivity due to scattering by impurity ions. Since the mean free path associated with lattice scattering[2] is inversely proportional to temperature,

$$\rho = AT^{3/2}/n, \tag{1}$$

where A is a constant characteristic of the material and n is the density of conduction electrons or holes. By assuming that carriers are subject to Rutherford scattering by impurity ions, it has been shown[3] that

$$\rho_I = 9\times 10^{11}\pi^{3/2}e^2m^{1/2}2^{-7/2}\kappa^{-2}(kT)^{-3/2}(N_S/n) \times \ln\{1+36\kappa^2d^2(kT)^2e^{-4}\}, \tag{2}$$

where κ = dielectric constant, e and m electron charge and mass, and d one-half the average distance between the N_S scattering ions per unit volume.

Above 100°K the measured resistivities of most germanium samples agree very well with values calculated as the sum of $\rho_L+\rho_I$, with N_S set equal to n in calculating ρ_I. For samples of high impurity content ($>10^{18}$ cm^{-3}) the measured resistivity agrees with the values calculated taking $N_S=n$, down to temperatures as low as 4°K, provided that Eq. (2) is modified by using quantum statistics.[4] For samples having smaller impurity content, the measured resistivity[5] curve at low temperatures rises more rapidly with falling temperature than does the curve calculated in the manner described. At low temperatures, ρ_L becomes increasingly negligible compared to ρ_I, and so one cannot look to ρ_L behavior for explanation. The deviations cannot be explained as due to grain boundary effects because single crystal and polycrystalline samples show the same behavior. The observed resistivity behavior is such as would arise if N_S becomes increasingly large compared to n as T decreases. This would happen if N_S remains approximately constant while n falls off rapidly with decreasing temperature.

A germanium sample of either N- or P-type usually contains impurities of the opposite type in smaller concentration. Let N_N represent the maximum density of ionized donor levels and N_P the maximum density of ionized acceptor levels. For an N-type sample, $N_N>N_P$ and the N_P acceptor levels are filled with electrons from the donor levels, even at 0°K. These electrons are "frozen" in the acceptor levels and are not available for conduction at any temperature. At 0°K, with $n=0$, there are $N_0=2N_P$ scattering centers present. As T rises, n electrons are excited to the conduction band from donor levels, creating an additional n positive impurity ions. The concentration of scatterers may be taken as

$$N_S=n+N_0=n+2N_P, \tag{3}$$

where n has a temperature dependence found from the measured Hall coefficient, increasing from zero at 0°K to N_N-N_P at exhaustion. At very low temperatures $N_S\approx N_0$ and thus independent of temperature. An analogous model applies to P-type samples.

In calculating the resistivity by use of Eqs (2) and (3), the number N_0 is so chosen as to give agreement of the calculated and measured resistivities at an arbitrarily chosen low temperature.

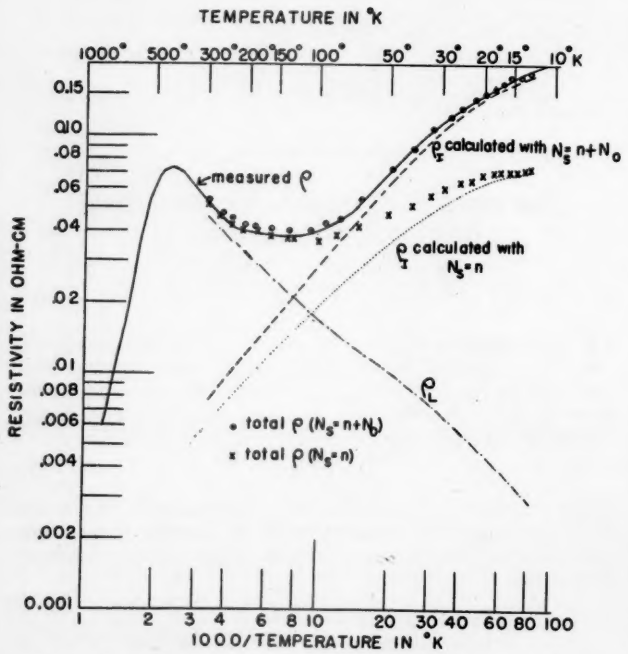

FIG. 1. Analysis of low temperature resistivity curve for germanium sample 33N (N-type, antimony added). N, impurity ion density at exhaustion, $=1.0\times10^{17}$/cm³. Agreement between theory and experiment is obtained by taking $N_0=2.4\times10^{16}$/cm³.

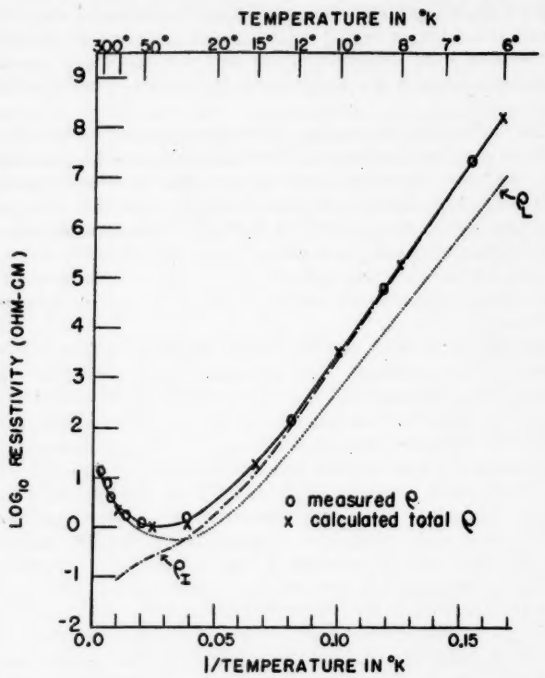
TEMPERATURE IN °K
300° 50° 20° 15° 12° 10° 8° 7° 6°
LOG10 RESISTIVITY (OHM-CM)
9 8 7 6 5 4 3 2 1 0 -1 -2
o measured ρ
x calculated total ρ
ρ_L
ρ_I
0.0 0.05 0.10 0.15
1/TEMPERATURE IN °K

FIG. 2. Analysis of low temperature resistivity curve for germanium sample 43W-81 (high purity N-type). N, impurity ion density at exhaustion, $=1.16\times10^{14}$/cm³. Number of scattering centers at 0°K, $N_0=1.04\times10^{14}$/cm³.

This N_0 is used in computing ρ_I from Eq. (2) throughout the impurity range. Figures 1 and 2 show, for two N-type samples of different impurity densities, the discrepancies appearing when N_S is taken as n and the good agreement obtained by considering the additional N_0 scattering ions. It is generally found for high resistivity samples that N_0 is of the same order of magnitude as the carrier concentration in the exhaustion range.

* Work assisted in part by Signal Corps contract.

[1] K. Lark-Horovitz and V. A. Johnson, Phys. Rev. **69**, 258 (1946); K. Lark-Horovitz (unpublished work).
[2] A. Sommerfeld and H. Bethe, *Handbuch d. Physik* (1933), Vol. 24, No. 2, p. 560.
[3] E. Conwell and V. F. Weisskopf, Phys. Rev. **69**, 258 (1946); **77**, 388 (1950).
[4] V. A. Johnson and K. Lark-Horovitz, Phys. Rev. 374, 909 (1947); **72**, 531 (1947).
[5] C. S. Hung and J. R. Gliessman (to be published).

Note on the Revision of the Hyperfine Structure of the Spectrum of Mercury

K. MURAKAWA
Institute of Science and Technology, Komba, Meguro-ku, Tokyo, Japan
June 15, 1950

OWING to an unfortunate misreading of the literature, a reference was given in an erroneous manner in our earlier Letter[1] on this subject. The last row of Table I should be omitted. The sentence from line 4 below the table commencing with "The value of . . ." to line 7, ending with ". . . the last row," should be omitted. The portion of the sentence of lines 8 and 9 below the table reading "not only different from that obtained by the nuclear absorption method, but is also" should be omitted.

A recent more accurate study has necessitated a change in the numerical values given in columns 2 and 7 of the last row but one of Table I from $-182._3$ and -2.86 ± 0.05 to -175.4 and -2.756 ± 0.017, respectively. The conclusion is not altered by these changes.

[1] K. Murakawa, Phys. Rev. **78**, 480 (1950).

On the Isomerism of Kr^{85}

INGMAR BERGSTRÖM AND SIGVARD THULIN
Nobel Institute of Physics, Stockholm, Sweden
June 9, 1950

OF great interest for the nuclear shell theory is Kr^{85}, since the neutron number is 49; i.e., it represents the filled 50 shell minus one nucleon. Two different activities of this isotope with half-lives 4.5 hr. and 9.4 yr. have been reported[1] indicating an isomeric pair. Two γ-rays of energies 0.17 and 0.37 Mev and a β-continuum with the upper limit of 1.0 Mev have been assigned to the shorter activity by absorption measurements.[1] The upper limit[1] for the β-spectrum of the longer activity is 0.74 Mev (abs.). No β-spectrometer measurements have been reported previously.

By using the electromagnetic isotope separator[2] and the high transmission β-spectrometer[3] of this Institute, we have studied the 4.5-hr. activity of Kr^{85} produced in uranium fission. The experimental technique was the same as that recently described[4] in an investigation of Kr^{83m}.

The β-spectrometer results are presented in Fig. 1 and Table I. The γ-rays of energies 149 and 300 kev are probably the same as those reported by Hoagland and Sugarman[1] (0.17 and 0.37 Mev abs.). The Fermi plot is a straight line from the upper limit 817 down to about 35 kev, where the backscattering effect in the collector foils (0.15 mg Al/cm²) probably begins. Thus the β-spectrum is simple and $f \cdot t \sim 1 \cdot 10^5$ corresponding to an allowed unfavored transition.[5]

The K_1 and the Auger electrons but not the K_2 electrons are in coincidence with the β-spectrum ($e^-\beta^-$-coincidence measurements in β-spectrometer). The half-lives for all the lines are the same as for the β-spectrum ($\sim$4.5 hr.). The possibility of an isomeric state with a short half-life in Rb^{85} cannot be definitely excluded by internal conversion considerations. Because of the presence of the other γ-ray this question can hardly be decided by critical absorption measurements. As we also found a weak (25 c/min. close to a β-tube) very long activity in our separated Kr^{85} sample and no isomer of Rb^{85} has been reported, it is most probable that the 300-kev γ-ray is emitted in an isomeric transition in Kr^{85}. This conclusion is also supported by the decay scheme of Fig. 2 as will follow from the discussion below.

For the isomeric transition $l=5$ seems to be consistent with out measurements. From Bethe's formula we estimate the half-life $\tau_{\frac{1}{2}}$ for the γ_2-transition. Thus $\tau_{\frac{1}{2}}=3.10^7$ sec. for $l=5$ and 35 sec. for $l=4$. $\tau_{\frac{1}{2}}$ for electric radiation can also be calculated using the experimental intensity ratio e^-/β^- for the K_2 line, the total half-life 4.5 hr., N_K/N_L (Hebb and Nelson) and the conversion coefficient α_K of Rose *et al.* In this way we obtain $\tau_{\frac{1}{2}}=2\cdot10^5$ sec. for $l=5$ and $7\cdot10^4$ sec. for $l=4$. The first l-value is in good agreement with the curves of Axel and Dancoff.[6] From the data above the branching ratio λ_2/λ_1 is about 0.19.

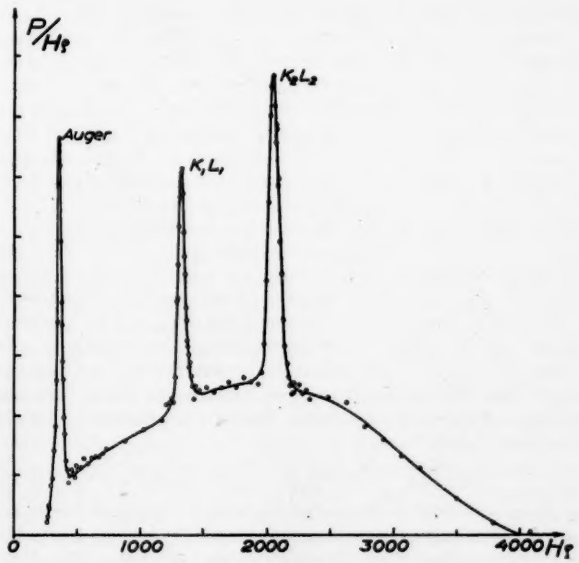

FIG. 1. β-spectrum of Kr^{85} (4.4 hr.).

TABLE I. β-spectrometer results for Kr^{85}.

	$H\rho$	$E(e^-)$ (kev)	$h\nu$ or E_{max} (kev)	e^-/β^-	$f \cdot t$
Lines					
A_1	350	10.7			
K_1	1311	134	149	0.09 ±0.01	
K_2	2033	285	300	0.051 ±0.006	
β-spectrum					
β_1			817		$\sim10^5$
β_2			666[a]		$\sim10^{9b}$

[a] Obtained from the decay scheme of Fig. 2.
[b] The half-life of Thode *et al.* was used (reference 1).

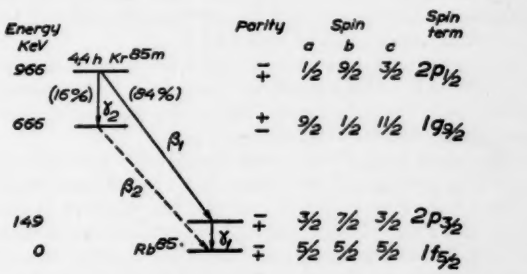

FIG. 2. Decay scheme of Kr^{85}, showing spin and parity discussed in text. Spin term according to M. G. Mayer (reference 7).

From the known spin 5/2 of Rb^{85} and the spin changes at the γ_1-, γ_2-, and β_1-transitions we arrive at the spin and parity relations shown in Fig. 2. All spin alternatives with $J>11/2$ have been excluded and spin alternative *c* can be ruled out since it is unlikely to find the spin 11/2 in the nucleon number region to which Kr^{85} belongs.[7] If the γ_2-transition is associated with no parity change the spin difference would be 5 leading to impossible $(-\frac{1}{2}, 19/2)$ and unprobable (11/2) spins of the ground state of Kr^{85}. Assuming instead parity change this would give the spins $\frac{1}{2}$ and 9/2 for the lowest levels of Kr^{85}. Spin alternative *a* is in excellent agreement with the nuclear shell model of Mayer and Jensen *et al.*[7] When the L conversion coefficient calculations of Rose *et al.*[7] When the L conversion coefficient calculations of Rose *et al.* are available this alternative can experimentally be established by measuring N_K/N_L with high resolving power.

Another consequence of our decay scheme will be that the β_2-transition would occur with a spin change of 2 and with change in parity. Shull and Feenberg[8] have given the formula (W_0^2-1). $f \cdot t \sim 10^{10}$ for a β-transition of the type mentioned. From our decay scheme we get the upper limit for $\beta_2=666$ kev, which gives $(W_0^2-1)f \cdot t = 0.4 \cdot 10^{10}$ (using the half-life 9.4 yr. measured Thode[1]), in good agreement with the suggested spin and partity relations. The β_2-spectrum would then have the forbidden shape and will soon be measured here with a much stronger sample.

[1] G. T. Seaborg and I. Perlman, Rev. Mod. Phys. 20, 585 (1948). Mattauch-Flammersfeld, Isotopic Report, Tübingen (1949).
[2] Bergström, Thulin, Svartholm, and Siegbahn, Arkiv. f. fysik 1, 281 (1949).
[3] H. Slätis and K. Siegbahn, Phys. Rev. 75, 1955 (1949).
[4] Bergström, Thulin, Andersson, Phys. Rev. 77, 851 (1950).
[5] E. Feenberg and K. C. Hammack, Phys. Rev. 75, 1877 (1949).
[6] P. Axel and S. M. Dancoff, Phys. Rev. 76, 892 (1949).
[7] M. G. Mayer, Phys. Rev. 78, 16 (1950), Jensen, Suess, and Haxel, Naturwiss. 36, 155 (1949).
[8] F. B. Shull and E. Feenberg, Phys. Rev. 75, 1768 (1949).

On the Decay of Xe^{133m}

INGMAR BERGSTRÖM AND SIGVARD THULIN
Nobel Institute of Physics, Stockholm, Sweden
June 9, 1950

OF interest for the nuclear shell theory is Xe^{133} which has the neutron number 79 representing the filled 82 shell minus three nucleons. By absorption measurements different investigators[1] have found β-particles having maximum energy 0.26 to 0.42 Mev. A strongly converted γ-ray of energy 83 to 85 kev has also been reported.[1] The same γ-energy has been found[1] in the K-capture of Ba^{133} from which it can be concluded that the 83- to 85-kev γ-ray is probably emitted from a level in Cs^{133}. No complete β-spectrometer measurements have been reported earlier. The half-life for Xe^{133} has recently been measured with high precision by Macnamara *et al.*[2] who found 5.270 days.

Using the same experimental technique as in an investigation[3] on Kr^{83m} it has been possible to measure the β-spectrum of Xe^{133}, produced in uranium fission. The results of these measurements are presented in Fig. 1 and Table I.

The upper limit for the β-spectrum is 345 kev and the corresponding $f\cdot t$-value $4\cdot10^5$ (unfavored allowed transition[4]). The K and L conversion lines (K_1 and L_1, Fig. 1) of the 81-kev γ-ray were very strong. In addition we have established the existence of a weak 232-kev γ-ray (K_2 and L_2, Fig. 1) earlier reported preliminarily by us.[5] This γ-ray is most probably emitted in an isomeric transition in Xe^{133}, which will follow from the following discussion.

The half-lives for the K_1 and K_2 conversion lines are the same as for the β-spectrum (~5.5 days). ϵ-β^--coincidence measurements in the β-spectrometer showed a very strong coincidence effect for the K_1 and L_1 lines, but no effect was found for the K_2 line. Thus there must be an isomeric state either in Cs^{133} ($\tau_\gamma<5.5$ days) or in Xe^{133} ($\tau_\gamma\gg5.5$ days for intensity reasons). The first possibility can be excluded by comparing the measured intensity ratio $K_2/\beta^-=0.025$ with those computed from the internal conversion coefficients α_K of Rose *et al.* Thus for electric radiation and $l=1$, 2, 3 we obtain $K_2/\beta^-=0.017$, 0.075, 0.24, respectively, showing that only $l=1$ can be considered. Still for 2^2 pole electric radiation however, the half-life obtained from Bethe's formula is $\sim5\cdot10^{-10}$ sec., which would give ϵ-β^--coincidences as the ressolving power of the coincidence amplifier was $3\cdot10^{-7}$ sec.

If the isomeric transition takes place in Xe^{133} the half-life $\tau_\frac{1}{2}$ for the γ_2-transition estimated from Bethe's formula is $\sim1\cdot10^8$ sec. for $l=5$ and $\sim1\cdot10^2$ sec. for $l=4$. $\tau_\frac{1}{2}$ can also be calculated from the measured intensity ratio K_2/β^-, the half-life 5.3 days and the theoretical α_K. Using these data we obtain $\tau_\frac{1}{2}=7\cdot10^7$ sec. for $l=5$ and $2\cdot10^7$ sec. for $l=4$. From the same data the branching ratio λ_2/λ_1 is 0.04. Thus $l=5$ is consistent with our measurements. As in the case[6] of Kr^{85} this is in agreement with the classification of Axel and Dancoff.[7] The curves of Hebb and Nelson give $N_K/N_L\sim1.4$ for $l=5$ and $N_K/N_L\sim2.6$ for $l=4$ and electric radiation. The experimentally obtained N_K/N_L is 2.2, indicating a mixture of electric 2^5 pole and magnetic 2^4 pole radiation (spin change 4, parity change).

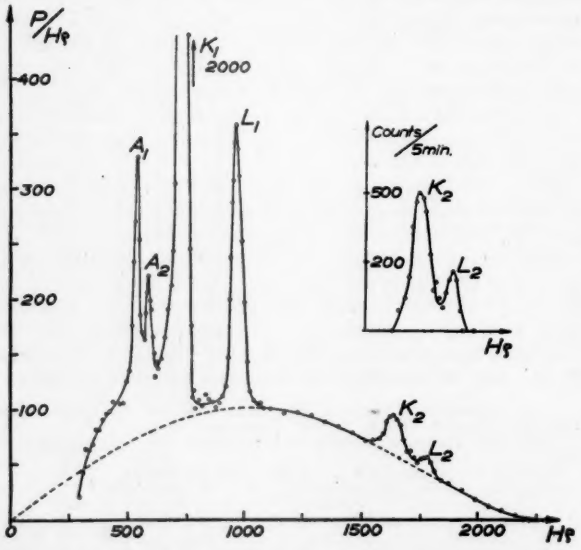

FIG. 1. β-spectrum of Xe^{133} (5.3 days).

TABLE I. β-spectrometer results for Xe^{133}.

	$H\rho$	$E(e^-)$ (kev)	$h\nu$ or E_{max} (kev)	N_K/N_L	$e^-\beta^-$	$f\cdot t$
Lines						
A_1	536	24.7				
A_2	586	29.4				
K_1	729	44.8	80.7	5.9±0.4	0.66	
L_1	962	75.8	81.5		±0.06	
K_2	1630	196	232	2.2±0.4	0.025	
					±0.006	
L_2	1780	227	233			
β-spectrum						
β_1			345			$4\cdot10^5$
β_2			194[a]			~10^{10}[b]

[a] Obtained from the decay scheme of Fig. 2.
[b] Obtained from the formula $(W_0^2-1)f\cdot t\sim10^{10}$.

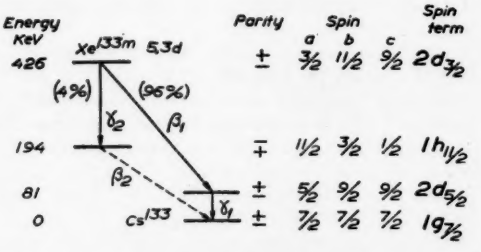

FIG. 2. Decay of Xe^{133} showing spin and parity discussed in text. Spin term according to M. G. Mayer (reference 8).

From the discussion above and the spin 7/2 of Cs^{133} the decay scheme of Fig. 2 has been drawn. All spin alternatives with $J>11/2$ and spin alternative c have been excluded for the same reasons[6] as for Kr^{85}. The spins 3/2 and 11/2 (alternative a) of the lowest levels in Xe^{133} and the parity change are consistent with the nuclear shell model of Mayer and Jensen *et al.*[8] According to our decay scheme the β_2-transition would have an upper limit of 194 kev and be first-forbidden, as the spin change is 2 and parity change occurs. The half-life computed from the formula $(W_0^2-1)f\cdot t\sim10^{10}$ of Shull and Feenberg[9] is about 2700 yr. Thus it would be quite impossible to detect the predicted activity in our sample because of the long half-life and the small branching ratio. A β-transition from the ground state of Xe^{133} to the 81-kev level is Cs^{133} would also give a very long half-life (third-forbidden).

The β-spectrum of Xe^{133} offers a possibility of studying the Auger effect. By comparison of the intensities of the K lines and the Auger lines we obtain a value for the x-ray fluorescence yield w_K of the K shell.[10]

$$w_K=(N_{K1}+N_{K2}-N_{A1}-N_{A2})/(N_{K1}+N_{K2}).$$

As the cut-off of the G-M window in the β-spectrometer is 5.0 kev, no absorption corrections are necessary, which also was controlled by measuring the low energy region of the Co^{60} β-spectrum. Here w_K corresponds to a mixture of x-rays from Xe^{133} and Cs^{133} but

since the fluorescence yield differs only slightly for elements with $\Delta Z=1$ and the intensity ratio of the K electrons from Xe^{132} and Cs^{133} is 1:32, the obtained value can be considered as the fluorescence yield of Cs. Our value 0.89 ± 0.08 is higher than that obtained by Auger[11] in Xe (0.71) but is in good agreement with the value 0.91 from the semi-empirical curve given by Haas[12] from the theory of Wentzel.[13] The ratio of the intensities of the A_1 and A_2 lines 0.48, gives the probability ratio for ejection of an Auger electron from the L shell and from the M, N, $\cdots$shells.

[1] G. T. Seaborg and I. Perlman, Rev. Mod. Phys. **20**, 585 (1948), Mattauch-Flammersfeld, Isotopic Report, Tübingen (1949).
[2] Macnamara, Collins, and Thode, Phys. Rev. **78**, 129 (1950).
[3] Bergström, Thulin, and Andersson, Phys. Rev. **77**, 851 (1950).
[4] E. Feenberg and K. C. Hammack, Phys. Rev. **75**, 1877 (1949).
[5] Thulin, Bergström, and Hedgran, Phys. Rev. **76**, 874 (1949).
[6] I. Bergström and S. Thulin, Phys. Rev. **79**, 537 (1950), preceding letter.
[7] P. Axel and S. M. Dancoff, Phys. Rev. **76**, 892 (1949).
[8] M. G. Mayer, Phys. Rev. **78**, 16 (1950), Jensen, Suess, and Haxel, Naturwiss. **36**, 155 (1949).
[9] B. Shull and E. Feenberg, Phys. Rev. **75**, 1768 (1949).
[10] A. H. Compton and S. K. Allison, *X-ray in Theory and Experiment* (D. Van Nostrand Company, Inc., New York, 1935).
[11] P. Auger, Ann. de physique **6**, 183 (1926).
[12] M. Haas, Ann. d. Physik (5), **16**, 473 (1933).
[13] G. Wentzel, Zeits. f. Physik **43**, 524 (1927).

Scattering of 3.27-Mev Neutrons by Deuterons in the Wilson Chamber

I. Hamouda, J. Halter and P. Scherrer
Physikalisches Institut der E. T. H. Zürich, Switzerland

June 13, 1950

THE scattering of neutrons by deuterons is known to give a clue regarding the nature of the force between two nucleons, even at relatively small neutron energies.[1] The two main angular distribution measurements in this field with neutrons of 2.6 Mev from a (d, d) reaction, are those of Coon and Barschall[2] with 12,000 deuteron recoils in an ionization chamber, and of Darby and Swan[3] with 1500 deuteron tracks in a cloud chamber. However, as Darby and Swan maintain, their angular distribution data agree very closely with the "ordinary force" curve of Massey and Buckingham,[4] whereas Massey and Buckingham[4] point out that the data of Coon and Barschall fit better with their "exchange force" curve.

We investigated the angular distribution of neutrons scattered by deuterons with 3.27-Mev (d, d) neutrons in the cloud chamber. To eliminate the disturbing effects of the neutrons scattered into the chamber from the surrounding material and to account for corrections due to the geometry of the apparatus, the angular distribution of neutron-proton scattering was also investigated with the same neutron source and under the same geometrical conditions. Assuming that the (n, p) distribution is isotropic, one obtains a correction factor for the disturbing effects which is just the deviation from isotropy of the measured distribution. In two separate runs of photographs under different geometrical conditions 5000 proton recoils and 10,000 deuteron recoils were investigated. The two independently measured (n, d) angular distributions were found to agree well within the limits of statistical fluctuation. In Fig. 1 the angular distribution data for protons and deuterons in the second run of photographs (2800 proton recoils and 8200 deuteron recoils) are plotted in the center-of-mass system. Our data agree with those of Coon and Barschall.

In a recent theoretical work on the elastic scattering of neutrons by deuterons at 20 Mev, Verde[5] points out that a pronounced maximum occurring only at 180° is a characteristic feature of the "exchange force" theory and is also produced at smaller energies. This is in disagreement with the results of Buckingham and Massey[1] who find for neutrons of 11.5 Mev a pronounced maximum only at 0° for exchange as well as for ordinary force theories. Coon and Taschek,[6] who have extrapolated their data to a pronounced maximum at 0° from measurements made at 20° and above, point out that their angular distribution data at 14 Mev fit better with the "exchange force" curve of Buckingham and Massey[1] at 11.5 Mev. On the other hand, this shape disagrees, according to Verde, with the "characteristic feature" of the "exchange force" theory, and fits qualitatively with the "ordinary force" curve of Verde at 20 Mev. If the data of the present experiment are compared with the curves of Massey and Buckingham[4] at 2.53 Mev, they fit much better with the "exchange-" than with the "ordinary-force" curve.

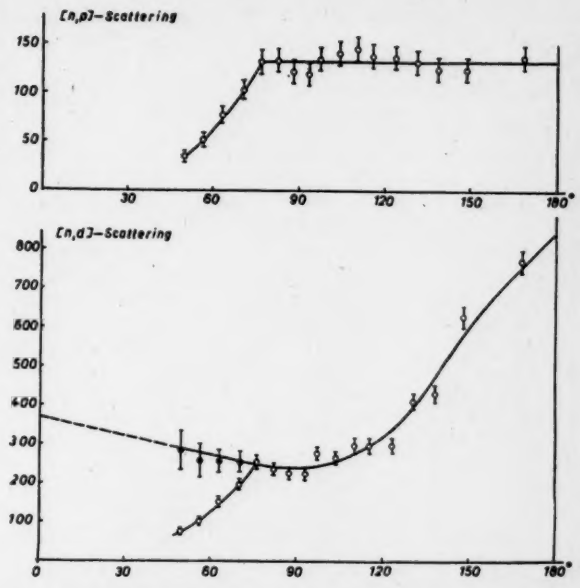

FIG. 1. Intensity of scattered neutrons *versus* angle of scattering in center-of-mass system. The empty circles represent the measured intensities; the full circles represent the corrected intensities, considering the isotropy of the (n, p) angular distribution. The dashed part of the curve is an extrapolation drawn to give a total number of recoils corresponding to the experimental total scattering cross-section values for the two processes.

We wish to thank Dr. M. Verde for very interesting and useful theoretical discussions, also Dr. W. Zünti for help in carrying out the radiation with the neutron generator.

The detailed experiment will be published in *Helvetica Physica Acta*.

[1] R. A. Buckingham and H. S. Massey, Proc. Roy. Soc. **A179**, 123 (1941).
[2] J. H. Coon and H. H. Barschall, Phys. Rev. **70**, 592 (1946).
[3] J. F. Darby and J. B. Swan, Australian J. Sci. Research **A1**, 18 (1948).
[4] H. S. W. Massey and R. A. Buckingham, Phys. Rev. **71**, 558 (1947).
[5] M. Verde, Helv. Phys. Acta **22**, 339 (1949).
[6] J. H. Coon and R. F. Taschek, Phys. Rev. **76**, 710 (1949).

Note on Angular Asymmetries in (γ, n) Reactions*

H. L. Poss
Brookhaven National Laboratory, Upton, New York

June 9, 1950

THE (n, p) threshold reaction in aluminum has been used to detect photo-neutrons emitted from bismuth, lead, and tungsten targets irradiated with x-rays produced by the 20-Mev betatron at the Picatinny Arsenal. Emission of photo-neutrons was found to be more prevalent at right angles to the x-ray beam than in the direction of the beam. This asymmetry for fast neutrons [the (n, p) reaction in aluminum has a threshold of 4.6 Mev for a probability[1] of barrier penetration by the emitted proton of $\frac{1}{2}$] is in contrast to the symmetrical distributions found for lead and iron by Price and Kerst[2] who used a detector responding to slow neutrons as well.

The detector consisted of a stack of aluminum plates[3] enclosed in $\frac{1}{32}$" cadmium. Their activity was measured with a thin-walled cylindrical Geiger counter following the end of a 10-min. irradiation. A decay curve was plotted in each case. With the exception of the first few minutes, during which an activity attributed to

2.3-min. Al^{28} was noticeable, the points could be fitted to a 9.6-min. half-life which has been established for the Mg^{27} end product of the aluminum (n, p) reaction.[4]

Targets were $\frac{3}{4}''$ diameter cylinders, 3" long, the tungsten being in the form of the metal powder while the lead and bismuth were solid cylinders. The x-ray beam was perpendicular to the axis of the cylinder. During an irradiation, the betatron intensity as indicated by a monitor ionization chamber was kept constant to about 10 percent. Partial corrections for fluctuations in intensity were made by normalizing each initial activity to the same total number of roentgens.

The background of fast neutrons generated by the betatron made it necessary to sacrifice resolution by placing the detector adjacent to the target. Measurements were made at 0° and at both 90° positions with respect to the beam. A carbon target was used to take into account the background. The threshold of the detector together with the high (γ, n) threshold for carbon would prevent photo-neutrons from being detected in this case. The resultant activities, about the same for each position, are attributed to neutrons in the x-ray beam being scattered by the target or reaching the detector directly. Since the carbon target scatters neutrons to roughly the same extent as do the other target matrials used, these activities were just subtracted from the others to obtain the net photo-neutron effect. The results of at least two independent sets of measurements on each element are in the range

$$N_{90°}/N_{0°}=2.0\pm0.5.$$

Within the limits of error, no significant differences for the different targets were noticed.

An angular dependence of the form $A+B\sin^2\theta$ would be expected if photo-disintegrations are principally due to dipole transitions. Because of the continuous nature of both the x-ray spectrum and the energy sensitivity of the detector, as well as the poor resolution, the experimental ratio is difficult to compare directly with theory, but is in qualitative agreement with considerations based on a shell structure model of nuclei.[5] If an average cross section of 0.025 barn for the aluminum (n, p) reaction is assumed, then comparing the results of these measurements with those of Price and Kerst on total neutron yields,[2] it appears that of the order of 1/10 of the total photo-neutrons from lead or bismuth are fast enough to activate the aluminum detector.

Acknowledgment is due Dr. E. O. Salant, who suggested this problem, and Dr. E. D. Courant for helpful discussions. I am also indebted to the officers and men of Picatinny Arsenal, in particular, to Mr. L. P. Goldberg and Dr. B. A. Lloyd, for enabling us to use the betatron and for rendering valuable assistance throughout.

* Research carried out at the Brookhaven National Laboratory under the auspices of AEC.

[1] Feld, Scalettar, and Szilard, Phys. Rev. **71**, 464(A) (1947).

[2] G. A. Price and D. W. Kerst, Phys. Rev. **77**, 806 (1950). M. Goldhaber has informed me that an asymmetry for fast neutrons of the type reported in this note has also been observed by a group at Illinois in connection with an experiment to detect nuclear scattering of x-rays.

[3] The plates were pressed from spectroscopically pure aluminum rods supplied by A. D. Mackay, New York, New York.

[4] S. Eklund and N. Hole, Arkiv. Mat. Astron. Fysik **29A**, No. 26 (1943).

[5] E. D. Courant (to be published).

[6] B. Cohen, Technical Report No. 3, Carnegie Institute of Technology (1949).

A Large Fluctuation in the Rate of Production of Nuclear Disintegrations Following a Solar Flare*

J. J. Lord, A. W. Elston, and Marcel Schein
Department of Physics, University of Chicago, Chicago, Illinois
June 7, 1950

In the course of a series of balloon flights in the stratosphere for the purpose of measuring the nuclear disintegration intensity in photographic emulsions as a function of altitude, one flight gave a very much larger intensity than normal. This flight was launched from Camp Ripley, Minnesota (56°N geomagnetic latitude) on May 11, 1949 and remained in the air from 18:48 to 22:30 Universal Time and reached a maximum altitude of 95,000 ft. This was about 23 hr. following the occurrence of the large solar flare[1] of May 10, 1949.

The intensity measurement of the production of nuclear disintegrations in photographic emulsions was referred to an altitude of 95,000 ft.; corrections having been made for the time of ascent and descent. These corrections were made possible since recent data to be published soon give a more detailed altitude variation[2] of stars of a specific number of prongs. The active volume of the emulsion examined for the determination of the frequency of stars was measured after processing it. The change in the volume due to shrinkage was determined from a number of sample plates selected at random from the plates used in the experiment. One-half of each plate was processed along with the others in the experiment, the other half was left unprocessed. Measurements of mass, area, and thickness of emulsion were made on both halves of the plates and compared with each other.

The intensity for the production of nuclear disintegrations during the flight of May 11 is compared in Fig. 1 with that during

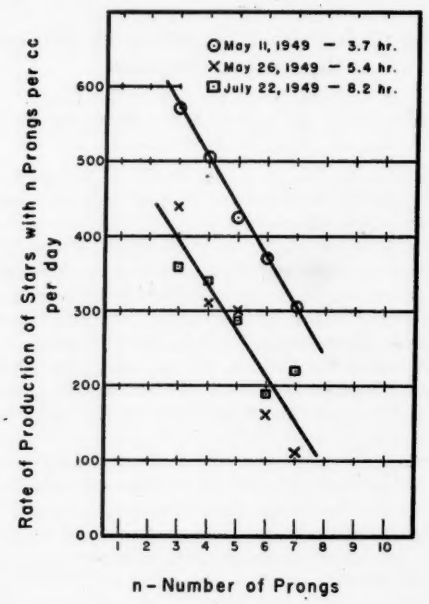
May 11, 1949 — 3.7 hr.
May 26, 1949 — 5.4 hr.
July 22, 1949 — 8.2 hr.
Rate of Production of Stars with n Prongs per cc per day
600
500
400
300
200
100
0
1 2 3 4 5 6 7 8 9 10
n – Number of Prongs

FIG. 1.

two other flights reaching the same altitude. During the flight of May 11, the intensity of production of stars having 3 to 8 prongs was 50±13 percent greater than the normal value. The intensity of heavy nuclei having atomic numbers greater than approximately 10 was within statistical error the same as that for a normal flight during the day.

The flare of May 10, 1949 began at 20:00–20:03 UT as reported by Shapley and Davis[1] and was rated 3^+ by observers at the McMath-Hulbert observatory.[3] Following the solar flare, a magnetic storm commenced at 06:24 UT on May 12, 1949. Observations by Forbush[4] at Cheltenham, Maryland (72 meters elevation) and Huanacayo, Peru (3350 meters elevation) with shielded ionization chambers showed no measurable change in the cosmic-ray intensity during the period from the start of the flare to the occurrence of the magnetic storm; however, a decrease of a few percent was observed during the magnetic storm.

Only four significant increases of cosmic-ray intensity have been observed in the past 13 yr. and all seem to have been closely associated with solar flares.[3,5] The unusually large latitude dependence of these increases indicates that they must be due predominantly

to low energy charged primary particles which would then account for the relatively large increase, 50 percent of intensity in the stratosphere of May 11 compared to the absence of a measurable effect (less than two percent) at sea level.

Johnson and Korff[6] measured the total cosmic-ray intensity at 64,000 ft. elevation during a solar flare of July 27, 1938 but found no change from the normal within the accuracy afforded by their apparatus. The measurement was made with a counter telescope so that at this elevation a large fraction of the counts would be due to electrons produced by the higher energy primary particles of the cosmic radiation.

We wish to thank the Office of Naval Research for arranging these balloon flights with the General Mills Aeronautical Laboratory and Mr. C. B. Moore of the latter laboratory for his great assistance.

* Assisted by the joint program of ONR and AEC.

[1] A. H. Shapley and R. M. Davis, Science **110**, 159 (1949).
[2] J. J. Lord and Marcel Schein, Phys. Rev. **75**, 1956 (1949).
[3] Helen W. Dodson, Astrophys. J. **110**, 382 (1949).
[4] S. E. Forbush (private communication, 1949).
[5] S. E. Forbush, Phys. Rev. **70**, 771 (1946).
[6] T. H. Johnson and S. A. Korff, Terr. Mag. **44**, 23 (1939).

The Beta-Spectra of Zn^{62} and Cu^{62}

RAYMOND W. HAYWARD
Department of Physics, University of California, Berkeley, California
May 29, 1950

THE beta-spectrum of the ten-minute Cu^{62} isotope has recently been studied by Becker, Kirn, and Buck[1] in a beta-spectrometer using sources of copper foil which had been irradiated with 22-Mev x-rays from the Illinois betatron. The method of observation required the use of rather thick sources (11 mg/cm²). Also because of the short lifetime of Cu^{62} a number of samples had to be used making it necessary to normalize each observed interval with the preceding one.

A more convenient method of observing the Cu^{62} spectrum would be to use its parent Zn^{62} as a source. Zn^{62} was reported by Miller, Thompson, and Cunningham[2] as a K-capture activity with a half-life of 9.5 hours; thus the Cu^{62} formed by the decay of Zn^{62} would appear to decay with this longer lifetime. A sample of Zn^{62} was prepared by bombarding a thick copper target with 100-Mev deuterons in the 184-inch Berkeley cyclotron. The Zn^{62} was separated by first electroplating out the majority of the copper and then performing a chemical separation on the remainder using 100 micrograms of carrier. The source was prepared by mounting a portion of the sample of ZnS on a backing of Formvar film so that the total source thickness was less than 0.1 mg/cm². The beta-spectrum is shown in Fig. 1. There are three features in this

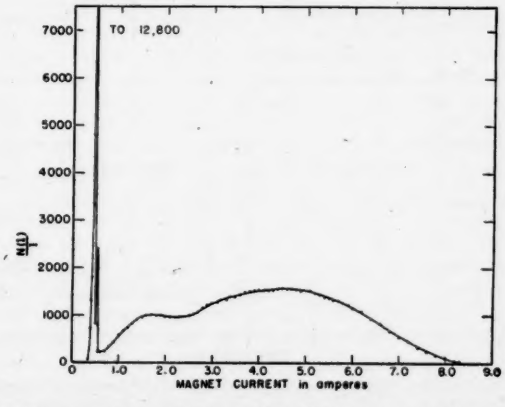

FIG. 1. The momentum spectrum of the positrons and conversion electrons from a source of Zn^{62} and its daughter Cu^{62}.

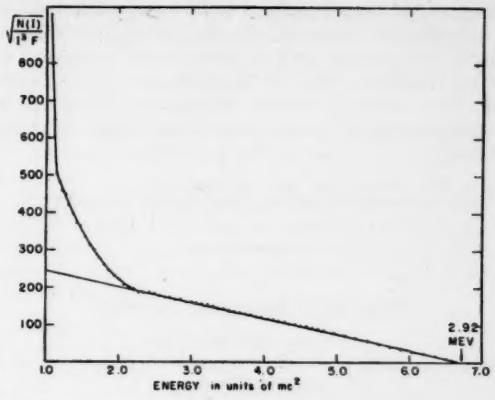

FIG. 2. The Fermi plot of the positron spectrum from a source of Zn^{62} and Cu^{62}.

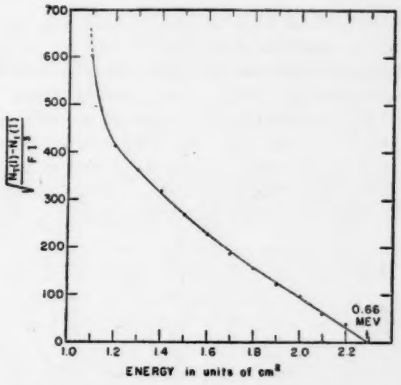

FIG. 3. The Fermi plot of the positron spectrum of Zn^{62} after the contribution of the daughter Cu^{62} has been subtracted.

spectrum, a high energy positron component arising from the decay of Cu^{62}, a lower energy positron component arising from the decay of Zn^{62}, and two conversion lines corresponding to the K and L conversion peaks of a 41.8±0.2 kev gamma-ray following the decay of Zn^{62} since the energy separation of the K and L lines is equal to the separation of the K and L binding energies in copper. At this low energy the absorption of the 0.4 mg/cm² Nylon window of the Geiger counter has considerable effect so that the K conversion line is absorbed more than the L conversion line. Hence the observed ratio of the number of K and L conversion electrons would set a lower limit of the actual ratio. The observed ratio is 6.4 and would correspond to either an electric or magnetic dipole transition. A Fermi plot of the positron spectrum is shown in Fig. 2. The upper limit of the Cu^{62} positron spectrum is 2.92±0.02 Mev, slightly higher than the value of Becker. Subtraction of the extrapolated straight line Fermi plot for Cu^{62} from the total spectrum gives the Fermi plot for Zn^{62} shown in Fig. 3. The upper energy limit is 0.66±0.01 Mev. The curvature in this Fermi plot can be attributed to a small amount of back-scattering from the much more intense Cu^{62} spectrum. The measured half-life is 9.33 hours. Comparison of the number of positrons in both the Zn^{62} and Cu^{62} spectra indicates that Zn^{62} decays about 10 percent of the time by positron emission and the remainder by K-capture. According to the Fermi theory of beta-decay positrons should be emitted 25 percent of the time. This sort of discrepancy is common because of the strong energy dependence of the probability for positron emission. The nuclear matrix elements should be the same for positron emission and K-capture. Perhaps a slight error in the determination of the upper energy limit would account for the discrepancy. However, another possibility is the lack of

UNIVERSITY OF MICHIGAN LIBRARIES

knowledge of the branching ratio of Zn^{62} decay where the decay might take place to two states separated by 41.8 kev. This would be difficult to determine without experimental knowledge of the conversion coefficient. The Cu^{62} has a $f\tau_{\frac{1}{2}}$ value of 13.4×10^4 and Zn^{62} has a $f\tau_{\frac{1}{2}}$ value of 5.3×10^4 (taking into account the decay by K-capture and positron emission) which classifies both spectra as allowed.

[1] Becker, Kirn, Buck, Phys. Rev. 76, 1406 (1949).
[2] Miller, Thompson, Cunningham, Phys. Rev. 74, 347 (1948).

The Sn^{117} Isomeric Activity

RAYMOND W. HAYWARD
Department of Physics, University of California, Berkeley, California
May 29, 1950

THE 14-day tin activity has recently been assigned to Sn^{117} by Mihelich and Hill[1] and by Mallary and Poole[2] who activated electromagnetically enriched isotopes of tin with slow neutrons.

A sample of Sn^{117} of high specific activity was prepared for observation in a magnetic lens spectrometer by bombarding a thick target of antimony with 100-Mev deuterons in the 184-inch Berkeley cyclotron. The Sn^{117} activity was separated from the antimony target by selective precipitation as sulfides thus requiring the addition of a relatively large amount (5 mg) of tin carrier. A source was prepared by mounting the SnS_2 on a Formvar film backing so that the total source thickness was about 1 mg/cm². The observed spectrum is shown in Fig. 1. Two conversion peaks are present at 127.0 and 152.5 kev corresponding to the K and L conversion for a transition with an energy of 0.157 ± 0.002 Mev. This value is slightly smaller than the value of 0.159 Mev obtained by Mihelich and Hill.

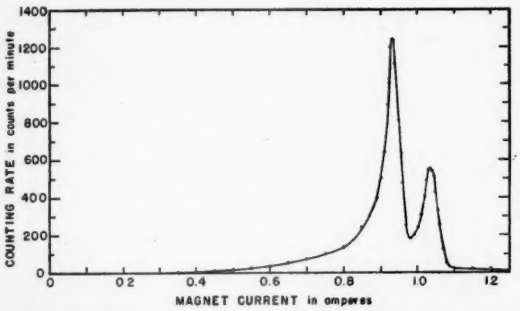

FIG. 1. The observed spectrum of conversion electrons from Sn^{117} before correction for the finite resolution of the spectrometer.

From the half-life of 14 days and the energy of 0.157 Mev the transition corresponds to a transition of order five according to the classification of Axel and Dancoff.[3] The experimental ratio of the number of K and L conversion electrons is 2.2 taking into account the resolution of the spectrometer. With a value $l=5$ the theory of Hebb and Nelson[4] gives 0.95 as the theoretical K/L ratio for electric transitions and 2.85 for magnetic transitions. With $l=4$ the theoretical K/L ratio is 3.84 for magnetic transitions. Therefore in order to account for the experimental value of the K/L ratio, a mixture of 2^5 pole electric and 2^4 pole magnetic radiation must be postulated.

The author wishes to thank Professor A. C. Helmholz for helpful discussions during the course of the experimental work described in this and the preceding letter and also to thank the Radiation Laboratory of the University of California for making some of their facilities available to him.

[1] J. W. Mihelich and R. D. Hill, Phys. Rev. 77, 743 (1950).
[2] E. C. Mallary and M. L. Poole, Phys. Rev. 77, 75 (1950).
[3] P. Axel and S. M. Dancoff, Phys. Rev. 76, 892 (1949).
[4] M. H. Hebb and E. Nelson, Phys. Rev. 58, 436 (1940).

Magnetic Resonance in Antiferromagnetic Materials near the Curie Temperature*

E. P. TROUNSON, D. F. BLEIL, R. K. WANGSNESS, AND L. R. MAXWELL
U. S. Naval Ordnance Laboratory, Silver Spring, Maryland
May 26, 1950

AN investigation[1,2] has been made of the magnetic resonance absorption of an antiferromagnetic material. Cr_2O_3 was selected for the initial experiments because it is a stable compound that has a Curie point at a convenient temperature. Honda and Sone[3] have reported a Curie temperature of 34°C for Cr_2O_3 while Foex and Graff[4] gave a higher value of 47°C.

The material was introduced into a rectangular cavity which formed one arm of a microwave bridge. The absorption was obtained by measuring the change of intensity of the reflection from the cavity which was slightly mismatched with respect to the line A d.c. magnetic field was set perpendicular to the microwave magnetic field. The procedure followed was to hold the frequency constant at 9300 Mc and sweep the d.c. magnetic field through the resonance peak at various temperatures, ranging from 150°C to liquid air temperature. A small field-dependent absorption has been eliminated from the data given below. We obtain, as a function of the temperature, the height of the absorption peak (h), and the value of the d.c. magnetic field (H_0) at the point of resonance.

We have found that h varies with the temperature of the powdered sample as shown by Fig. 1. It is noticed that h decreases abruptly at about 38°C indicating a drastic change in the nature of the absorption. Through the paramagnetic range, H_0 was constant at approximately 3450 oersteds.

Magnetic susceptibility measurements[5] made on the sintered Cr_2O_3 used are shown in Fig. 2. It is noticed for this material that the Curie temperature is 38°C, close to the point where the break in the resonance absorption occurs. It is believed, therefore, that the sudden decrease in the resonance absorption can be attributed to the change of Cr_2O_3 from the paramagnetic to the antiferromagnetic state.

The amount of absorption occurring below the Curie temperature depended upon the nature of the material. When the Cr_2O_3 was in a powdered form two absorption peaks were found. H_0 for one peak was independent of temperature and equal to the value found in the paramagnetic region. H_0 for the second peak decreased as the temperature decreased as illustrated in Fig. 3. At −64°C the two peaks are well resolved, occurring at 3450 and 660 oersteds, respectively. When the Cr_2O_3 was prepared as

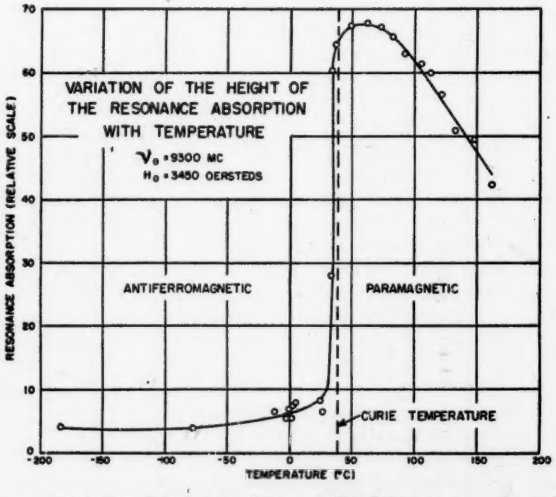

FIG. 1. Variation of the height of the peak (h) of the resonance absorption with temperature of powdered Cr_2O_3. The vertical broken line indicates the Curie point as determined by an independent measurement of the paramagnetic susceptibility on the sintered material investigated.

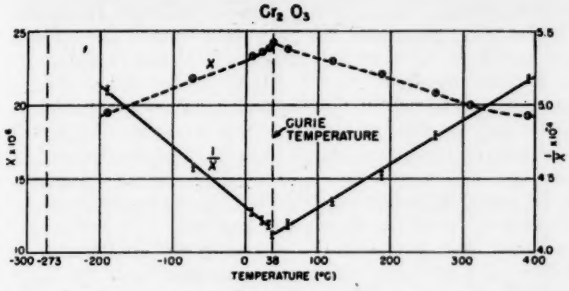

FIG. 2. Variation of paramagnetic susceptibility of sintered Cr_2O_3 with temperature.

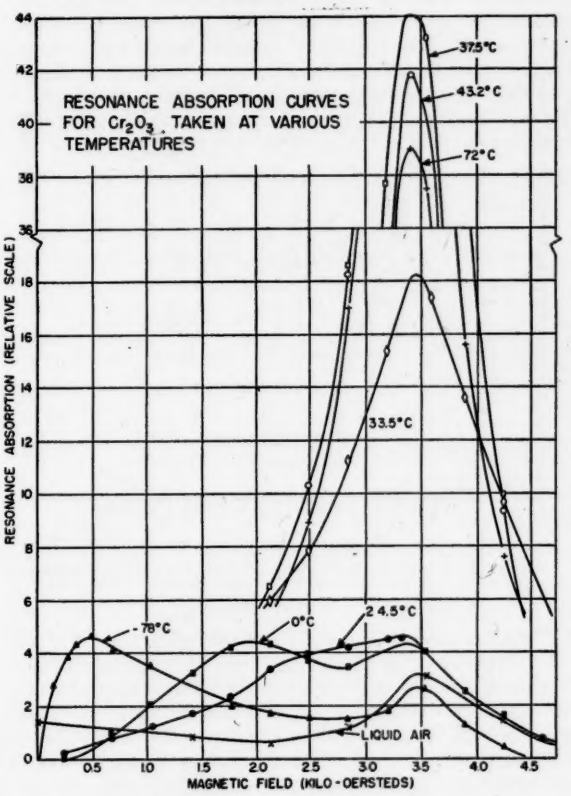

FIG. 3. Resonance absorption curves for powdered Cr_2O_3 taken at various temperatures below the Curie temperature.

sintered material the absorption decreased to zero below the Curie temperature.

The striking correlation of the decrease in peak absorption with the Curie temperature suggests the possibility of interpreting these results in terms of the large local fields associated with the spontaneous magnetization. In the ferromagnetic case the applied torque, in the classical sense, is independent of the internal field arising from the exchange integral because the exchange field and the magnetization vectors are parallel. The effective field required for resonance is then determined by the applied field which is independent of temperature. In contrast to the ferromagnetic case, the spontaneous magnetization for an antiferromagnetic material need not be parallel to the total magnetic moment.[6] On the basis of this simplified microscopic picture, it has been suggested[2] that the cross product of the magnetization and the exchange field is not always zero, making the resultant torque depend on the combined internal and external fields. Kittel,[7] however, has indicated that even in the case of antiferromagnetic resonance absorption the spin systems precess together and the exchange torques mutually cancel.

The small absorption remaining below the Curie temperature for the powdered material is described above as consisting of two parts, one which indicates the growth of an internal field with decreasing temperature. This field is of the order of magnitude of a magnetic dipole field.

Antiferromagnetic resonance is being investigated for NiO, MnO, CoO, and αFe_2O_3 and will be included in a forthcoming paper.

The writers are indebted to Dr. J. W. Beams of the University of Virginia for suggesting that the nature of the internal field of antiferromagnetic materials might be studied by microwave resonance absorption and to Dr. J. Samuel Smart for his interest and helpful discussions.

* Supported in part by the ONR.

[1] Trounson, Bleil, and Maxwell, Phys. Rev. **79**, 226 (1950).
[2] D. F. Bleil and R. K. Wangsness, Phys. Rev. **79**, 227 (1950).
[3] K. Honda and T. Sone, Sci. Rep. Tohoku Imp. Univ. **3**, 223 (1914).
[4] G. Foex and M. Graff, Comptes Rendus **209**, 160 (1939).
[5] The data given here were kindly furnished by Dr. T. R. McGuire of the Naval Ordnance Laboratory.
[6] J. H. Van Vleck, J. Chem. Phys. **9**, 85 (1941).
[7] C. Kittel (private communication, May 1, 1950).

Single Synthetic Zinc Sulfide Crystals

D. C. REYNOLDS AND S. J. CZYZAK
Battelle Memorial Institute, Columbus, Ohio
June 14, 1950

SINGLE synthetic zinc sulfide crystals have been grown under pressure in a hydrogen sulfide atmosphere. Chemically pure zinc sulfide powder was distributed in a quartz tube over a length of 2½ inches. After inserting the quartz tube in the combustion furnace, the tube was evacuated and hydrogen sulfide gas was passed into the system until a pressure of 6 p.s.i. was obtained. The tube was then heated to a temperature of 1150°C for a period of 48 to 96 hours.

An attempt was made previously to grow zinc sulfide crystals in vacuum; however, no satisfactory crystals were produced and as

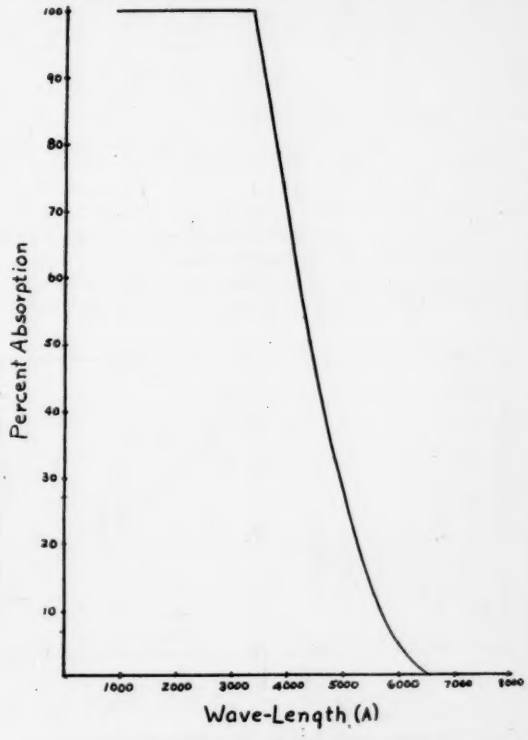

FIG. 1. Optical absorption of zinc sulfide.

UNIVERSITY OF MICHIGAN LIBRARIES

a result of this the growing of crystals in a hydrogen sulfide atmosphere was tried.[1]

The size of the largest crystals that were obtained by hydrogen sulfide method was approximately 2×2×10 mm. Since there are two forms of zinc sulfide crystals, i.e., alpha-form or wurtzite and the beta-form or sphalerite, the crystals were examined with polarized light and were found to be of the alpha-form.

The optical absorption of the zinc sulfide crystals was measured with a photospectrometer at room temperature to determine the absorption cut-off. The data obtained are shown in Fig. 1. The absorption cut-off for the crystals was found to be at 3350A and they are entirely opaque below this. This agrees with the value for powders obtained by Gislof.[2] The absorption decreases until in the red and infra-red region the crystals are completely transparent.

The purity of the crystals was determined by subjecting them to ultraviolet light. The crystals showed no sign of phosphorescence and only in rare cases did they fluoresce. The fluorescence in these few cases was the typical blue fluorescence supposedly due to an excess of zinc atoms predicted by theory. In general the zinc sulfide crystals grown in a hydrogen sulfide atmosphere exhibited neither phosphorescence nor fluorescence which indicates a high degree of purity.

[1] D. C. Reynolds, M.S. thesis (unpublished), University of Iowa (1948).
[2] J. H. Gislof, Physica **6**, 84 (1939).

The Thermal Neutron Scattering by Ammonium Chloride

MOTOHARU KIMURA
Scientific Research Institute, Tokyo, Japan
May 18, 1950

NEUTRON scattering has proved to be a very powerful means of investigating crystalline states, especially those containing hydrogen atoms.[1] The following experiments[2] were performed during the last war, and as we have no facilities for continuing the experiment, it seems appropriate to report here briefly what we did. The transformation of NH_4Cl at −30.8°C has been interpreted as the mutation between the ordered and the disordered states in the orientation of the ammonium ions.[3,4] If this is the case it is to be expected that the diffractive scattering of thermal neutrons may not be the same for the two states. The transmission of thermal neutrons was measured as a function of the temperature of NH_4Cl ranging from about −70°C to room temperature. The experimental arrangement was much the same as that of Beyer and Whitaker,[5] the scatterer being put in a Dewar vessel. The scattering cross section showed a maximum (or minimum in transmission) at the transformation point. It had somewhat larger values at higher temperatures as compared with the values below −30°C as shown in Fig. 1. It is not an established matter, however, to interpret the above results as the mutation between the ordered and the disordered state of the NH_4 ions. The change in the secondary structure (the state of mosaic block or internal distortion) of the NH_4Cl crystal might cause the larger part, if not all, of the observed variation in the scattering, as we may naturally expect a lattice distortion of the crystal near the transformation temperature.[6,7] If this is the case, however, the scattering cross section must depend on the grain size of the powdered scatterer of NH_4Cl of the same temperature as in the case of a polycrystalline metal scatterer.[8,9] We measured the variation using scatterers of various grain size ranging from 2×10^{-4} to 4×10^{-1} cm, and found no change within the limits of error of ±2 percent. This result implies that, contrary to perfect crystals such as SiO_2, the crystal of NH_4Cl belongs to an imperfect type such as those of sulfur and lead[10,11] and cannot show any variation in scattering cross section by internal distortion. Further experiments are desired, however, for the final conclusion.

The author wishes to express his sincere thanks to Professor S. Nishikawa for his encouragement throughout this work. The author also wishes to express his gratitude to the Japanese Foundation for Cancer Research for the supply of radon.

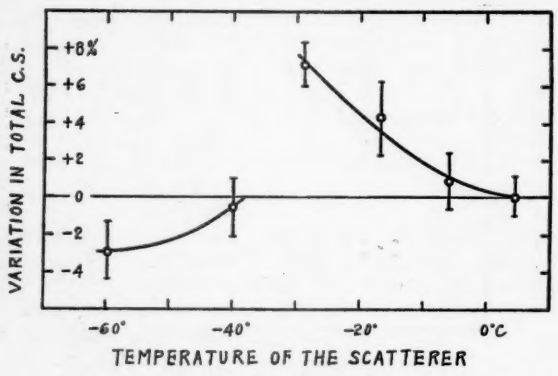

FIG. 1. Scattering cross section of thermal neutrons near the transformation point of ammonium chloride.

[1] Shull, Wollan, Morton, and Davidson, Phys. Rev. **73**, 842 (1948).
[2] M. Kimura, Proc. Imp. Acad. Tokyo **19**, 244 (1943).
[3] J. Frankel, Acta Physicochimica **3**, 23 (1935).
[4] T. Nagamiya, Proc. Phys. Math. Soc. Japan **24**, 137 (1942).
[5] Beyer, Whitaker, Phys. Rev. **57**, 976 (1940).
[6] M. Kimura and R. Hashiguchi, Proc. Phys. Math. Soc. Japan **25**, 530 (1943).
[7] See reference **2**, p. 152.
[8] See reference 6, p. 495.
[9] F. C. Nix and G. F. Clement, Phys. Rev. **68**, 159 (1945).
[10] F. Rasetti, Phys. Rev. **58**, 321 (1940).
[11] M. Kimura and J. Akutsu, Sci. Pap. Inst. Phys. Chem. Research **38**, 63 (1940).

The Shape of the Rossi Curve

W. BOTHE AND H. THURN
Institut für Physik im Max Planck-Institut für med. Forschung and Physikalisches Institut der Universität, Heidelberg, Germany
June 12, 1950

THE second maximum of the Rossi curve, first observed by Ackemann and Hummel,[1,2] was investigated in greater detail some time ago in our laboratory.[3,4] These experiments led to the conclusion that the second maximum indicates production of a special kind of shower differing from cascade showers in origin and properties: (1) most, if not all, of these showers contain two particles only, (2) the shower particles are probably mesons, (3) the angular spread is small (around 10°), (4) the showers are produced by the meson component of cosmic rays, (5) the cross section for production is approximately proportional to Z.

Cloud-chamber experiments,[5,6] as far as they go, have confirmed these results with regard to points (1) to (4), and to absolute rate of production. On the other hand, several investigators using counter arrangements obtained more or less divergent results.[7–9]

We have started fresh experiments with a counter arrangement much more effective than the original one (Fig. 1). Showers are recorded by the two crossed counter trays A, B. Fourfold coincidences between two counters each are recorded. The angular spread is determined by the diagonal distance between the intersecting squares of the four counters. A third counter tray, C, is arranged above the shower-producing lead layer. Connections between C and A, B can be made in different ways, so that the showers are recorded if produced either (a) by ionizing as well as non-ionizing rays or showers (tray C removed), or (b) by showers of at least three ionizing particles, or (c) by ionizing single particles, no second ionizing particle hitting tray C, or (d) by non-ionizing rays, no ionizing particle hitting tray C.

Experiments have so far been performed at an altitude of 100 meters under about 290 g/cm² of concrete ceiling. We believe that all possible sources of misinterpretation of the results, as an in-

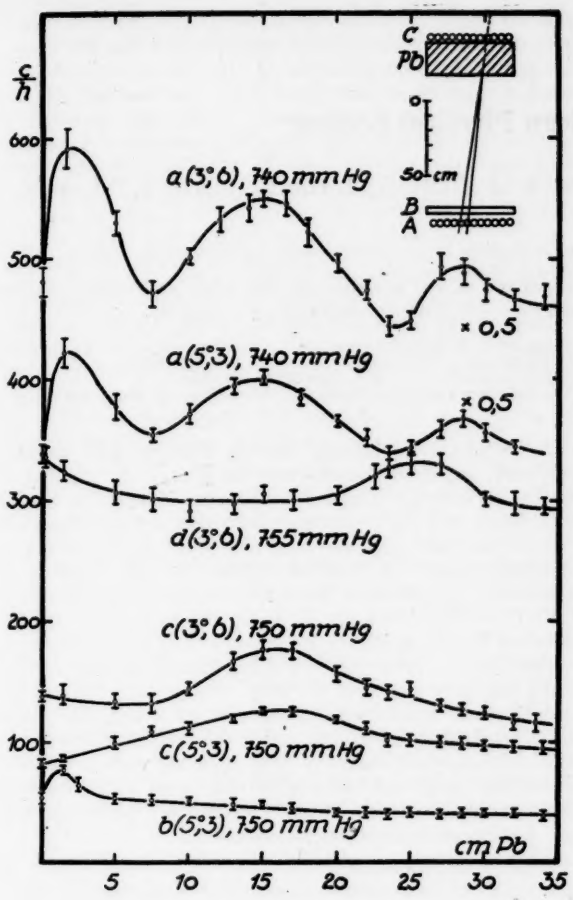

FIG. 1.

fluence of the supporting frame, shape of the lead screen, knock-on electrons from the counter walls, have been ruled out. Some of the Rossi curves obtained for cases (a) to (d) are presented in Fig. 1. Our earlier results concerning the second maximum could be reproduced with much greater accuracy, and some more remarkable facts are revealed. In curves *a* not only the first and second maxima are well pronounced, but in addition a third maximum appears at about 28 cm of lead. Clay,[10] too, has reported, besides the second maximum, a third maximum in about the same region. Curves *b*, *c*, *d* show that each of the three maxima can be completely isolated from the others by controlling conditions of shower production. In this way evidence on the origin of the maxima is obtained. Absolute intensities in the different curves cannot be compared. The initial drop in curves *c* (3°, 6) and *d* springs from imperfections in the apparatus.

The first maximum appears in curve *b* only, and therefore is evidently produced by cascade showers originating in the ceiling and enhanced by the lead.

The second maximum, as previously shown,[3] indicates production of hard narrow showers. Curve *c* is additional proof that the primaries are single ionizing particles.[4] For reasons of penetrating power and rate of shower production it seems almost certain that the primaries can only be μ-mesons. Assuming this, the shower-producing cross section of the lead atom can be estimated as a few percent of the geometric nuclear cross section. As to the nature of the shower particles there is little doubt that our former assumption of mesons is correct (compare the cloud-chamber photographs[5,6]). Experiments are in progress to discriminate between μ- and π-mesons.

It seems difficult at the moment to explain the showers or pairs responsible for the second maximum by one of the known interaction processes. Apparently there is little or no relation to the penetrating meson showers connected with star production.

The third maximum is not easily explained either. It indicates shower production by some non-ionizing radiation, as the comparison of curves *c* and *d* shows. Since high energy neutrons are rare at sea level it will possibly be necessary to assume a new long-lived neutral meson (neutretto). The position of the third maximum depends markedly on the barometric pressure. This explains the shift of the third maximum between curves *a* and *d*, and might also explain discrepancies on the third maximum found by other investigators.

The experiments are being continued.

[1] M. Ackemann, Naturwiss. **22**, 169 (1934).
[2] J. N. Hummel, Naturwiss. **22**, 170 (1934).
[3] K. Schmeiser and W. Bothe, Ann. d. Physik (5) **32**, 161 (1938).
[4] K. Schmeiser, Zeits. f. Physik **110**, 443 (1938); **112**, 501 (1939).
[5] H. Maier-Leibnitz, Zeits. f. Physik **112**, 569 (1939). S. Leisegang, Zeits. f. Physik **116**, 515 (1940).
[6] R. P. Shutt, Phys. Rev. **69**, 261 (1946).
[7] Altmann, Walker and Hess, Phys. Rev. **58**, 1011 (1940).
[8] George, Janossy and McCaig, Proc. Roy. Soc. (A)**180**, 219 (1942).
[9] Z. Ozorai, Zeits. f. Physik **122**, 413 (1944).
[10] Clay, Venema and Jonker, Physica **7**, 673 (1940).
[11] J. Clay and G. Klein, Physica **16**, 293 (1950).

UNIVERSITY OF MICHIGAN LIBRARIES

Proceedings of the American Physical Society

SIXTH MEETING OF THE DIVISION OF FLUID DYNAMICS AT URBANA, ILLINOIS, MAY 12, 13, 1950

Symposium on Hypersonic Flow and Low Density Flow

(J. H. Bartlett, presiding)

A1. Results of Recent Hypersonic Flow Research in the Army Ordnance-California Institute of Technology Hypersonic Wind Tunnel. HENRY J. NAGAMATSU, *California Institute of Technology.*

A2. Hypersonic Research Facilities at the Ames Aeronautical Laboratory. V. J. STEVENS, *NACA, Ames Aeronautical Laboratory.*

A3. Recent Research at the Naval Ordnance Laboratory on Hypersonic Flow. R. SMELT, *Naval Ordnance Laboratory.*

A4. Hypersonic Flow. L. LEES, *Princeton University.*

A5. The Effect of Thermal Radiation on Hypersonic Flow in Wind Tunnels and Free Flight. H. G. STEVER, *Massachusetts Institute of Technology.*

A6. Some Experiments in the Field of Rarefied Gas Dynamics. R. G. FOLSOM AND S. A. SCHAAF, *University of California.*

Contributed Papers

(A. T. NORDSIECK, presiding)

B1. Transonic Flow Measurements.[1] WAYLAND C. GRIFFITH, *Princeton University.*—Experimental results on the flow around two-dimensional wedges and diamond airfoils have been obtained in the Princeton shock tube. Wedge angles studied are 10, 20, 40, 60, 90, and 180° (square ended wedge). Symmetrical diamond airfoils of 10 and 15° total angle are used for a preliminary study of shock wave and boundary layer growth in the transonic region. Density contours throughout the field are found from the fringe shifts observed with a Mach-Zehnder interferometer. The Mach numbers used in these experiments are between 0.8 and 1.6. The distance between detached bow waves and the shoulder of a wedge are found to depend only on the Mach number, and not on the wedge angle as long as the flow is not near the attachment Mach number. In many cases the change in stagnation density across the chock is only a few percent. An average may be chosen and the sonic line located simply by computing the appropriate density ratio. Slides illustrating the methods used for analyzing pictures will be included.

[1] Assisted by an AEC Fellowship and ONR contract.

B2. Diffraction of a Shock Wave through a Small Angle.[1] C. H. FLETCHER, *Princeton University.*—The theories of Bargmann[2] and Lighthill[3] for the diffraction of a shock wave near a corner which deviates the flow by only a small angle ϵ are applicable in first order whether ϵ is positive or negative. Since we have already measured[4] the density field, using a shock tube and interferometer, for ϵ of one sign, it is of interest to carry the investigations to ϵ of opposite sign as well. Shocks of small amplitude have been photographed as they suffered a diffraction through a small angle away from the flow yielding density patterns very similar to those predicted by theory. Photographs of the phenomena will be shown and comparison of the pressures on the walls and other features with theoretical predictions will be discussed.

[1] Supported by ONR contract.
[2] V. Bargmann, AMP 108.2R, N.D.R.C. (March, 1945).
[3] M. J. Lighthill, Proc. Roy. Soc. **A198**, 454 (1949).
[4] W. Bleakney and A. H. Taub, Rev. Mod. Phys. **21**, 604 (1949).

B3. Diffraction of Shock Waves around, and Surface Pressures on, Two-Dimensional Objects.[1] W. BLEAKNEY AND D. R. WHITE, *Princeton University.*—The diffraction of shock waves and the resulting density field has been observed when a plane shock passes around a right-angled corner, a rectangular block, a cylinder, a triangle and other two-dimensional objects in the shock tube. Using a shock strength of $P_1/P_0=2$ the pressures P/P_0 at different points on the surface of the obstacle vary all the way from 0.9 to 2.3. Sharp gradients in the pressure are evident especially near corners during the early stages of the flow. The pressure behind the incident shock is sufficiently constant and of sufficient duration to establish quasi-equilibrium in the wind pressures on the object. No adequate theory of large angle diffraction of shocks has yet been proposed, but qualitatively most of the observed effects are explainable in terms of elementary notions of fluid flow. Extensive illustrations will be given.

[1] Supported by ONR contract.

B4. Supersonic Flow in a Shock Tube.[1] DAVID WEIMER, *Princeton University.*—The evolution of the shock tube technique for the study of shock waves, blast waves, and transonic flow problems has been well described in the literature. The purpose of this paper is to discuss some of the properties of the flow in the region behind the cold front. A number of schlieren pictures will be shown of the flow behind the main shocks in the region of mixing of the hot and cold gases and in the cold gas alone for shocks strong enough to produce supersonic flow (up to $M=3.7$). The Mach numbers of the flow in the hot and cold regions as observed by the angles of attached bow waves are consistent with each other. Considerable turbulence is observed as the cold front passes and then the flow becomes more uniform again.

[1] Supported by ONR contract.

B5. Breaking of Waves by an Opposing Current. YI-YUAN YU, *Northwestern University (Introduced by E. R. Peck).*—A wave beomes unstable and breaks when the forward velocity of the water particles at the crest exceeds the wave celerity. Ordinarily the criterion for breaking is given by the wave steepness, which is not to exceed 1/7 according to Michell. When waves propagate upstream against an opposing current, their breaking is further closely related to the velocity at which energy is transmitted by the wave. A criterion for their breaking may be obtained by considering the critical situation when energy can no longer be transmitted upstream by the wave. In the case in which deep-water waves propagate from still water into a moving current, the criterion comes out to be that waves break when the velocity of the opposing current reaches $\frac{1}{4}$ of the initial wave celerity. Experiments were conducted in a flume consisting of two section of different depths,

Waves were produced in the deeper section in which the water was practically still, and they propagated upstream into the shallower section against an opposing current. The $\frac{1}{4}$ ratio relation was verified, and it was further observed that partial breaking of waves had occured before the current velocity reached $\frac{1}{4}$ of the wave celerity. When the current velocity was smaller than about 1/7 of the celerity, there seemed no breaking.

B6. Axially Symmetrical Jet Mixing of a Compressible Fluid. S. I. PAI, *Institute for Fluid Dynamics and Applied Mathematics, University of Maryland (Introduced by R. J. Seeger).*—The flow of an axially symmetrical jet of a compressible fluid exhausting into a uniform stream is investigated theoretically. The flow of the jet is assumed to be under full expansion from a nozzle. The pressure gradient in the jet is assumed to be negligible. The first part of the paper is concerned with the laminar flow. Ordinary assumptions of boundary layer are used to simplify the Navier-Stokes equations. A solution by the method of small perturbation is first obtained which is expressed in terms of integral of Bessel functions. Exact solution is then obtained by successive approximation from the small perturbation solution. The second part of the paper is concerned with the turbulent flow. The fundamental equation of motion of axially symmetrical jet mixing is derived by the help of Taylor's transport of vorticity hypothesis and Reichardt's assumption of free turbulence that the exchange coefficient over each cross section of the mixing zone is constant. By suitable transformation of variables, it has been shown that the equations of turbulent axially symmetrical jet mixing are identical to those of the laminar case. Hence the solution of the first part can be used to the turbulent case provided that the characteristic constant, i.e., the eddy viscosity, has been properly chosen.

B7. Aerodynamic Behavior and Interaction of Supersonic and Subsonic Axially Symmetric Flows. BERTRAND DES CLERS AND CHIEH-CHIEN CHANG, *The Johns Hopkins University (Introduced by F. H. Clauser).*—This paper analyzes the linearized aerodynamic problems of the axially symmetric body in a subsonic and/or supersonic flow which may be confined in a closed or open wind tunnel, as well as the free flight condition. In order to illustrate the physical aspects of the problem clearly, the arbitrary body shape is decomposed into its Fourier components, and only one component is treated thoroughly. This component is equivalent to an infinitely long cylinder with a wavy surface traveling in a compressible fluid. First, such a wavy-walled cylinder in an axially symmetric subsonic or supersonic flow in a closed- or open-throat wind tunnel is investigated. Next, the subsonic annular flow between the cylinder and an infinite supersonic flow field is considered because of its resemblance to the supersonic boundary-layer effect on the wave drag. Some interesting results are obtained, such as wind tunnel correction and compressibility correction factors. In the supersonic flight of the axially symmetric body, the pressure distribution is not proportional to the local slope as in the two-dimensional case, but lags behind. Besides, the wave drag coefficient is finite at Mach number unity as shown by von Kármán. The thickness of the subsonic layer affects appreciably the wave drag and the pressure distribution of the body.

B8. Explicit Representation of the Flow in the Region of Interaction of Two Arbitrary Simple Waves in One-Dimensional Compressible Fluid Flow. R. SHAW, *New York University (Introduced by George E. Hudson).*—The hodograph transformation is exploited to express the space coordinate x and the time t in the region of interaction in terms of two radially symmetric solutions of the ordinary linear wave equation in spaces whose dimensionality depends on the adiabatic constant γ of the gas, the dimensionality for both solutions being odd integers if $\gamma=3$, 5/3, 7/5 (air), ... From the character of the simple waves, or, from the equations representing the arbitrary motion of two pistons at the ends of a gas-filled tube, which would produce such simple waves, initial data can be calculated along the two characteristics bounding the interaction region. In the hodograph space these characteristics are represented by forward and backward characteristic cones enclosing a spindle-shaped region which corresponds to the interaction flow. For the above values of γ the solutions of the resulting double characteristic initial value problems are obtained explicitly in terms of the initial data and a number (depending on γ) of integrals of these data. For other values of γ, a new method of descent and ascent transforms a radial solution of the wave equation for an odd number of dimensions to a solution for any other number of dimensions (not necessarily integral). This provides general solutions analogous to the form used in the above method.

B9. Nucleation in Very Rapid Vapor Expansions. ARTHUR KANTROWITZ, *Cornell University.*—In the steady state Becker-Döring theory, sub-critical droplets (embryos), with vapor pressure greater than their surroundings, nevertheless grow statistically because they exist in sufficiently greater numbers than neighboring larger droplets. Thus the formation of nuclei against the thermodynamic barrier presupposes the presence of very large numbers of embryos of all sizes. An approximate lower bound for the time required for the formation of this system of embryos can be calculated readily by: (1) neglecting the thermodynamic barrier which impedes their formation; (2) assuming that when droplets contain a certain supercritical number, G, of molecules they grow very rapidly because their vapor pressure is considerably lower than their surroundings; (3) assuming that the formation of the embryo system begins when the vapor first becomes saturated. The equation for the rate of formation of embryos then reduces to the heat conduction equation yielding a simple solution. The lower bound sought is found to be inversely proportional to the fourth power of the degree of supercooling. Comparison with experiments indicates that in some nozzle expansions the occurrence of nucleation is determined by this process.

B10. Effect of Variable Viscosity and Thermal Conductivity on the High Speed Plane Couette Flow of a Semirarefied Gas. T. C. LIN, *University of Washington (Introduced by R. E. Street).*—Schamberg has solved the problem of plane Couette flow in semirarefied gases, under the assumption of constant coefficients of viscosity and thermal conductivity. This paper extends Schamberg's solution to include the effect of variable viscosity and thermal conductivity. For the case of equal wall temperatures the effect of variable viscosity and thermal conductivity tends to increase the velocity slip and the temperature jump, as well as the friction coefficient and the heat transfer, especially at high Mach number and for decreasing density of the gas. Furthermore, at high Mach number the temperature jump plays a more important part in the friction through the coefficient of viscosity, and overbalances the reduction in friction due to velocity slip. This investigation is based on Burnett's expressions for the stresses and the heat flux and Schamberg's expressions for the slip velocity and the temperature discontinuity, as deduced from the third-order approximation to the molecular velocity distribution function of a non-uniform gas.

B11. The Existence and Limit Behavior of the One-Dimensional Shock Layer. DAVID GILBARG, *Indiana University.*—Designate by *shock layer* a steady one-dimensional flow of a viscous, heat-conducting fluid approaching limit values at $x=-\infty$ and $x=+\infty$ which are possible initial and final states

UNIVERSITY OF MICHIGAN LIBRARIES

of a normal shock wave. Rayleigh, Becker, and others have established the existence of the shock layer for ideal gases of a special type. Here the existence and uniqueness of the shock layer is proved for general fluids with viscosity and heat conductivity arbitrary functions of the thermodynamic state. It is also proved, in the same generality, that the shock layers corresponding to a fixed initial and final state converge to a shock wave if viscosity and heat conductivity approach zero (whatever the manner of approach). The limit of the shock layers as heat conductivity tends to zero, viscosity remaining fixed, is seen always to be continuous, whereas, with fixed heat conductivity, the limit, as viscosity vanishes, is discontinuous in general.

B12. Interferometric Studies of Laminar and Turbulent Boundary Layers along a Flat Plate in Supersonic Flow.* R. LADENBURG AND P. WATCHELL, *Princeton University.*— In continuation of our interferometric studies of boundary layers[1] it was found that refraction of light within regions of appreciable density gradients may produce errors in the evaluation. By minimizing those effects through suitable focusing[2] the measured velocity profile near the nose of the flat plate is at a Mach number $M\sim 2.3$ at low Reynolds number ($Re_x\sim 2\times 10^5$) in agreement with Crocco's theory[3] within the experimental uncertainties. With increasing distance from the nose of the plate the profile changes more and more and approaches a profile observed at high Reynolds numbers ($Re_x\sim 3\times 10^6$). This change can be explained by "transverse contamination" by turbulence starting near the corners of the plate.[4] The observed velocity profile at higher density in the test section, corresponding to $Re_x\sim 3\times 10^6$, follows the logarithmic law deduced recently by Kalikhman[5] for compressible turbulent flow.

* Supported by ONR.

[1] R. Ladenburg and D. Bershader, Rev. Mod. Phys. **21**, 510 (1949); Proc. Symposium N. O. L. (June 29, 1949).

[2] P. Wachtell, Phys. Rev. **78**, 333 (1950).

[3] Luigi Crocco, Monogr. Scient. di Aeron., No. 3 (December, 1946).

[4] A. C. Charters, N. A. C. A. Tech. Note No. 891 (1943). Dr. H. Liepmann informed us that he has observed such contamination also in supersonic flow.

[5] L. E. Kalikhman, N. A. C. A. Memo. No. 1229 (1949).